

SYNTHESIS AND ASSESSMENT
OF LASER RELATED PARAMETERS
IN COLOUR CENTRE CONTAINING
DIAMOND

THESIS SUBMITTED FOR THE DEGREE OF
DOCTOR OF PHILOSOPHY

DEPARTMENT OF PHYSICS
INSTITUTE OF PHOTONICS
UNIVERSITY OF STRATHCLYDE

BY ELISABETH FRACZEK

2020

This thesis is the result of the author's original research. It has been composed by the author and has not been previously submitted for examination which has led to the award of a degree.

The copyright of this thesis belongs to the author under the terms of the United Kingdom Copyright Acts as qualified by the University of Strathclyde Regulation 3.50. Due acknowledgement must always be made of the use of any material contained in, or derived from, this thesis.

Signed:  _____

Date: 23.04.2020 _____

First printing, April 2020

Contents

Glossary	ix
Defects in diamond	xi
1 Introduction	1
1.1 Motivation for study	2
1.2 Statement of significance	4
1.3 Publications	6
1.4 Thesis outline	7
References	8
2 Literature review of optically-active defects in diamond	9
2.1 Structure and material properties of diamond	10
2.2 Fundamentals of crystallographic defects	17
2.3 Common defects in diamond	22
2.4 Natural and synthetic diamond	28
2.5 Summary	32
References	33
3 Synthesis of colour centres in diamond	37
3.1 Irradiation	38
3.2 Experimental procedure for electron irradiation	41
3.3 Diffusion, aggregation and dissociation of defects	45
3.4 Experimental procedure for thermal treatment	59
3.5 Summary	63
References	64
4 Defect quantification and spectroscopic methods	67
4.1 Defect quantification in diamond	68
4.2 Dispersive spectroscopy	71
4.3 Fourier transform spectroscopy	74
4.4 EPR spectroscopy	76
4.5 Summary	78
References	79
5 Results of the colour centre synthesis	81

5.1	Introduction	82
5.2	NV synthesis	85
5.3	N_2V^0 synthesis	90
5.4	Spectroscopic analysis	96
5.5	Summary	127
	References	128
6	Progress towards a laser based on colour centres in diamond	129
6.1	Interaction of light and matter	130
6.2	Key parameters for solid state lasers	139
6.3	Luminescence spectroscopy	146
6.4	Diamond in laser engineering	149
6.5	A potential diamond colour centre laser	152
6.6	Summary	168
	References	169
7	Assessment of laser related properties	173
7.1	Sample selection	174
7.2	Assessment of NV containing samples	176
7.3	Assessment of N_2V^0 containing samples	188
7.4	Re-evaluation of laser potential	198
7.5	Summary	203
	References	204
8	Summary and future work	207
8.1	Synthesis	208
8.2	Assessment of laser related properties	211
8.3	Further work	212
	References	215

Acknowledgments

There were numerous obstacles in the way to have this work submitted. I am grateful to everyone who stood besides me during this long and sometimes difficult journey. There are too many to mention all by name, but you all know who you are.

I am grateful to have had the opportunity to spend four years of my life in Scotland. To experience the beautiful nature, the friendly people and welcoming culture of this country.

To my family, thank you for all the unconditional support. And thank you for very rarely asking about the progress of my PhD.

Alan, thank you for caring, for always encouraging my strengths and accepting my weaknesses. In particular, for keeping in touch in the years I dropped out due to my depression. I don't think I can put into words the enormous difference this made to me. I wish I had been an easier student for you to supervise.

None of the results of this work would have been here without you, Vasili. I appreciate all your effort and your perseverance.

I am grateful to the wonderful Diamond Research Group at the University of Warwick, everyone who helped us at the MAMI at the University of Mainz and at the Geoinstitut at the University of Bayreuth. To Jeff Harris, for lending me a whole box of natural diamonds, and never ending encouragement; To the European Research Council for funding, and Element Six for guidance and diamond samples to help me with this research.

To my colleagues and all the people I've met in Scotland. Thank you for many happy memories and experiences!

To the friends I made in Scotland, I am glad I have met you here and I hope to keep in touch and share many happy moments with you in the future.

To my friends at home and all over the world, thank you for being my foundation.

Abstract

Synthesis and Assessment of Laser Related Parameters in Colour Centre Containing Diamond

This thesis reports research on the fabrication and assessment of colour centre containing diamond. The advent of affordable single crystal synthetic diamond with low background absorption has motivated renewed interest in whether efficient colour centre lasers can be realised based on diamond. Two types of colour centres were investigated, composed of one or two nitrogen (N) atoms and a vacancy (V): NV and N_2V^0 . Laser action was first reported in 1985 by Rand and DeShazer in a N_2V^0 containing diamond. The NV centre is one of the most studied defects in diamond, due to the amount of applications harnessing the specific quantum properties of its negatively charged state.

A variety of synthesis techniques were used to produce these centres in nitrogen containing diamond. Specifically, irradiation with electrons with the energy of several MeV in combination with high-temperature and high-pressure annealing. Techniques to characterise samples include infrared and ultraviolet-visible absorption and photoluminescence spectroscopy. Up to 0.65 ppm¹ of NV^0 and 0.85 ppm of NV^- were generated in synthetic diamond. Up to 2.2 ppm of N_2V^0 was generated in natural diamond and up to 0.5 ppm in synthetic diamond. These were consistent with the estimations for concentrations thought to be required for efficient pump absorption in a laser context, 0.6 and 0.9 ppm of NV^- and N_2V^0 . Luminescence lifetimes of 8 ± 1 and 20 ± 1 ns and peak emission cross-sections of $(3.6 \pm 0.1) \cdot 10^{-17}$ and $(1.7 \pm 0.1) \cdot 10^{-17}$ cm² were measured for NV^- and NV^0 , respectively; as well as 12 ± 1 ns and $(1.5 \pm 0.1) \cdot 10^{-17}$ cm² for N_2V^0 .

The gain spectrum was estimated using the emission cross section and absorption spectrum. The potential for positive net gain in a NV^- containing sample, for realistic inversion levels of $\beta = 0.3$, was inferred from these calculations. Although laser operation may be possible with such samples, this has yet to be achieved, indicating that further study of the fabrication and spectroscopy is required. The best N_2V^0 sample showed less promise, requiring inversion levels of $\beta > 0.5$ to achieve positive net gain.

¹ parts per million ($1.77 \cdot 10^{17}$ cm⁻³ for diamond)

Glossary

bcc	body-centered cubic
CCD	Charge-Coupled Device
CVD	Chemical Vapour Deposition
cw	continuous wave
EPR	Electron Paramagnetic Resonance
ESA	Excited State Absorption
fcc	face-centered cubic
FEL	Free-Electron Laser
FTIR	Fourier Transform Infra Red
HeNe	Helium-Neon
HPHT	High Pressure High Temperature
InGaAs	Indium gallium arsenide
IR	InfraRed (0.78-1000 μm)
LaCrO ₃	lanthanum chromate
LED	Light-Emitting Diode
LiF:F ₂ ⁺	Lithium fluoride with an F ₂ ⁺ colour centre
MAMI	MAInzer MIkrotron
MgO	Magnesium oxide
MW	MicroWave
NaCl:F ₂ ⁺ :OH	Sodium chloride with an F ₂ ⁺ colour centre in combination with hydroxide
NIR	Near-InfraRed (0.78-3 μm)
OC	Output Coupler
ODMR	Optically Detected Magnetic Resonance
PbS	Lead sulfide
PCD	Polycrystalline Diamond
PMT	PhotoMultiplier Tube
ppb	parts per billion
ppm	parts per million ($1.77 \cdot 10^{17} \text{cm}^{-3}$ for diamond)
QY	Quantum Yield
RE	Rare Earth

RT	Room Temperature (293 <i>K</i>)
STED	Stimulated Emission Depletion
TCSPC	Time-Correlated Single Photon Counting
Ti:sapphire	titanium-sapphire - $\text{Ti}^{3+}:\text{Al}_2\text{O}_3$
TM	Transition Metal
UV	UltraViolet (10-380 <i>nm</i>)
UV-VIS	UltraViolet-Visible
VECSEL	Vertical-External-Cavity-Surface Emitting Laser
VIS	Visible (380-780 <i>nm</i>)
ZPL	Zero Phonon Line

Defects in diamond

B'	Platelets associated with a sharp line with a position varying between 1358 to 1380 cm^{-1}
C_I	Carbon interstitial
colour centre	A type of structural defect, which produces absorption and emission bands that are different to those of the pure crystal [Sole]
N_2	Two adjacent substitutional nitrogen atoms (A centre)
N_2V	A vacancy and two substitutional nitrogen atoms in C_{2v} symmetry
N_2V^0	The neutrally charged state of N_2V (H3)
N_2V^-	The negatively charged state of N_2V (H2)
N_2VH	A nitrogen pair with a vacancy and a hydrogen
N_2VH^0	The neutral form of N_2VH
N_3V^0	A vacancy and three substitutional nitrogen atoms with a C_{3v} symmetry (N3)
N_4V	Four substitutional nitrogen surrounding a vacancy (B centre)
N_4V_2	Two vacancy and four substitutional nitrogen atoms with a C_{1h} symmetry (H4)
N_s	Single substitutional nitrogen (C centre)
N_s^+	Positively charged N_s
N_s^0	Neutrally charged N_s
NV	A substitutional nitrogen adjacent to a vacancy with a C_{3v} symmetry
NV^+	Proposed positive form of NV
NV^0	The neutral form of NV
NV^-	The negative form of NV
V	Lattice vacancy
V^0	Neutral vacancy (GR1)
V^-	Negative vacancy (ND1)

1

Introduction

Contents

1.1	Motivation for study	2
1.2	Statement of significance	4
1.3	Publications	6
1.4	Thesis outline	7
	References	8

1.1 Motivation for study

THIS WORK addresses the question of whether colour centre¹ containing diamond could in the future be routinely utilised as a laser gain material. Specifically, if a diamond sample can be fabricated with methods presently available in such a way that laser oscillation based on the emission of a particular nitrogen-vacancy colour centre, NV² or N₂V³, is achievable.

Colour centres generate energy levels within the energy gap of the host material. Transitions between those levels can cause the appearance of optical bands.

Many colour centres in alkali halides have been used to build lasers. Such lasers can have high emission cross-sections ($\sigma > 10^{-16} \text{ cm}^2$) and gain coefficients, resulting in low threshold pump powers (as low as tens of mW) and relatively high output powers of hundreds of mW. Their broad luminescence facilitates combined tunability in the IR⁴ between 0.8 to 4 μm and operation with femtosecond pulses [2, 3, 4].

Operation at cryogenic temperatures is needed for most of those alkali halide based lasers to prevent the bleaching and destruction of the optically active centres and the generation of different centres that act as parasitic absorbers. Many colour centres in diamond are thermally stable. They could enable room temperature operation, dramatically simplifying the laser setup [1].

Diamond is an appealing candidate to be utilized in laser engineering due to its outstanding thermo-optical material properties [5].

The conventional approach to harness a material as a laser host is to dope it with RE⁵ or TM⁶ laser ions. This is difficult in the closely packed diamond lattice, as laser ions are large in comparison to the lattice spacing. Successful incorporation of any laser ion into the diamond structure has not been reported yet.

Colour centres could solve the challenge of finding suitable optically active centres in diamond. Such a laser could combine the advantages of the material properties of diamond with the efficiency, tunability and short pulse generation known from alkali halide colour centre lasers [1, 6]. About five hundred luminescent colour centres are known in diamond, jointly covering an emission range from blue to NIR⁷ [7].

For the last 30 years Ti:sapphire⁸ and dye lasers were the most important sources for broadly tunable and ultrafast lasers⁹, covering the spectral range from VIS¹⁰ to NIR [9].

This region is not fully covered by direct emission in available laser materials and often indirect conversion techniques are used to access it [9].

¹ A type of structural defect, which produces absorption and emission bands that are different to those of the pure crystal [1]

² A substitutional nitrogen adjacent to a vacancy with a C_{3v} symmetry

³ A vacancy and two substitutional nitrogen atoms in C_{2v} symmetry

⁴ InfraRed (0.78-1000 μm)

⁵ Rare Earth

⁶ Transition Metal

⁷ Near-InfraRed (0.78-3 μm)

⁸ titanium-sapphire - Ti³⁺:Al₂O₃

⁹ A laser which can generate pulses in the order of picoseconds to femtoseconds [8]

¹⁰ Visible (380-780 nm)

Additionally, an alternative to dye lasers would be welcome. A complex setup of dye jets, flammable solvents and carcinogenic dyes makes them impractical in many applications.

An efficient diode pumped solid-state laser with direct light generation in those spectral regions would be the preferable solution. It would enable more practical and versatile setups, making them accessible to be taken out of the lab or incorporated into extended setups, to be used by a wider audience and more flexible to meet the criteria of real world applications [9].

Laser action at 530 nm in a N_2V^0 ¹¹ containing sample was reported in 1985 [6]. The demonstration of an ultrafast, tunable laser, once diamond with improved optical quality becomes available, was described as promising [10, 11]. Since then high-quality, low cost synthetic diamond has appeared on the market and knowledge about certain colour centres in diamond has deepened with ongoing research.

¹¹ The neutrally charged state of N_2V (H3)

This is the cue for another attempt to investigate the feasibility of using a colour centre containing diamond as a solid state laser material.

In this study we aimed for the synthesis of a few ppm of either NV or N_2V^0 in natural and synthetic diamond samples of a few mm thickness. Suitable concentrations were predicted with estimations for pump absorption calculated using literature values for those centres.

Diamond starting material was obtained with nitrogen already incorporated during the growth process. N_2V^0 and NV were generated using a combination of electron irradiation, annealing and HPHT¹² approaches. Electron irradiation was used to produce vacancies in the diamond lattice. Annealing at moderate temperatures (around 800°C) is needed to mobilize vacancies and form nitrogen-vacancy clusters. Thermal treatment at high pressures and high temperatures (HPHT - $P > 5$ GPa, $T > 1500^\circ\text{C}$) is needed to mobilize nitrogen atoms to form nitrogen clusters. This formation of clusters will be referred to as aggregation in this work.

¹² High Pressure High Temperature

Samples were successfully fabricated with the targeted concentrations of NV and N_2V^0 . The most promising samples were characterised both in terms of their laser-related spectroscopic properties and the relative composition of the target defects and other, potentially parasitic, defects.

Although laser action was not demonstrated with these first-generation samples, the outcomes of the spectroscopic studies were promising in terms of the prospects for future laser demonstrations following iterative improvement of the colour centre fabrication processes. Future directions in this regard will be discussed.

1.2 Statement of significance

In this work the following original contributions were made:

- The emission cross section at the maximum of the emission band has been more firmly established for NV⁻¹³. In 2006, Vins et al. cited a value of $3.2 \cdot 10^{-16} \text{cm}^2$ at 690 nm [11]. In this work, based on assessment of two NV containing CVD¹⁴ samples, a significantly lower value of $(3.6 \pm 0.1) \cdot 10^{-17} \text{cm}^2$ at 710 nm (after subtraction of the contribution of NV⁰¹⁵) was calculated [12]. The accuracy of the lower value was subsequently confirm by Subedi et al., who measured $4.3 \cdot 10^{-17} \text{cm}^2$ at 690 nm [13]
- To the best of the authors' knowledge no values for the emission cross section of NV⁰ have been published in literature to date. In this work the peak emission cross section of NV⁰ was measured as $(1.7 \pm 0.1) \cdot 10^{-17} \text{cm}^2$ at 660 nm [12].
- The emission cross section of N₂V⁰ was given in 2006 by Vins et al. as $1.6 \cdot 10^{-16} \text{cm}^2$ at 525 nm [11]. Calculation of laser threshold by Rand et al. in 1985 [6] imply an emission cross section of $2.3 \cdot 10^{-17} \text{cm}^2$. The value measured in this work was $(1.5 \pm 0.1) \cdot 10^{-17} \text{cm}^2$ at maximum emission (525 nm).

¹³ The negative form of NV

¹⁴ Chemical Vapour Deposition

¹⁵ The neutral form of NV

The calculated emission cross sections for the colour centres under study are shown in fig. 1.1. They span over a combined wavelength range from 500 to 800 nm with a FWHM from 70 to 150 nm for N₂V⁰ and NV.

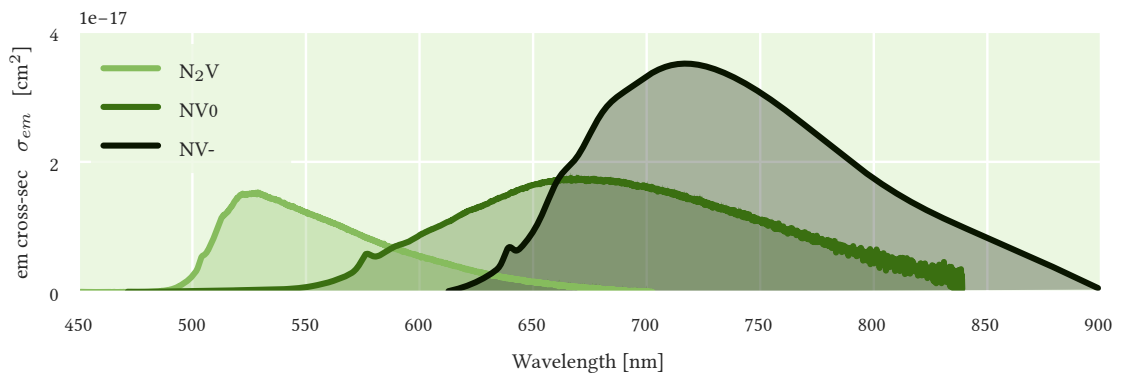


Figure 1.1: Overview of the emission cross section spectra obtained in this work.

- NV assisted aggregation of nitrogen into N₂V⁰ was reported in literature many times as part of HPHT studies of diamond, among others

by [14, 15, 16], discussing the process and qualitative changes in the samples. In this work we report the first quantitative assessment of NV assisted N_2V^0 synthesis.

After treatment, a conversion of 26% of the initial nitrogen concentration into N_2V^0 was found in a CVD sample with ~ 3.8 ppm of single nitrogen. In comparison, literature aggregation constants for the a classical nitrogen aggregation into pairs [17] only predict 0.12% of nitrogen to be converted into N_2 ¹⁶ centres at the same conditions.

- The fabrication of a sample set with ppm levels of a relevant colour centre, low background absorption and high optical quality, aimed specifically for the assessment of laser suitability, was a novel endeavour. Since then further research progress has been made; in particular the study of NV in single crystal and nano diamonds, by the *Compact Solid-State Lasers* group at the University of Strathclyde [12], Jeske et al. [18] in 2017 and Subedi et al. [13] in 2018. While Jeske et al. concluded that NV^- centres are suitable as a laser medium, Subedi et al. reported that stimulated emission of NV^- centres is suppressed by photoionization and ESA¹⁷, and rated the possibility of diamond lasers based on NV^- centres as low.

It is clear that colour centres in diamond continue to be of interest, and more work needs to be done to fully understand the processes involved. The work reported in this thesis contributes to that effort.

¹⁶ Two adjacent substitutional nitrogen atoms (A centre)

¹⁷ Excited State Absorption

1.3 Publications

Journal Papers

- “Laser spectroscopy of NV- and NV0 colour centres in synthetic diamond”. By E. Fraczek, V. G. Savitski, M. Dale, B. G. Breeze, P. Diggle, M. Markham, A. Bennett, H. Dhillon, M. E. Newton, and A. J. Kemp. In: *Optical Materials Express* 7.7 (2017). ISSN: 21593930. DOI: 10.1364/OME.7.002571

Conference Proceedings

- “Progress towards the fabrication and characterisation of colour centres in diamond for laser applications”. By E. Fraczek, V. G. Savitski, S. Shcheka, M. Dale, D. J. Frost, M. E. Newton, and A. J. Kemp. In: *De Beers Diamond Conference*. 2014
- “Fabrication and characterisation of NV and H3 centres in diamond for laser applications”. By E. Fraczek, V. G. Savitski, S. Shcheka, M. Dale, B. G. Breeze, H. Dhillon, A. Bennett, D. J. Frost, M. E. Newton, and A. J. Kemp. In: *De Beers Diamond Conference*. 2015
- “Spectroscopy of colour centres in diamond for possible laser applications”. By E. Fraczek, V. G. Savitski, M. Dale, B. G. Breeze, H. Dhillon, A. Bennett, M. E. Newton, and A. J. Kemp. In: *Advanced Solid State Lasers, ASSL*. 2015. ISBN: 9781943580026. DOI: 10.1364/ASSL.2015.ATu2A.21
- “Synthesis of H3 and NV colour centres in bulk diamond with laser applications in mind - towards higher purity and quantum efficiency with lower parasitic absorption”. By E. Fraczek, V. G. Savitski, D. Pabœuf, S. Shcheka, M. Dale, B. G. Breeze, P. Diggle, M. Markham, A. Bennett, H. Dhillon, J. Hall, D. J. Frost, M. E. Newton, and A. J. Kemp. In: *De Beers Diamond Conference*. 2016
- “Laser-related spectroscopic parameters of NV colour centres in diamond”. By V. G. Savitski, E. Fraczek, M. Dale, B. G. Breeze, L. Dziechciarzyk, P. Diggle, M. Markham, A. Bennett, H. Dhillon, M. E. Newton, and A. J. Kemp. In: *2017 Conference on Lasers and Electro-Optics Europe & European Quantum Electronics Conference (CLEO/Europe-EQEC)*. IEEE, June 2017, pp. 1–1. ISBN: 978-1-5090-6736-7. DOI: 10.1109/CLEOE-EQEC.2017.8086316. URL: <http://ieeexplore.ieee.org/document/8086316/>

Presentations

Oral:

- De Beers Diamond Conference, 2015

Poster:

- De Beers Diamond Conference, 2014
- Advanced Solid State Lasers Conference and Exhibition (ASSL), 2015
- De Beers Diamond Conference, 2016

1.4 Thesis outline

This thesis is structured into the following chapters:

- Chapter 1, Introduction. A brief motivation for the investigation of NV and N_2V^0 colour centres in diamond for the purpose of building a solid state laser.

Colour centre synthesis and characterisation

- Chapter 2, Literature review of optically-active defects in diamond. Structure, material properties, and growth methods of diamond. Introduction of crystallographic defects, in particular colour centres.
- Chapter 3, Synthesis of colour centres in diamond. Review of synthesis techniques for colour centres in diamond, in particular irradiation of diamond for the generation of vacancies and heat treatment for the aggregation and formation of defects. Information about the experimental facilities and procedures used.
- Chapter 4, Defect quantification and spectroscopic methods. Information about the quantification methods for colour centres of interest and the spectroscopic techniques used.
- Chapter 5, Results of the colour centre synthesis. Results of the synthesis of NV and N_2V^0 in synthetic and natural diamond.

Laser related spectroscopy

- Chapter 6, Progress towards a laser based on colour centres in diamond. Introduction to laser physics, in particular solid state lasers, and key laser parameters. Applications of diamond in laser engineering and literature review of the work towards NV and N_2V^0 based diamond lasers.
- Chapter 7, Assessment of laser related properties. A selection of diamond samples with promising characteristics, most importantly colour centre concentration, background absorption and residual defect composition, are assessed for their laser related parameters, such as luminescence lifetime, quantum yield, transition cross-sections and gain coefficient.
- Chapter 8, Summary and future work. A summary of the work conducted. An overview of challenges and ideas for future work.

References

- [1] J. Solé, L. Bausá, and D. Jaque. *An Introduction to the Optical Spectroscopy of Inorganic Solids*. 2005. DOI: 10.1002/0470016043.
- [2] L. F. Mollenauer and J. C. White. *Tunable Lasers*. Springer-Verlag Berlin Heidelberg, 1987, pp. 225–277. ISBN: 978-3-662-10637-2. DOI: 10.1007/978-3-662-10635-8.
- [3] C. R. Pollock, J. F. Pinto, and E. Georgiou. “Recent progress in color center lasers”. In: *Applied Physics B Photophysics and Laser Chemistry* 48.4 (Apr. 1989), pp. 287–292. ISSN: 0721-7269. DOI: 10.1007/BF00694183. URL: <http://link.springer.com/10.1007/BF00694183>.
- [4] F. Träger. *Springer handbook of lasers and optics*. Springer, 2012, pp. 87–156. ISBN: 9783642194085. DOI: 10.1007/978-3-642-19409-2.
- [5] R. P. Mildren and J. R. Rabeau. *Optical Engineering of Diamond*. Ed. by R. P. Mildren and J. R. Rabeau. Weinheim, Germany: Wiley-VCH, Apr. 2013. ISBN: 352741102X. DOI: 10.1002/9783527648603.
- [6] S. C. Rand and L. G. Deshazer. “Visible color-center laser in diamond”. In: *Optics letters* 10.10 (Oct. 1985), pp. 481–483. ISSN: 0146-9592. DOI: 10.1364/OL.10.000481.
- [7] A. M. Zaitsev. *Optical Properties of Diamond: A Data Handbook*. Springer, 2001, p. 502. ISBN: 354066582X. DOI: 10.1007/978-3-662-04548-0.
- [8] *RP Photonics Consulting GmbH - technical consulting on laser technology, nonlinear optics, fiber optics; simulation and design software; encyclopedia and buyer’s guide*. URL: <https://www.rp-photonics.com/>.
- [9] G. Huber, C. Kränkel, and K. Petermann. “Solid-state lasers: status and future”. EN. In: *Josa B* 27.11 (Oct. 2010), pp. 93–105. ISSN: 0740-3224. DOI: 10.1364/JOSAB.27.000B93.
- [10] S. Rand. “Synthetic Diamond for Color Center Lasers”. In: *Advanced Solid State Lasers*. Optical Society of America, 1986, FA9. DOI: 10.1364/ASSL.1986.FA9.
- [11] V. G. Vins and E. V. Pestryakov. “Color centers in diamond crystals: Their potential use in tunable and femtosecond lasers”. In: *Diamond and Related Materials* 15.4-8 (Apr. 2006), pp. 569–571. ISSN: 09259635. DOI: 10.1016/j.diamond.2005.11.038.
- [12] E. Fraczek et al. “Laser spectroscopy of NV- and NV0 colour centres in synthetic diamond”. In: *Optical Materials Express* 7.7 (2017). ISSN: 21593930. DOI: 10.1364/OME.7.002571.
- [13] S. Subedi et al. “Laser spectroscopy of highly doped NV-centers in diamond”. In: *Solid State Lasers XXVII: Technology and Devices* 10511 (Feb. 2018). Ed. by W. A. Clarkson and R. K. Shori, p. 84. DOI: 10.1117/12.2290705.
- [14] Y. Mita et al. “Photochromism of H2 and H3 centres in synthetic type Ib diamonds”. In: *Journal of Physics: Condensed Matter* 2.43 (Oct. 1999), pp. 8567–8574. ISSN: 0953-8984. DOI: 10.1088/0953-8984/2/43/002.
- [15] S. C. Lawson et al. “The ‘H2’ optical transition in diamond: the effects of uniaxial stress perturbations, temperature and isotopic substitution”. In: *Journal of Physics: Condensed Matter* 4.13 (Mar. 1992), pp. 3439–3452. ISSN: 0953-8984. DOI: 10.1088/0953-8984/4/13/008.
- [16] A. T. Collins et al. “High-temperature annealing of optical centers in type-I diamond”. In: *Journal of Applied Physics* 97.8 (Apr. 2005), p. 083517. ISSN: 00218979. DOI: 10.1063/1.1866501.
- [17] R. Jones et al. “Diffusion of nitrogen in diamond and the formation of A-centres”. In: *Diamond and Related Materials* 53. Supplement C (2015), pp. 35–39. DOI: 10.1016/j.diamond.2015.01.002.
- [18] J. Jeske et al. “Stimulated emission from NV centres in diamond”. In: *Nature Communications* 8 (Jan. 2017), pp. 1–10. ISSN: 2041-1723. DOI: 10.1038/ncomms14000.
- [19] E. Fraczek et al. “Progress towards the fabrication and characterisation of colour centres in diamond for laser applications”. In: *De Beers Diamond Conference*. 2014.
- [20] E. Fraczek et al. “Fabrication and characterisation of NV and H3 centres in diamond for laser applications”. In: *De Beers Diamond Conference*. 2015.
- [21] E. Fraczek et al. “Spectroscopy of colour centres in diamond for possible laser applications”. In: *Advanced Solid State Lasers, ASSL*. 2015. ISBN: 9781943580026. DOI: 10.1364/ASSL.2015.ATu2A.21.
- [22] E. Fraczek et al. “Synthesis of H3 and NV colour centres in bulk diamond with laser applications in mind - towards higher purity and quantum efficiency with lower parasitic absorption”. In: *De Beers Diamond Conference*. 2016.
- [23] V. G. Savitski et al. “Laser-related spectroscopic parameters of NV colour centres in diamond”. In: *2017 Conference on Lasers and Electro-Optics Europe & European Quantum Electronics Conference (CLEO/Europe-EQEC)*. IEEE, June 2017, pp. 1–1. ISBN: 978-1-5090-6736-7. DOI: 10.1109/CLEOE-EQEC.2017.8086316. URL: <http://ieeexplore.ieee.org/document/8086316/>.

2

Literature review of optically-active defects in diamond

Contents

2.1	Structure and material properties of diamond	10
	Crystal structure	10
	Band structure	13
	Material properties	14
	Applications	15
2.2	Fundamentals of crystallographic defects	17
	Defect types	17
	Optically active centres in a crystal and electron phonon coupling	18
	Non-radiative deexcitation and energy transfer	20
2.3	Common defects in diamond	22
	An overview of defects found in diamond	22
	Charged state and transfer between defects	25
2.4	Natural and synthetic diamond	28
	Growth conditions	28
	Natural diamond	29
	HPHT grown diamond	29
	CVD grown diamond	30
2.5	Summary	32
	References	33

2.1 Structure and material properties of diamond

CARBON can exist in covalent bonds in a tetrahedral geometry and form a stable, highly symmetric and tight crystal lattice. This crystalline structure of carbon is named diamond [1].

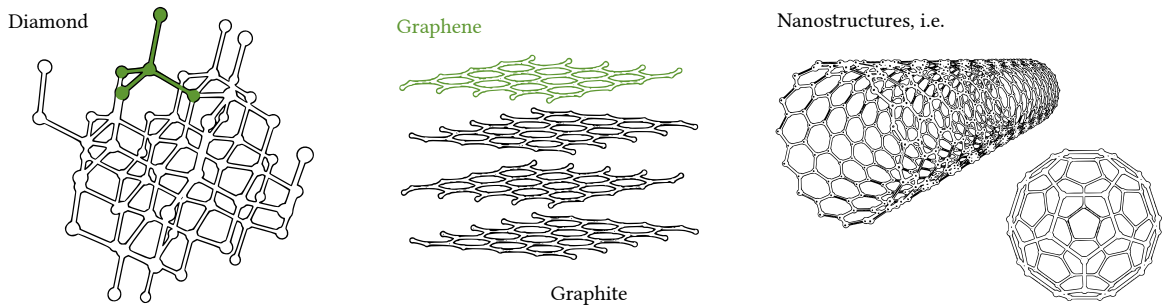
The combination of structure and atomic properties brings about a wide range of outstanding material properties. For many applications where thermal management and optical quality are crucial parameters, for example laser engineering, diamond is a pursued material choice. Simultaneously, doping with RE¹ or TM² ions is restricted by the tight crystal lattice, thus preventing the conventional utilization of diamond as a laser host material [1, 2].

¹ Rare Earth

² Transition Metal

Crystal structure

Carbon can form many different structures at the same temperature and pressure. Such structures are called allotropes. Well known forms of carbon are diamond, graphene, graphite and nanostructures like fullerenes, as shown in fig. 2.1.



Graphite is the energetically favourable solid form of carbon under standard laboratory conditions. Diamond is meta stable and can be converted into graphite after overcoming an activation energy.

The diamond lattice has a characteristic tetrahedral structure, formed by 4 equal-length, covalent σ -bonds [4] illustrated in fig. 2.2.

The crystal structure of diamond is a variation of the fcc³ lattice structure. Two fcc lattices are combined and diagonally shifted with respect to each other by a fourth of the lattice constant a in each direction, illustrated in fig. 2.3. One base is $(0, 0, 0)$ and the other $(a/4, a/4, a/4)$. Each atom has 4 nearest neighbours and $4 \times 3 = 12$ next nearest neighbours. The diamond lattice is the most compact lattice structure, with 18 atoms per unit cell and a lattice constant of $a = 3.567 \text{ \AA}$ [6].

Figure 2.1: Allotropes of carbon adapted from [3]. **Diamond** - tetrahedral bonds between atoms. **Graphene** - single sheet of carbon in a hexagonal lattice. **Graphite** - multiple sheets of graphene. **Fullerenes** - atoms are bonded together in spherical, tubular, or ellipsoidal formations.

³ face-centered cubic

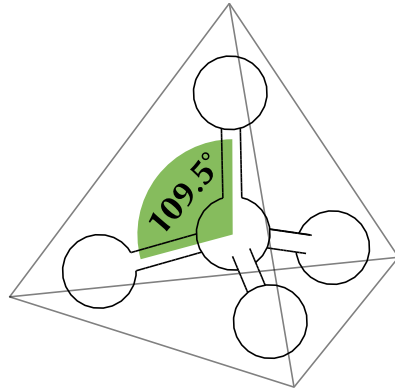


Figure 2.2: The 4 valence electrons of a carbon atom in diamond form sp^3 orbitals which are aligned at an angle of 109.5° to each other. This is the characteristic tetrahedral structure of diamond. Adapted from [5].

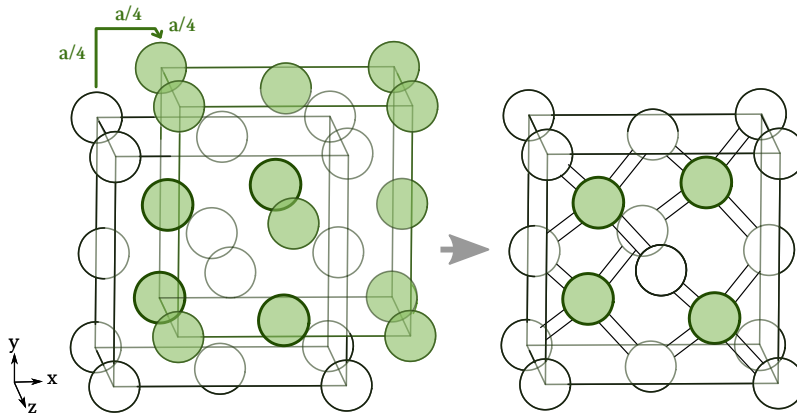


Figure 2.3: Two diagonally shifted fcc lattices illustrate the diamond lattice [6].

On the left a fcc unit cell (unfilled circles) is overlapped with a fcc unit cell shifted diagonally by $a/4$ in each direction (filled circles). On the right the diamond unit cell is pictured with the atoms that originate from the original fcc cell and the four atoms from the shifted cell, together with the bonds between atoms.

The maximum fraction of the volume in the structure that can be occupied by spheres without overlapping, called atomic packing factor, is $APF_{Dia} = \pi\sqrt{3}/16 \approx 0.34$ for diamond - less than half of the filling factor for a closest-packed structure such as fcc or bcc⁴ lattices [7].

Even though the structure is relatively empty, the small atomic radii and short distances between atoms result in a high atomic density. The bond lengths in diamond are only about 1.54 Å. The resulting atomic density of $\rho_{Dia} = 1.76 \cdot 10^{23} \text{ cm}^{-3}$ is the highest of any solid [8].

When defects in diamond are illustrated, it is useful to shift the diamond unit by $a/2$ in any direction, because it puts a carbon atom right at the centre of cell, surrounded by all nearest and next-nearest neighbours, instead of being offset. For 2D representations the (120) orientation is chosen for illustration purposes, as there is no overlap of atoms and the connections between atoms are relatively clear (See fig. 2.4).

⁴ body-centered cubic

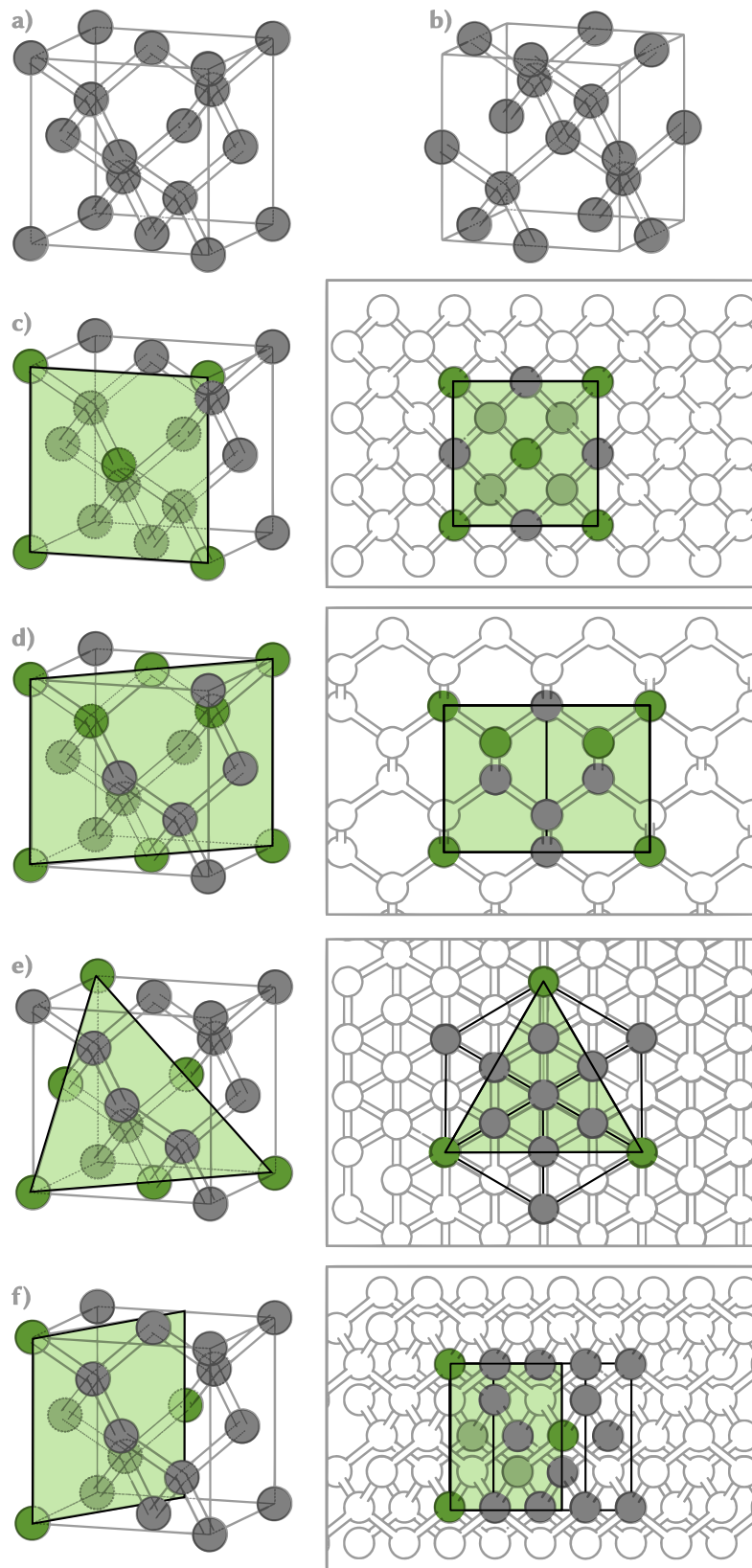


Figure 2.4:

a) Diamond unit cell

b) Diamond unit cell shifted by $a/2$ in any direction. This representation has one atom in the middle of the unit cell and all four atoms bonded to it inside the cell and it therefore more intuitive to represent defects in diamond, especially if they are a combination of multiple atoms or vacancy-atom combinations.

c) - f) are 3D (left side) and 2D (right side) representations of different orientations in diamond.

c) (100) orientation

d) (110) orientation

e) (111) orientation

f) (120) orientation. In the 2D representation of this orientation there are no overlapping atoms. All 18 atoms in the unit cell, together with all 4 tetrahedral bonds are visible. This representation will be used in this work to visualize the diamond structure and defects in it in 2D.

Band structure

Carbon can form many different structures due to its valency, a measure of the affinity to share electrons between atoms. In the ground state it has the electronic configuration $1s^2 2s^2 2p^2$. The 4 valence electrons of each carbon atom ($2s^2$ and $2p^2$) are sp^3 hybridized in diamond ($(2sp^3)^4$), shown in fig. 2.5.

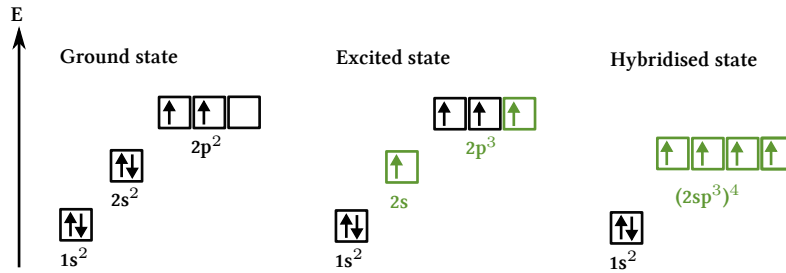


Figure 2.5: Diamond hybridization adapted from [9].

The band structure describes the range of energies that the electrons may (energy bands) or may not (band gaps) occupy. Transitions between these bands happen through photons or phonons [6].

It results from the overlap of the original $2s^2$ and $2p^2$ orbitals as illustrated in fig. 2.6, where the band structure for the valence electrons is shown as a function of the atom spacing.

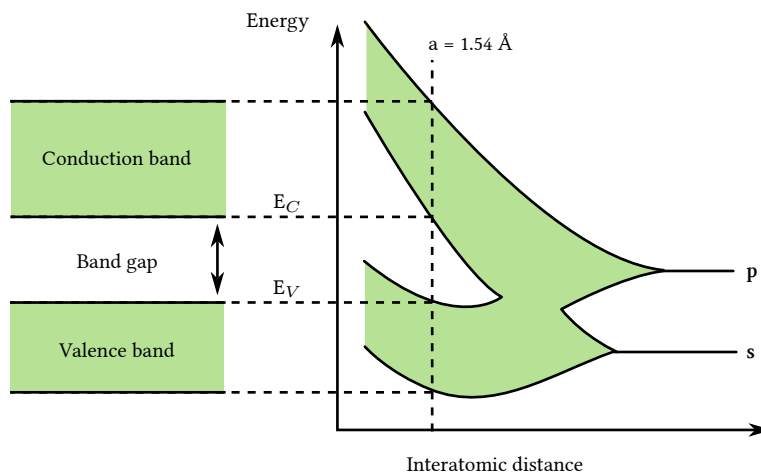


Figure 2.6: Diamond hybridization illustrated with band structure Adapted from [10].

Material properties

Diamond has a wide range of outstanding material properties. A selection of these properties for diamond is presented in table 2.1 along with comparisons to some common semiconductor materials.

	Si	SiC	GaN	Diamond
Band-gap (eV)	1.1	3.2	3.4	5.5
Electron mobility ($\text{cm}^2 (\text{Vs})^{-1}$)	1450	900	440	4500
Hole mobility ($\text{cm}^2 (\text{Vs})^{-1}$)	480	120	200	3800
Thermal conductivity ($\text{W} (\text{mK})^{-1}$)	150	500	130	2000

Table 2.1: Material properties of diamond compared to semiconductor materials [1, 11].

The covalent bonding of diamond together with the large $C - C$ binding energy of 348 kJ/mol are the cause for its hardness [4], which is used as the maximum of the Mohs hardness scale [12].

The stronger the bonding configuration and the purer the crystal, the less free electrons are available to conduct electricity, but the faster and further phonons can disperse [13]. Unlike in metals, where thermodynamic properties and heat capacity are mediated by electrons, in diamond they are characterized by the phonon structure. Thermal conductivity of natural diamond at room temperature was measured to be about $2000 \text{ W}/(\text{m} \cdot \text{K})$, five times the conductivity of copper [1].

A broad transmission spectrum and high thermal conductivity results from the wide band gap and high phonon propagation frequency [1]. Photon absorption in solids is mediated through excitations of valence electrons in the UV⁵-NIR⁶, where the wavelength is much larger than the distances between atoms, and lattice vibrations in the IR⁷, where atoms in solids vibrate [14].

The transmission spectrum is the widest spectrum of any known material and extends from UV (225 nm) to far IR ($>15 \mu\text{m}$). Intrinsic absorption decreases at longer wavelengths as fewer phonon modes are available. Low absorption samples have been reported up to and beyond $500 \mu\text{m}$ [1].

The spectrum is mostly featureless, besides the a characteristic absorption feature in the mid-IR called lattice or multiphonon absorption, in the range of 2.6 to $6.2 \mu\text{m}$ [1, 15]. An illustration of this can be seen in fig. 2.7. Single phonon absorption is prevented in the perfect diamond lattice due to its symmetry, but can occur when imperfections are present [16]. These features have been associated with defects like nitrogen [17] and will be further discussed in section 2.2, Fundamentals of crystallographic defects.

⁵ UltraViolet (10-380 nm)

⁶ Near-InfraRed (0.78-3 μm)

⁷ InfraRed (0.78-1000 μm)

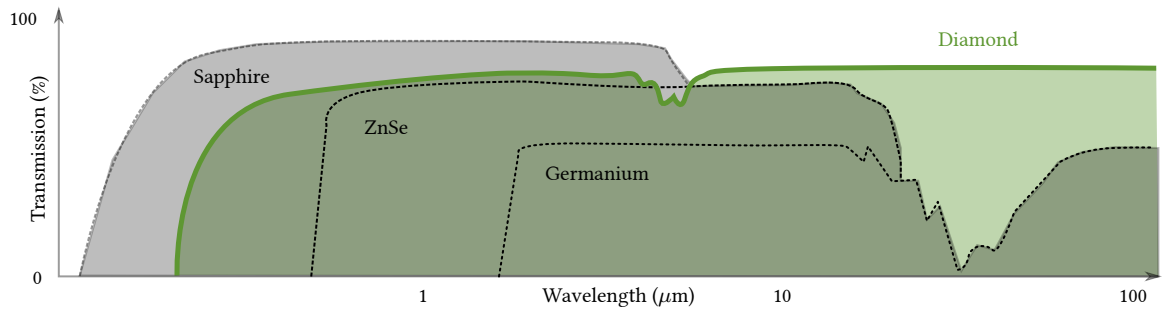


Figure 2.7: Transmission spectrum diamond in comparison to Sapphire, ZnSe and Germanium. Adapted from [18].

Diamond has a band gap of 5.5 eV , which is associated with the fundamental absorption edge at 225 nm ($E = hc/\lambda$). This gap is significantly larger than that of other common semiconductor materials [6, 19], as can be seen in table 2.1.

The maximum frequency at which a phonon can propagate through a crystal lattice is known as the Raman frequency. Phonon-Raman scattering is the inelastic scattering of photons on atoms, where the energy difference is transferred through phonons. This energy can be either transferred from the photon to the lattice (Stokes-Raman) or from the lattice to the photon (Anti-Stokes-Raman).

In diamond this frequency is 1332 cm^{-1} [20]. In crystals with regularly arranged identical atoms there is one dominant Raman band. The Raman shift in diamond is high because it is proportional to the bond strength and inversely proportional to the atom masses.

A perfect diamond lattice is isotropic and therefore devoid of birefringence. In practice defects in the lattice are present to some degree, introduced during the growth process, due to strain or other outside influences, which modify the isotropic properties [21].

Diamond is chemically and biologically inert [12]. At high electron energies ($>0.1 \text{ GeV}$), where radiation damage is dominated by the inelastic cross section of the radiation particle and material, diamond is an order of magnitude more radiation hard than silicon. At lower energies this difference is small [22].

Applications

The outstanding thermal conductivity of diamond, together with the rigidity of the lattice, make it an excellent material for purposes where efficient cooling and low thermal deformation are crucial. A high thermal conductivity is usually directly correlated with a high electrical conductivity in

most materials. In diamond phonons transport heat through the lattice. This makes diamond an ideal choice as heat spreader for a range of applications, in particular high power electronics [23].

The high thermal conductivity together with the large spectral transmission window, high refractive index and moderate dispersion makes it an ideal material for optical applications, for example as an intracavity heat-spreader for lasers and optical windows [1].

Diamond is used in solid state particle detectors, as for example at the Large Hadron Collider at CERN. In comparison to silicon it is highly resistive and has no free carriers that contribute to noise in the electric signal. The thermal conductivity eliminates the need for extensive cooling. It is also more radiation hard than silicon and therefore has an extended lifetime [24].

2.2 Fundamentals of crystallographic defects

DEFECTS IN A CRYSTAL can affect its material properties, like color and electrical and thermal conductivity. This makes the characterisation, quantification and synthesis of defects in diamond and their possible applications a popular field of study.

One of these possible applications is the topic of this work, the utilisation of luminescent nitrogen-vacancy complexes in diamond to manufacture a laser crystal.

Defect types

Crystals are characterized by a periodic lattice structure. A crystallographic defect is an irregularity in this pattern. Defects are categorized into point and extended defects, depending on their extent in the crystal, and into intrinsic and extrinsic defects, depending on the inclusion of impurities.

Many point defects are referred to as *centres*, for historical reasons. Defects that produce colouration in the otherwise colourless crystal are called colour centres ⁸ [14].

Point defects affect the area in or around a single lattice site and seldom extend further than the unit cell. They typically involve missing and/or additional atoms.

Intrinsic defects only include displaced lattice atoms and vacancies. Extrinsic defects, sometimes referred to as impurities or inclusions, are atoms or larger clusters that are not part of the original crystal setup.

The most important point defects are [1]:

- Vacancies, lattice sites which should be occupied by an atom but are empty. The stability of the crystal lattice prevents the surrounding atoms from collapsing into the empty space. Vacancies are formed during crystal growth, plastic deformation and irradiation damage.
- Interstitials, atoms located in between lattice sites. They can form when a lattice atom is displaced and a vacancy is created or when impurities are introduced in the crystal, which have a different size to the original lattice atoms and therefore have an energetically favourable position on off lattice sites.
- Frenkel defect, an interstitial-vacancy pair. They form when an atom leaves its place in the lattice, creating a vacancy, and becomes an interstitial by occupying a nearby location in between lattice sites [25].

Defect complexes are a combination of different kind of point defects.

⁸ A type of structural defect, which produces absorption and emission bands that are different to those of the pure crystal [14]

Figure 2.8 illustrates point defects in a simplified lattice. This illustration doesn't take into account different interstitial sites or lattice relaxations, which would result in a deformation of the surrounding lattice around defects to reach a configuration of minimal potential energy.

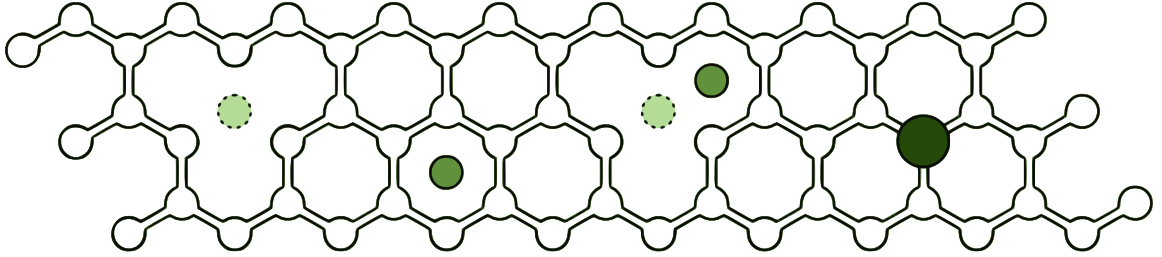


Figure 2.8: Defect types illustrated on a hexagonal lattice. Left to right: Vacancy, interstitial, Frenkel defect and extrinsic defect on a lattice site.

Optically active centres in a crystal and electron phonon coupling

Optically active centres have electronic states within the energy gap of the material. This enables the possibility for optical transitions at wavelengths longer than the fundamental absorption edge, and cause a coloration of the crystal [14]. Due to the large bandgap a perfect diamond crystal is colourless. The band structure of diamond has been covered in section 2.1 (see fig. 2.6).

Unlike transitions in an isolated atom, the centres in a crystal often have a characteristic broadened absorption and emission spectrum as a result of the interactions with lattice phonons. A brief introduction to the interaction between colour centres and a vibronic⁹ crystal is given in this subsection. In fig. 2.9 the broadening of the discrete electronic states into continuous bands by the vibronic coupling of the atom and the crystal vibrations is shown [26].

⁹ A system where vibrational and electronic interactions are coupled (electron-phonon coupling)

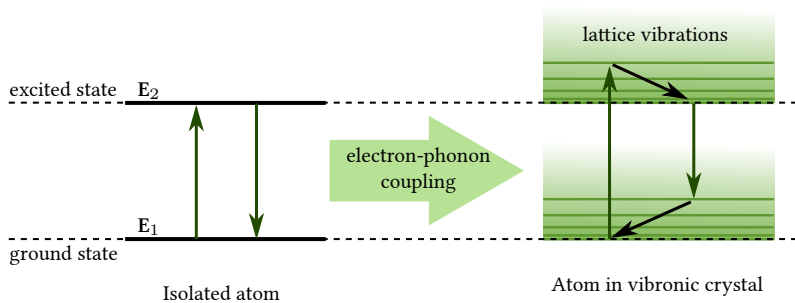


Figure 2.9: Optical transitions between the ground state and an excited state of (Left) an isolated atom and (Right) an atom within a crystal lattice, where the electronic states are coupled to a continuous band of phonons by electron-phonon interactions. Adapted from [26].

To illustrate the effect of the lattice coupling a defect A surrounded by lattice atoms B can be considered (fig. 2.10). In a static lattice A and B are

fixed at equilibrium positions. But in a real lattice A is coupled to the lattice vibrations through the atoms B.

If the electronic and atomic motions are practically independent of one another A is weakly coupled to the lattice phonons. If the electronic motions are strongly dependent on the atom positions at any given time, A is strongly coupled to the lattice phonons [14].

If A is an isolated atom with two electronic states (fig. 2.9 left), a photon with the energy $\Delta E = E_2 - E_1$ can be absorbed and emitted. In a crystal photons with higher energies can be absorbed, exciting the electron into a higher level in the excited state band by creating lattice phonons (fig. 2.9 right). The electron then relaxes to the bottom of the excited state band by nonradiative processes¹⁰.

Finally, the electron can relax into an upper level of the ground state band, again generating phonons and relaxing to the bottom by nonradiative processes.

The transition between the bottom of the ground state band and the bottom of the excited state band is called ZPL¹¹, as neither excitation nor relaxation is coupled to phonons.

The energy difference between the maximum of the absorption and emission spectrum, as seen in fig. 2.9 and represented by the difference of the arrow lengths, is called the Stokes shift.

The Stokes shift can be explained using the configurational coordinate model, illustrated in an configuration diagram¹² in fig. 2.11. The harmonic potentials illustrate the electron-phonon coupling. Inside the potentials the electron states ($n, m = 0, 1, 2, \dots$) and corresponding probability densities of the electrons are indicated. The configurational coordinate model is based on the following approximations.

The adiabatic approximation [27] considers the fact that electrons are much lighter than the lattice atoms. Their movement is so much faster than that of the lattice, that the lattice can be considered static in comparison.

One mode of vibration, where the atoms B pulsate radially around A in an 'in and out' motion, is considered. Because of its dynamics, this is called the *breathing model*. This reduces the spacial coordinates in this system to one configurational coordinate Q , which corresponds to the distance A-B (see fig. 2.10). When A is strongly coupled, the minimum of the ground and excited state will in be positioned at different values of Q , Q_0 and Q_0' , respectively [14].

The Franck Condon principle implies that electronic transitions are represented by vertical arrows in fig. 2.11 at the same configurational coordinate Q , as the electronic transitions happen on much faster timescales than

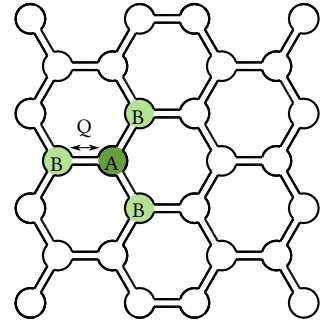


Figure 2.10: Illustration of an optical centre. Adapted from [14].

¹⁰ Transitions that do not involve radiation. The energy is dissipated for example through spreading of the lattice vibrations in the crystal.

¹¹ Zero Phonon Line

¹² The electronic energy of a system is shown as a function of the configuration coordinates

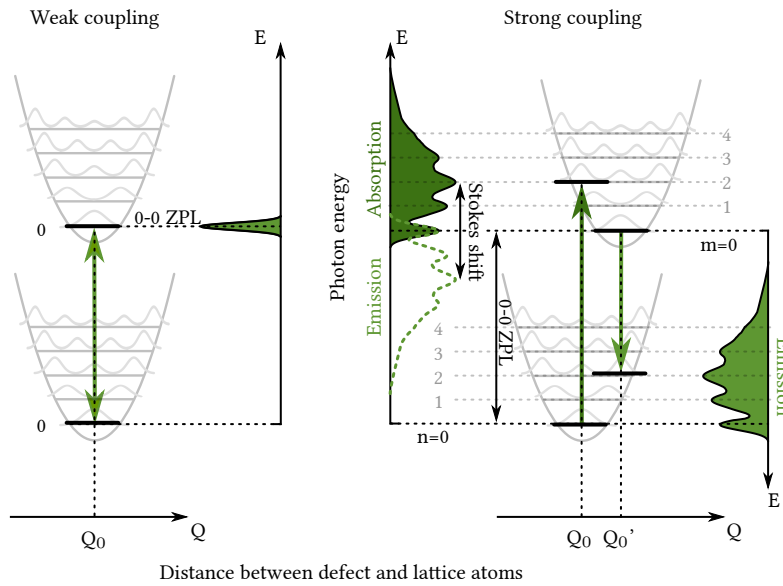


Figure 2.11: Strong and weak coupling and its influence on the absorption and emission features illustrated. Adapted from [14].

the atomic movements. The strength of the transition is dependent on the overlap of the probability densities of the two vibrational states [14]. This is the reason why the strongest emission and absorption don't necessarily occur at the ZPL in a strongly coupled system, but at the transitions where the overlap of the the probability densities is largest.

The transitions as pictured in fig. 2.11 would imply discrete lines in the spectrum. In a real crystal there are many different phonon modes available and therefore the spectrum is continuous.

Non-radiative deexcitation and energy transfer

Besides the shape of the emission and absorption, covered in the previous subsection, we are interested in the efficiencies of the processes for a certain optically active centre under study. As the samples are intended to be examined for their potential as laser gain material, a large product of emission cross section and luminescence lifetime is desirable. This will be discussed in more detail in chapter 6, Progress towards a laser based on colour centres in diamond.

Concentration quenching and parasitic absorption by other centres can influence this product negatively. These are linked to the concentrations of the optically active centre and to the presence and concentration of other defects.

In a lattice an excited centre can relax back into the initial state after excitation by additional, non-radiative processes. This means that instead of the emission of a photon it relaxes through dipole-dipole interactions

between two nearby centres, multi-phonon emission or a combination of both. Excitation energy can be transported between centres of the same type, to different luminescent centres or to other defects that then de-excite through non-radiative channels.

Energy transport is dependent on the average distance between centres, and therefore their concentration. Below a critical concentration, an increase in the concentration of the luminescent centre corresponds with an increase in the intensity of the emitted light. At the critical concentration the luminescence intensity starts to decrease again. This is referred to as concentration quenching of luminescence [14]. Quenching occurs when the average distance between the centres is small enough for energy transfer to become a competing mechanism for luminescence.

Concentration quenching will result in a reduction in the luminescence decay time. The critical concentration for which the lifetime starts to be reduced can be determined by measuring the lifetime of the excited centres as a function of the concentration [14].

2.3 Common defects in diamond

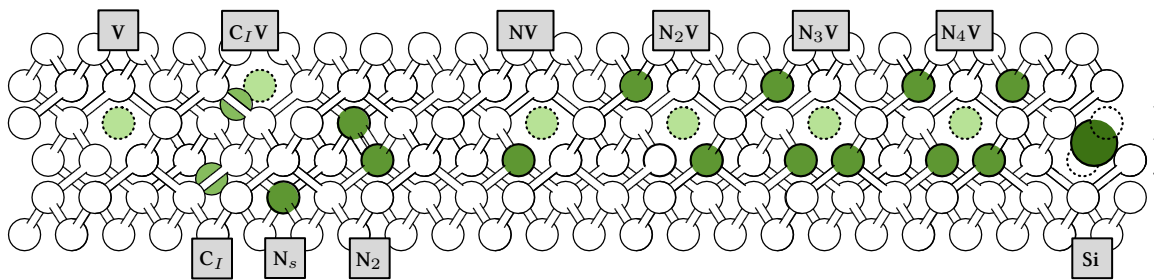
RADIATIVE ELECTRONIC TRANSITIONS in a crystal require that both ground and excited state of a centre lie within the band-gap of the crystal. The huge bandgap in diamond allows for many different centres to exist within the bandgap and to exhibit optical absorption and emission.

More than five hundred optical centres are known in diamond. Of those only a few have been artificially produced so far and a wide field is still to be explored [20, 28].

An overview of defects found in diamond

Intrinsic defects in diamond include carbon atoms located outside of lattice sites, C_I ¹³, and vacancies. Extrinsic defects in diamond include a range of impurities. The most common ones among these are H, B, N, O and Si [20].

Nitrogen is the most common extrinsic defect in diamond. The historical classification of diamond is based on its nitrogen content. It is still commonly used today and therefore will be briefly introduced below. Nitrogen can be found as a single substitutional defect N_s ¹⁴, as a nitrogen pair N_2 ¹⁵ or as a combination of nitrogen and vacancies, forming bigger clusters [1, 20]. Among those the most important for this work are NV¹⁶ and N_2V ¹⁷. An illustration of some intrinsic and extrinsic defects in the diamond lattice is given in fig. 2.12



¹³ Carbon interstitial

¹⁴ Single substitutional nitrogen (C centre)

¹⁵ Two adjacent substitutional nitrogen atoms (A centre)

¹⁶ A substitutional nitrogen adjacent to a vacancy with a C_{3v} symmetry

¹⁷ A vacancy and two substitutional nitrogen atoms in C_{2v} symmetry

Historically, diamond has been classified into two types, called type I and II, depending on their nitrogen content [15]. The type categorization is presented in table 2.2

The most common sample type at the time was called type I. Diamonds in this category absorb UV radiation below 300 nm and display character-

Figure 2.12: Nitrogen-vacancy defects in diamond illustrated on the 2D diamond lattice in (120) orientation. Atoms are scaled to 50% of their actual size (relative to the bond lengths) in this representation. Silicon atom at an interstitial site with two carbon atoms missing from the lattice to make space for the large atom.

Type		Category	Sub- category
I	II		
Aggregated nitrogen	< 1 ppm nitrogen or boron	a	
A centres (N ₂)			A
B centres (N ₄ V)			B
A & B centres			AB
Single nitrogen	Boron	b	

Table 2.2: The type categorisation of diamonds. Illustration based on [29].

istic absorption features in the range of 7000 - 20000 nm ($500-1400\text{ cm}^{-1}$). These features in the IR were later associated with the presence of nitrogen in the lattice [30]. The smaller group was called type II. Diamonds in this group lacked those absorption features and were believed to have a perfect lattice structure [15, 31].

Later subdivisions have been added to the two categories. Type I diamonds were subdivided into type Ia, where nitrogen was present in aggregated form, and type Ib, with single substitutional nitrogen [32]. The majority of natural diamonds are type Ia, only few are found to be type Ib [33] or type II [34]. Type Ia can be further subdivided based on the nature of the nitrogen aggregation. In type IaA diamond, nitrogen is found as N₂ [33], in type IaB it is found as N₄V¹⁸ and in type IaAB both aggregates are present. Larger aggregates of nitrogen are possible, too, but are not included in the type categorization [35, 36]. Type II diamonds were split into type IIa and type IIb [34]. Type IIb diamonds conduct electricity [37], which was later correlated with the presence of boron in the lattice [38, 39]. Many of the most interesting optically active centres in diamond are connected to nitrogen. A summary of those is presented in table 2.3.

¹⁸ Four substitutional nitrogen surrounding a vacancy (B centre)

ZPL Wavelength [nm]	Structure	Name	Colour	Luminescence	Source
393.6	V ⁻	ND1	UV absorption	-	[40]
415.2	N ₃ V ⁰	N3	yellow color	blue	[29, 40]
477.2	unknown	N2	yellow color	blue	[29]
496.2	N ₄ V ₂	H4	yellow	green	[29, 40]
503.2	N ₂ V ⁰	H3	green to yellow	green	[29]
575	NV ⁰	NV0	pink	red	[29, 40]
637	NV ⁻	NV-	pink	red	[29, 40]
740.9 (744.4)	V ⁰	GR1	green or blue	-	[29, 40]
986.3	N ₂ V ⁻	H2	green	-	[29, 40]
Wavenumber [cm ⁻¹]					
2803	B	Boron	blue	red	[40]
1130	N _s	C centre	yellow	-	[40]

Table 2.3: Overview of optical centers in diamond.

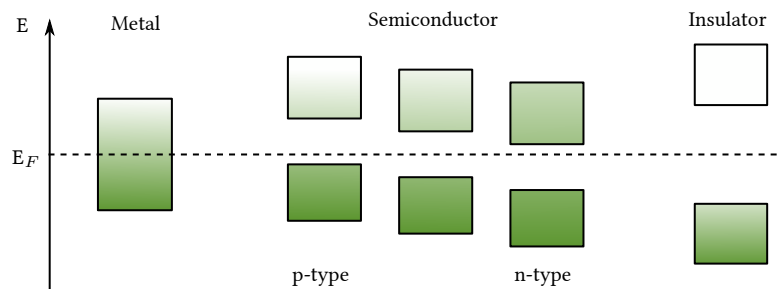
Charged state and transfer between defects

This work will deal with different charged states of the same defect type. In particular N_s in the charged states N_s^+ ¹⁹ and N_s^0 ²⁰, V ²¹ in V^- ²² and V^0 ²³, NV in the charged states NV^- ²⁴ and NV^0 ²⁵ and N_2V in the charged states N_2V^0 ²⁶ and N_2V^- ²⁷. In the same sample, different charged states of the same defect can be found.

A simple visualisation to understand electronic behaviour in a solid is by relation of the Fermi level to the conduction band of the material.

In section 2.1, Structure and material properties of diamond, the band theory of solids was briefly covered. The electron distribution in these bands is determined by the Fermi-Dirac distribution. The energy level, whether hypothetical or real, at which the occupation probability is 50%, is referred to as Fermi level E_F .

In fig. 2.13 the electron distribution in different materials in relation to the Fermi level is illustrated. The electron filling is indicated by the shading. In materials with a bandgap the Fermi level lies within the gap.



¹⁹ Positively charged N_s

²⁰ Neutrally charged N_s

²¹ Lattice vacancy

²² Negative vacancy (ND1)

²³ Neutral vacancy (GR1)

²⁴ The negative form of NV

²⁵ The neutral form of NV

²⁶ The neutrally charged state of N_2V (H3)

²⁷ The negatively charged state of N_2V (H2)

Figure 2.13: Illustration for band-filling in different materials at equilibrium. In a semiconductor or insulator the Fermi level lies inside the band gap Adapted from [41].

Diamond can be considered as a *wide-gap* semiconductor, a material with electronic properties in between semiconductors and insulators [42]. Doping a semiconductor or insulator with impurities with a different number of valence electrons than the base atoms modifies its conductivity.

If the dopant has less valence electrons (p-doping), it removes an electron from the valence band and creates a hole. This kind of dopant is referred to as acceptor. If the dopant has more valence electrons (n-doping), it adds an electron to the conduction band, which can then move as a free electron. This kind of dopant is referred to as donor.

At room temperature the Fermi energy is determined by the energy position of the dominant donor or acceptor in the system. In semiconductors with shallow donors and acceptors the charged states of the defects in the system are determined by the Fermi level [43]. Most of the donor and

acceptor levels in diamond are deep in comparison to conventional semiconductor materials. An impurity is called deep if the energy to remove an electron or hole is much larger than the characteristic thermal energy $k_B T$.

In diamond it is proposed that the charged state of a defect is influenced by the proximity to a donor or acceptor rather than by the Fermi level. This would explain why in one sample the same defect can be found in different charge states [43].

In fig. 2.14 the estimated and measured energy levels of some common defects in diamond within the bandgap are illustrated. Donor and acceptor energy levels are labelled with (0/+) and (-/0) respectively, adapted from [44].

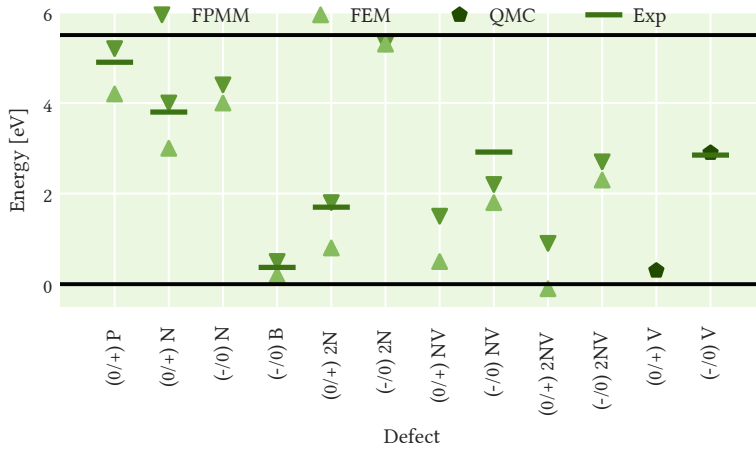


Figure 2.14: Energy levels of defects in the diamond band gap, based on values found in [44, 45, 46, 47, 48, 49]. Values are presented for phosphorus (P), boron (B), and nitrogen (N) - vacancy (V) complexes. Theoretical calculations are based on density functional theory with the first-principles marker method (FPMM) or formation energy method (FEM) and Quantum Monte Carlo (QMC) [44].

The donor level of N_s^0 in diamond lies approximately 1.7 eV below the conduction band [47]. N_s^0 is a major electron donor in diamond and its concentration determines the charged state of many optical defects found in diamond [50]. Boron forms an acceptor in diamond with an ionization energy of 0.37 eV above the valence band [49].

Other defects lie deep within the band gap. N_2 centres behave like very deep donors in diamond with an ionization energy of 4 eV [46]. Vacancies can exist in two charged states; neutral (V^0) and negative (V^-) [51]. The electronic level for V^0 is located at 2.85 eV above the valence band [48]. The energy level for NV^- has been measured at 2.9 eV [44].

The existence of these donor and acceptor states leads to the potential for charge transfer. Charge transfer is the process in which charge is trans-

ferred between defects through electrons in the conduction band or holes in the valence band. Temporary charge transfer can be induced by optical illumination and thermal treatment. This is illustrated for the example of nitrogen in fig. 2.15.

Thermochromic charge transfer occurs when energy levels close to the valence band are thermally populated. We assume a defect X^0 with its ground state energy level close to the valence band. An electron-hole pair is generated, with the electron combining with X^0 , generating a negatively charged state X^- , and the hole in the valence band. The hole can then recombine with an electron donated by N_s^0 , creating N_s^+ . During optical illumination with suitable wavelengths the electron from X^- can be excited into the conduction band and from there recombine with the N_s^+ , creating N_s^0 .

These processes are reversible; optical illumination will reverse changes induced by thermal treatment and vice versa [45]:

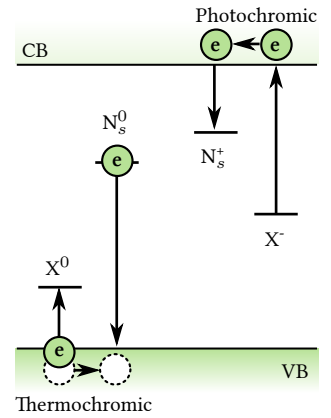
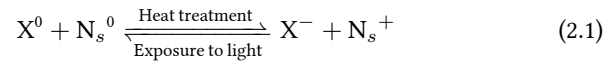


Figure 2.15: Illustration of charge transfer driven by optical illumination and thermal treatment.

2.4 Natural and synthetic diamond

DIAMOND CRYSTALS are divided in natural diamond, formed by geological processes, and synthetic diamond, grown in the laboratory. Both have the same crystal structure, but specific properties of the samples can differ. In natural diamond crystal size, quality and lattice defects are dependent on the growth conditions in nature and hence are statistically dispersed. These parameters can be controlled to some degree in synthetic diamond. Synthetic diamond is of particular interest for industrial applications and research due to its customizability and comparatively low cost.

A wide range of relevant research has been performed on natural diamonds. Partly historically due to a lack of synthetic diamond and partly because certain relevant defects occur in natural diamond and can be studied in such samples. Both natural diamond and synthetic diamond will be briefly introduced in this section.

Growth conditions

Two growth methods for diamond are common, HPHT²⁸ and CVD²⁹ growth. They produce diamonds with different characteristics and shall be referred to as synthetic HPHT and synthetic CVD diamond respectively in this work.

Specific thermodynamic or chemical conditions must be met during diamond growth, since it is metastable at room temperature and pressure. In fig. 2.16 the carbon pressure-temperature diagram is shown and regions where HPHT and CVD synthesis are possible are marked.

While HPHT growth imitates formation conditions of diamond in the earth, at temperatures and pressures above 1200°C and 5 GPa, CVD growth takes advantage of reaction kinetics to work at less extreme conditions, around 800-1000°C and one-tenth of atmospheric pressure [52].

CVD synthesis was first demonstrated in 1952 [54], a few years earlier than HPHT synthesis [55, 56]. Growth rates in early CVD processes were low, while HPHT synthesis could produce diamond on an industrial scale. 30 years later CVD growth rates improved [57] and both synthesis techniques are used on an industrial scale nowadays [1].

There are different kinds of synthetic diamonds, mainly single crystal samples and PCD³⁰. Optical quality PCD, with the same transmission in the IR region above 8 μm as single crystal, is available and has a range of advantages, like being available in large areas suitable for optical windows of CO₂ lasers [58]. Single crystal diamond is the preferred choice for appli-

²⁸ High Pressure High Temperature

²⁹ Chemical Vapour Deposition

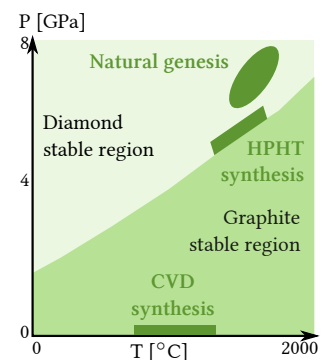


Figure 2.16: The carbon pressure-temperature diagram. Adapted from [1, 53].

³⁰ Polycrystalline Diamond

cations in the UV to NIR, due to lower birefringence and scattering [1].

Natural diamond

Natural diamond forms under pressures above 4 GPa and in a temperature range of 950 - 1400°C [59]. Suitable temperatures and pressures are found at least 150 km deep in the earth's mantle, the area between core and crust [60]. Carbon that originates from carbon containing minerals is the source for diamond growth. Most natural diamonds are between 1 and up to 3.5 billion years old, three quarters the age of the earth [61].

Deep volcanic eruptions transport the diamonds from areas of diamond stable conditions to the earth's surface [59]. While the majority of diamonds are from the crust and upper mantle, samples from greater depths up to at least 700 km have been identified. Mineral inclusions in such ultradeep diamonds allow the study of the composition of the earth's lower mantle [62].

HPHT grown diamond

HPHT growth requires, as the name suggests, high pressures and temperatures. Typical conditions range between 1200 - 1500°C and 5 to 6 GPa [63, 64, 65].

To reach such conditions large presses are required. There are different types of press designs, usually belt, BARS (based on a split-sphere concept), cubic, and toroid presses [66, 67, 68, 69] More detail about cubic presses and the HPHT process in this work can be found in section 3.4, Experimental procedure for thermal treatment.

The growth process is illustrated in fig. 2.17. Synthetic or natural diamond seeds are placed in a capsule along with a metal solvent-catalyst (a group VIII element such as iron or its alloys) and a carbon source. A temperature gradient is produced so that the carbon source is located at a higher temperature than the seed. In this way the source material dissolves, while the seed remains stable. The solvent then transports the carbon from the carbon source to the diamond seed [71]. There the solvent-carbon mixture cools down and carbon becomes supersaturated in the solvent. It then crystallizes on the diamond seed and the diamond grows [72]. Additionally, the solvent acts as a catalyst, lowering the temperature for diamond growth [73].

Most HPHT grown diamonds are yellow due to a nitrogen concentration of hundreds of ppm³¹ [74]. Nitrogen can originate from the solvent, the carbon source or gas in pores and spaces of the HPHT capsule [75].

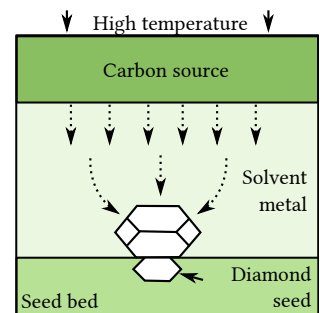


Figure 2.17: Schematic of HPHT diamond growth. Adapted from [70].

³¹ parts per million
($1.77 \cdot 10^{17} \text{ cm}^{-3}$ for diamond)

To reduce the nitrogen concentration in HPHT grown stones it is necessary to introduce a nitrogen getter. A nitrogen getter is a material with a strong affinity for nitrogen, that can be used in the solvent to bind the nitrogen and reduce its concentration in the growing diamond [66]

The specific combination of dopants, getters and surrounding material can yield a variety of coloured stones. Aluminium, titanium and zirconium produce clear stones, while adding boron leads to blue coloration [76]. These materials get incorporated in the diamond lattice, which can be a drawback if a perfect diamond lattice without defects is desired. To reduce the amount of impurities the growth rate can be reduced by adjusting the temperature of the process [72]. Approaching gigagrams of diamond are produced by the HPHT growth method each year. Most of it for industrial applications [77].

CVD grown diamond

Unlike HPHT growth, CVD growth is very different from the natural diamond growth process. The process is illustrated in fig. 2.18.

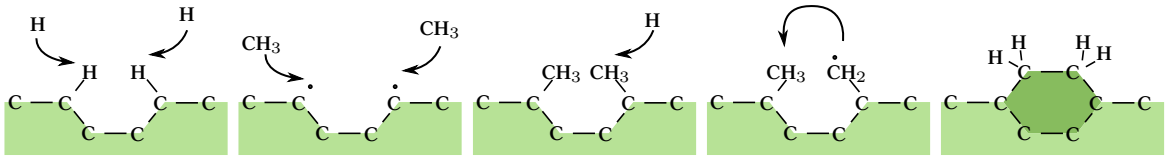


Figure 2.18: Schematic of the Standard Growth Model for CVD diamond. Adapted from [78].

A substrate is placed in a chamber and varying gases are energized to provide the conditions for diamond growth. The gases include a source of carbon and hydrogen, typically a mix of hydrocarbons like methane (CH_4) and hydrogen. A synthetic or natural diamond seed is placed in the gas chamber. The gases are then broken up into hydrocarbon and hydrogen radicals. To do this different energy sources can be used. The most important methods are hot filament and microwave assisted CVD growth [77].

Hydrogen is used to prevent graphite growth by attaching to any non-diamond bonded (sp^2) carbon and remove it from the crystal surface. If it attaches to another hydrogen that terminates the diamond surface, H_2 is formed and a dangling bond is left behind. The high H fraction ensures the etching of sp^2 bonded carbon dominates the growth of sp^3 bonded carbon. CH_3 can then attach and form an sp^3 bond. In this way, even though it is not a thermodynamically favoured process, diamond can grow slowly, atomic layer by layer, in a kinetic process [78, 79]. The growth of single crystal CVD diamond requires a single crystal substrate [80].

As with HPHT samples, nitrogen can be incorporated into the lattice dur-

ing growth as single substitutional nitrogen. While HPHT grown diamond typically contains more than 200 ppm of nitrogen, CVD grown diamond doesn't contain more than 50 ppm [81]. Nitrogen can be mixed into the gas as either N_2 or NH_3 [82]. It has been shown to act as a catalyst for the growth, significantly increasing growth rates even when added in small concentrations [83].

Adding boron to the gas results in blue diamonds. Other colors can be created with different mixtures of gases [77]. CVD grown diamond often contains silicon that originates from silica windows used as part of the growth chambers or from the silicon substrate used to grow the diamond on [84].

2.5 Summary

DIAMOND IS OF GREAT INTEREST as a material due to its outstanding thermo-optical properties, its hardness, rigidity and chemical and biological inertness. Those properties result from the strong covalent sp^3 bonding and large carbon binding energy. The high thermal conductivity, rigidity and the wide spectral transmission range make it particularly interesting for applications in laser engineering. The compact crystal lattice makes doping with laser-ions difficult, hence an alternative route to direct light generation within the crystal is desirable.

One such alternative could be the utilization of luminescent defects in diamond. These defects often have broadened spectra due to their interaction with lattice phonons. Among these, two nitrogen based colour centres are of particular interest for us due to previous research and a positive outlook on their suitability in literature. These are NV and N_2V^0 .

Diamond samples can be obtained both by mining of natural diamond or growth of synthetic diamond. Synthetic diamond is cost efficient and its size and optical quality can be controlled to some degree, as opposed to natural diamond, which first has to be found with the desired characteristics. For this research different single nitrogen concentrations were of interest, leading to experiments on both HPHT (high nitrogen samples >100 ppm) and CVD (low nitrogen samples <5 ppm) grown diamond samples. Samples with a low overall nitrogen concentration were desired for colour centre synthesis, to prevent parasitic absorption and concentration quenching of leftover nitrogen or a high density of colour centre. Because of the low nitrogen aggregation efficiency in CVD diamond [81], discussed in detail in the next chapter, natural samples, containing nitrogen clusters, were used to synthesise N_2V^0 in ppm concentrations.

In the next part, chapter 3, Synthesis of colour centres in diamond, methods to generate NV and N_2V^0 in synthetic and natural diamond will be described. Later on, in chapter 6, Progress towards a laser based on colour centres in diamond, the utilization of those centres for laser engineering will be discussed.

References

- [1] R. P. Mildren and J. R. Rabeau. *Optical Engineering of Diamond*. Ed. by R. P. Mildren and J. R. Rabeau. Weinheim, Germany: Wiley-VCH, Apr. 2013. ISBN: 352741102X. DOI: 10.1002/9783527648603.
- [2] G. Huber, C. Kränkel, and K. Petermann. "Solid-state lasers : status and future". EN. In: *Josa B* 27.11 (Oct. 2010), pp. 93–105. ISSN: 0740-3224. DOI: 10.1364/JOSAB.27.000B93.
- [3] M. Ströck. *Eight Allotropes of Carbon*. 2006. URL: https://en.wikipedia.org/wiki/Allotropes_of_carbon#/media/File:Eight_Allotropes_of_Carbon.png.
- [4] H. Briehl. *Chemie der Werkstoffe*. Vol. 53. 9. B.G. Teubner Verlag / GWV Fachverlage GmbH, Wiesbaden, 2014, pp. 10–10. ISBN: 978-3-658-06224-8. DOI: 10.1007/978-3-658-06225-5.
- [5] Sven. *sp3-Orbital*. URL: <https://de.wikipedia.org/wiki/Datei:Sp3-Orbital.png>.
- [6] C. Kittel. *Introduction to Solid State Physics*. Wiley, 2005. ISBN: 978-0-471-41526-8.
- [7] W. Kleber, H.-J. Bautsch, and J. Bohm. *Einführung in die Kristallographie*. De Gruyter, 2002, p. 420. ISBN: 9783486598858.
- [8] R. J. Narayan, R. D. Boehm, and A. V. Sumant. "Medical applications of diamond particles & surfaces". In: *Materials Today*. Vol. 14. 4. 2011, pp. 154–163. DOI: 10.1016/S1369-7021(11)70087-6.
- [9] A. Vinke, G. Marbach, and J. Vinke. *Chemie für Ingenieure*. ISBN: 9783486780963.
- [10] Chetvorno. *Solid state electronic band structure*. URL: https://commons.wikimedia.org/wiki/File:3ASolid_state_electronic_band_structure.svg.
- [11] S. Hadlington. "Hot rocks (single crystal diamond for power semiconductor devices)". In: *IEE Review* 51.4 (Apr. 2005), p. 30. ISSN: 09535683. DOI: 10.1049/ir:20050402.
- [12] C. Klein. *Minerals and Rocks: Exercises in crystal and mineral chemistry, crystallography, x-ray diffraction, and ore mineralogy*. Wiley, 2008. ISBN: 0471772771.
- [13] H. Vogel. *Gerthsen Physik*. Springer Berlin Heidelberg, 1995. ISBN: 978-3-662-07466-4. DOI: 10.1007/978-3-662-07466-4.
- [14] J. Solé, L. Bausá, and D. Jaque. *An Introduction to the Optical Spectroscopy of Inorganic Solids*. 2005. DOI: 10.1002/0470016043.
- [15] R. Robertson, J. J. Fox, and A. E. Martin. "Two Types of Diamond". In: *Philosophical Transactions of the Royal Society A: Mathematical, Physical and Engineering Sciences* 232.707-720 (1934), pp. 463–535. ISSN: 1364-503X. DOI: 10.1098/rsta.1934.0013.
- [16] M. Lax and E. Burstein. "Infrared lattice absorption in ionic and homopolar crystals". In: *Physical Review* 97.1 (Jan. 1955), pp. 39–52. ISSN: 0031899X. DOI: 10.1103/PhysRev.97.39.
- [17] C. D. Clark and S. T. Davey. "One-phonon infrared absorption in diamond". In: *Journal of Physics C: Solid State Physics* 17.6 (Feb. 2000), pp. 1127–1140. ISSN: 0022-3719. DOI: 10.1088/0022-3719/17/6/020.
- [18] *Optische Eigenschaften von CVD-Diamant*. URL: http://www.diamond-materials.com/DE/cvd_diamond/optical_properties.htm.
- [19] J. F. H. Custers and F. A. Raal. "Fundamental Absorption Edge of Diamond". In: *Nature* 179.4553 (Feb. 1957), pp. 268–269. ISSN: 0028-0836. DOI: 10.1038/179268a0.
- [20] A. M. Zaitsev. *Optical Properties of Diamond : A Data Handbook*. Springer, 2001, p. 502. ISBN: 354066582X. DOI: 10.1007/978-3-662-04548-0.
- [21] D. Howell. "Strain-induced birefringence in natural diamond: a review". In: *European Journal of Mineralogy* 24.4 (2012), pp. 575–585. DOI: 10.1127/0935-1221/2012/0024-2205.
- [22] W. de Boer et al. "Radiation hardness of diamond and silicon sensors compared". In: (May 2007). DOI: 10.1002/pssa.200776327. arXiv: 0705.0171.
- [23] R. S. Balmer et al. "Chemical vapour deposition synthetic diamond: materials, technology and applications". In: *Journal of Physics: Condensed Matter* 21.36 (Sept. 2009), p. 364221. ISSN: 1361-648X. DOI: 10.1088/0953-8984/21/36/364221.
- [24] M. Červ. "The ATLAS Diamond Beam Monitor". In: *Journal of Instrumentation* 9.02 (Feb. 2014). ISSN: 1748-0221. DOI: 10.1088/1748-0221/9/02/C02026.
- [25] J. Walker. "Optical absorption and luminescence in diamond". In: *Reports on Progress in Physics* 42.10 (1979), p. 1605. DOI: 10.1088/0034-4885/42/10/001.
- [26] M. Fox. *Optical properties of solids*. 2010. ISBN: 0199573360.
- [27] M. Born and R. Oppenheimer. "Zur Quantentheorie der Molekeln". In: *Annalen der Physik* 389.20 (1927), pp. 457–484. ISSN: 15213889. DOI: 10.1002/andp.19273892002.
- [28] S. Pezzagna et al. "Creation and nature of optical centres in diamond for single-photon emission-overview and critical remarks". In: *New Journal of Physics* 13.3 (Mar. 2011), p. 035024. ISSN: 13672630. DOI: 10.1088/1367-2630/13/3/035024.
- [29] C. M. Breeding and J. E. Shigley. "The type classification system of diamonds and its importance in geology". In: *Gems and Gemology* 45.2 (2009), pp. 96–111. URL: [http://northarrowminerals.com/_resources/The-%20Type%20Classification-System-of-Diamonds%20\(4\).pdf](http://northarrowminerals.com/_resources/The-%20Type%20Classification-System-of-Diamonds%20(4).pdf).
- [30] W. Kaiser and W. L. Bond. "Nitrogen, a major impurity in common type I diamond". In: *Physical Review* 115.4 (Aug. 1959), pp. 857–863. ISSN: 0031899X. DOI: 10.1103/PhysRev.115.857.
- [31] R. Robertson, J. J. Fox, and A. E. Martin. "Further Work on Two Types of Diamond". In: *Proceedings of the Royal Society of London A: Mathematical, Physical and Engineering Sciences* 157.892 (1936). DOI: 10.1098/rspa.1936.0217.

- [32] H. B. Dyer et al. "Optical absorption features associated with paramagnetic nitrogen in diamond". In: *Philosophical Magazine* 11.112 (Apr. 1965), pp. 763–774. ISSN: 0031-8086. DOI: 10.1080/14786436508230081.
- [33] G. Davies. "The A nitrogen aggregate in diamond-its symmetry and possible structure". In: *Journal of Physics C: Solid State Physics* 9.19 (Oct. 1976), p. L537. ISSN: 0022-3719. DOI: 10.1088/0022-3719/9/19/005.
- [34] J. F. H. Custers. "Unusual phosphorescence of a diamond". In: *Physica* 18.8 (Aug. 1952), pp. 489–493. ISSN: 0031-8914. DOI: 10.1016/S0031-8914(52)80049-7.
- [35] A. T. Collins and G. S. Woods. "An anomaly in the infrared absorption spectrum of synthetic diamond". In: *Philosophical Magazine Part B* 46.1 (July 1982), pp. 77–83. ISSN: 1364-2812. DOI: 10.1080/13642818208246424.
- [36] A. T. Collins. "The colour of diamond and how it may be changed". In: *Journal of Gemmology* 27.6 (2001), pp. 341–359. URL: https://gem-a.com/images/Documents/JoG/Archive/JoG2001_27_6.pdf#page=23.
- [37] J. F. H. Custers. "Semiconductivity of a Type IIb Diamond". In: *Nature* 176.4473 (July 1955), pp. 173–174. ISSN: 0028-0836. DOI: 10.1038/176173a0.
- [38] R. H. Wentorf and H. P. Bovenkerk. "Preparation of Semiconducting Diamonds". In: *The Journal of Chemical Physics* 36.8 (Apr. 1962), p. 1987. ISSN: 00219606. DOI: 10.1063/1.1732815.
- [39] R. M. Chrenko. "Boron, the dominant acceptor in semiconducting diamond". In: *Physical Review B* 7.10 (May 1973), pp. 4560–4567. ISSN: 01631829. DOI: 10.1103/PhysRevB.7.4560.
- [40] J. E. Shigley and C. M. Breeding. "Optical Defects in Diamond: A Quick Reference Chart". In: *Gems & Gemology* 49.2 (2013), pp. 5–6. URL: <https://www.gia.edu/gems-gemology/summer-2013-shigley-optical-defects-diamond>.
- [41] Nanite. *Band filling diagram*. URL: https://en.wikipedia.org/wiki/File:Band_filling_diagram.svg.
- [42] M. A. Prelas et al. *Wide Band Gap Electronic Materials*. Vol. 1. Springer Science & Business Media, 1995. ISBN: 9789401040785. DOI: 10.1007/978-94-011-0173-8.
- [43] A. T. Collins. "The Fermi level in diamond". In: *Journal of Physics: Condensed Matter* 14.14 (2002), p. 3743. DOI: 10.1088/0953-8984/14/14/307.
- [44] J. P. Goss et al. "Donor and acceptor states in diamond". In: *Diamond and Related Materials* 13.4 (2004), pp. 684–690. DOI: 10.1016/j.diamond.2003.08.028.
- [45] R. U. A. Khan et al. "Charge transfer effects, thermo and photochromism in single crystal CVD synthetic diamond". In: *Journal of Physics: Condensed Matter* 21.36 (Sept. 2009), p. 364214. ISSN: 1361-648X. DOI: 10.1088/0953-8984/21/36/364214.
- [46] P. Denham, E. C. Lightowers, and P. J. Dean. "Ultraviolet intrinsic and extrinsic photoconductivity of natural diamond". In: *Physical Review* 161.3 (1967), p. 762. DOI: 10.1103/PhysRev.161.762.
- [47] R. G. Farrer. "On the substitutional nitrogen donor in diamond". In: *Solid State Communications* 7.9 (1969), pp. 685–688. DOI: 10.1016/0038-1098(69)90593-6.
- [48] S. Dannefaer, A. Pu, and D. Kerr. "Positron annihilation study of vacancies in type IIa diamonds illuminated with monochromatic light". In: *Diamond and related materials* 10.12 (2001), pp. 2113–2117. DOI: 10.1016/S0925-9635(01)00489-7.
- [49] A. T. Collins and A. W. S. Williams. "The nature of the acceptor centre in semiconducting diamond". In: *Journal of Physics C: Solid State Physics* 4.13 (1971), p. 1789. DOI: 10.1088/0022-3719/4/13/030.
- [50] T. Gaebel et al. "Photochromism in single nitrogen-vacancy defect in diamond". In: *Applied Physics B: Lasers and Optics* 82.2 SPEC. ISS. (2006), pp. 243–246. ISSN: 09462171. DOI: 10.1007/s00340-005-2056-2.
- [51] S. C. Lawson et al. "On the existence of positively charged single-substitutional nitrogen in diamond". In: *Journal of Physics: Condensed Matter* 10.27 (July 1998), pp. 6171–6180. ISSN: 0953-8984. DOI: 10.1088/0953-8984/10/27/016.
- [52] P. M. Martineau et al. "Identification of synthetic diamond grown using chemical vapor deposition (CVD)". In: *Gems & Gemology* 40.1 (2004), pp. 2–25.
- [53] F. P. Bundy. "Pressure-temperature phase diagram of elemental carbon". In: *Physica A: Statistical Mechanics and its Applications* 156.1 (Mar. 1989), pp. 169–178. ISSN: 03784371. DOI: 10.1016/0378-4371(89)90115-5.
- [54] A. D. Kiffer. "Synthesis of diamond from carbon monoxide". In: *Report from the Tonawanda Laboratories, Linde Air Products Co, Tonawanda NY* 6 (1956).
- [55] F. Bundy et al. "Man-Made Diamonds". In: *Nature* 176.4471 (1955), pp. 51–55. ISSN: 0028-0836. DOI: 10.1038/176051a0.
- [56] E. Hoffmann and H. Schiff-Shenhav. "Some observations on the synthesis of phthaloylamino acids." In: *Journal of Organic Chemistry* 27 (1962), pp. 4686–4688. ISSN: 0022-3263. DOI: 10.1021/jo01059a531.
- [57] S. Matsumoto et al. "Growth of diamond particles from methane-hydrogen gas". In: *Journal of Materials Science* 17.11 (Nov. 1982), pp. 3106–3112. ISSN: 00222461. DOI: 10.1007/BF01203472.
- [58] *Enable extreme performance photonics*. URL: https://e6cvd.com/media/catalog/category/Element_Six_Optical.pdf.
- [59] T. Stachel and J. W. Harris. "Formation of diamond in the Earth's mantle." In: *Journal of physics. Condensed matter: an Institute of Physics journal* 21.36 (Sept. 2009), p. 364206. ISSN: 0953-8984. DOI: 10.1088/0953-8984/21/36/364206.
- [60] F. R. Boyd and J. J. Gurney. "Diamonds and the african lithosphere." In: *Science (New York, N.Y.)* 232.2 (1986), pp. 472–477. ISSN: 0036-8075. DOI: 10.1126/science.232.4749.472.
- [61] D. Pay, J. Shigley, and P. Padua. *Tiny Inclusions Reveal Diamond Age and Earth's History: Research at the Carnegie Institution*. 2014. URL: <https://www.gia.edu/>

- gia-news-research-tiny-inclusions-reveal-diamond-age (visited on 04/26/2017).
- [62] T. Stachel, G. P. Brey, and J. W. Harris. "Inclusions in sublithospheric diamonds: Glimpses of deep Earth". In: *Elements* 1.2 (2005), pp. 73–78. ISSN: 1811-5209. DOI: 10.2113/gselements.1.2.73.
- [63] S. Ferro. "Synthesis of diamond". In: *Journal of Materials Chemistry* 12.10 (2002), pp. 2843–2855. ISSN: 09599428. DOI: 10.1039/b204143j.
- [64] R. A. Spits and C. Dodge. *High pressure high temperature (HPHT) method for the production of single crystal diamonds*. 2010. URL: <https://www.google.com/patents/W02010082029A1?cl=en>.
- [65] D. Borse et al. *Process for manufacturing synthetic single crystal diamond material*. 2013. URL: <https://www.google.com/patents/W02013135785A1?cl=en>.
- [66] H. M. Strong and R. M. Chrenko. "Diamond growth rates and physical properties of laboratory-made diamond". In: *The Journal of Physical Chemistry* 75.12 (1971), pp. 1838–1843. ISSN: 0022-3654. DOI: 10.1021/j100681a014.
- [67] F. P. Bundy, H. M. Strong, and R. H. Wentorf. "Methods and mechanisms of synthetic diamond growth". In: *Chem. Phys. Carbon* 10 (1973), pp. 213–272.
- [68] J. E. Shigley et al. "The gemological properties of the Sumitomo gem-quality synthetic yellow diamonds". In: *Gems & Gemology* 22.4 (1986), pp. 192–208. ISSN: 0016-626X. DOI: 10.5741/GEMS.22.4.192.
- [69] J. E. Shigley, C. M. Breeding, and A. H.-T. Shen. "An Updated Chart on the Characteristics of HPHT-Grown Synthetic Diamonds". In: *Gems & Gemology* 40.4 (2004), pp. 303–313. URL: <http://www.gia.edu/UK-EN/gems-gemology/winter-2004-characteristics-hpht-grown-synthetic-diamonds-shigley>.
- [70] C. Y. Zang, M. Li, and L. J. Chen. "Growth and characterization of large, high quality cubic diamond crystals". In: *Chinese Science Bulletin* 57.14 (May 2012), pp. 1733–1738. ISSN: 10016538. DOI: 10.1007/s11434-012-5023-4.
- [71] J. E. Field. *The Properties of Natural and Synthetic Diamond*. Academic Press, 1992. ISBN: 9780122553523.
- [72] U. F. D'Haenens-Johansson et al. "Near-Colorless HPHT Synthetic Diamonds from AOTC Group". In: *Gems & Gemology* 50.1 (2014), pp. 1–19. ISSN: 0016626X. DOI: 10.5741/GEMS.50.1.30.
- [73] F. P. Bundy et al. "The pressure-temperature phase and transformation diagram for carbon; updated through 1994". In: *Carbon* 34.2 (1996), pp. 141–153. ISSN: 00086223. DOI: 10.1016/0008-6223(96)00170-4.
- [74] A. T. Collins and S. C. Lawson. "Spectroscopic studies of a thermochromic centre in synthetic diamonds grown by the temperature-gradient method". In: *Philos. Mag. Lett.* 60.3 (1989), pp. 117–122. ISSN: 0950-0839. DOI: 10.1080/09500838908206445.
- [75] R. Burns et al. "Growth of high purity large synthetic diamond crystals". In: *Diamond and Related Materials* 8.8-9 (1999), pp. 1433–1437. ISSN: 09259635. DOI: 10.1016/S0925-9635(99)00042-4.
- [76] H. Strong. *Manufacture of diamond products*. 1978. URL: <https://www.google.ch/patents/US4082185>.
- [77] I. D. Technologies. *CVD-Grown Synthetic Diamonds*. 2013. URL: <https://www.gia.edu/news-research-CVD-grown-part1> (visited on 05/01/2017).
- [78] *CVD Diamond Group - School of Chemistry - Bristol University*. 2007. URL: <http://www.chm.bris.ac.uk/pt/diamond/othergps.htm> (visited on 05/01/2017).
- [79] J. C. Angus, H. A. Will, and W. S. Stanko. "Growth of diamond seed crystal by vapor deposition". In: *Journal of Applied Physics* 39.6 (1968), pp. 2915–2922.
- [80] *The Element Six CVD Diamond Handbook*. Tech. rep. 2015. URL: https://e6cvd.com/media/wysiwyg/pdf/E6_CVD_Diamond_Handbook.pdf.
- [81] K. Iakoubovskii, G. Adriaenssens, and Y. Vohra. "Nitrogen incorporation in CVD diamond". In: *Diamond and Related Materials* 10.3-7 (Mar. 2001), pp. 485–489. ISSN: 0925-9635. DOI: 10.1016/S0925-9635(00)00436-2.
- [82] M. Werner and R. Locher. "Growth and application of undoped and doped diamond films". In: *Reports on Progress in Physics* 61.12 (1998), pp. 1665–1710. ISSN: 0034-4885. DOI: 10.1088/0034-4885/61/12/002.
- [83] Q. Liang et al. "Recent advances in high-growth rate single-crystal CVD diamond". In: *Diamond and Related Materials* 18.5-8 (2009), pp. 698–703. ISSN: 09259635. DOI: 10.1016/j.diamond.2008.12.002.
- [84] J. Barjon et al. "Silicon incorporation in CVD diamond layers". In: *Physica Status Solidi (A) Applications and Materials Science* 202.11 (2005), pp. 2177–2181. ISSN: 18626300. DOI: 10.1002/pssa.200561920.

3

Synthesis of colour centres in diamond

Contents

3.1	Irradiation	38
	Overview of radiation types	38
	Energy transfer	39
3.2	Experimental procedure for electron irradiation	41
3.3	Diffusion, aggregation and dissociation of defects	45
	Thermal stability of diamond	45
	Activation energies	46
	Diffusion and aggregation rate constants	51
	Annealing	54
	HPHT treatment	56
3.4	Experimental procedure for thermal treatment	59
	Thermal treatment at atmospheric pressure or in a vacuum	59
	Thermal treatment at high temperatures and pressures	59
3.5	Summary	63
	References	64

3.1 Irradiation

THE GENERATION OF VACANCIES by irradiation will be explained in this chapter. This is a necessary step in the synthesis of nitrogen-vacancy defects when starting with as-grown, single nitrogen containing diamond.

Irradiation refers to the exposure of an object to radiation. The first laboratory experiments to change the colour of diamond using radiation were performed in 1904. Colourless diamonds turned blueish-green after they were embedded in radium bromide for 12 months [1]. In the following decades experiments were performed with different types of radiation: Cyclotron radiation using alpha particles, deuterons and protons, electrons from line accelerators, neutrons and gamma rays [2].

Overview of radiation types

A particle can create a vacancy in the diamond lattice if enough energy is transferred to displace a carbon atom. Experiments show the displacement energy for carbon in the diamond lattice is ~ 40 eV [3].

The aim in this work is the generation of a few ppm¹ of evenly distributed single vacancies in samples of several mm thickness. The sample thickness is determined by the availability of suitable samples for purchase. From this the estimation for the colour centre² concentration has been made based on literature values for the respective centres. This will be discussed in detail in section 6.2, Key parameters for solid state lasers, and section 6.5, A potential diamond colour centre laser.

Mass and charge are important parameters for the choice of irradiation particle. Particles with a mass similar to that of carbon can transfer a larger part of their energy to the carbon atoms (which is discussed in detail in section 3.1). A comparison of the mass for particles commonly used for irradiation can be found in table 3.1

Charged particles, like protons and alpha particles, lose a lot of their energy through ionization and Rutherford scattering. The main difference is the even shorter penetration depth of alpha particles, because of the greater mass and charge. Although neutrons and protons have the same mass, the neutron mainly interacts with the material through collisions with the atoms and therefore has a longer penetration depth.

Gamma radiation displaces carbon atoms indirectly: Electrons produced by Compton scattering and pair production displace the carbon atoms [6]. Gamma rays around 1 MeV can colour a diamond evenly, but the process is slow and treatment takes several months [7]. From the variety of different irradiation types, gamma irradiation is the least common and won't be considered further.

¹ parts per million ($1.77 \cdot 10^{17} \text{ cm}^{-3}$ for diamond)

² A type of structural defect, which produces absorption and emission bands that are different to those of the pure crystal [4]

Particle	Mass [u]
Carbon	12
Neutron	1
Proton	1
Alpha	4
Electron	$5.5 \cdot 10^{-4}$

Table 3.1: Comparison of the masses of carbon and particles used for irradiation in atomic mass unit[5].

A comparison of the number of vacancies generated by 1 MeV particles of the respective radiation type is given in table 3.2. A penetration depth of the order of mm is possible with electrons and neutrons, but not with heavy ions, which only penetrate of the order of a few μm [8]. Hence the specification of vacancy numbers per cm in table 3.2 for electrons and neutrons. 1 MeV neutrons generate 68 vacancies per cm per particle. In contrast, protons and alpha particles both stop within the diamond and generate 8 and 51 vacancies respectively, per particle. Electrons generate 1.5 vacancies per cm per particle.

Irradiation using neutrons or high-energy electrons is most common [2]. They allow for a deep penetration depth in comparison to alpha particles and protons, and the generation of single vacancies without complex damage in the case of electrons.

Neutrons can transfer enough energy so that the displaced carbon atom can displace further atoms in the lattice, causing a cascade of damage. In that way complex damage can be generated, rather than single vacancies. Many of the absorption features in the complex spectrum after neutron irradiation have not yet been interpreted [9].

In contrast, the kinetic energy transferred by an electron to a carbon atom is so small that the carbon atom won't cause any further displacements [8]. Complex damage has been linked to an increase of the refractive index, dependent on the induced damage density, and increased absorption in the visible wavelength range [10]. An even distribution of single vacancies in the diamond lattice without the generation of complex damage is best done by electron irradiation. This approach was chosen for the work described in this thesis.

Energy transfer

For most relevant irradiation methods a simple model for the interaction of two particles can be considered: the elastic collision of two hard spheres. The de Broglie wavelength ($\lambda_B = h/p$) of electrons reduces with increasing momentum p . At energies above a few hundred eV electrons will interact only with single atoms and the electron-solid interactions can be described by atomic models [11]. Below that, for example for electrons used in cathodoluminescence, electrons interact with the material through inelastic scattering and ultimately the process can lead to the excitation of valence electrons into the conduction band.

Figure 3.1 shows the collision of a mass m , with kinetic energy E and velocity $v_{m,0}$, with a resting mass M . After the collision M moves with kinetic energy T and velocity v_M in a direction at θ with regard to the incoming direction of m . The particle m now has a reduced kinetic energy ($E - T$) and scatters with velocity $v_{m,1}$ at angle ϕ to its original direction.

Particle with 1 MeV	Vacancies per particle
Neutron	68 (cm^{-1})
Proton	7.9
Alpha	51
Electron	1.5 (cm^{-1})

Table 3.2: Comparison of the number of vacancies created by radiation with an energy of 1 MeV[8].

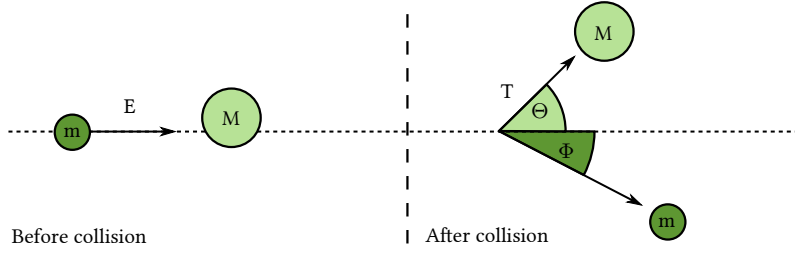


Figure 3.1: Illustration of the elastic scattering of two particles. A particle of mass m and kinetic energy E collides with a stationary particle of mass M . After the collision M is scattered at angle θ and now has a kinetic energy of T . Mass m is scattered at angle ϕ .

The conservation of total energy and momentum leads to the equation for the transferred energy [12]:

$$T = \frac{4mM}{(m + M)^2} \cos^2(\theta) \cdot E \quad (3.1)$$

The electron mass is much smaller than that of a carbon atom (table 3.1); Relativistic effects have to be considered for the energy transfer using electrons at energies above a hundred keV [13].

The maximum energy transferred by an electron is [3]:

$$T_{max} = 2 \frac{m_0}{M} E \left(2 + \frac{E}{m_0 c^2} \right) \quad (3.2)$$

Figure 3.2 shows the maximum energy transfer to carbon atoms by electrons and neutrons depending on their kinetic energy. The displacement energy of a carbon atom in diamond is ~ 40 eV [3]. Neutrons require energies above 100 eV and electrons above 180 keV to displace a carbon atom [3, 14].

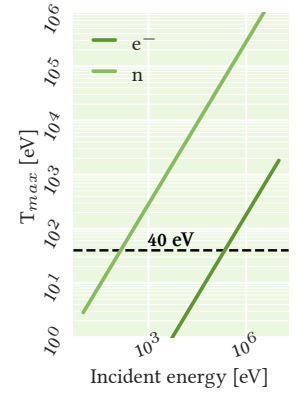


Figure 3.2: Maximum energy transfer in elastic scattering from neutrons (eq. (3.1)) and electrons (eq. (3.2)) to carbon atoms.

3.2 Experimental procedure for electron irradiation

ELECTRON IRRADIATION was performed in collaboration with the University of Mainz, Germany, and at Synergy Health Ltd., Swindon, UK.

Irradiation at the University of Mainz was performed at the MAMI³. It is a microtron that provides a continuous wave, high intensity, polarized electron beam with an energy up to 1.6 GeV. A 14 MeV stage with an unpolarized 50 μ A electron beam, able to homogeneously irradiate an area of 1 cm², was used for the irradiation. Diamond samples were wrapped in aluminium foil and placed into a metal holder, which was connected to water-cooling.

In the early stages of this project the boundaries for a suitable starting concentration of single nitrogen were not well understood. Experiments using diamonds with high nitrogen concentrations (\sim 100 ppm) were important to determine their usefulness in this project. In an attempt to produce as many NV⁴ centres as possible, the setup and procedure in Mainz were used to match the concentration of nitrogen in those samples with vacancies. It was discovered that for the parameters described here complex damage was incurred in the diamond and the background absorption in the visible spectral region made those samples unsuitable for laser purposes. As a result following work concentrated on samples with lower nitrogen concentration in the range of a few to a few tens of ppm. The setup is shown in fig. 3.3.

³ MAinzer Mikrotron

⁴ A substitutional nitrogen adjacent to a vacancy with a C_{3v} symmetry

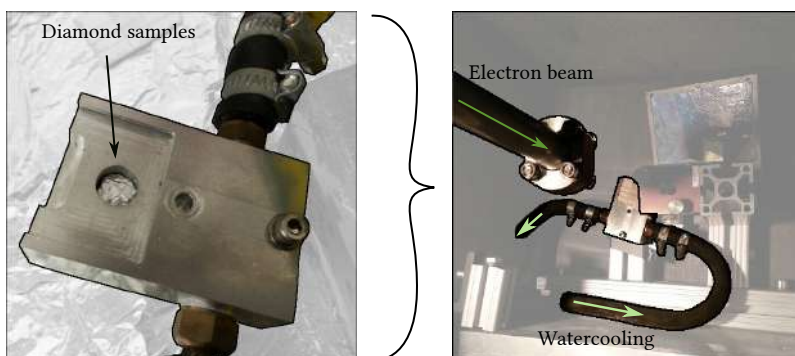


Figure 3.3: Experimental setup at the University of Mainz.

Left: Diamond samples wrapped in aluminium foil inside metal holder with water-cooling connections.

Right: Sample holder in the experimental setup with the output for the electron beam.

Irradiation at Synergy Health, Swindon, was performed with an 4.5 MeV and 20 mA electron beam. Figure 3.4 shows the experimental setup of the electron source and the placement of diamond samples on the metal table below. The diamonds were placed directly on the metal bench, with thermal paste applied to the bench beforehand, in accordance with previous experimental setups performed by scientists at the University of Warwick.

This is probably redundant according to Synergy Health staff, as the paste turns to powder within seconds of irradiation and thermal contact isn't provided any longer. According to Synergy Health staff no difference was detected by Element Six after irradiation without thermal paste or other means of cooling when using the irradiation parameters mentioned above.

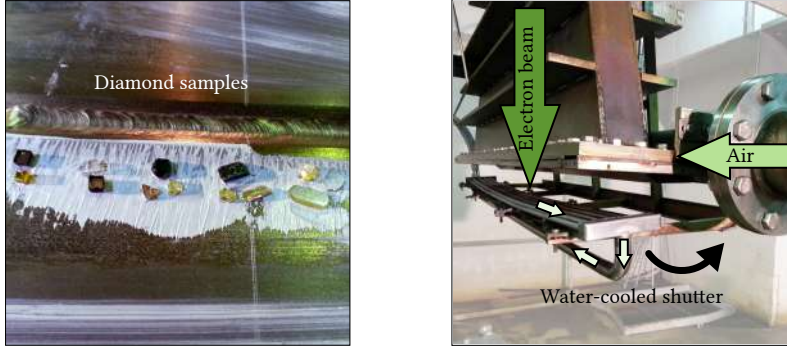


Figure 3.4: Experimental setup at Synergy Health.

Left: Diamond samples placed on a metal bench covered with a layer of thermal paste. The bench is placed below the electron beam exit.

Right: Electron beam exits through air cooled foil. The shutter for the beam is water-cooled and can be hinged aside.

The total number of vacancies per volume $N_v(t, E)$ after an irradiation time t can be calculated if the total electron dose, $d(t)$, and the number of vacancies created per electron and cm at a given incident energy E , $L(E)$, are known.

The total electron dose $d(t)$ is the total number of electrons per area after the irradiation time t :

$$d(t) = \frac{I}{A_b} \cdot t \quad (3.3)$$

I is the number of electrons per second that the electron source produces and A_b is the beam area.

The number of vacancies per unit volume $N_v(t, E)$ can then be calculated with:

$$N_v(t, E) = d(t) \cdot L(E) \quad (3.4)$$

Monte Carlo simulations are used to calculate the number of vacancies per electron and cm and the penetration depth, for different incident energies [6]. These are shown in fig. 3.5. Experimental results with electron energies between 1 - 2 MeV have shown to produce isolated vacancies and interstitials with a penetration depth of about 1 mm [15].

Electron incident energies available are $E_{Syn} = 4.5 \text{ MeV}$ and $E_{MAMI} = 14 \text{ MeV}$. The number of vacancies created per electron and cm for these incident energies are: $L(4.5 \text{ MeV})$ ranges from $2.2 \text{ v}/(e \cdot \text{cm})^5$ up to $2.85 \text{ v}/(e \cdot \text{cm})$ [6]. Based on the highest electron energy calculated in [6], at the MAMI we assume $L(14 \text{ MeV}) \sim 3.5 \text{ v}/(e \cdot \text{cm})$.

⁵ Based on calculations by Andrew Edmonds, Element Six, 09.10.2014 for irradiation at Synergy Health

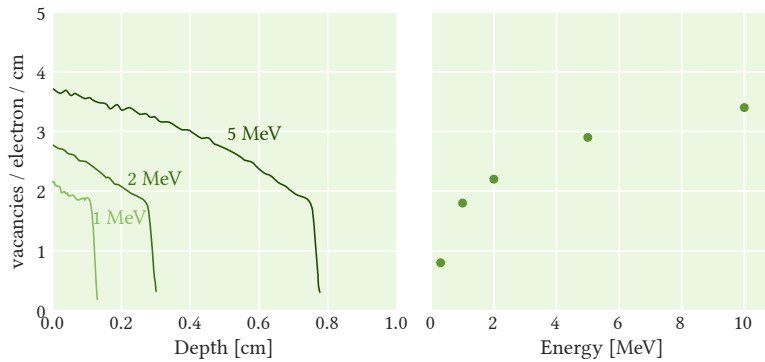


Figure 3.5: Number of vacancies generated per electron and cm calculated by Monte Carlo simulations [6].

Left: For different incident electron energies as a function of penetration depth.

Right: As a function of incident electron energies.

Figure 3.6 shows the vacancy generation in the two different experimental setups calculated with eq. (3.4).

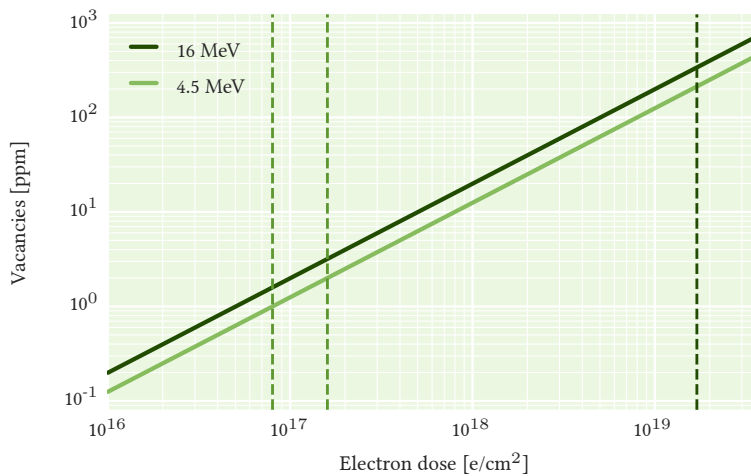


Figure 3.6: Number of vacancies per electron and cm as a function of the electron dose based on eq. (3.4). The dotted lines represent the region of electron doses used in the experiments. 16 MeV represent the conditions at the MAMI, while 4.5 MeV correspond to those at Synergy Health.

The number of vacancies generated was likely to be two orders of magnitude higher in Mainz than at Synergy Health. This reflects the different concentrations of NV and N₂V⁰ ⁶ aimed for during the evolution of this project. During the experiments performed at Mainz the starting material was chosen to be HPHT⁷ grown diamond with hundreds of ppm of nitrogen. This was due to the fact that this material was readily available to us at the time, while samples with lower concentrations were not yet accessible. In this early phase of the project our aim was to match the number of nitrogen with the number of vacancies to generate as many NV centres as possible. It was found later that complex damage and high absorption in the visible wavelength region made the samples treated in Mainz unsuitable for laser purposes.

⁶The neutrally charged state of N₂V (H3)

⁷High Pressure High Temperature

Later CVD⁸ grown diamond became accessible. The aim here was to generate a couple ppm of vacancies in the samples in order to match the \sim ppm nitrogen concentration in the CVD samples. This material was deemed a more promising choice for a laser material, because of lower parasitic background absorption in the emission region and potentially good enough pump absorption, which is discussed in more detail in section 6.5. A potential diamond colour centre laser.

⁸ Chemical Vapour Deposition

3.3 Diffusion, aggregation and dissociation of defects

DIFFUSION AND AGGREGATION of nitrogen and vacancies in the diamond lattice is required for the formation of NV and N_2V^0 . They are enabled by thermal treatment of diamond.

At the time this work was carried out no diamond samples with a few to a few dozen ppm of NV and N_2V^0 already present could be purchased. The target concentration for the centres is discussed in greater detail in section 6.5, A potential diamond colour centre laser. Both NV and N_2V^0 centres can be found in natural, untreated diamonds [16, 17]. But obtaining a suitable natural sample, in terms of size and optical properties, is difficult. NV centres have been found in as grown CVD diamond [18, 19] in concentrations < 100 ppb⁹ [20]. But these concentrations are too low for our purposes. The most promising starting material seems to be type Ib synthetic diamond, a material readily available commercially in a range of different nitrogen concentrations.

In this section it is assumed that nitrogen and vacancies are already present in the sample. The generation of vacancies is discussed in the previous section 3.1, Irradiation. Nitrogen is already incorporated into the starting material, as mentioned in section 2.3, Common defects in diamond.

Activation energies determine the temperature ranges for defect diffusion, aggregation and dissociation. Rate constants are used to describe the rate of a given process at a certain temperature and pressure and can be used to determine treatment times. These concepts are described in the following section.

Thermal stability of diamond

In the following subsections diffusion of vacancies and nitrogen in diamond through heating of the samples will be discussed. For some of these processes, in particular the diffusion of nitrogen, temperatures in excess of $1700^\circ C$ are required.

The stability of diamond is important to keep in mind in order to preserve the samples during thermal treatment. At room temperature and pressure the sp^3 bond between carbon atoms in the lattice is shorter than it would be in equilibrium, this is causing internal pressure, about 2 GPa at room temperature (represented as the diamond-graphite stability line in fig. 3.7 and fig. 3.14), in the lattice. This is the reason that diamond is metastable at room temperature and pressure. With increasing temperature this internal pressure grows and diamond becomes increasingly metastable [23]. A metastable state is a local minimum separated from an

⁹ parts per billion

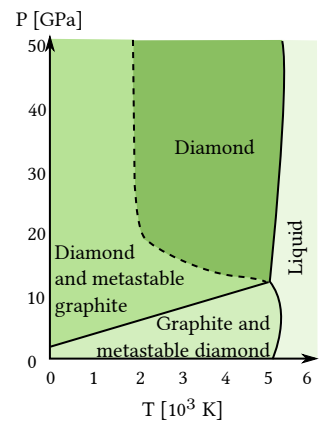


Figure 3.7: P-T phase and transformation diagram for carbon [21, 22]. Solid lines represent equilibrium phase boundaries.

energetically favourable minimum by an activated state (fig. 3.8).

The transition of diamond to graphite is thermodynamically favourable with $E_{\text{graphite}} - E_{\text{diamond}} = \Delta E < 0$. Later we'll see that the rate of the process is determined by the activation energy via eq. (3.9). The activation energy for the transition from diamond to graphite per atom is 3.5 eV. This energy is large enough that the process is not observable at room temperature in reasonable timescales [24].

Increasing the temperature changes the situation and makes graphitization of the samples likely. This effectively destroys the samples and should be prevented.

Surface graphitization is considered to occur in two steps rather than by direct diamond to graphite transformation. First, a single carbon atom detaches from the surface and forms a disordered bonding. Second, multiple of those atoms form graphite microcrystals [25]. The reaction becomes observable above 700°C at atmospheric pressure [26]. At temperatures below 900°C the rate of oxidization exceeds the rate of graphitization [27]. Diamond can be heated up to 1700°C in vacuum, or at atmospheric pressure using a high-purity gas like nitrogen, although some surface graphitization can occur under those conditions [25, 28].

Up to $\sim 1700^\circ\text{C}$ graphitization is considered a surface phenomenon. At temperatures above it starts to penetrate the insides of the crystal [27]. Applying high pressure during treatment with high temperatures keeps the diamond stable. The stability regions for diamond are illustrated in in fig. 3.7. The phase boundary between the diamond stability region and the graphite stability region determines the pressure needed in HPHT experiments at a given temperature to prevent phase transitions. In this way diamond can withstand temperatures up to 2500°C [29] and even above 3000°C [30].

Activation energies

Defect diffusion and aggregation can be thought of as state transitions. To describe a transition we consider a system with two equilibrium states [31], as illustrated before in fig. 3.8.

To transform a system in the initial state with energy E_1 into a final state with energy E_2 , a potential barrier for the intermediate state has to be overcome. The energy difference between the initial state and the activated state E_a is called activation energy. The transition from the initial state is energetically favourable if $E_2 - E_1 = \Delta E < 0$.

Diffusion activation energies describe the activation energy for a certain defect to become mobile in the diamond lattice. For defect complexes the

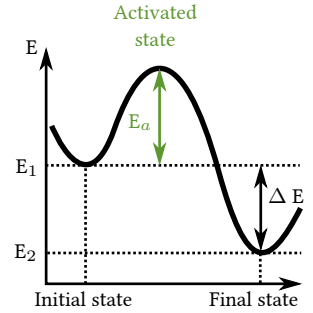


Figure 3.8: Illustration of the transition between two equilibrium states. The initial state has an energy of E_1 and the final state of E_2 . The energy difference between the initial state and the intermediate state is called activation energy E_a .

binding energy determines the activation energy for dissociation. Aggregation and vacancy capture are thermodynamically favourable processes in diamond. Internal stress in the diamond lattice, as mentioned before in section 3.3, Thermal stability of diamond, is reduced by the presence of atoms with atomic radii greater than carbon, like nitrogen atoms. This reduction is even greater for larger nitrogen and nitrogen-vacancy clusters [23].

This is illustrated in fig. 3.9, where the energies of the aggregates are calculated relative to the energy of their constituents at distant positions [32].

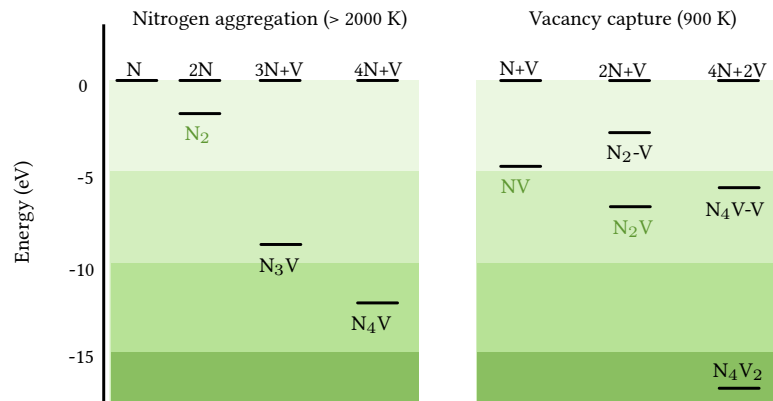


Figure 3.9: The energy of the nitrogen and nitrogen-vacancy complexes by [32]. - denotes defects at first neighbor positions and + denotes distant defects.

It is the aim here to outline defect formation, considering both experimental and theoretical values for activation energies and temperatures used. Experimental values vary considerably in some cases. They depend on the pressure and on the defect composition of the samples used [23, 33] and the relevant information is not always provided in every experimental description.

The simplest case to consider is the formation of NV. If single nitrogen atoms and vacancies are present in the lattice, then they only need to be aggregated. The activation energy of vacancy diffusion is 2.3 eV [32]. The dissociation barrier at 5.8 eV is the sum of the vacancy diffusion energy and the binding energy of NV, $\sim 3.5 \text{ eV}$ [34]. The lower temperature limits for these processes have been reported at 600°C and 1800°C respectively [23, 35].

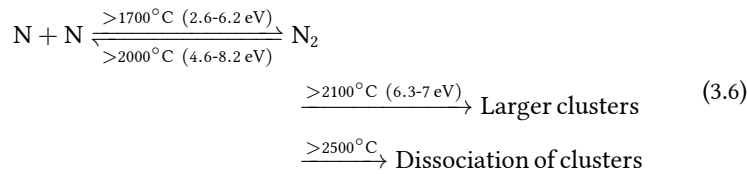


The concentration of NV is expected to plateau at about half the original nitrogen concentration in the sample, provided enough vacancies are available to reach that concentration in the first place [36]. Thermo-chromic

charge transfer during the annealing process leads to an exchange of an electron between NV^0 ¹⁰ and N_s^0 ¹¹, resulting in the formation of NV^- ¹² and N_s^+ ¹³. When the concentration of NV is approximately equal to the remaining nitrogen concentration, all the leftover single nitrogen is believed to exist in a positively charged state. The leftover vacancies can form NV^+ ¹⁴ with the remaining N_s^+ , a defect with a much lower binding energy. Low enough that it immediately breaks apart after formation during the annealing procedure [36].

N_2V ¹⁵ is a more complex defect and it can be synthesized in different ways. One is to produce N_2 ¹⁶ centres by nitrogen aggregation and subsequent irradiation and annealing [16, 23, 37, 38, 39]. Another method is the production of NV , as described above (eq. (3.5)), followed by HPHT treatment to mobilise NV in the lattice so it can combine with a single nitrogen to form N_2V . Synthesis of N_2V^0 was also demonstrated in brown natural Ia diamond by short time HPHT anneals [16, 40, 41].

We consider nitrogen aggregation in type Ib diamond first. Experimental values for the diffusion activation energy of N_s ¹⁷ in diamond range from 2.6 to 6.2 eV [23, 42, 43], depending on the samples and conditions used. Diamonds with moderate nitrogen concentrations, below a few hundred ppm, do not show significant aggregation of nitrogen below 1700°C [23]. Anneals at temperatures above 2000°C result in the formation of N_s from dissociation of N_2 centres [23]. The dissociation energy for N_2 is the sum of the diffusion energy of N_s and the binding energy of N_2 , 2 eV [32]. At temperatures above 2100°C larger nitrogen clusters start to form [23], with an activation energy in the range of 6.3-7 eV [23, 38]. At temperatures above 2500°C nitrogen clusters and platelets start to dissociate again, and single nitrogen is created [23, 39].



To form N_2 temperatures between 1700 and 2100°C are required. The most suitable temperature choice depends on further parameters, such as nitrogen concentration in the sample and treatment time available, and will be discussed further in section 3.3, Diffusion and aggregation rate constants.

When N_2 is successfully produced, the sample needs to be irradiated to create vacancies. Then, this sample that contains N_2 and V ¹⁸, needs to be annealed in order to create N_2V . The energy needed to form N_2V is higher

¹⁰ The neutral form of NV

¹¹ Neutrally charged N_s

¹² The negative form of NV

¹³ Positively charged N_s

¹⁴ Proposed positive form of NV

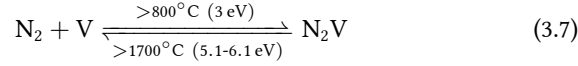
¹⁵ A vacancy and two substitutional nitrogen atoms in C_{2v} symmetry

¹⁶ Two adjacent substitutional nitrogen atoms (A centre)

¹⁷ Single substitutional nitrogen (C centre)

¹⁸ Lattice vacancy

than the activation energy for vacancy diffusion ($>600^\circ\text{C}$ (2.3 eV)). This is due to the needed for reordering from $\text{N}_2\text{-V}$ to N-V-N , which happens at $>800^\circ\text{C}$ (3 eV) [32, 44]. N_2V dissociates into N_2 and a vacancy at temperatures in the range of $1700\text{--}2200^\circ\text{C}$ ($5.1\text{--}6.5\text{ eV}$) [34, 38, 39]:



Annealing temperatures above 800°C are required for the formation of N_2V .

For the second synthesis route of N_2V , the generation of NV with subsequent thermal treatment, we first assume that there is single nitrogen and NV present in the sample. Some theoretical models predict that vacancy-assisted nitrogen diffusion is energetically favourable over direct or interstitial diffusion mechanisms [32, 45]. This means that the aggregation of NV and N_s to N_2V can happen at temperatures below nitrogen diffusion, simply due to the presence of NV.

The activation energy of vacancy assisted nitrogen diffusion in pre-irradiated diamond is reported to lie between $3\text{ eV}\text{--}4.8\text{ eV}$ [34, 46, 47]. The dissociation energy for NV (5.8 eV eq. (3.5)) is larger than the proposed migration energy. This strengthens the assumption that in an appropriate temperature range NV migrates through the lattice without fully dissociating.

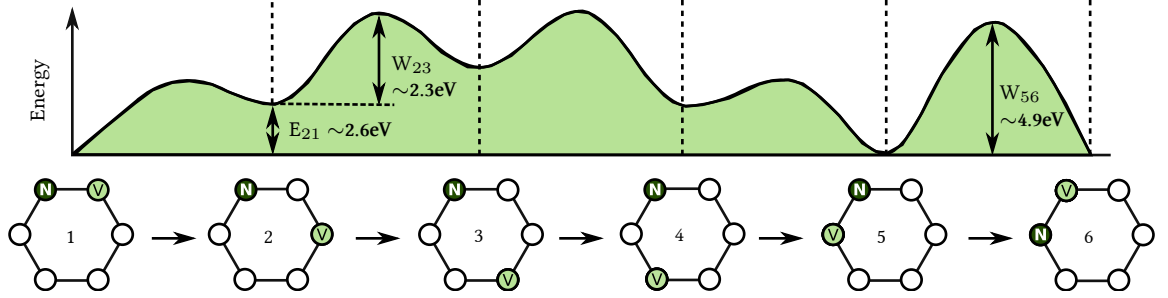
Formation of N_2 in pre-irradiated diamond has been found in type Ib diamond with concentrations between $50\text{--}500\text{ ppm}$ in vacuum and at temperatures between 1500°C [48] and as low as 1300°C [49]. The addition of external pressure is believed to promote interstitial and slow down vacancy assisted diffusion [33], this might reduce its effect during HPHT treatment.

Figure 3.10 illustrates the movement and energy profile of vacancy assisted migration by a partial dissociation process, where the nitrogen and vacancy stay in the vicinity of each other [34]. During this movement N_s and V are separated only by a few bond lengths. The attractive force between them then promotes the recombination of both. For every complete circle 1-6 the nitrogen atom is transported one place further in the lattice.

NV is assumed to migrate through the lattice until it combines with another N_s to form N_2V [40]. This is supported by experimental results, where HPHT treatment at about 1700°C of pink synthetic diamond containing NV resulted in a weakening of the NV absorption and a change into an intense green colour as a result of N_2V^0 and N_2V^{-19} absorption [50, 51].

Long-time annealing of irradiated type Ib diamond at 800°C , during which NV could form, increases the aggregation into N_2 and N_2V after subsequent heating at temperatures as low as 1500°C [23, 52].

¹⁹ The negatively charged state of N_2V (H_2)



Further heating may result in the vacancy breaking away, effectively leading to an enhanced nitrogen aggregation [48, 53] as seen in eq. (3.7) previously. Heating at higher temperatures will lead to the formation of bigger nitrogen clusters as shown in eq. (3.6):

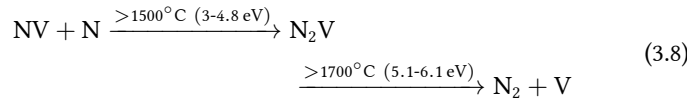


Figure 3.10: An illustration of vacancy assisted migration of nitrogen adapted from [34]. The diffusion activation energy is represented by the barrier E_{21} plus W_{23} . The reorientation energy is represented by W_{56} . All energies are relative to the stable energy of NV. As NV migrates through the lattice it can trap an additional N_s atom forming N_2V .

For a laser sample we have to consider that NV contributes to parasitic absorption in the emission range of N_2V^0 [54]. If this synthesis route is taken, residual NV should be minimized.

If both N_s and N_2 are present in a sample, they compete for vacancy capture. Some experimental work suggests that N_s traps vacancies between eight [55] and fifty times [48, 56] more efficiently than N_2 . As discussed above, in the theoretical model the vacancy capture of N_2 and the reordering of $\text{N}_2\text{-V}$ to N-V-N involve activation energies above the vacancy migration barrier of ~ 2.4 eV, while the formation of NV occurs with activation energies all within this energy [32]. This makes the latter process statistically more likely.

To produce a N_2V^0 sample suitable to be used as a laser crystal, aggregation is required to be as complete as possible, as any single nitrogen present in the sample is likely to form NV after subsequent irradiation and annealing.

For the production of N_2V^0 in samples with low nitrogen concentration (<5 ppm) this seems to be the preferable path due to the low aggregation efficiency of nitrogen in those samples. This will be discussed in greater detail in the following subsection.

HPHT treatment of brown natural Ia diamond was demonstrated to yield luminescent N_2V^0 containing samples [16, 40, 41]. Formation of N_2V^0

occurs much faster than dissociation of N_2 , as HPHT experiments with brown type Ia, in particular IaA and IaAB, natural diamond have shown. Short time anneals, about 2-5 minutes at 2000-2100°C, turn those stones green, while prolonged anneals turn them yellow. The green color is an indication for the formation of N_2V^0 , while the yellow one occurs due to the presence of single N_s after dissociation of N_2V^0 and N_2 . Brown Ia diamonds should be treated with short time HPHT treatments in order to produce N_2V^0 [16, 41].

Diffusion and aggregation rate constants

In this part the timescales for the diffusion and aggregation of defects are taken into account. The aggregation in particular is dependent on the defect concentrations in the samples. If the defect concentration is high, the mean path for two defects to meet is short. In comparison, if the concentration is low, the mean path is longer and it takes more time for defects to travel these distances. This explains why the aggregation of single nitrogen into pairs is difficult in samples with low nitrogen concentrations.

To describe the interplay of defects a similar construct can be used as the one to describe chemical reactions. The reaction rate constant k quantifies the speed of a chemical reaction.

In the case of diffusion k can be thought of as a *hopping rate*, which describes the jump of a defect to another lattice site per time unit [34]. In the case of aggregation and dissociation the rate equations are used to link the rate of a reaction to the concentration of each of the reactants. The reactions are described by the reactants and the products of the reaction, as seen in the previous subsection. How such a rate equation is constructed depends on the nature of the reaction, the concentrations of the reactants and how complex the reaction is [57].

In first order reactions the influence of the temperature on the reaction rate is described by the Arrhenius equation [31, 57]:

$$k = \nu \cdot \exp(-E_a/k_B T) \quad (3.9)$$

The equation relates the reaction rate constant k with the activation energy E_a , temperature T and attempt frequency ν . k_B is the Boltzmann constant. In other words, ν describes the number of collisions per second that may or may not end in a reaction (reaction attempts), $\exp(-E_a/k_B T)$ is the probability for a reaction to occur and k is the number of collisions that result in a reaction per second. When eq. (3.9) is used in conjunction with rate equations, the effects of concentration can also be included.

Rate equations are a convenient way to determine rate constants experimentally, by measuring the concentrations of the reactants before and

after thermal treatment. If the rate constants are known, they can be used to determine the treatment time to get a desired concentration of the reaction product.

We consider a defect species X, with the concentration $[X]$. If the change in concentration of defect X is dependent on the concentration of X, then first order kinetics describe the system. This is approximately true for the capture of vacancies in type Ib diamond due to the formation of NV centres $N_s + V \rightarrow NV$ in a nitrogen rich diamond with $[N_s] \gg [V]$ [58]. Nitrogen acts as a vacancy trap in this example [59]. Dissociation of NV is not taken into account and the nitrogen concentration is assumed to be much larger than the concentration of vacancies, so that $[N_s]_{t=0} \approx [N_s]$.

The rate equation for the change of the concentration of defect X in such a system has the form:

$$d[X]/dt = -k \cdot [X] \quad (3.10)$$

with the solution:

$$[X] = [X]_0 \cdot \exp(-kt) \quad (3.11)$$

Second order kinetics have to be considered if the rate equation is dependent on two variables, X and Y. Those can be different defects or different aggregation states of one defect. If the reaction is such that $X + Y \rightarrow P$, we get:

$$\frac{d[X]}{dt} = \frac{d[Y]}{dt} = -k \cdot [X][Y] \quad (3.12)$$

In a type IIa, diamond vacancies will anneal out through the surface of the crystal or form aggregates. The process then becomes a combination of first and second order kinetics [35, 59].

In a special case X and Y describe the same defect. The aggregation of N_2 follows this case of second order kinetics. Single nitrogen aggregates into pairs via $N_s + N_s \rightarrow N_2$. Dissociation of nitrogen pairs is not considered here. In this case $[X]_0 = [Y]_0$ and eq. (3.12) then becomes:

$$\frac{d[X]}{dt} = \frac{d[Y]}{dt} = -k \cdot [X]^2 = -k \cdot [Y]^2 \quad (3.13)$$

with the solution:

$$[X] = \frac{1}{[X]_0^{-1} + kt} \quad (3.14)$$

The only variable that is relevant is the initial single nitrogen concentration $[X]_0 = [N_s]_0$.

In fig. 3.11 the conversion of X into the reaction product as a fraction of the starting concentration $[X]_0$ is visualized for different reaction orders.

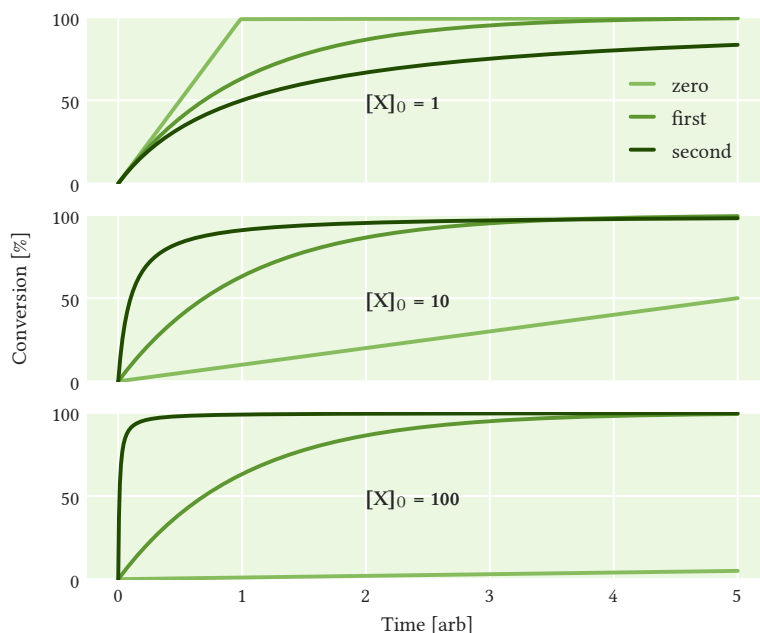


Figure 3.11: Illustration of the conversion $([X]_0 - [X])/[X]_0$, depending on the starting concentration $[X]_0$ of 1, 10 and 100 per unit volume. For zero, first and second order rate equations and an arbitrary rate $k = M^{(1-n)}/[time]$, with the concentration unit $M = 1$, and the order of the reaction n .

The fractional conversion rate of first order kinetics is not dependent on the initial concentration. The conversion time for all processes that follow second order kinetics, including most aggregation processes, is prolonged in samples with lower concentrations.

An intuitive way to counteract the slower conversion of $N_s + N_s \rightarrow N_2$ in diamond samples with low initial nitrogen concentrations is to increase the treatment temperature of the process, as implied by eq. (3.9). This is only feasible until a temperature is reached where considerable amounts of aggregates dissociate. The dissociation process is considered a first order reaction and hence the conversion efficiency is not dependent on the initial nitrogen concentration. This means that in samples with low concentrations the aggregation efficiency is reduced, while the dissociation efficiency isn't affected. The lower the initial nitrogen concentration of a sample, the more difficult aggregation becomes.

Most of the samples under study in this work were type Ib synthetic diamond. That is why we consider the simple case where all the nitrogen is present in single substitutional form $[N_s]_0 \neq 0$ and no pairs are present initially $[N_2]_0 \approx 0$. The rate of reduction of $[N_s]$ due to aggregation can

be expressed by the second order rate equation eq. (3.13):

$$\frac{d[N_s]}{dt}_{\text{aggregation}} = -k_1 \cdot [N_s]^2 \quad (3.15)$$

and the increase in single nitrogen from pairs dissociating takes the form of a first order rate equation (eq. (3.10)), as it is not dependent on the single nitrogen concentration:

$$\frac{d[N_s]}{dt}_{\text{dissociation}} = -2 \cdot \frac{d[N_2]}{dt} = 2k_2 \cdot [N_2] \quad (3.16)$$

with $[N_2] = ([N_s]_0 - [N_s])/2$ and the rate constants $k_1 = k_{\text{aggregation}}$ and $k_2 = k_{\text{dissociation}}$. The combined rate equation can be written as [43]:

$$\frac{d[N_s]}{dt} = -k_1[N_s]^2 + k_2([N_s]_0 - [N_s]) \quad (3.17)$$

Dissociation of N_2 appears at around 2000°C with a rate that is small in comparison to the aggregation of nitrogen [43, 60]. The equation takes the form of eq. (3.15) $\lesssim 2000^\circ\text{C}$, when dissociation can be neglected [42].

The rate constant of nitrogen-pair dissociation into single nitrogen, k_2 , depends on the annealing temperature, pressure and initial nitrogen concentration [42, 61]. It was found to be enhanced in the graphite stable region for HPHT experiments, in comparison to the diamond stable region. In an HPHT experiment at 2300°C with a pressure of 5-6 GPa k_2 was enhanced by a factor of ~ 10 , in comparison to using 8.5 GPa [62].

In fig. 3.12 the slowed aggregation for samples with low initial nitrogen concentrations is illustrated.

The aggregation for different initial nitrogen concentrations as a function of time is compared for two temperatures and literature rate constants. Above 2000°C dissociation is taken into account with plausible values for the rate constants $k_1 = 10^{-4} (\text{ppm})^{-1} \text{s}^{-1}$ and $k_2 = 0.5 \cdot 10^{-3} \text{s}^{-1}$ [62]. At 1900°C the aggregation rate is $k_1 \approx 7.5 \cdot 10^{-7} (\text{ppm})^{-1} \text{s}^{-1}$ [36], while dissociation can be neglected with $k_2 \rightarrow 0$ [43]. Dissociation as a competing process to aggregation has a stronger influence in samples with lower nitrogen concentrations. The starting concentration determines the maximum conversion that can be reached at thermodynamic equilibrium. If full conversion is required temperatures have to be adjusted to prevent dissociation. This is especially relevant for samples with low concentrations.

Annealing

Annealing in this work refers to the heat treatment of diamond specifically to mobilize vacancies in order to form colour centres.

As discussed previously, vacancy diffusion starts at 600°C (2.3 eV) while 800°C is needed for the final reordering step (N-N-V to N-V-N) in the pro-

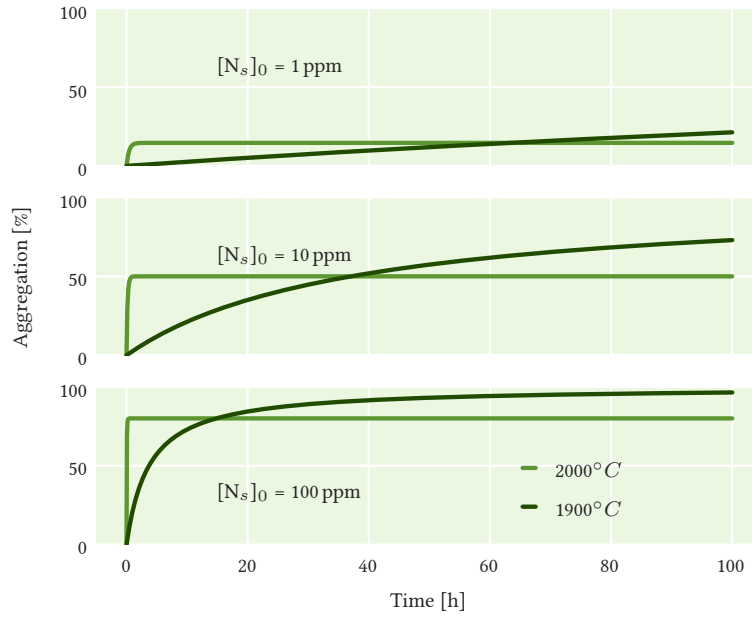


Figure 3.12: The solutions to eq. (3.15) and eq. (3.17) are compared for starting concentrations $[N_s]_0$ of 1, 10 and 100 ppm. Plausible values for the rate constants above 2000°C, $k_1 = 10^{-4} (\text{ppm})^{-1} \text{s}^{-1}$ and $k_2 = 0.5 \cdot 10^{-3} \text{s}^{-1}$ [62], have been compared to the rate $k_1 \approx 7.5 \cdot 10^{-7} (\text{ppm})^{-1} \text{s}^{-1}$ at 1900°C [36], where $k_2 \rightarrow 0$ [43].

duction of N_2V . Higher temperatures lead to a faster diffusion, but the temperature is limited by the dissociation temperature of the respective defect ($\sim 1700^\circ\text{C}$ for both NV and N_2V^0) and the prevention of graphitization in order to preserve the quality of the sample.

Taking into account the stability considerations from the previous subsection anneals should be performed in protective atmosphere, vacuum or covered in diamond grit in order to prevent oxidization and graphitization. The diffusion distance of the vacancies during annealing can be estimate with a variation of eq. (3.9):

$$k_D = k_0 \cdot \exp(-E_a/k_B T) \quad (3.18)$$

where k_D is the diffusion coefficient and $k_0 = 3.6 \cdot 10^{-6} \text{cm}^2/\text{s}$ is a pre-factor obtained by computational simulations from vacancy diffusion near the diamond surface [63].

Diffusion near the surface is more rapid than in bulk diamond, so the diffusion distance obtained with this pre-factor is an overestimation of the actual distance in bulk diamond. The diffusion distance d can be estimated with the equation [64]:

$$d \approx \sqrt{k_D \cdot t} \quad (3.19)$$

where t represents the annealing time.

If we consider a sample with an evenly distributed nitrogen concentration of $n = 1$ ppm, the average distance between the nitrogen atoms is approximately $\langle r \rangle = 1/\sqrt[3]{n} \sim 18 \text{ nm}$. Typical anneals of diamond at the University of Warwick for the synthesis of NV and N_2V were performed at 800°C for 5 hours. In fig. 3.13 the diffusion distance at 800°C is plotted.

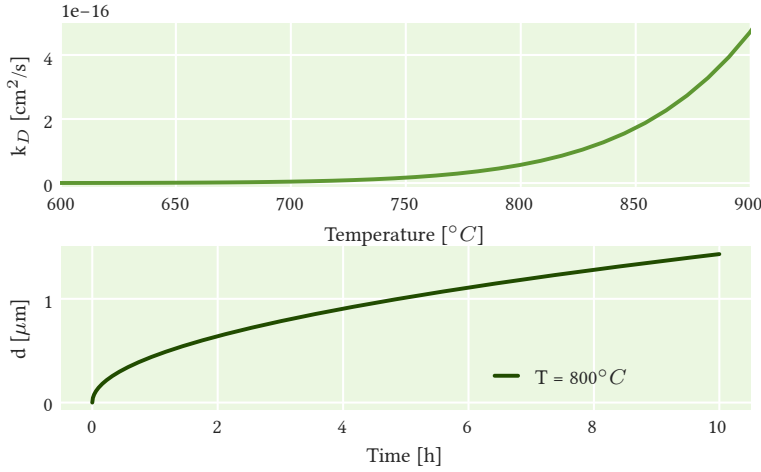


Figure 3.13: Vacancy diffusion coefficient and distance (eqs. (3.18) and (3.19)) estimated with literature values for vacancy diffusion near the surface [63, 64]. For an annealing temperature of 800°C a maximum diffusion distance of $1 \mu\text{m}$ is estimated after 5 hours of annealing.

In theory, with a perfectly even distribution of centres, anneals at shorter times should be sufficient for full conversion into NV, but experimental results show a residue of vacancies after 3 hour anneals at 800°C in our samples (see section 5.4) and after discussion with the Diamond group at the University of Warwick, an annealing time of 5 hours at 800°C was suggested to us as an empirical value for maximum conversion into NV, determined by them during their experiments.

HPHT treatment

For the synthesis of N_2V^0 the diffusion and aggregation of nitrogen into nitrogen pairs is needed. As described in section 3.3, Activation energies, this happens at temperatures above 1500°C . As discussed in the beginning of this section, in order to avoid graphitization, stabilizing pressure is needed when treating diamond at high temperatures.

HPHT treatment refers to the annealing of diamond at high temperatures under high pressures [23]. The experimental details of the HPHT setup are discussed in the following section 3.4, Experimental procedure for thermal treatment.

At a pressure of 7 GPa diamond can last hours without any graphitization at 1900°C , while it can be completely graphitized in a minute at 2500°C [23].

Because of that it is important to carefully select the pressure for a given temperature. A guideline for this is the diamond-graphite stability transition shown in fig. 3.7. Pressure and treatment time are the most crucial parameters to control graphitization during HPHT treatment, next to the temperature.

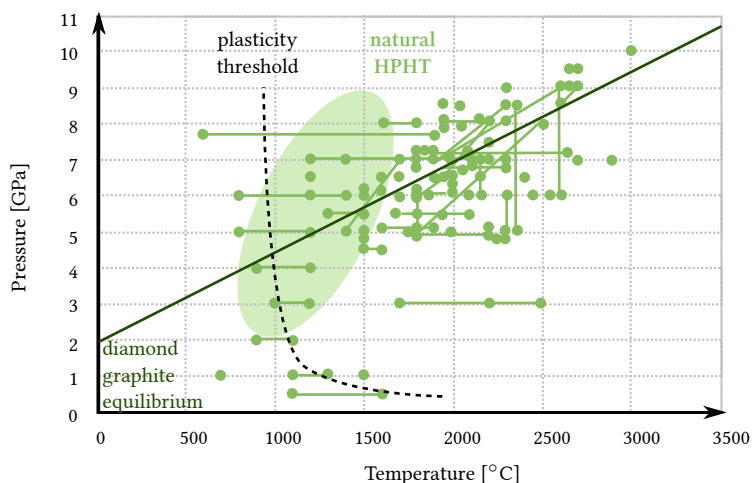


Figure 3.14: P-T diagram of published experimental parameters (dots) and ranges (horizontal lines) for diamonds subjected to HPHT treatment.

The diagonal line indicates the diamond-graphite equilibrium line. The dashed line indicates the pressure-temperature threshold of diamond plasticity. The range of possible natural HPHT growth and annealing is indicated by the green ellipse. Adapted from [65].

For most defects the diffusion is most efficient when diamond is in a plastic state [65]. The transition between rigid and plastic states starts in a pressure region of 4-7 GPa for temperatures between 900-1200°C [66, 67] (indicated by a dashed line in fig. 3.14).

External pressure promotes the transition of diamond from a rigid state into the range of plasticity. It has been found that at low pressures, even at temperatures as high as 2200°C, diamond still remains in the rigid state. Applying a pressure of just 5 GPa leads to diamond reaching a plastic state at temperatures as low as 1000°C [23]. Most HPHT experiments are performed around the area of the diamond-graphite equilibrium line. Lower pressures and temperatures are easier to reach and maintain experimentally and so some HPHT experiments are performed in the range of graphite stability. In these cases it is important to minimize treatment time and to work with diamond without major inclusions or voidites to prevent graphitization [65].

One way to study the aggregation of nitrogen is by comparison of aggregation rates. A selection of rate constants for different temperatures from literature values is presented in table 3.3. Up till 1500°C the aggregation rate increases by an order of magnitude for every 100°C [68], above that it does so for every ~200°C in the temperature range of this data.

Depending on the experimental circumstances different temperatures

are better suited. For example, if the HPHT treatment time has to be kept as short as possible, a higher percentage of aggregated nitrogen can be achieved when choosing higher temperatures, even though dissociation starts to happen there. This can be seen in fig. 3.12.

Aggregation of single nitrogen and dissociation of nitrogen pairs become observable at moderate temperatures around 1900-2100°C. Additionally, this temperature range is used to remove brown colouration from diamonds. Depending on the initial defect composition these will turn transparent or a fancy colour [65]. At high temperatures in the range of 2100-2300°C the removal of brown colour and the aggregation and dissociation of nitrogen defects occur most effectively [65].

Diffusion coefficients for carbon and nitrogen can change by about 30% for a 1 GPa change in pressure [69]. External pressure impedes the dissociation of defects with a radius larger than carbon. For example, while in an experiment at 2300°C at 8.5 GPa for 15 minutes 10% of N₂ centres dissociated, the rate jumped to 50% at the same temperature and even shorter treatment time for a pressure of 5-6 GPa [62].

For defects with a smaller radius the opposite is true. Here dissociation is promoted under external pressure. This is true for example for vacancies and vacancy clusters. This is believed to be the reason why the reduction of brown coloration in diamond is more effective for HPHT treatment at elevated pressures [65].

According to this nitrogen aggregation should be performed at large pressures in order to suppress nitrogen dissociation. At the same conditions brown coloration that might have been present in the sample would be more efficiently removed, removing background absorption from the sample.

Temperature [°C]	k [ppm ⁻¹ s ⁻¹]
2200	$1.3 \cdot 10^{-5}$
2100	$6.7 \cdot 10^{-6}$
1900	$7.5 \cdot 10^{-7}$
1700	$5.0 \cdot 10^{-8}$
1500	$1.8 \cdot 10^{-9}$
1400	$2.5 \cdot 10^{-10}$
1300	$2.8 \cdot 10^{-11}$
1200	$2.3 \cdot 10^{-12}$
1100	$1.3 \cdot 10^{-13}$

Table 3.3: Rate constants for the aggregation of nitrogen in diamond at various temperatures [36, 43].

3.4 Experimental procedure for thermal treatment

Thermal treatment of diamond is used to reach activation energies for different processes described in detail in section 3.3, Diffusion, aggregation and dissociation of defects.

Thermal treatment at atmospheric pressure or in a vacuum

Annealing was performed both at the University of Edinburgh and the University of Warwick. For the first synthesis protocol, annealing was performed at the University of Edinburgh in a vacuum at 800°C for 3 hours. For further iterations, annealing was performed at the University of Warwick with an Elite Thermal Systems horizontal tube furnace with a setup as described in [36, 49] at 800°C for 5 hours (as discussed in section 3.3). Nitrogen gas was used in order to prevent graphitisation of the samples. A schematic of a horizontal tube furnace is presented in fig. 3.15.

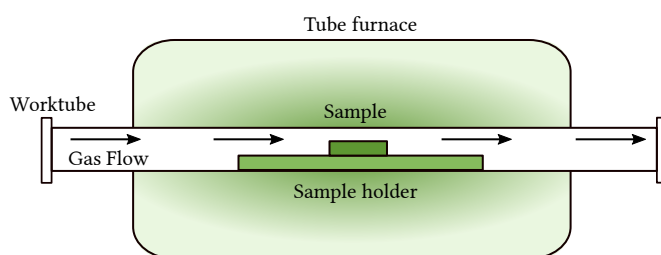


Figure 3.15: Schematic of an annealing furnace as described in [70].

The sample is placed on a thermally resistant sample holder, covered in diamond grit to further prevent graphitization. A continuous gas flow can be sent through the worktube.

Anneals at 800°C are sufficient for the diffusion of vacancies and the formation of NV, in samples containing single nitrogen and vacancies, as well as the formation of N_2V , in samples containing N_2 and vacancies. The formation processes and their temperature dependence is described in more detail in section 3.3, Diffusion, aggregation and dissociation of defects.

Thermal treatment at high temperatures and pressures

HPHT experiments were performed in a collaboration with the Geoinstitut at the University of Bayreuth, Germany.

A so called multi-anvil apparatus was used for this purpose. It is designed to generate high pressures (tens of GPa) and high temperatures (above 2500°C) under laboratory conditions. These conditions are interesting for research in material science and geology, as well as for the

industrial production of minerals, like synthetic diamond. They are able to reproduce pressures and temperatures that exist in deep layers of the earth [71].

The multi-anvil apparatus used in this work are categorized as Large Volume Presses (LVP) since they allow for a relatively large sample volume in the order of cubic millimetres [72]. Creating laser sized samples is therefore a non-trivial endeavour, as our sample sizes reach the limits of the allowed sample volumes. A multi-anvil apparatus consists of three components. A hydraulic press to generate force, a high-pressure module with anvils to compress the sample volume and the sample assembly.

An illustration of the sample assembly placed inside a high pressure module with anvils can be seen in fig. 3.16.

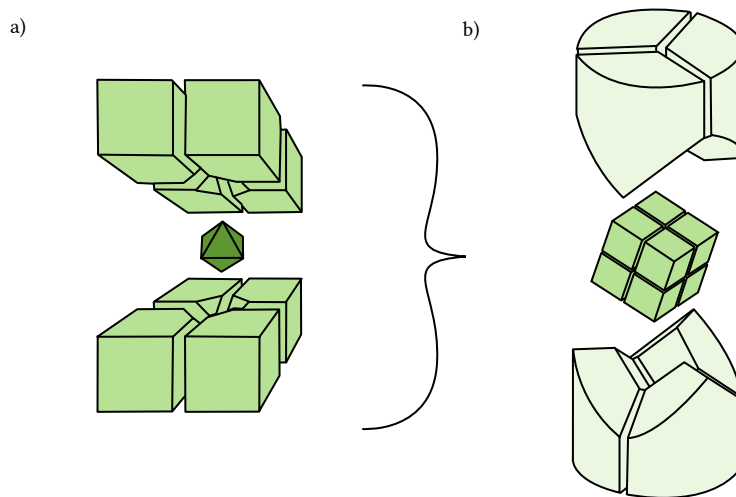


Figure 3.16:

a) Pressure medium between 8 tungsten carbide anvils.

b) 8 tungsten carbide anvils between 6 steel anvils.

This is a typical Kawai cell 6-8 multi-anvil apparatus setup. Illustration adapted from [72].

Sample assemblies usually include a soft pressure medium, a furnace that converts current into heat, a soft medium to cushion the sample and a sample jacket that protects the sample from touching other parts of the assembly. Pictures of the assembly as it was used in this work, together with a diamond sample inside an MgO²⁰ sleeve, can be seen in fig. 3.17.

The interior corners of the anvils are truncated to fit an octahedral assembly. These octahedra can have edge lengths from 8 to 25 mm. They are made of easily deformable material that provides electrical insulation between the furnace and the anvils, in the case of this work made of MgO doped with Cr₂O₃ (grey) and ZrO₂ (white) (as seen in fig. 3.17).

The octahedral assembly is larger than the space between the anvils. When pressure is applied, the material will squeeze out into the spaces between the anvils until the pressure between the octahedral assembly and the anvils balances the pressure generated inside the total sample assem-

²⁰ Magnesium oxide

bly [72].

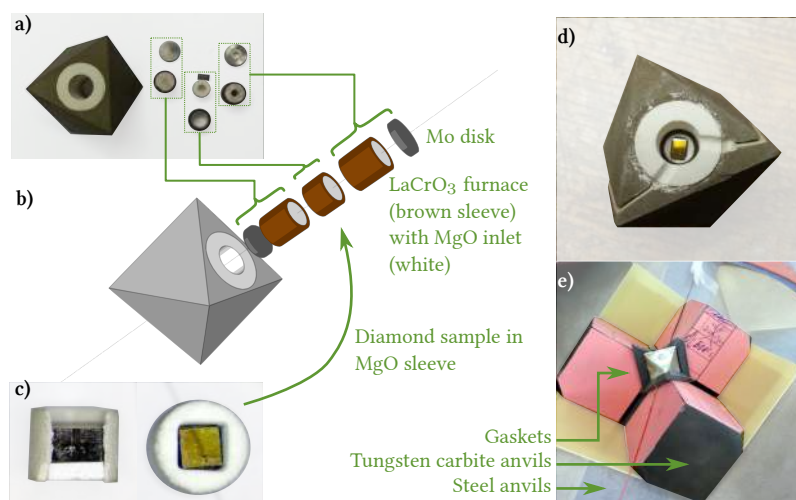


Figure 3.17: HPHT setup with

a) Octahedral assembly, including all small parts to host the sample. These include:

A soft pressure medium in the form of an octahedron, made from MgO doped with Cr_2O_3 (grey) and ZrO_2 (white),

A furnace that converts current into heat, in this case LaCrO_3 (brown sleeve).

A soft medium to cushion the sample and a sample jacket that protects the sample from touching other parts of the assembly, in this case MgO.

Two Molybdenum (Mo) disks to cap the inner assembly.

b) Assembly of all parts.

c) Diamond sample surrounded by MgO sleeve.

d) Sample in octahedral assembly.

e) Octahedral assembly placed on 4 tungsten carbide anvils, which are placed on 3 steel anvils. Gaskets are placed on the truncated sides of the anvils.

Gaskets are placed on the truncated sides of the anvils to help distribute the pressure evenly along the sides of the octahedron. They are made of pyrophyllite, a soft, chemically inert material with a high melting temperature.

The hydraulic press in the HPHT setup generates the force to push the anvils together. By pressurization of a hydraulic fluid a ram is driven towards a stationary plate to compress the high-pressure module. This design must be very sturdy to withstand the forces generated.

Most experiments were performed using a Voggenreiter split sphere Kawai-type multi-anvil assembly compressed with a 5000-ton press. Other presses available were a Hymag split sphere Kawai-type multi-anvil assembly compressed with a 1000-ton press, a Sumitomo split sphere Kawai-type multi-anvil assembly compressed with a 1200-ton press and piston-cylinder press. All presses used in this work, besides the piston-cylinder press, were of the type Kawai cell 6-8 multi-anvil apparatus. The original concept of this type of press was introduced by Kawai et al. in 1970 [73]. They consist of six steel anvils, three on the ram facing up, and three on the stationary plate facing down. In these eight anvils can be places (Figure 3.16).

This design is used for force magnification to amplify pressure. The pressure P is related to the force F applied to the area A via $P = F/A$. A smaller area means larger pressures. The anvils are composed of very strong material, in our case tungsten carbide. They have a large surface area on the sides that are in contact with the steel anvils and a small sur-

face area on one side, the truncated edge seen in fig. 3.16, that is in contact with the octahedral sample assembly. The smaller the area of the truncated edges, and as a consequence the sample assembly, the larger the pressure on the sample. This is limited by the sample dimensions and the compressive strength of the tungsten carbide cubes. All Kawai-type presses are able to be operated up to about 25 GPa and 3000 K. The piston-cylinder press can be operated up to 4 GPa and 2100 K [72].

Heating is produced by electrical resistance in graphite or LaCrO_3 ²¹ furnaces. These materials are compressed into cylinders which can be assembled to surround the MgO inlets in a) and b) of fig. 3.17. They are connected to two of the anvils by a conductive material, in this case the Mo disks pictured in fig. 3.17. Electrical current runs through the two connecting anvils. All the anvils are electrically insulated from each other using cardboard plates (pink cardboard in fig. 3.17 e)). Graphite furnaces can transform into diamond at higher pressures, making LaCrO_3 the material of choice for such conditions [74].

²¹ lanthanum chromate

Temperatures in the setup are either measured with a thermocouple or estimated with calibration curves. The calibration curves relate the temperature inside the cell to the electrical power provided to the furnace.

Accurate temperature measurements in HPHT experiments are still a challenge. Temperatures up to 1700°C can be measured using thermocouples. At higher temperatures, where calibrations are used, the real temperature can differ. Above 2500°C, the error of the temperature measurements can exceed 100°C. This error is one of the main reasons for discrepancy between the results reported by different authors [23].

The exact pressure in the sample assembly is not easy to determine. The frictional force and the degree to which the pressure media squeezes out is unknown. Therefore calibration curves for each sample assembly are used to estimate the pressure inside the sample assembly. For this the pressure in the hydraulic fluid that drives the hydraulic rams is used [72].

3.5 Summary

THE SYNTHESIS OF NITROGEN BASED DEFECTS starts with nitrogen containing samples. In synthetic diamond, nitrogen is present predominantly as single atoms (type Ib), while natural diamond can have a variety of nitrogen clusters (type IaA/B). The defects of interest, NV and N_2V^0 , consist of a single nitrogen and a vacancy and two nitrogen atoms and a vacancy respectively.

For the generation of NV, vacancies have to be generated in a synthetic diamond containing single nitrogen and finally the vacancies and nitrogen atoms have to be combined. For the generation of N_2V^0 , single nitrogen in synthetic diamond has to be aggregated into pairs and combined with a vacancy or natural diamond containing nitrogen clusters has to be treated at high temperatures and pressures.

The generation of single vacancies in diamond, as opposed to vacancy clusters, is done most commonly by electron irradiation. Diffusion of those vacancies starts above 600°C and is commonly performed at 800°C for 3-5 hours.

Diffusion of nitrogen starts at 1700°C and to prevent graphitization has to be performed at high pressures. Rate constants describe the aggregation or dissociation efficiency of defects at different temperatures. The nitrogen concentration determines the timescales of the aggregation. The lower the concentration, the longer the timescales get. With higher temperatures, aggregation accelerates, but competing dissociation occurs, lowering the overall efficiency of the aggregation process.

The next chapter, Defect quantification and spectroscopic methods, describes how to measure the defect concentrations in a diamond sample. In chapter 5, Results of the colour centre synthesis, the synthesis of a selection of diamond samples is described. In chapter 6 and chapter 7 the concept of a NV or N_2V^0 based diamond laser is described and the most promising samples of the synthesis for the use as a laser gain medium are evaluated.

References

- [1] W. Crookes. *Diamonds*. Harper & Brothers, London, New York, 1909. URL: <http://farlang.com/books/william-crookes-diamonds>.
- [2] T. W. Overton and J. E. Shigley. "A History of Diamond Treatments". In: *The Global Diamond Industry*. London: Palgrave Macmillan UK, 2008, pp. 181–228. DOI: 10.1057/9781137537614_8.
- [3] J. Koike, D. M. Parkin, and T. E. Mitchell. "Displacement threshold energy for type IIa diamond". In: *Applied Physics Letters* 60.12 (Mar. 1992), pp. 1450–1452. ISSN: 00036951. DOI: 10.1063/1.107267.
- [4] J. Solé, L. Bausá, and D. Jaque. *An Introduction to the Optical Spectroscopy of Inorganic Solids*. 2005. DOI: 10.1002/0470016043.
- [5] P. Mohr, B. Taylor, and D. Newell. "CODATA recommended values of the fundamental physical constants: 2010". In: *Reviews of Modern Physics* 84.4 (July 2012), pp. 1527–1605. ISSN: 0034-6861. DOI: 10.1103/RevModPhys.84.1527.
- [6] B. Campbell and A. Mainwood. "Radiation damage of diamond by electron and gamma irradiation". en. In: *Physica Status Solidi (A) Applied Research* 181.1 (Sept. 2000), pp. 99–107. ISSN: 00318965. DOI: 10.1002/1521-396X(200009)181:1<99::AID-PSSA99>3.0.CO;2-5. URL: [http://onlinelibrary.wiley.com/doi/10.1002/1521-396X\(200009\)181:1%3C99::AID-PSSA99%3E3.0.CO;2-5/abstract](http://onlinelibrary.wiley.com/doi/10.1002/1521-396X(200009)181:1%3C99::AID-PSSA99%3E3.0.CO;2-5/abstract).
- [7] A. T. Collins. "Colour centres in diamond". In: *Journal of Gemmology* 18.1 (1982), pp. 37–75. URL: <https://gem-a.com/component/edocman/?task=document.viewdoc%7B%5C%7D&id=2940%7B%5C%7D&Itemid=>
- [8] A. Mainwood. "CVD diamond particle detectors". In: *Diamond and Related Materials* 7.2-5 (Feb. 1998), pp. 504–509. ISSN: 0925-9635. DOI: 10.1016/S0925-9635(97)00248-3.
- [9] A. T. Collins. "Optical Centres Produced in Diamond by Radiation Damage". In: *New Diamond and Frontier Carbon Technology* 17.2 (2007), pp. 47–61. ISSN: 13449931. URL: http://myukk.xsrv.jp/free_journal/download.php?fn=NDFCT532_full.pdf.
- [10] S. Lagomarsino et al. "Refractive index variation in a free-standing diamond thin film induced by irradiation with fully transmitted high-energy protons". In: *Scientific reports* 7.1 (2017), pp. 1–8.
- [11] B. Ziaja, R. A. London, and J. Hajdu. "Ionization by impact electrons in solids: Electron mean free path fitted over a wide energy range". In: *Journal of Applied Physics* 99.3 (Feb. 2006), p. 033514. ISSN: 00218979. DOI: 10.1063/1.2161821.
- [12] W. Nolting. *Grundkurs Theoretische Physik 1 Klassische Mechanik*. Springer Berlin Heidelberg, 2013. ISBN: 9783642299360. DOI: 10.1007/978-3-642-29937-7.
- [13] W. Bertozzi. "Speed and Kinetic Energy of Relativistic Electrons". In: *American Journal of Physics* 32.7 (1964), pp. 551–555. DOI: 10.1119/1.1970770.
- [14] T. Nöbauer et al. "Creation of ensembles of nitrogen-vacancy centers in diamond by neutron and electron irradiation". In: *arXiv preprint arXiv:1309.0453* (2013).
- [15] C. D. Clark, R. W. Ditchburn, and H. B. Dyer. "The Absorption Spectra of Natural and Irradiated Diamonds". In: *Proceedings of the Royal Society of London. Series A. Mathematical and Physical Sciences* 234.1198 (Feb. 1956), pp. 363–381. ISSN: 1364-5021, 1471-2946. DOI: 10.1098/rspa.1956.0040.
- [16] A. T. Collins, H. Kanda, and H. Kitawaki. "Colour changes produced in natural brown diamonds by high-pressure, high-temperature treatment". In: *Diamond and Related Materials* 9.2 (Mar. 2000), pp. 113–122. ISSN: 09259635. DOI: 10.1016/S0925-9635(00)00249-1.
- [17] E. Gaillou and G. R. Rossman. "Color in Natural Diamonds: The Beauty of Defects". In: *Rocks & Minerals* 89.1 (2014), pp. 66–75. DOI: 10.1080/00357529.2014.842839.
- [18] I. I. Vlasov et al. "Relative abundance of single and vacancy-bonded substitutional nitrogen in CVD diamond". In: *Physica Status Solidi (A) Applied Research* 181.1 (2000), pp. 83–90. ISSN: 00318965. DOI: 10.1002/1521-396X(200009)181:1<83::AID-PSSA83>3.0.CO;2-6.
- [19] A. M. Edmonds et al. "Production of oriented nitrogen-vacancy color centers in synthetic diamond". In: *Physical Review B* 86.3 (2012), p. 35201. DOI: 10.1103/PhysRevB.86.035201.
- [20] A. Tallaire et al. "Highly photostable NV centre ensembles in CVD diamond produced by using N₂O as the doping gas". In: *Applied Physics Letters* 111.14 (2017), p. 143101. DOI: 10.1063/1.5004106.
- [21] F. P. Bundy et al. "The pressure-temperature phase and transformation diagram for carbon; updated through 1994". In: *Carbon* 34.2 (1996), pp. 141–153. ISSN: 00086223. DOI: 10.1016/0008-6223(96)00170-4.
- [22] Y. Chen and L. Zhang. "Understanding the Material Removal Mechanisms". In: *Polishing of Diamond Materials*. Springer, 2013, pp. 11–23. DOI: 10.1007/978-1-84996-408-1_2.
- [23] I. A. Dobrinets, V. G. Vins, and A. M. Zaitsev. *HPHT-Treated Diamonds*. Vol. 181. Springer, 2013. ISBN: 978-3-642-37489-0. DOI: 10.1007/978-3-642-37490-6.
- [24] T. R. Anthony. "Metastable synthesis of diamond". In: *Vacuum* 41.4 (1990), pp. 1356–1359. DOI: 10.1016/0042-207X(90)93956-J.
- [25] G. Davies and T. Evans. "Graphitization of diamond at zero pressure and at a high pressure". In: *Proceedings of the Royal Society of London* 328.1972 (June 1972), pp. 413–427. ISSN: 1364-5021. DOI: 10.1098/rspa.1972.0086.
- [26] P. John et al. "The oxidation of (100) textured diamond". In: *Diamond and Related Materials* 11.3-6 (Mar. 2002), pp. 861–866. ISSN: 09259635. DOI: 10.1016/S0925-9635(01)00673-2.
- [27] R. A. Khmel'nitsky and A. A. Gippius. "Transformation of diamond to graphite under heat treatment at low pres-

- sure". In: *Phase Transitions* 87.2 (2014), pp. 175–192. DOI: 10.1080/01411594.2013.807429.
- [28] T. Evans et al. "A Study of the Transformation of Diamond to Graphite A study of the transformation of diamond to graphite". In: *Society* 277.1369 (Jan. 1964), pp. 260–269. ISSN: 1364-5021. DOI: 10.1098/rspa.1964.0020.
- [29] T. Evans, Z. Qi, and J. Maguire. "The stages of nitrogen aggregation in diamond". In: *Journal of Physics C: Solid State Physics* 14.12 (Apr. 1981), pp. L379–L384. ISSN: 0022-3719. DOI: 10.1088/0022-3719/14/12/005.
- [30] A. Shatskiy et al. "Boron-doped diamond heater and its application to large-volume, high-pressure, and high-temperature experiments". In: *Review of Scientific Instruments* 80.2 (Feb. 2009), p. 023907. ISSN: 00346748. DOI: 10.1063/1.3084209.
- [31] A. Vinke, G. Marbach, and J. Vinke. *Chemie für Ingenieure*. ISBN: 9783486780963.
- [32] A. Mainwood. "Nitrogen and nitrogen-vacancy complexes and their formation in diamond". In: *Physical Review B* 49.12 (Mar. 1994), pp. 7934–7940. ISSN: 01631829. DOI: 10.1103/PhysRevB.49.7934.
- [33] A. A. Shiryaev, D. J. Frost, and F. Langenhorst. "Impurity diffusion and microstructure in diamonds deformed at high pressures and temperatures". In: *Diamond and Related Materials* 16.3 (2007), pp. 503–511. ISSN: 0925-9635. DOI: <https://doi.org/10.1016/j.diamond.2006.10.001>.
- [34] H. Pinto et al. "On the diffusion of NV defects in diamond". In: *Physica Status Solidi (A) Applications and Materials Science* 209.9 (Sept. 2012), pp. 1765–1768. ISSN: 18626300. DOI: 10.1002/pssa.201200050.
- [35] G. Davies et al. "Vacancy-related centers in diamond". In: *Physical Review B* 46.20 (Nov. 1992), pp. 13157–13170. ISSN: 01631829. DOI: 10.1103/PhysRevB.46.13157.
- [36] C. B. Hartland. *A study of point defects in CVD diamond using electron paramagnetic resonance and optical spectroscopy*. Aug. 2014. URL: <http://wrap.warwick.ac.uk/id/eprint/67156>.
- [37] I. Kiflawi et al. "The aggregation of nitrogen and the formation of A centres in diamonds". In: *Diamond and Related Materials* 6.11 (Oct. 1997), pp. 1643–1649. ISSN: 09259635. DOI: 10.1016/S0925-9635(97)00207-0. URL: <http://www.sciencedirect.com/science/article/pii/S0925963597002070>.
- [38] J. Goss et al. "Extended defects in diamond: The interstitial platelet". In: *Physical Review B* 67.16 (Apr. 2003), pp. 1–15. ISSN: 0163-1829. DOI: 10.1103/PhysRevB.67.165208.
- [39] R. Jones et al. "Diffusion of nitrogen in diamond and the formation of A-centres". In: *Diamond and Related Materials* 53. Supplement C (2015), pp. 35–39. DOI: 10.1016/j.diamond.2015.01.002.
- [40] A. T. Collins et al. "High-temperature annealing of optical centers in type-I diamond". In: *Journal of Applied Physics* 97.8 (Apr. 2005), p. 083517. ISSN: 00218979. DOI: 10.1063/1.1866501.
- [41] F. De Weerd and A. T. Collins. "HPHT annealing of natural diamond". In: *New Diam. Front. Carbon Technol* 17.2 (2007), pp. 91–103.
- [42] R. M. Chrenko, R. E. Tuft, and H. M. Strong. "Transformation of the state of nitrogen in diamond". In: *Nature* 270. November (Nov. 1977), pp. 141–144. ISSN: 0028-0836. DOI: 10.1038/270141a0.
- [43] T. Evans and Z. Qi. "The Kinetics of the Aggregation of Nitrogen Atoms in Diamond". In: *Proceedings of the Royal Society A: Mathematical, Physical and Engineering Sciences* 381.1780 (May 1982), pp. 159–178. ISSN: 1364-5021. DOI: 10.1098/rspa.1982.0063.
- [44] S. C. Rand and L. G. DeShazer. *Solid state laser employing diamond having color centers as a laser active material*. 1985. URL: <https://www.google.com/patents/WO1986003347A1?c1=en>.
- [45] J. Bernholc et al. "Mechanism of self-diffusion in diamond". In: *Phys. Rev. Lett.* 61.23 (Dec. 1988), pp. 2689–2692. DOI: 10.1103/PhysRevLett.61.2689.
- [46] E. B. Lombardi et al. "Computational models of the single substitutional nitrogen atom in diamond". In: *Journal of Physics: Condensed Matter* 15.19 (May 2003), pp. 3135–3149. ISSN: 0953-8984. DOI: 10.1088/0953-8984/15/19/314.
- [47] J. R. Kim et al. "High pressure and high temperature annealing on nitrogen aggregation in lab-grown diamonds". In: *Journal of materials science* 46.19 (2011), pp. 6264–6272. DOI: 10.1007/s10853-011-5383-1.
- [48] A. T. Collins. "Vacancy enhanced aggregation of nitrogen in diamond". In: *Journal of Physics C: Solid State Physics* 13.14 (May 1980), pp. 2641–2650. ISSN: 0022-3719. DOI: 10.1088/0022-3719/13/14/006.
- [49] M. W. Dale. "Colour centres on demand in diamond". PhD thesis. University of Warwick, 2015. URL: <http://wrap.warwick.ac.uk/id/eprint/80044>.
- [50] Y. Mita et al. "Photochromism of H2 and H3 centres in synthetic type Ib diamonds". In: *Journal of Physics: Condensed Matter* 2.43 (Oct. 1999), pp. 8567–8574. ISSN: 0953-8984. DOI: 10.1088/0953-8984/2/43/002.
- [51] S. C. Lawson et al. "The 'H2' optical transition in diamond: the effects of uniaxial stress perturbations, temperature and isotopic substitution". In: *Journal of Physics: Condensed Matter* 4.13 (Mar. 1992), pp. 3439–3452. ISSN: 0953-8984. DOI: 10.1088/0953-8984/4/13/008.
- [52] A. T. Collins. "The colour of diamond and how it may be changed". In: *Journal of Gemmology* 27.6 (2001), pp. 341–359. URL: https://gem-a.com/images/Documents/JoG/Archive/JoG2001_27_6.pdf#page=23.
- [53] L. A. Bunsnl and R. W. Grusmn. "Aggregation and dissolution of small and extended defect structures in type Ia diamond". In: *American Mineralogist* 70 (1985), p. 608418.
- [54] K. T. Takeru Nakashima, Shuichi Satoh. *Diamond laser crystal and method manufacturing the same*. Aug. 1990. URL: <https://www.google.com/patents/US4950625>.
- [55] K. Iakoubovskii and G. J. Adriaenssens. "Trapping of vacancies by defects in diamond". In: *Journal of Physics: Con-*

- densed Matter* 13.26 (2001), p. 6015. DOI: 10.1088/0953-8984/13/26/316.
- [56] G. Davies. "Current problems in diamond: Towards a quantitative understanding". In: *Physica B: Condensed Matter* 273-274 (Dec. 1999), pp. 15-23. ISSN: 09214526. DOI: 10.1016/S0921-4526(99)00398-1.
- [57] IUPAC. *Compendium of Chemical Terminology, 2nd ed. (the "Gold Book")*. Compiled by A. D. McNaught and A. Wilkinson. XML on-line corrected version: <http://goldbook.iupac.org> (2006-) created by M. Nic, J. Jirat, B. Kosata; updates compiled by A. Jenkins. Blackwell Scientific Publications, Oxford (1997). DOI: 10.1351/goldbook.
- [58] A. T. Collins and I. Kiflawi. "The annealing of radiation damage in type Ia diamond." en. In: *Journal of physics. Condensed matter : an Institute of Physics journal* 21.36 (Sept. 2009), p. 364209. ISSN: 0953-8984. DOI: 10.1088/0953-8984/21/36/364209.
- [59] A. M. Zaitsev. *Optical Properties of Diamond : A Data Handbook*. Springer, 2001, p. 502. ISBN: 354066582X. DOI: 10.1007/978-3-662-04548-0.
- [60] M. R. Brozel, T. Evans, and R. F. Stephenson. "Partial dissociation of nitrogen aggregates in diamond by high temperature-high pressure treatments". In: *Proceedings of the Royal Society of London A: Mathematical, Physical and Engineering Sciences* 361.1704 (1978), pp. 109-127. ISSN: 0080-4630. DOI: 10.1098/rspa.1978.0094.
- [61] J. Van Royen and Y. N. Pal'yanov. "High-pressure-high-temperature treatment of natural diamonds". In: *Journal of Physics: Condensed Matter* 14.44 (2002), p. 10953. DOI: 10.1088/0953-8984/14/44/408.
- [62] F. De Weerd and A. T. Collins. "The influence of pressure on high-pressure, high-temperature annealing of type Ia diamond". In: *Diamond and Related Materials* 12.3-7 (Mar. 2003), pp. 507-510. ISSN: 09259635. DOI: 10.1016/S0925-9635(02)00319-9.
- [63] X. J. Hu et al. "The diffusion of vacancies near a diamond (001) surface". In: *Solid state communications* 122.1 (2002), pp. 45-48. DOI: 10.1016/S0038-1098(02)00069-8.
- [64] J. Orwa et al. "An upper limit on the lateral vacancy diffusion length in diamond". In: *Diamond and Related Materials* 24 (Apr. 2012), pp. 6-10. ISSN: 0925-9635. DOI: 10.1016/J.DIAMOND.2012.02.009.
- [65] I. A. Dobrinets, V. G. Vins, and A. M. Zaitsev. *Diamonds Used for HPHT Treatment*. Berlin, Heidelberg: Springer Berlin Heidelberg, 2013, pp. 5-25. ISBN: 978-3-642-37490-6. DOI: 10.1007/978-3-642-37490-6_2.
- [66] G. P. Bulanova. "The formation of diamond". In: *Journal of Geochemical Exploration* 53.1-3 (1995), pp. 1-23. DOI: 10.1016/0375-6742(94)00016-5.
- [67] R. C. DeVries. "Plastic deformation and "work-hardening" of diamond". In: *Materials Research Bulletin* 10.11 (1975), pp. 1193-1199. ISSN: 00255408. DOI: 10.1016/0025-5408(75)90026-4.
- [68] T. Evans and P. Rainey. "Changes in the defect structure of diamond due to high temperature+ high pressure treatment". In: *Proceedings of the Royal Society of London A: Mathematical, Physical and Engineering Sciences*. Vol. 344. 1636. The Royal Society, 1975, pp. 111-130. DOI: 10.1098/rspa.1975.0093.
- [69] K. T. Koga, J. A. Van Orman, and M. J. Walter. "Diffusive relaxation of carbon and nitrogen isotope heterogeneity in diamond: a new thermochronometer". In: *Physics of the Earth and Planetary Interiors* 139.1 (2003), pp. 35-43. DOI: 10.1016/S0031-9201(03)00141-9.
- [70] *Elite Furnaces - 1200 Single Zone Tube Furnaces*. URL: <http://www.elitefurnaces.com/eng/products/furnaces/1200%20Single%20Zone%20Tube%20Furnaces.php> (visited on 01/04/2019).
- [71] R. C. Liebermann. "Multi-anvil, high pressure apparatus: a half-century of development and progress". In: *High Pressure Research* 31.4 (Dec. 2011), pp. 493-532. ISSN: 0895-7959. DOI: 10.1080/08957959.2011.618698. URL: <http://www.tandfonline.com/doi/abs/10.1080/08957959.2011.618698>.
- [72] J. Chantel. "Measurement of elastic properties of silicates at realistic mantle pressures". PhD thesis. Bayreuth, 2012, pp. 1-154. URL: <https://epub.uni-bayreuth.de/83/>.
- [73] N. Kawai and S. Endo. "The Generation of Ultrahigh Hydrostatic Pressures by a Split Sphere Apparatus". In: *Review of Scientific Instruments* 41.8 (Aug. 1970), pp. 1178-1181. ISSN: 0034-6748. DOI: 10.1063/1.1684753. URL: <http://aip.scitation.org/doi/10.1063/1.1684753>.
- [74] D. Walker, M. A. Carpenter, and C. M. Hitch. "Some simplifications to multianvil devices for high pressure experiments". In: *American Mineralogist* 75.9-10 (1990), pp. 1020-1028. ISSN: 0003004X. URL: http://www.minsocam.org/ammin/AM75/AM75_1020.pdf.

4

Defect quantification and spectroscopic methods

Contents

4.1 Defect quantification in diamond	68
Absorption coefficient	68
4.2 Dispersive spectroscopy	71
Spectrometer setup	71
Absorption spectroscopy	72
Spectral sensitivity	73
4.3 Fourier transform spectroscopy	74
4.4 EPR spectroscopy	76
4.5 Summary	78
References	79

4.1 Defect quantification in diamond

THE INTRODUCTION of any defect into the diamond lattice breaks the lattice symmetry. This makes one-phonon absorption processes possible. The shape and location of these absorption features are characteristic for the specific defect. The strength of the absorption can be used to determine the concentration of the defect [1, 2]. Literature calibration constants and the defect ZPL¹s measured at low temperatures with optical spectroscopy techniques are used to calculate defect concentrations in this work.

¹ Zero Phonon Line

Absorption coefficient

The Beer–Lambert law describes the attenuation of light travelling through a material connected to two sample properties: the concentrations of the attenuating species and the thickness of the material d .

The transmittance $T(\lambda)$ of a sample can be expressed as the fraction of the intensity of the incident light beam I_0 and the intensity of the light beam after it passed through the sample I , neglecting Fresnel reflection at the interfaces. Both can be measured experimentally.

$$T(\lambda) = \frac{I(d, \lambda)}{I_0} = \exp(-\alpha(\lambda) \cdot d) = 10^{-A} \quad (4.1)$$

A is called absorbance. The absorption coefficient $\alpha(\lambda)$

$$\alpha(\lambda) = -\frac{\ln(T)}{d} = \frac{\ln(10)}{d} \cdot A \quad (4.2)$$

is the product of the concentration and the absorption cross-section $\sigma_{abs}(\lambda)$.

The concentration of the defect X , $[X]$, can be linked to the absorption coefficient at a certain wavelength via calibration constants. The total integrated strength of an electronic absorption is proportional to the concentration of the defect. Room temperature absorption can be very broad. Cooling the sample shifts the intensity of the absorption from the phonon sideband to the ZPL. This allows to estimate the concentration of a defect in a sample through the strength of the ZPL at a specified temperature.

For UV-VIS² measurements the strength of the absorption A_X is linked to the relevant calibration constant f via:

² UltraViolet-Visible

$$[X]_{UV-VIS} = \frac{A_X}{f} \quad (4.3)$$

f is the calibration constant in $meV \cdot cm^2$, $[X]$ the concentration in cm^{-3} (which can be expressed in ppm³ by $[X]_{ppm} = [X]/(1.77 \cdot 10^{17} cm^{-3})$). A_X is the strength of the absorption caused by defect X (after subtraction

³ parts per million ($1.77 \cdot 10^{17} cm^{-3}$ for diamond)

of the background) in $meV \cdot cm^{-1}$ obtained by integration of the absorption coefficient at the photon energy E over the defect ZPL [3]:

$$A_X = \int_{ZPL} dE \alpha(E) \quad (4.4)$$

Literature calibration constants for important diamond defects in the UV-VIS are presented in table 4.1.

Absorption spectrum at 80 K				
Defect	ZPL		Calibration constant [$meV \text{ cm}^2$]	Reference
	[nm]	[eV]		
V^0	741	1.673	$(1.2 \pm 0.3) \cdot 10^{-16}$	[3]
V^-	394	3.150	$(4.8 \pm 0.2) \cdot 10^{-16}$	[3]
NV^0	575	2.156	$(9.8 \pm 0.6) \cdot 10^{-17}$	[4]
NV^-	637	1.945	$(1.7 \pm 0.08) \cdot 10^{-16}$	[4]
N_2V^0	503	2.462	$(7.7 \pm 1.2) \cdot 10^{-17}$	[4]
N_2V^-	986.3	1.256	$(6.8 \pm 1) \cdot 10^{-17}$	[4]
N_3V^0	415	2.985	$(8.6 \pm 2) \cdot 10^{-17}$	[5]

Table 4.1: Calibration constants for absorption data taken at 80 K in literature

For IR⁴ measurements the calibration constant is directly linked to the absorption coefficient at a characteristic wavenumber [6]:

$$[X]_{IR} = \alpha(\lambda) \cdot f \quad (4.5)$$

f is the calibration constant in $ppm \cdot cm$, $[X]$ the concentration in ppm and $\alpha(\lambda)$ the absorption coefficient of the characteristic feature in cm^{-1} .

⁴ InfraRed (0.78-1000 μm)

FTIR spectrum at room temperature			
Defect	Wavenumber	Calibration constant [ppm cm]	Reference
	[cm^{-1}]		
N_s^0	1344	37 ± 1	[7]
N_s^0	1130	25 ± 2	[6]
N_s^+	1332	5.5 ± 1	[7]
N_2	1282	16.5 ± 1	[8]
N_4V	1282	79.4 ± 8	[9]

Table 4.2: Calibration constants for FTIR data taken at room temperature in literature

Literature calibration constants for important diamond defects are presented in table 4.2.

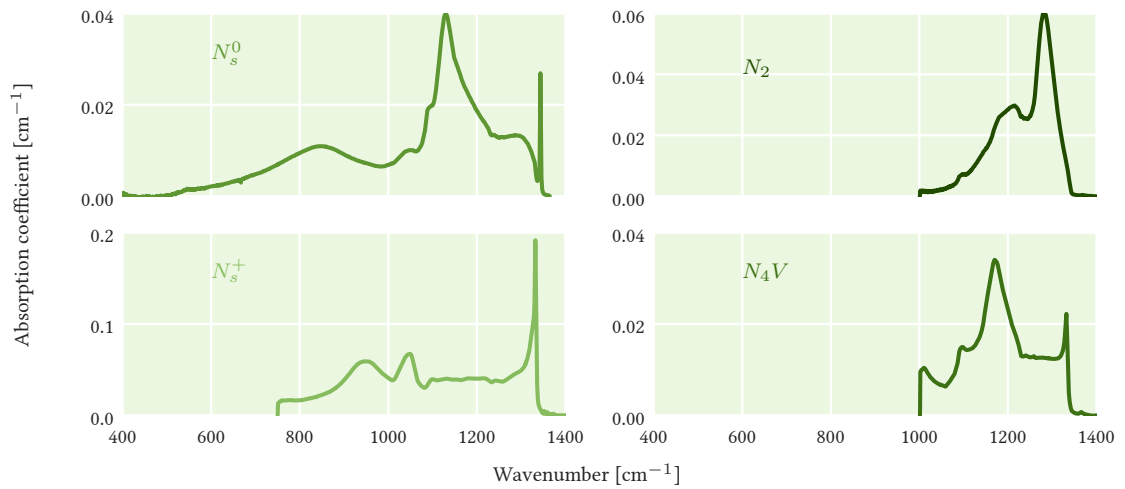


Figure 4.1: Calibration spectra for nitrogen in the IR. Each spectrum represents a concentration of 1 ppm of nitrogen in the respective form of the defect [4].

In practice the program *SpectrumManipulator*, developed by M. Dale from the Diamond Group at the University of Warwick [4], was used in this work for the deconvolution of measured IR absorption spectra and quantification of nitrogen defects. The strength of the two-phonon absorption is proportional to the thickness of the samples. This is used as a standard to normalize the IR absorption spectra of diamond samples according to their thickness. Characteristic one-phonon spectra for each of the defects were calibrated using the constants in table 4.2.

The calibrated spectra are presented in fig. 4.1. These can be used to fit a measured spectrum and determine both the concentration of nitrogen as well as its aggregation form [4].

For N_s ⁵-V⁶ related defects the characteristic absorption features lie in the UV-VIS (see table 2.3). The absorption is measured at low temperatures to resolve the corresponding ZPL. After subtraction of the background, the ZPL is integrated and concentrations are determined using calibration constants in table 4.1.

For single N_s and its aggregates characteristic features lie in the IR spectrum. Measured spectra are normalized and then deconvoluted with the spectra in fig. 4.1 using the *SpectrumManipulator*.

⁵ Single substitutional nitrogen (C centre)

⁶ Lattice vacancy

4.2 Dispersive spectroscopy

SPECTROSCOPIC MEASUREMENTS in the UV-VIS are used to characterise certain defects in diamond, most importantly for this work N_s -V complexes. As described in the previous section, the absorption at certain wavelengths can give us quantitative and qualitative information about the defect composition of a sample.

For the purpose of this work a short overview of the optical spectroscopy of solids is given in this section based on [10].

A solid sample is illuminated by a light beam of intensity I_0 . The intensity of the light beam after passing through the sample can be attenuated by absorption, reflection and scattering processes. Absorption in the material happens when the frequency of the beam is resonant with a ground state to excited state transition of the atoms in the material. The intensity of the light beam after the sample I , corrected for reflection and scattering processes, and the initial intensity I_0 are used to determine the absorption coefficient of a sample.

In some cases the deexcitation happens through the emission of photons, usually at a lower frequency. The emitted light is measured and analysed in luminescence spectroscopy. Luminescence spectra are an additional source of information and have been used to measure luminescence lifetime and estimate the QY⁷ and emission cross-section of NV⁸ and N_2V^0 ⁹ as described in section 6.2, Key parameters for solid state lasers. The details of luminescence spectroscopy and luminescence lifetime measurements are described in section 6.3, Luminescence spectroscopy.

Spectrometer setup

In a spectrometers a light beam is spatially separated into its wavelength components, making it possible to measure the intensity at a given wavelength. A simple spectroscopic setup consists of a light source, a dispersive optical element and a detector. There are two approaches to record the full spectrum, point and array detectors. The setup for a single point detector and for a CCD detector can be seen in fig. 4.2.

In a point detector the spectrum is recorded by rotation of the diffraction grating in the monochromator, recording the signal for each interval. The intensity is measured by a detector over a narrow wavelength range at a time. The grating, slit width and the acquisition time used determine the sensitivity and resolution of the spectrum.

In a CCD¹⁰ detector a fixed diffraction grating and an array of detectors are used. CCD spectrometers are relatively compact, as there is no

⁷ Quantum Yield

⁸ A substitutional nitrogen adjacent to a vacancy with a C_{3v} symmetry

⁹ The neutrally charged state of N_2V (H3)

¹⁰ Charge-Coupled Device

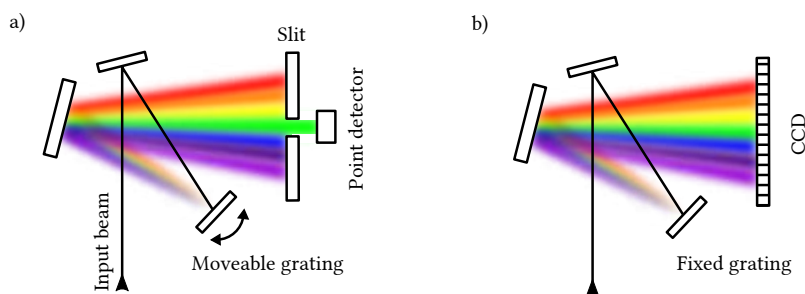


Figure 4.2: Two types of dispersion spectrometers. a) Moveable diffraction grating. The light is directed through a slit to a detector. b) Fixed diffraction grating with CCD detector. Adapted from [4].

need for moving parts in the setup. They typically have a lower resolution and sensitivity in comparison to what can be achieved by a dispersive spectrometer with a point detector.

Absorption spectroscopy

Room temperature UV-VIS measurements were taken with a Varian Cary 5000 UV-VIS-NIR spectrometer. This is a dual beam spectrometer with a wavelength range from 190 - 3300 nm. The UV-VIS detector is a R928 PMT¹¹ and the IR detector a cooled PbS¹² photocell. The spectrometer was operated at a resolution of 1 nm for all measurements in this thesis.

The setup of a dual beam spectrometer is illustrated in fig. 4.3. In such a system the intensity of the initial beam I_0 and the beam after the sample I are collected at the same time. In a single beam setup a additional reference scan has to be performed to calculate the absorption. This makes measurements taken with dual beam spectrometers less sensitive to fluctuations caused by the light source or detector.

¹¹ PhotoMultiplier Tube

¹² Lead sulfide

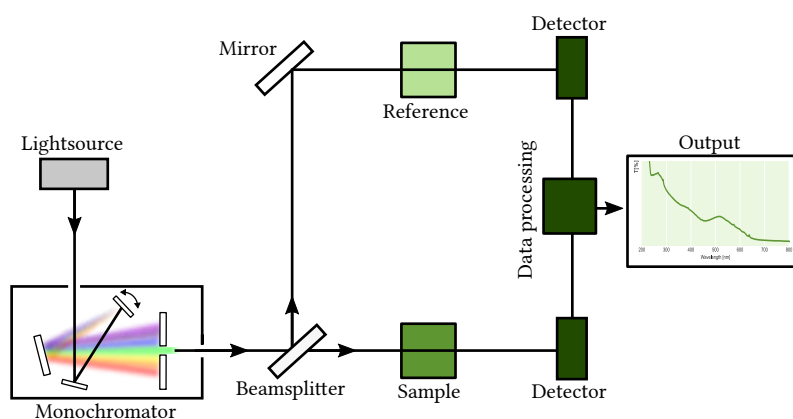


Figure 4.3: Schematic of a double beam UV-VIS spectrometer [10].

UV-VIS measurements at cryogenic temperatures were measured in collaboration with the University of Warwick.

Spectra were recorded with a PerkinElmer Lambda 1050 spectrometer at 1 nm resolution. A deuterium lamp is used inside the spectrometer for the UV¹³ wavelength range ($175 < \lambda < 319$ nm) and a tungsten filament halogen lamp for the NIR¹⁴-VIS¹⁵ range ($319 < \lambda < 3300$ nm). The light is depolarized, monochromated and alternated between sample and reference beam with a rotating mirror. Both sample and reference beam are focused onto the detector. A InGaAs¹⁶ detector is used for NIR measurements and a PMT for UV-VIS.

The sample was placed into an Oxford Instruments continuous flow cryostat, mounted onto an aperture with indium. The temperature was regulated by a heater set by an Oxford Instruments ITC5035 intelligent temperature controller. Measurements were performed at liquid nitrogen temperature (77 K).

Spectral sensitivity

If not otherwise specified then the spectral sensitivity of the detection system was calibrated using an Ocean Optics HL-2000-FHSA tungsten lamp. As an approximation the HL-2000 bulb can be treated as a blackbody source with a colour temperature of 2500 K¹⁷. According to Planck's law the spectral radiance of a body $I(\lambda, T)$ is dependent on the wavelength λ and the temperature T via:

$$I(\lambda, T) = \frac{2hc^2}{\lambda^5} \cdot \frac{1}{e^{hc/\lambda k_B T} - 1} \quad (4.6)$$

with the Boltzmann constant k_B , the Planck constant h , and the speed of light in the medium c .

The normalized theoretical spectrum obtained by eq. (4.6) is then divided by the normalized measured spectrum of the tungsten lamp to obtain the spectral response as a function of the wavelength.

¹³ UltraViolet (10-380 nm)

¹⁴ Near-InfraRed (0.78-3 μ m)

¹⁵ Visible (380-780 nm)

¹⁶ Indium gallium arsenide

¹⁷ Private communication with Nick Barnett, Ocean Optics EMEA

4.3 Fourier transform spectroscopy

SPECTROSCOPIC MEASUREMENTS in the IR can be used to determine the state of aggregation and quantity of nitrogen in diamond. This has been covered in section 4.1, Defect quantification in diamond. In this section the technique to measure spectra in the IR is introduced.

In contrast to a dispersive spectrometer, Fourier transform spectroscopy collects high spectral resolution data over a large wavelength range at the same time [10]. A beam containing many different wavelengths at once is directed into a Michelson Interferometer. An illustration of such a setup is shown in fig. 4.4.

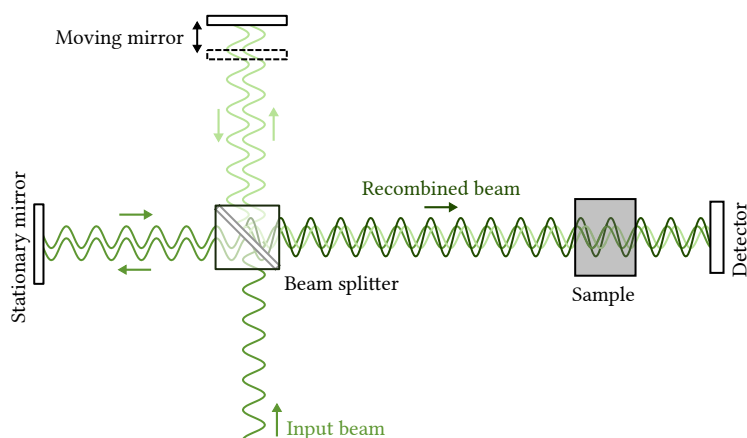


Figure 4.4: A Michelson interferometer in a FTIR setup. Light from a broadband source is split by a beam splitter. One split beam is reflected by a stationary mirror. The other split beam is reflected by a movable mirror, changing the path the light has to travel by the mirror movement. The beam going through the sample is a recombination of both beams. Adapted from [4].

The beam is directed into a beam splitter, which splits it in two directions. One towards a stationary mirror, the other towards a mobile one attached to a motor. The beams are reflected off the mirrors and recombined by the same beam splitter before entering a detector. The mobile mirror will change the length of the optical path of one beam. The two beams will arrive for recombination at the beam splitter either in phase or out of phase, causing constructive or destructive interference. The intensity measured at the detector, as a function of the path difference, is called interferogram. If a wide band light source is used, the interferogram measured by the detector is a sum of the monochromatic interferograms of each wavelength component. The interferogram can be converted into a spectrum by inverse Fourier transform.

FTIR¹⁸ spectrometer have some advantages over dispersive spectrometers:

¹⁸ Fourier Transform Infra Red

- The input beam has a broad spectrum so light from many different wavelengths is collected simultaneously. The signal to noise ratio is improved in comparison to dispersive spectroscopy measurements for measurements where the signal noise is mostly caused by detector noise. (The improvement scales with \sqrt{m} , where m is the number of sample points in the spectrum) (Fellgett's advantage)
- The light that reaches the detector in a dispersive spectrometer is limited by the entrance and exit slits of the monochromator. This is not the case in an FTIR spectrometer. (Jacquinot's advantage)
- The measurements are constantly calibrated against a HeNe¹⁹ laser used as reference wavelength. (Conne's advantage)

Fourier transform based spectrometer in the UV-VIS region are possible in principle. But the advantages of signal averaging are not as significant in the UV-VIS region as in the IR. In the detector used for light in the UV-VIS (typically photomultipliers), the noise is caused by the incoming radiation and is proportional to \sqrt{m} , exactly offsetting Fellgett's advantage. Detectors in the IR react to thermal fluctuations and are more prone to thermal noise by the environment and not the IR radiation itself [11]. Additionally, if a sample is photosensitive the higher throughput of light can cause charge transfers in a sample, as for example in certain defects in diamond mentioned earlier. Because of that it is common to use dispersive spectrometer in the UV-VIS region and Fourier transform spectrometer in the IR.

IR measurements were taken with a bench-top FTIR spectrometer at the University of Strathclyde, or with a higher resolution FTIR spectrometer with a nitrogen-gas purged chamber at the University of Warwick. At the University of Strathclyde an Agilent Cary 630 FTIR spectrometer with a spectral resolution $< 2 \text{ cm}^{-1}$ was used. At the University of Warwick a Perkin Elmer Spectrum-GX with a wavenumber range of $370 - 3300 \text{ cm}^{-1}$ and a resolution set to 1 cm^{-1} was used. For all measurements a 5x beam condenser was used, changing the beam diameter to $\sim 1 \text{ mm}$. The sample was placed on top of a (1 mm) aperture with the beam going through the sample vertically. The sample chamber was continuously purged with a nitrogen gas in order to avoid absorption from H_2O and CO_2 in the atmosphere. The spectral region and transmission of these in comparison to type IIa diamond can be seen in fig. 4.5. As can be seen, CO_2 and H_2O can add noise to the diamond spectra in regions that are useful for the characterisation of a diamond sample.

¹⁹ Helium-Neon

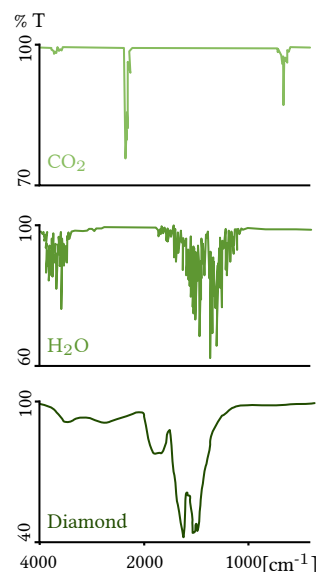


Figure 4.5: Comparison of the transmission spectrum of Top: CO_2 , Middle: H_2O , Bottom: Diamond, in the range between $4000\text{-}500 \text{ cm}^{-1}$ [12, 13].

4.4 EPR spectroscopy

PARAMAGNETIC POINT DEFECTS in diamond can be characterized by EPR²⁰ measurements. The measurements have been carried out and evaluated by members of the Diamond Research Group at the University of Warwick, UK. A Bruker EMX spectrometer was used for the measurements. In this section a short introduction to the technique is given.

²⁰ Electron Resonance Paramagnetic

EPR is a spectroscopic technique to study the transitions of unpaired electrons in a sample when placed in a magnetic field [14]. An illustration of the setup and working principle can be seen in fig. 4.6

The unpaired electron orients itself either parallel or antiparallel to the direction of the external magnetic field (Zeeman effect), creating two distinct energy levels that can be occupied (fig. 4.6 2). The electrons can be moved between the levels through absorption and emission of microwave radiation (fig. 4.6 3). Due to the Boltzmann-Maxwell distribution, there are more electrons in the lower energy level. To measure the absorption, which is proportional to the number of spins in the sample and hence the concentration of the relevant defect, the gap of the energy levels must match the energy of the microwaves. This can be done by either keeping the magnetic field constant and sweeping the microwave frequency or vice versa. In practice usually the microwave frequency is kept constant while sweeping through the magnetic field (fig. 4.6 4).

The concentration of paramagnetic defects like N_s^0 ²¹, NV^- ²² and N_2V^- ²³ can be quantified by EPR measurements [4, 15]. Despite having an unpaired electron, the signal from NV^0 ²⁴ is presumably too broad for EPR detection [16]. NV^- has an extra electron forming a spin $S=1$ pair with one of the vacancy electrons. In that way the $m_s = \pm 1$ and $m_s = \pm 2$ transitions can be measured [4]. N_2V^0 is diamagnetic and therefore doesn't yield an EPR signal [15].

²¹ Neutrally charged N_s

²² The negative form of NV

²³ The negatively charged state of N_2V (H2)

²⁴ The neutral form of NV

In the scope of this work EPR measurements have been used to measure the N_s^0 and NV^- concentrations of a selection of samples.

1. EPR spectrometer setup

An EPR setup typically consists of a **microwave bridge**, a **magnet** and a **sample cavity**.

The microwave bridge includes a source and detector, together with a modulation input to accurately control the microwave power. The magnet is either an electromagnet or superconducting magnet, designed so that the magnetic field is constant across the sample. The sample cavity is a resonator that is designed to enhance the microwave field at the sample.

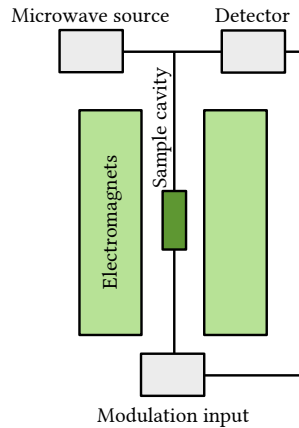
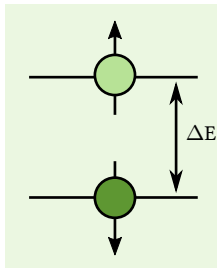


Figure 4.6: Schematic of an EPR setup. Adapted from [14].

2. Energy levels are separated by an magnetic field

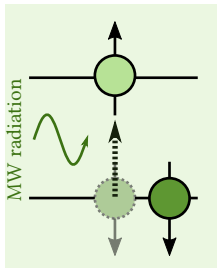


When an external magnetic field is applied, the unpaired electron's magnetic moment orients itself parallel or antiparallel to the direction of the field. According to the **Zeemann effect**, the splitting is directly proportional to the magnetic field:

$$\Delta E = g_e \mu_B B_0$$

with the g -factor g_e , the Bohr magneton μ_B and the magnetic field B_0 .

3. Electrons are moved between the levels by microwave radiation

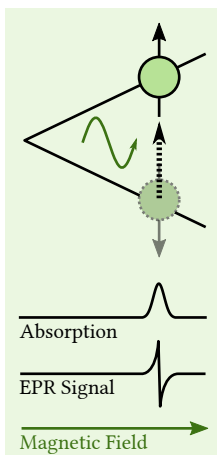


Electrons can be moved between those levels by absorption or emission of a photon with suitable energy. This leads to the **resonance condition**:

$$h\nu = \Delta E$$

with the Planck constant h and the frequency of the photons ν . Experimentally, the frequency often lies in the microwave region.

4. Absorption is measured by sweeping the magnetic field at constant microwave frequency



Due to the **Maxwell-Boltzmann distribution** there are typically more electrons in the lower energy level:

$$\frac{N_{upper}}{N_{lower}} = \exp\left(-\frac{\Delta E}{kT}\right)$$

with the number of paramagnetic centres N , the Boltzmann constant k and the temperature T .

The magnetic field strength is varied while the radiation frequency is kept constant. A net absorption that can be measured when the resonance condition is met.

The most common way to record and publish EPR spectra is to take the first derivative of the absorption spectrum.

The shape of the spectrum is determined by the interaction of the electron with its surroundings.

4.5 *Summary*

DEFECTS IN DIAMOND are quantified using calibration constants and the characteristic signal of the defect in the spectrum. Depending on the defect type, either UV-VIS spectra at 77 K (sample cooled with liquid nitrogen) or IR spectra are used for the quantification. Additionally, EPR spectroscopy can be used to precisely determine the concentration of paramagnetic defects. Most measurements were performed in collaboration with the University of Warwick. As far as possible the characterisation of each diamond sample after each treatment step was aimed for.

Single nitrogen and nitrogen clusters often have more complex spectra in the IR, as opposed to a single ZPL. The sample spectra have been deconvoluted, using the program SpectrumManipulator and appropriate reference spectra, to determine the concentrations of the defects.

Vacancies and nitrogen-vacancy complexes have features in the UV-VIS and their concentrations are estimated with the characteristic ZPLs.

The defect quantities throughout our synthesis attempt are presented in the following chapter, Results of the colour centre synthesis. The motivation for the synthesis protocols used and the assessment of the outcome are presented in chapter 6 and chapter 7.

References

- [1] J. Walker. "Optical absorption and luminescence in diamond". In: *Reports on Progress in Physics* 42.10 (1979), p. 1605. DOI: 10.1088/0034-4885/42/10/001.
- [2] A. M. Zaitsev. *Optical Properties of Diamond: A Data Handbook*. Springer, 2001, p. 502. ISBN: 354066582X. DOI: 10.1007/978-3-662-04548-0.
- [3] D. Twitchen et al. "Correlation between ND1 optical absorption and the concentration of negative vacancies determined by electron paramagnetic resonance (EPR)". In: *Diamond and Related Materials* 8.8 (1999), pp. 1572-1575. ISSN: 09259635. DOI: 10.1016/S0925-9635(99)00038-2.
- [4] M. W. Dale. "Colour centres on demand in diamond". PhD thesis. University of Warwick, 2015. URL: <http://wrap.warwick.ac.uk/id/eprint/80044>.
- [5] G. Davies. "Current problems in diamond: Towards a quantitative understanding". In: *Physica B: Condensed Matter* 273-274 (Dec. 1999), pp. 15-23. ISSN: 09214526. DOI: 10.1016/S0921-4526(99)00398-1.
- [6] I. Kiflawi et al. "Infrared absorption by the single nitrogen and A defect centres in diamond". In: *Philosophical Magazine Part B* 69.6 (June 1994), pp. 1141-1147. ISSN: 1364-2812. DOI: 10.1080/01418639408240184.
- [7] S. C. Lawson et al. "On the existence of positively charged single-substitutional nitrogen in diamond". In: *Journal of Physics: Condensed Matter* 10.27 (July 1998), pp. 6171-6180. ISSN: 0953-8984. DOI: 10.1088/0953-8984/10/27/016.
- [8] S. R. Boyd, I. Kiflawi, and G. S. Woods. "The relationship between infrared absorption and the A defect concentration in diamond". In: *Philosophical Magazine Part B* 69.6 (June 1994), pp. 1149-1153. ISSN: 1364-2812. DOI: 10.1080/01418639408240185.
- [9] S. R. Boyd, I. Kiflawi, and G. S. Woods. "Infrared absorption by the B nitrogen aggregate in diamond". In: *Philosophical Magazine Part B* 72.3 (Sept. 1995), pp. 351-361. ISSN: 1364-2812. DOI: 10.1080/13642819508239089.
- [10] J. Solé, L. Bausá, and D. Jaque. *An Introduction to the Optical Spectroscopy of Inorganic Solids*. 2005. DOI: 10.1002/0470016043.
- [11] M. F. Vitha. *Spectroscopy: principles and instrumentation*. ISBN: 9781119436607. URL: <https://www.wiley.com/en-bf/Spectroscopy%3A+Principles+and+Instrumentation-p-9781119436607>.
- [12] *Q: Is FTIR affected by the environment?: SHIMADZU (Shimadzu Corporation)*. URL: <http://www.shimadzu.com/an/ftir/support/faq/1.html> (visited on 08/07/2017).
- [13] *Gemology Online: Online Gemological Expertise*. URL: <https://www.gemologyonline.com/> (visited on 08/07/2017).
- [14] K. Rangelova. *EPR-The 'workhorse technique' that is still enabling scientists to break new ground after 70+ years*. Tech. rep. 2017. URL: https://www.europeanpharmaceuticalreview.com/wp-content/uploads/BBS.R.098-EPR-Whitepaper_LayoutFULL-1.pdf.
- [15] B. L. Green et al. "Electron paramagnetic resonance of the N2V - defect in N15-doped synthetic diamond". In: *Physical Review B* 92.16 (Oct. 2015), p. 165204. ISSN: 1098-0121. DOI: 10.1103/PhysRevB.92.165204.
- [16] S. Felton et al. "Electron paramagnetic resonance studies of the neutral nitrogen vacancy in diamond". In: *Physical Review B* 77.8 (Feb. 2008), p. 081201. ISSN: 1098-0121. DOI: 10.1103/PhysRevB.77.081201.

5

Results of the colour centre synthesis

Contents

5.1	Introduction	82
5.2	NV synthesis	85
	Synthesis using CVD diamonds	85
	Loaned, pre-treated CVD samples	87
5.3	N_2V^0 synthesis	90
	Synthesis using CVD diamonds	90
	Synthesis using Natural diamonds	92
5.4	Spectroscopic analysis	96
	Illustration of defect quantification	96
	CVD samples	97
	Natural samples	118
5.5	Summary	127
	References	128

5.1 Introduction

THE UNIQUE MATERIAL PROPERTIES of diamond make it an interesting material for optical applications. In particular, CVD grown diamond seems to be a promising candidate for colour centre¹ synthesis in synthetic diamond with laser applications in mind. The high optical quality and low parasitic defect concentration results in low background absorption and loss of luminescence due to quenching [2, 3, 4].

The samples studied in this work were intended for the study of laser related properties. The concentration required for 50% pump absorption was taken as a preliminary aim for the colour centre synthesis, which is discussed in section 6.5, A potential diamond colour centre laser. Based on literature values for the absorption cross sections and lifetimes [5, 6, 7, 8, 9] and a 2 mm sample thickness, the estimated concentrations required for 50% pump absorption are $\sim 0.6 \text{ ppm}^2$ for NV^- ³ and 0.9 ppm for N_2V^0 ⁴.

The conversion of NV^5 centres plateaus at half the initial nitrogen concentration [10] (see section 3.3). To achieve at least 0.6 ppm of NV , at least 1.2 ppm of nitrogen in the sample is needed. For the aggregation of N_2V^0 , where the aggregation of single nitrogen into pairs is a crucial first step, good conversion efficiency into the target colour centre is tough with low to moderate nitrogen concentrations and reasonable experimental parameters, as discussed in section 3.3. Therefore, N_2V^0 synthesis through NV assisted migration was explored in synthetic diamond with initial nitrogen concentrations below 5 ppm; and additionally in natural diamonds, where samples with fully aggregated nitrogen-pairs are available (type IaA) and where N_2V^0 can be produced by HPHT⁶ treatment of type IaAB samples.

All synthesis treatments were performed as described previously in chapter 3, Synthesis of colour centres in diamond.

Some CVD⁷ diamond samples were purchased as grown from Element Six and Applied Diamond, Inc. They were subjected to electron irradiation and annealing in order to generate NV . Eight samples were HPHT treated after the NV synthesis to generate N_2V^0 , of which one sample survived in sufficient optical quality to be presented here. Additionally, pre-treated samples have been loaned from Element Six and examined for their laser potential. Three samples with low amounts of N_2V^0 and leftover single nitrogen were irradiated and annealed to synthesise NV .

All synthetic samples had two parallel polished surfaces each when received and were repolished if they underwent HPHT treatment during the synthesis.

¹ A type of structural defect, which produces absorption and emission bands that are different to those of the pure crystal [1]

² parts per million ($1.77 \cdot 10^{17} \text{ cm}^{-3}$ for diamond)

³ The negative form of NV

⁴ The neutrally charged state of N_2V (H3)

⁵ A substitutional nitrogen adjacent to a vacancy with a C_{3v} symmetry

⁶ High Pressure High Temperature

⁷ Chemical Vapour Deposition

Natural samples used in this work have been kindly provided by Dr. Jeffrey W. Harris of the University of Glasgow. Samples available to us included IaA samples with an abundance of nitrogen (~ 1000 ppm) and IaB and IaAB samples with varying nitrogen concentrations (up to a few dozen ppm). All samples were received unpolished.

In this chapter only a subset of all the samples that were treated are shown. The samples have been selected for their promising characteristics: a large final concentration of the target colour centre, together with a relatively low background absorption in comparison to other samples, and good optical quality.

Figure 5.1 shows an illustration of the most important samples for this work, with an overview of treatment steps and initial single nitrogen and nitrogen aggregate concentrations, as well as final colour centre concentrations for NV and N_2V^0 . It can be seen that CVD grown samples started out with a few ppm of single nitrogen, while the selection of natural samples had a large quantity of nitrogen aggregates. A moderate amount (>0.5 ppm) of NV^0 ⁸ and NV^- could be generated in most CVD samples, with some traces of N_2V^0 . ppm level concentrations could only be achieved for the N_2V^0 synthesis in two natural samples.

Some samples started out with excess initial nitrogen (>100 ppm) or N_2 ⁹ centres (~ 1000 ppm) and all the luminescence was quenched as described in [11], despite large amounts (a few to tens of ppm) of the target colour centre being present. Some samples were destroyed during the synthesis. Either by excessive electron irradiation ($\sim 3.6 \cdot 10^{19}$ e/cm² at 14 MeV), which generated vacancy clusters and other complex damage, adding excessive absorption in the visible wavelength region, turning those samples dark-red to blackish (see section 3.1). Other samples were broken during HPHT treatment and the leftover pieces (if they did not fully turn into graphite) were too small to be repolished or reused.

⁸ The neutral form of NV

⁹ Two adjacent substitutional nitrogen atoms (A centre)

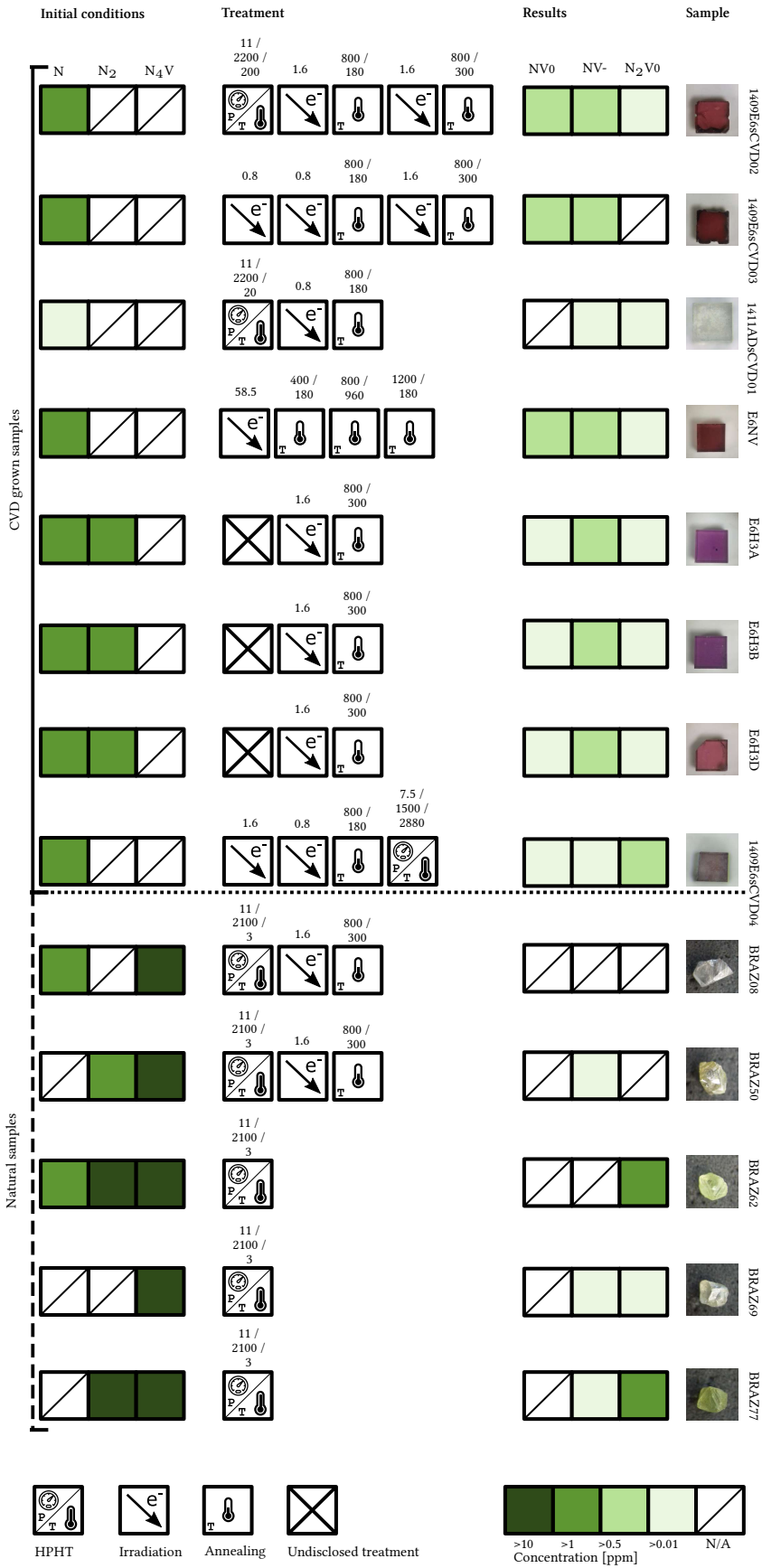


Figure 5.1: Overview over the most important samples in this work. From left to right:

Initial N_s, N₂ and N₄V concentrations.

Treatment sequence with HPHT (in GPa, °C and min), Irradiation (in 10⁻¹⁷ e/cm²) and Annealing (in °C and min).

Final NV⁰, NV⁻ and N₂V⁰ concentrations.

Photo and sample name.

5.2 NV synthesis

Synthesis using CVD diamonds

Two samples (1409E6sCVD02, 1409E6sCVD03) were obtained from Element Six as part of the same growth series. They were 3x3x2 mm in size. Their initial single nitrogen concentration was about 3.8 ppm, as determined by EPR¹⁰ measurements of one sample in the same series (1409E6sCVD05). All those samples had a brownish colouration, as can be seen in the leftmost picture of sample 1409E6sCVD02 in fig. 5.2.

Two samples (1411ADsCVD01 and 1411ADsCVD02) were obtained from Applied Diamond. They were 2x2x2 mm in size. After treatment, they were selected as reference samples with low colour centre concentrations and later used for analysis in chapter 7, Assessment of laser related properties. They had an initial single nitrogen concentration of 0.3 and 0.11 ppm as determined by EPR measurements of both samples.

¹⁰ Electron Paramagnetic Resonance

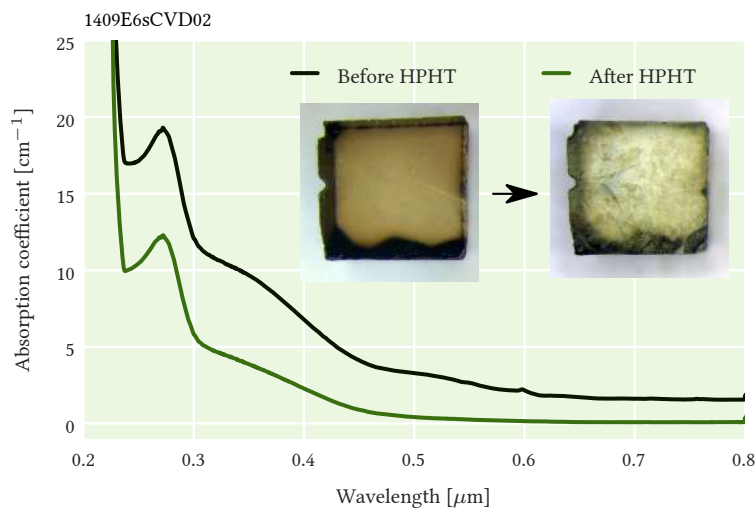


Figure 5.2: Absorption spectra of CVD diamond sample 1409E6sCVD02 before and after HPHT treatment. A reduction in brown color and a reduction in the absorption can be seen after treatment at 2200°C and 11 GPa for 20 minutes. Spectra corrected for Fresnel losses.

HPHT treatment at 2200°C and 11 GPa for 20 min of sample 1409E6sCVD02 was performed to reduce the brown color. Sample 1409E6sCVD03 was not HPHT treated as a comparison sample, to determine the effect of the HPHT treatment on the final outcome of the synthesis. As expected from literature [12], a weakening of the brown colouration and a lower background absorption in the visible can be seen in fig. 5.2, due to the removal of plastic deformation and vacancy clusters in the sample. Background absorption at the peak emission for NV⁻ (690 nm table 6.5) was reduced from 1.62 to 0.08 cm⁻¹, and at the peak emission for N₂V⁰ (525 nm table 6.5) from 3.02 to 0.31 cm⁻¹.

A small concentration of N_2V^0 (0.07 ppm, table 5.3) could be measured by absorption spectroscopy at liquid nitrogen temperature in the sample after subsequent irradiation (twice with $1.6 \cdot 10^{17} e/cm^2$ each) and annealing (800°C for 3h after first irradiation and 5h after second irradiation), indicating that at least 0.07 ppm of nitrogen pairs were generated after the HPHT treatment. Judging from the literature rate constants and assuming a temperature of 2200°C (table 3.3, $k = 1.3 \cdot 10^{-5}/ppm/s$, neglecting dissociation), we'd expect about 5.6% (0.21 ppm) of nitrogen aggregating into pairs after 20 min in a sample with a nitrogen starting concentration of 3.8 ppm. It has to be pointed out here that we didn't measure the N_2V^- ¹¹ concentration in the sample or leftover N_2 for such low concentrations, which might account for the rest of the generated N_2 .

¹¹ The negatively charged state of N_2V (H2)

For samples aimed for intra-cavity use in a laser, HPHT treatment of brown samples is recommended to significantly lower parasitic background absorption.

For the example of samples 1409E6sCVD02 and 1409E6sCVD03, where the synthesis protocol was identical, besides the additional initial HPHT treatment of sample 1409E6sCVD02, we observe the following: For sample 1409E6sCVD02, HPHT treatment reduced the absorption coefficient at 690 nm (peak emission of NV^-) from 1.62 to 0.08 cm^{-1} . After the complete synthesis, the absorption coefficient was 0.57 cm^{-1} . Sample 1409E6sCVD03, where the HPHT treatment was not included in the synthesis protocol, had a absorption coefficient of 1.34 cm^{-1} pre-treatment and 2.79 cm^{-1} (fig. 5.17) after the final treatment step.

The round trip loss (eq. (6.24)) before and after the synthesis, at 690 nm, the peak emission wavelength of NV^- , decreased by a factor of 2.4 ($\alpha_{before} = 1.62$, $\alpha_{after} = 0.57$, $1-I/I_0 = 0.48$ to 0.2, for a sample of $L=2$ mm length) for sample 1409E6sCVD02, while it increased by a factor of 1.6 ($\alpha_{before} = 1.34$, $\alpha_{after} = 2.79$, $1-I/I_0 = 0.41$ to 0.67) in sample 1409E6sCVD03.

After the HPHT treatment of sample 1409E6sCVD02, both 1409E6sCVD02 and 1409E6sCVD03 were irradiated with a total electron dose of $1.6 \cdot 10^{17} e/cm^2$ at 4.5 MeV, aiming to generate 2 ppm of vacancies (see fig. 3.6 in section 3.2). Sample 1409E6sCVD03 was irradiated two times with a dose of $8 \cdot 10^{16} e/cm^2$ each. Sample 1409E6sCVD02 was irradiated in one session, due to logistical reasons.

Subsequent annealing at 800°C for 3 hours resulted in the generation of ~ 1 ppm of NV in each sample, with a leftover V^0 ¹² concentration of 0.1-0.2 ppm, based on absorption spectroscopy measurements (see section 4.1 and section 5.4). To reduce leftover vacancies, annealing time was raised to 5 hours in following annealing procedures (as discussed in section 3.3).

¹² Neutral vacancy (GR1)

In order to increase the yield of NV , a second synthesis run was performed with samples 1409E6sCVD02 and 1409E6sCVD03 under identical

irradiation conditions as above. This time no absorption measurements could be taken to establish the real vacancy concentration generated, due to restrictions on access to the absorption spectrometer that allowed for measurements at liquid nitrogen temperature. It is assumed that a similar concentration of vacancies was generated as before. Annealing was performed at 800°C for 5 hours.

The increase in total NV concentration was ~ 0.2 - 0.3 ppm in both samples after the second irradiation and annealing, instead of an expected ~ 1 ppm, indicating a saturation of the NV concentration. As discussed in section 3.3, such a saturation would be expected at half of the total nitrogen concentration, $3.8/2 = 1.9$ ppm. The lower concentration might either be due to a reduction in the response to the NV formation process, as saturation is approached, or a lower overall nitrogen concentration in the samples in comparison to the reference sample, for which the nitrogen concentration was determined through EPR measurements by the Diamond group at the University of Warwick.

In total about 1.2 ppm of NV was generated in sample 1409E6sCVD02 and about 1.4 ppm in sample 1409E6sCVD03 (see table 5.3 and fig. 5.8 in section 5.4).

Samples 1411ADsCVD01 and 1411ADsCVD02 were irradiated with an electron dose of $8 \cdot 10^{16} \text{ e/cm}^2$ at 4.5 MeV, aiming to generate 1 ppm of vacancies (see fig. 3.6 in section 3.2). Subsequent absorption measurements at liquid nitrogen temperature indicated that the concentration of V^0 was ~ 0.5 ppm, but due to a damage in the spectrometer, measurements could not be taken in the spectral region for V^- ¹³.

About 0.1 and 0.03 ppm of NV^0 , respectively, were generated after annealing at 800°C for 3 hours. NV is present in the neutrally charged state NV^0 due to the low overall nitrogen concentration in the samples (see nitrogen as electron donor in section 2.3). The quantification was based on absorption measurements taken at liquid nitrogen temperature (see section 4.1 and section 5.4). This is slightly less than the possible maximum of 0.15 and 0.05 ppm, which is half the original nitrogen concentration. It might be that the 3 hour annealing time was too short for full NV synthesis in those samples. There is ~ 0.1 ppm of leftover V^0 present in both samples after annealing.

Loaned, pre-treated CVD samples

Five pre-treated CVD grown diamond samples were received on loan from Element Six. Sample E6NV¹⁴ was 2.5x2.5x2 mm and samples E6H3A, E6H3B, E6H3C and E6H3D were 3x3x2 mm in size. Two of these (E6NV and E6H3C) were studied as received. They were given to us as promising samples containing relatively large amounts of the target colour centres, in comparison

¹³ Negative vacancy (ND1)

¹⁴ 1242704-NID-02, referred to as E6NV for simplicity

to other samples available, by Element Six.

All treatment steps listed below were performed by Element Six. Treatment by Element Six was not done with this project in mind, but for other, unconnected, projects and subsequently offered to us as samples that might be of interest. The author didn't have any influence on the treatments used or any other specifications.

Sample E6NV was electron irradiated at 4.5 MeV with a total electron dosage of $5.85 \cdot 10^{18}$ e/cm². It was then annealed at 400°C for two hours to anneal out interstitial carbon. Another anneal at 800°C for 16 hours was used to create NV in the sample. A final anneal at 1200°C for 2 hours was done to remove any vacancy chains that might have built up [13, 14]. Samples E6H3A - D were subjected to prior treatment that wasn't disclosed in detail.

Based on FTIR¹⁵ measurements (as discussed in detail in section 5.4, fig. 5.13), E6NV has less than a ppm of leftover N_s¹⁶ (table 5.5). Based on absorption measurements taken at 77 K (see fig. 5.14 in section 5.4), a NV concentration of ~ 1.3 ppm was measured, approximately equally split between NV⁰ and NV⁻.

¹⁵ Fourier Transform Infra Red

¹⁶ Single substitutional nitrogen (C centre)

A few ppm of N_s, $\sim 0.05 - 0.11$ ppm of N₂V⁰ and traces of NV were present in samples E6H3A, E6H3B, E6H3C and E6H3D as received.

Sample E6H3C was kept as a reference sample, due to the highest concentration of N₂V⁰. Samples E6H3A, E6H3B and E6H3D were chosen for further NV synthesis. FTIR measurements suggest leftover nitrogen concentrations of 4-7 ppm in those samples (section 5.4). They were irradiated with a dose of $1.6 \cdot 10^{17}$ e/cm², aiming to generate 2 ppm of vacancies, with the goal to generate up to 2 ppm of NV, of which a majority should be present in the negatively charged state, due to sufficient leftover single nitrogen as electron donor. The amount of vacancies generated is unknown, as no data exists for those sample after irradiation. But as discussed previously, a concentration of at least 1.4 ppm of vacancies can be expected. Afterwards, the samples were annealed at 800°C for 5 hours at atmospheric pressure within this work to produce NV.

Based on absorption measurements at 77 K (see fig. 5.14), a total of ~ 1 ppm of NV was measured in samples E6H3A and E6H3B, and about 0.8 ppm in sample E6H3D. It is not obvious why there wasn't a larger yield of NV in those samples, as FTIR spectra suggest (fig. 5.13) that a few ppm of nitrogen should be present in those samples and between 1.4 to 2 ppm of vacancies should have been generated. Competing synthesis of N₂V⁻, which was not measured in this work, or other defects could be responsible for the disappearance of vacancies that did not end up contributing to the NV yield.

Unlike in the samples prepared in the previous subsections, which had a lower leftover single nitrogen concentration, NV is present predominantly

as NV^- . Between 74-87% of the total NV concentration is present in the negatively charged state, depending on the sample. This suggests an abundance of electron donors, most likely single nitrogen, and is in accordance with the increase in the intensity of the peak associated with N_s^+ ¹⁷ after irradiation and annealing of those samples, seen in fig. 5.13.

¹⁷ Positively charged N_s

All samples show a characteristic reddish NV luminescence under UV¹⁸ light as can be seen in fig. 5.15. Sample E6H3D has the most orange luminescence, possibly due to the contribution of green luminescence generated by N_2V^0 .

¹⁸ UltraViolet (10-380 nm)

5.3 N_2V^0 synthesis

Synthesis using CVD diamonds

Sample 1409E6sCVD04 was obtained from Element Six as part of the same growth series as the 1409E6sCVD samples introduced previously. It has the same size (3x3x2 mm) and estimated initial nitrogen concentration (3.8 ppm) as the other samples. The synthesis of a few hundred ppb¹⁹ of N_2V^0 , the largest in any CVD grown sample in this work, was achieved in this sample.

¹⁹ parts per billion

As discussed in section 3.3 and section 3.4, NV assisted aggregation of N_2V^0 is believed to have some advantages over the aggregation of nitrogen into pairs, followed by irradiation and annealing, in samples with low nitrogen concentrations [15, 16].

To reach significant aggregation in reasonable timescales, when single nitrogen is diffused (eq. (3.6)), in samples with ~ 1 ppm of nitrogen, dissociation has to be prevented as much as possible. This can be done by the selection of temperatures below 2000°C, where dissociation is believed to be negligible [17, 18]. But at these temperatures, experiments need to run more than 40 hours (for ~ 1 ppm of single nitrogen), even just to reach 10% aggregation (see fig. 3.12). In addition, the higher the temperature and pressure of an HPHT experiment, the harder it is to maintain stability of the experiment for prolonged periods of time. Experiments at less extreme conditions are easier to maintain [7].

These are arguments for a more detailed study of NV assisted synthesis of N_2V^0 , which could likely be performed at lower temperatures and pressures if the rate constant indeed is higher than for nitrogen aggregation.

Nevertheless, HPHT experiments can fail due to many reasons, such as material failure, even at lower temperatures and pressures. Out of 4 such experiments prepared here only 1 succeeded and yielded a sample that was in good enough optical condition to perform spectroscopic measurements on. Experiments either failed due to overheating as a result of the heating assembly malfunctioning (reaching an excess of 2200°C instead of the aimed for 1500-1700°C) and / or due to the diamond sample breaking and turning into graphite, so it was unusable for quantitative assessment.

For the synthesis of NV in sample 1409E6sCVD04, it was irradiated with a total dose of $2.4 \cdot 10^{17}$ e/cm² at 4.5 MeV (one irradiation at $1.6 \cdot 10^{17}$ e/cm² and one at $8 \cdot 10^{16}$ e/cm², due to logistical reasons), aiming to generate 3 ppm of vacancies in total (2 and 1 ppm respectively). The first irradiation yielded 0.95 ppm of V^- with no V^0 detectable. The second irradiation yielded 1.2 ppm of V^0 , but due to damage to the spectrometer, the spectral region for V^-

could not be measured and the amount of V^- after the second irradiation is unknown. The vacancy concentration after both irradiation experiments was at least the sum of both, 2.1 ppm, with possibly an unknown extra amount of V^- . As the only change in the sample between measurements was the generation of extra vacancies, there is no reason to believe that the concentration of V^- reduced after further irradiation.

After subsequent annealing at 800°C for 3 hours a total of about 1.4 ppm of NV was generated, divided into 0.8 ppm of NV^- and 0.6 ppm of NV^0 .

This sample was selected for NV assisted synthesis of N_2V^0 , due to its large NV concentration in comparison to other samples available. The original aim of this synthesis route was to compare NV assisted synthesis of N_2V^0 at different temperatures in long duration HPHT experiments, but only one sample survived in a good enough condition to measure defect concentrations with spectroscopic methods.

For the N_2V^0 synthesis, HPHT treatment was performed at 1500°C and 7.5 GPa for 48 hours. 0.5 ppm of N_2V^0 was measured afterwards. This result is in agreement with the overall reduction of NV concentration from ~ 1.4 to ~ 0.5 ppm, providing about 1 ppm of nitrogen needed for the creation of 0.5 ppm of N_2V^0 . In eq. (3.8) it is assumed that the process happens through the interaction of NV with single nitrogen. Since we don't have the concentration of N_2V^- available we cannot determine the total concentration of N_2V^- ²⁰. Judging from the 0.35 ppm of NV^- present in the sample after treatment and < 1 ppm of N_s^+ measured, we'd expect up to ~ 0.65 ppm of N_2V^- to be possibly present in the sample. This might be the case if NV combined with single nitrogen, of which about 2.4 ppm is present as single atoms, in the sample to form N_2V^- .

²⁰ A vacancy and two substitutional nitrogen atoms in C_{2v} symmetry

Nevertheless, with the limited data available, some approximations for the aggregation efficiencies and rate constants can be considered.

This result shows that 26% of initial nitrogen was converted into N_2V^0 , if we assume a total nitrogen concentration of 3.8 ppm. In comparison, as described in section 3.3, we would expect an aggregation of 0.12% of single nitrogen into pairs at 1500°C after 48 hours for a sample with 3.8 ppm of nitrogen, using the appropriate rate constant in table 3.3 for this calculation. This suggests that an NV assisted approach is a much more feasible approach for the N_2V^0 synthesis in samples with low nitrogen concentrations.

This experiment only provided one data point in the synthesis of N_2V^0 through NV aggregation. For a better understanding more experiments in the temperature range between 1500-1700°C, and possibly above, are needed in order to establish if a full transformation of NV to N_2V could be achieved.

For simplicity and as a first approximation it is assumed here that the reaction is described by the aggregation of an NV centre with a single nitrogen (eq. (3.8)). We start with equal concentrations of NV and N_s , $[NV]_0=[N]_0=1.4$ ppm, if we assumed we converted half the initial concentration of nitrogen in NV by irradiation and annealing previously. For simplicity, we consider that they aggregate with one another, so that $[NV]=[N]$ is given at all times. The reaction can be then written as $d[NV]/dt = -k \cdot [NV]^2$.

From the values mentioned above a rate constant of $k \approx (7.4 \pm 0.8) \cdot 10^{-6} \text{ ppm}^{-1}\text{s}^{-1}$ at 1500°C can be calculated. This rate constant is 4000 times larger than the one given in literature for the aggregation of single nitrogen into pairs at that temperature (table 3.3). If the rate constant were to behave similarly to those in table 3.3, we can assume an increase of a factor of ~ 30 when increasing the temperature from 1500 to 1700°C . If this were true, an HPHT experiment run at 1700°C for 48 hours with a sample containing 1.4 ppm of NV could potentially result in the aggregation of 98% of NV into N_2V . Further experiments are needed in order to examine the exact process and measure the associated rate constants. Again, as a comparison, with the rate constant at 1700°C (table 3.3) and assuming 2.8 ppm of total nitrogen, we'd expect an aggregation of only 2.4% of the initial nitrogen into pairs after 48 hours.

From the data obtained it seems that this synthesis route is preferable to nitrogen aggregation (eq. (3.6)) and subsequent irradiation and annealing as the aggregation rate is much larger at the same temperature. At this moment both routes yield a significant amount of leftover NV in the sample, contributing to parasitic absorption directly in the emission region of N_2V^0 . Further experiments are needed to determine the exact path and rate constants of NV assisted N_2V^0 synthesis at different temperatures and treatment times.

Synthesis using Natural diamonds

Four natural, transparent IaA samples were available to us and were investigated for N_2V^0 synthesis. All detectable nitrogen in the samples was present as N_2 in concentrations of about 1000 ppm.

Three samples were irradiated with a dose of $1.6 \cdot 10^{17} \text{ e/cm}^2$ at Synergy Health, with the aim to generate 2 ppm of vacancies (to produce up to 2 ppm of N_2V^0), and subsequently annealed at 800°C at atmospheric pressure for 5 hours, while one was kept as a reference.

Defect concentrations were determined from FTIR and UV-VIS²¹ absorption spectra. The N_2 concentration in two of the samples was determined to be 950 ± 60 ppm (in sample OR353-2) and 1000 ± 60 ppm (in sample OR357). 2.2 ± 0.4 ppm and 1.8 ± 0.3 ppm of N_2V^0 was generated in the samples, re-

²¹ UltraViolet-Visible

spectively, with no traces of NV and no leftover vacancies. These numbers agree well with the expected ~ 2 ppm of vacancies generated in the samples.

As expected, no luminescence was visible by eye under UV-illumination in any of the samples, despite the relatively large N_2V^0 concentration. N_2 is known to quench luminescence [19], rendering these samples unsuitable for luminescence studies. In the next subsection samples with similar N_2V^0 concentrations, but much lower N_2 concentrations, are shown. They show a bright green luminescence. (fig. 5.23 and fig. 5.24).

Background absorption at the peak emission for N_2V^0 (525 nm table 6.5) was measured to be $\sim 5 \text{ cm}^{-1}$ in sample OR358, at least 1 cm^{-1} larger than in those samples introduced before. If IaA samples with a lower concentration of N_2 would be available, ideally a few to a few dozen ppm judging from the luminescent samples introduced in the following subsection, they would be a very interesting material to produce luminescent N_2V^0 laser samples, without residue NV in the sample.

A secondary route to produce large amounts of N_2V^0 in diamond is suggested in literature [20, 21, 22]. Natural diamond with nitrogen present in aggregated form is used as a starting material.

As discussed previously in chapter 3, Synthesis of colour centres in diamond, the production of N_2V^0 in synthetic Ib diamond with a low concentration of nitrogen is difficult, as it involves prolonged HPHT treatment times. Additionally full conversion of N_s into N_2 is problematic. Leftover N_s will form NV after irradiation and annealing, which is a source of parasitic absorption for N_2V^0 samples [23].

Natural samples have undergone extensive HPHT treatment inside the earth for long enough time periods, so that even in samples with low nitrogen concentrations full aggregation into N_2 and N_4V ²² centres, without leftover single nitrogen, is achieved.

²² Four substitutional nitrogen surrounding a vacancy (B centre)

From a larger selection of samples containing both N_2 and N_4V , two IaAB samples with the largest initial concentration of N_2 available (about 35 and 50 ppm, BRAZ62 and BRAZ77) were selected, as well as a IaB sample with a comparable N_4V concentration for reference (BRAZ69). N_4V concentrations in those samples ranged from ~ 10 to 180 ppm.

Additionally, a IaAB (BRAZ50) and a IaB (BRAZ08) sample with low concentrations (< 2 ppm) of N_2 were chosen for reference. The IaAB samples were used for the synthesis of N_2V^0 and IaB samples as reference samples, to monitor and compare the outcomes with identical treatment conditions to those used for IaAB samples.

The IaB and IaAB samples were used to produce N_2V^0 by HPHT treatment

as suggested in literature. The aim was to produce samples with ~ 1 ppm of N_2V^0 to investigate samples for laser purposes.

Samples arrived untreated and unpolished, as seen in fig. 5.23. The shape was irregular and between 1 and 3 mm in diameter. FTIR measurements of natural diamond samples were obtained pre-polishing, as the higher signal-to-noise ratio of this technique allowed for a signal to be measured even under these conditions. UV-VIS spectroscopy measurements were only successful after polishing.

The samples were all HPHT treated at 2100°C and 11 GPa for 3 minutes, as discussed previously in section 3.3 and suggested in [20, 22] for the efficient synthesis of N_2V^0 in natural diamond samples. Treatment details are listed in table 5.6.

BRAZ08 and BRAZ50 were irradiated and annealed, to generate 2 ppm of vacancies. Sample BRAZ50 was then HPHT treatment in order to test the combination of N_2 with vacancies to possibly enhance the number of N_2V^0 . Sample BRAZ08 was used as a reference. But due to the difficulty of putting the natural diamonds in the low temperature absorption spectroscopy setup, spectra could be only obtained for sample BRAZ08 and BRAZ50 after the last treatment step, when they were polished. In conclusion, no N_2V^0 could be measured after additional irradiation and annealing in sample BRAZ50 and only 0.1 ppm of NV^- , suggesting that the majority of vacancies must have combined to form defects that we were not monitoring. This was tried in the first instance only in those samples, as not to accidentally generate any parasitic NV centres in other, more promising N_2V^0 samples.

$\sim 1.1 - 2.2$ ppm of N_2V^0 were generated in the most promising samples (BRAZ77 and BRAZ62) with very low NV concentrations (< 0.02 ppm, see table 5.8). While no UV-VIS absorption data is available pre polishing, and consequently pre synthesis, for those samples, it can be assumed that no significant N_2V^0 concentrations were present in those samples, as neither the yellow colour nor any luminescence was detectable. In contrast to the natural IaA samples discussed before, where a similar concentrations of N_2V^0 were generated, both samples show a bright yellow-green luminescence under UV light (Figures 5.23 and 5.24). This is likely due to the lower concentration of N_2 centres (between 35 and 50 ppm as opposed to ~ 1000 ppm in the IaA samples) and therefore less luminescence quenching.

The background absorption in those natural samples is 2.9 and 8.7 cm^{-1} in samples BRAZ62 and BRAZ77 respectively, at 525 nm, the peak emission of N_2V^0 (table 6.5).

Samples BRAZ62 and BRAZ77 show the brightest N_2V^0 related luminescence of all samples and are promising candidates to study N_2V^0 laser re-

lated properties, despite the difficulties that arise from being of natural origin, which include not being able to reliably generate samples of a desired size, quality and defect concentration. These samples were then selected as the most suitable N_2V^0 samples and assessed for their laser related parameters in section 7.3, Assessment of N_2V^0 containing samples.

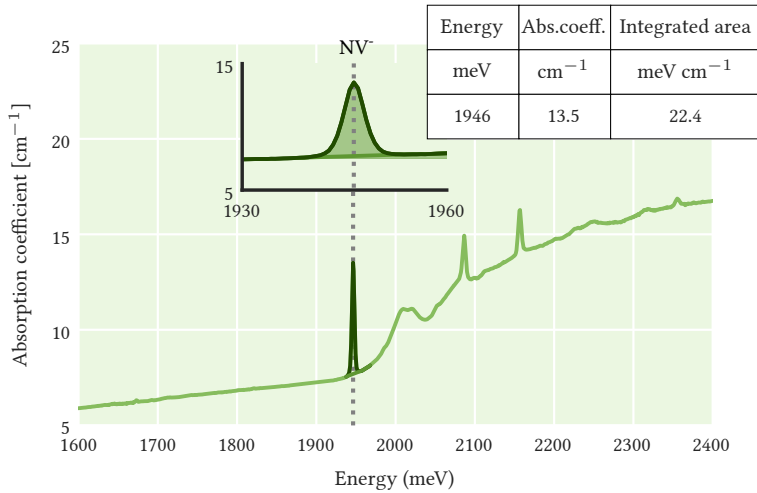
5.4 Spectroscopic analysis

Defect quantification was discussed in detail in chapter 4, Defect quantification and spectroscopic methods. In this section these methods are illustrated on the example of two diamond samples. Furthermore, the spectra obtained after the various steps of the synthesis process of the samples introduced in the previous section are presented and discussed.

Illustration of defect quantification on sample data

For the quantification of defects from absorption spectra taken at 77 K, using liquid nitrogen for cooling, the area under the ZPL²³ of the respective defect is needed. The process is illustrated on sample 1409E6sCVD03, after the last step of treatment. The sample is a CVD grown synthetic diamond that has undergone the following treatment (table 5.1): Electron irradiation with a total dose of $16 \cdot 10^{16} \text{ e/cm}^2$, followed by annealing at atmospheric pressure and 800°C for 3 hours to generate NV. Afterwards, the sample was irradiated with a dose of $16 \cdot 10^{16} \text{ e/cm}^2$ again and annealed at atmospheric pressure and 800°C for 5 hours to increase the yield of NV.

Figure 5.3 shows the sample absorption spectrum after the last treatment step.



²³ Zero Phonon Line

Figure 5.3: Absorption spectrum of sample 1409E6sCVD03, taken at 77 K.

The wavelength range has been converted to energy through the relationship $E = hc/\lambda$. The ZPL for NV⁻ is expected at 1.945 eV (638 nm, see table 4.1). In this example the peak is found at 1.946 eV and 13.5 cm^{-1} . The integration of the peak after subtraction of a baseline gives an integrated area of $A = 22.4 \text{ meV} \cdot \text{cm}^{-1}$. With eq. (4.3) and the calibration constant of $(1.7 \pm 0.08) \cdot 10^{-16} \text{ meV} \cdot \text{cm}^2$ (table 4.1), this leads to an estimated concentration of $[\text{NV}^-]_{UV-VIS} = (1.32 \pm 0.19) \cdot 10^{17} \text{ cm}^{-3} \approx 0.74 \pm 0.08 \text{ ppm}$.

The error given results from the uncertainty in the wavelength (wavelength accuracy ± 0.08 nm for UV-VIS) and the uncertainty in the measured absorbance A (photometric accuracy $\pm 0.0003 A$) of the spectrometer [24], as well as the precision of the calipers (0.02 mm) to measure the sample thickness and calculate the absorption coefficient from the absorbance (eq. (4.2)), and the error of the calibration constant.

For the quantification of defects from IR²⁴ spectra, the program SpectrumManipulator was used. Details about SpectrumManipulator can be found in [25]. As described, the intrinsic diamond spectrum was calibrated to have an absorption coefficient of 12.3 cm^{-1} at 2000 cm^{-1} . An experimental sample spectrum can be calibrated and deconvolved into its components using the SpectrumManipulator.

²⁴ InfraRed (0.78-1000 μm)

Figure 5.4 shows the calibrated IR spectrum of sample BRAZ77, the intrinsic diamond spectrum (IIa) and the reference spectra for defects N_2 (A) and N_4V (B). BRAZ77 is a natural IaAB diamond sample that was HPHT treated with 2100°C at 11 GPa for 3 minutes to produce $1.5 \pm 0.3 \text{ ppm}$ of N_2V^0 . The reference spectra are adjusted for the defect concentrations, in this case 35 ± 2 and $55 \pm 6 \text{ ppm}$ of A and B centres respectively, so the total spectrum overlaps with the calibrated experimental spectrum of BRAZ77, which can be seen in the inset in fig. 5.4.

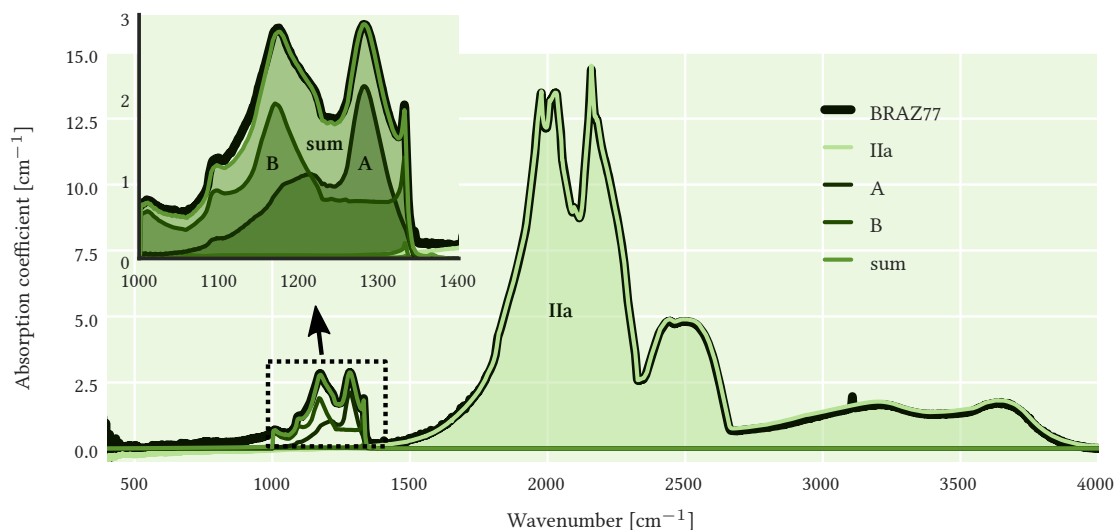


Figure 5.4: FTIR spectrum of sample BRAZ77 with reference spectra.

CVD samples

Figure 5.5 shows the FTIR spectra of samples 1409E6sCVD02 and 1409E6sCVD03 after the various steps of the synthesis process.

After HPHT treatment of sample 1409E6sCVD02 a slight shoulder appears where the feature for N_2 is expected. The spectrum of 1409E6sCVD03 doesn't show such a feature. This feature indicates that nitrogen aggregated into N_2 during HPHT treatment, although, for the treatment conditions, in low quantities (see section 5.2 for the discussion). There is an increase of N_s^+ and a decrease of N_s^0 ²⁵ after irradiation in both samples, which is consistent with charge transfer to the vacancies generated, forming V^- , as can be seen in fig. 5.6.

Both samples show a peak at 1450 cm^{-1} , which is in agreement with the feature described in Ia and Ib diamonds after irradiation and annealing in literature [5]. Sample 1409E6sCVD03 shows two peaks of unknown origin in between 1344 and 1371 cm^{-1} , which are absent in sample 1409E6sCVD02. They might be caused, to some degree, by the presence of platelets, extended planar defects, in the sample [5]. Sample 1409E6sCVD03 shows a peak at 1265 cm^{-1} of unknown origin after the first round of irradiation and annealing. After the second round, the peak disappears and a shoulder at 1240 cm^{-1} appears together with a pronounced broad feature at 1065 cm^{-1} . None of these features are present in sample 1409E6sCVD02. The feature at 1240 cm^{-1} is mentioned in literature, but its origin is not clear. The feature at 1065 cm^{-1} is attributed to irradiation damage [5], but it is unknown why it is present in one sample and not the other.

Figure 5.6 shows the UV-VIS absorption spectra of samples 1409E6sCVD02 and 1409E6sCVD03 taken at liquid nitrogen temperature (77 K) after the various steps of the synthesis process.

It can be seen that vacancies appear first in the form of V^- (plot b). After additional irradiation, vacancies in the form of V^0 appear (plot c). This is believed to be due to charge transfer between vacancies and the residual single nitrogen in the sample, and is in accordance with the increase in N_s^+ seen in fig. 5.5. Unfortunately, V^- concentrations could not be measured for sample 1409E6sCVD02 or 1409E6sCVD03 after the second irradiation. This was due to the spectrometer being broken in the particular spectral range at the time measurements were taken. Vacancy concentrations are estimated from the data available, which indicate that $\sim 0.8\text{ ppm}$ of V^0 and $\sim 0.6\text{ ppm}$ of V^- was generated, so the total vacancy generation was at least 1.4 ppm .

There is a peak at 595 nm , visible after irradiation with a total dose of $1.6 \cdot 10^{17}\text{ e/cm}^2$ in both samples, increasing in intensity after annealing and subsequent irradiation and annealing. It has been observed in literature in type I diamonds after radiation damage and anneals around 800°C and is believed to be caused by a nitrogen-vacancy defect [5].

The peak at 488 nm , with a small broad absorption next to it, appears in both samples after irradiation, but disappears again after annealing. Its origin is not clear from literature. It might be associated with N_4V_2 ²⁶ [5],

²⁵ Neutrally charged N_s

²⁶ Two vacancy and four substitutional nitrogen atoms with a C_{1h} symmetry (H4)

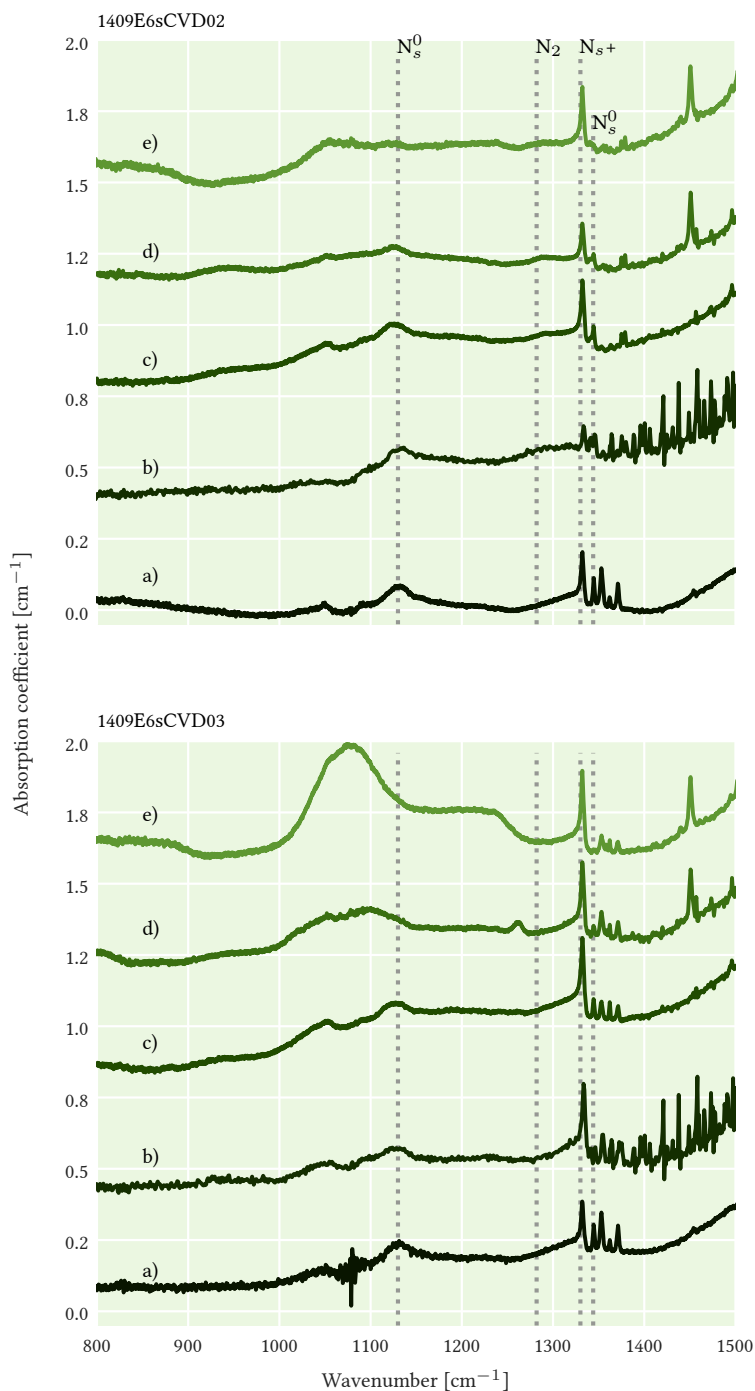


Figure 5.5: FTIR spectra of samples 1409E6sCVD02 and 1409E6sCVD03. The data for b) in both plots has been taken with the benchtop FTIR spectrometer and shows the characteristic absorption from H_2O above $\sim 1350 \text{ cm}^{-1}$. Spectra are vertically shifted by 0.4 cm^{-1} for visibility.

1409E6sCVD02:

- a) As received
- b) After HPHT treatment at 2200°C and 11 GPa for 20 minutes.
- c) After irradiation with $1.6 \cdot 10^{17} \text{ e/cm}^2$.
- d) After annealing at 800°C and atmospheric pressure for 3 hours.
- e) After irradiation with $1.6 \cdot 10^{17} \text{ e/cm}^2$ and annealing at 800°C and atmospheric pressure for 5 hours

1409E6sCVD03:

- a) As received
- b) After irradiation with $8 \cdot 10^{16} \text{ e/cm}^2$.
- c) After additional irradiation with $8 \cdot 10^{16} \text{ e/cm}^2$.
- d) After annealing at 800°C and atmospheric pressure for 3 hours.
- e) After irradiation with $1.6 \cdot 10^{17} \text{ e/cm}^2$ and annealing at 800°C and atmospheric pressure for 5 hours

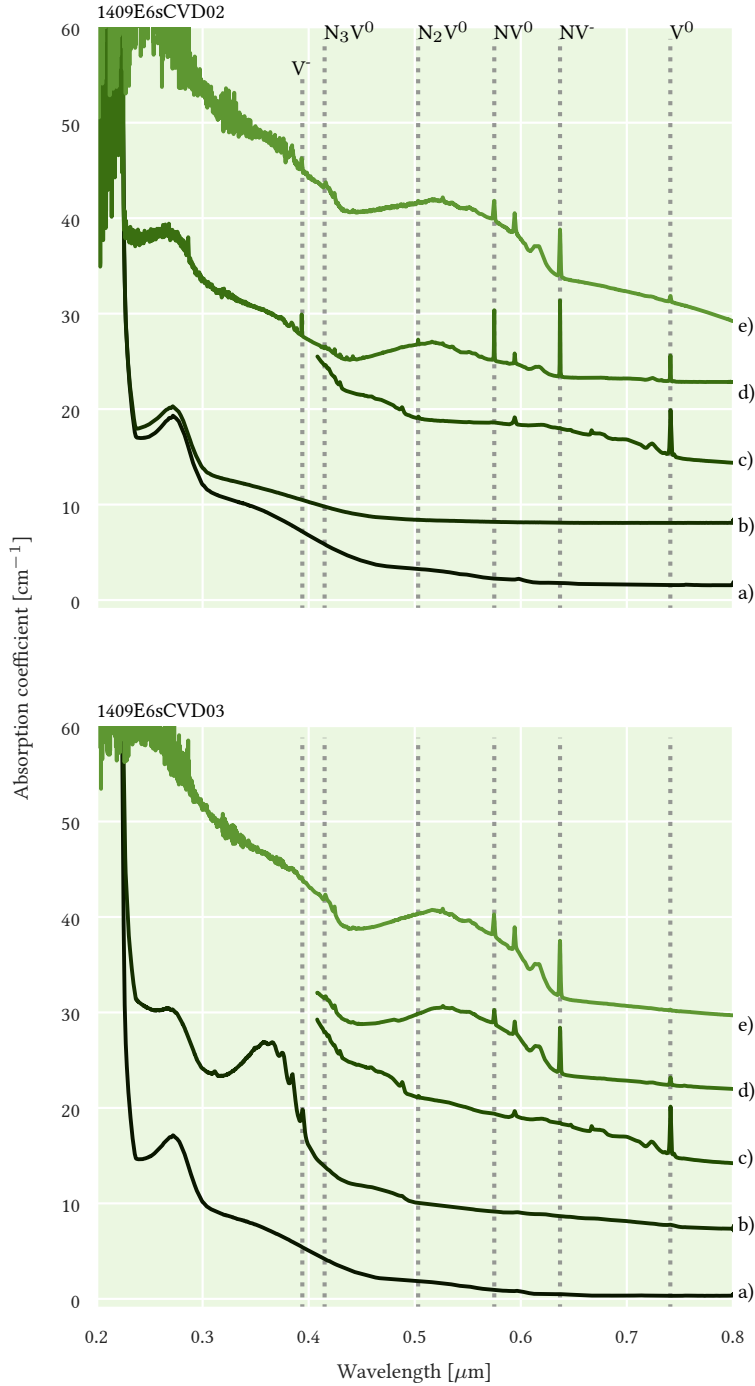


Figure 5.6: UV-VIS absorption spectra of samples 1409E6sCVD02 and 1409E6sCVD03 taken at liquid nitrogen temperature (77 K). Some spectra are cut off below $0.4 \mu\text{m}$ because the spectrometer was broken at the time of the measurements and full spectra couldn't be taken. Spectra are vertically shifted by 7 cm^{-1} for visibility.

1409E6sCVD02:

- As received
- After HPHT treatment at 2200°C and 11 GPa for 20 minutes.
- After irradiation with $1.6 \cdot 10^{17} \text{ e/cm}^2$.
- After annealing at 800°C and atmospheric pressure for 3 hours.
- After irradiation with $1.6 \cdot 10^{17} \text{ e/cm}^2$ and annealing at 800°C and atmospheric pressure for 5 hours

1409E6sCVD03:

- As received
- After irradiation with $8 \cdot 10^{16} \text{ e/cm}^2$.
- After additional irradiation with $8 \cdot 10^{16} \text{ e/cm}^2$.
- After annealing at 800°C and atmospheric pressure for 3 hours.
- After irradiation with $1.6 \cdot 10^{17} \text{ e/cm}^2$ and annealing at 800°C and atmospheric pressure for 5 hours

which seems unlikely in this case, as we don't expect larger nitrogen clusters present in these samples. Another possibility is the connection to a centre introduced by radiation damage with a ZPL at 489 nm, which anneals out above 350°C, and is believed to relate to a defect containing nitrogen and interstitial carbon [5].

Figure 5.7 shows the FTIR spectra of samples 1411ADsCVD01 and 1411ADsCVD02 after the various steps of the synthesis process. Concentrations in those samples were small and difficult to monitor with the techniques available to us.

The spectra show a broad feature between 1000 and 1100 cm^{-1} , similar to that seen in fig. 5.5 for sample 1409E6sCVD03. Here it seems to consist of an additional pronounced broad peak at 1020 cm^{-1} in addition to the one at 1065 cm^{-1} . Again, the origin of the feature is not clear and it is unclear why the feature seems to have disappeared in sample 1411ADsCVD01 after irradiation and then reappear after annealing. The feature at 1265 cm^{-1} , which was only present in sample 1409E6sCVD03 after the first round of irradiation and annealing and disappeared after additional irradiation and annealing, is present in almost all spectra. It disappears for sample 1411ADsCVD01 after HPHT treatment and reappears only after irradiation and annealing. N_s is present predominantly as N_s^+ .

Figure 5.8 shows the UV-VIS absorption spectra of samples 1411ADsCVD01 and 1411ADsCVD02 taken at liquid nitrogen temperature (77 K) after the various steps of the synthesis process.

The peak at 741 nm and the broad absorption band extending to about 500 nm are attributed to V^0 [5]. The peak appears after irradiation and is then reduced after annealing, as expected. A weak peak at 738 nm is present in both samples as grown and in sample 1411ADsCVD01 after HPHT treatment. It is associated with the ZPL of the negative silicon-vacancy centre [26]. Silicon can be present in CVD grown diamond, for example if a silicon substrate has been used during growth or silica containing components are present in the reactor [5].

After irradiation the peak at 738 nm disappears and a peak at 736.8 nm appears in both samples. After annealing, a second peak at 736.4 nm appears next to the one at 736.8 nm. The broadened shape of the peaks, visible in the insets, in the measurements after irradiation in comparison to the peaks after annealing could suggest that the temperature of the samples in the latter measurement was lower than in the first. The peak at 736.4 nm, as shown in the inset, might only appear due to a difference in temperature, and therefore sharper lines and more distinguishable features, rather than a new feature that appeared after annealing. Literature measurements of the ZPL of the negative silicon-vacancy at 8 K, show, that it is resolved into four components between 736.4 and 737 nm [26]. At 77 K these fea-

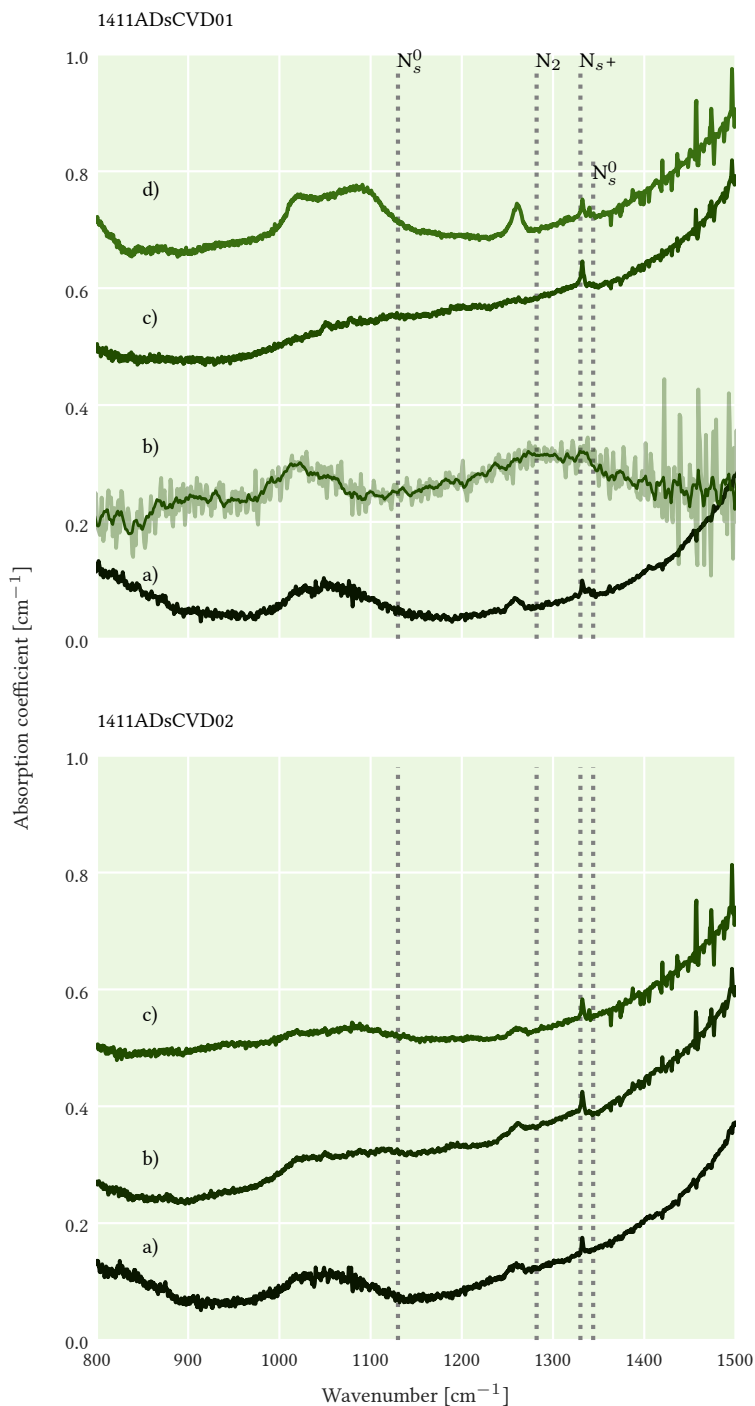


Figure 5.7: FTIR spectra of samples 1411ADsCVD01 and 1411ADsCVD02. Noisy data is smoothed using moving average, the original data is plotted in a lighter shade below.

Spectra are vertically shifted by 0.2 cm^{-1} for visibility.

1411ADsCVD01:

- a) As received
- b) After HPHT treatment at 2200°C and 11 GPa for 20 minutes.
- c) After irradiation with $8 \cdot 10^{16} \text{ e/cm}^2$.
- d) After annealing at 800°C and atmospheric pressure for 3 hours.

1411ADsCVD02:

- a) As received
- b) After irradiation with $8 \cdot 10^{16} \text{ e/cm}^2$.
- c) After annealing at 800°C and atmospheric pressure for 3 hours.

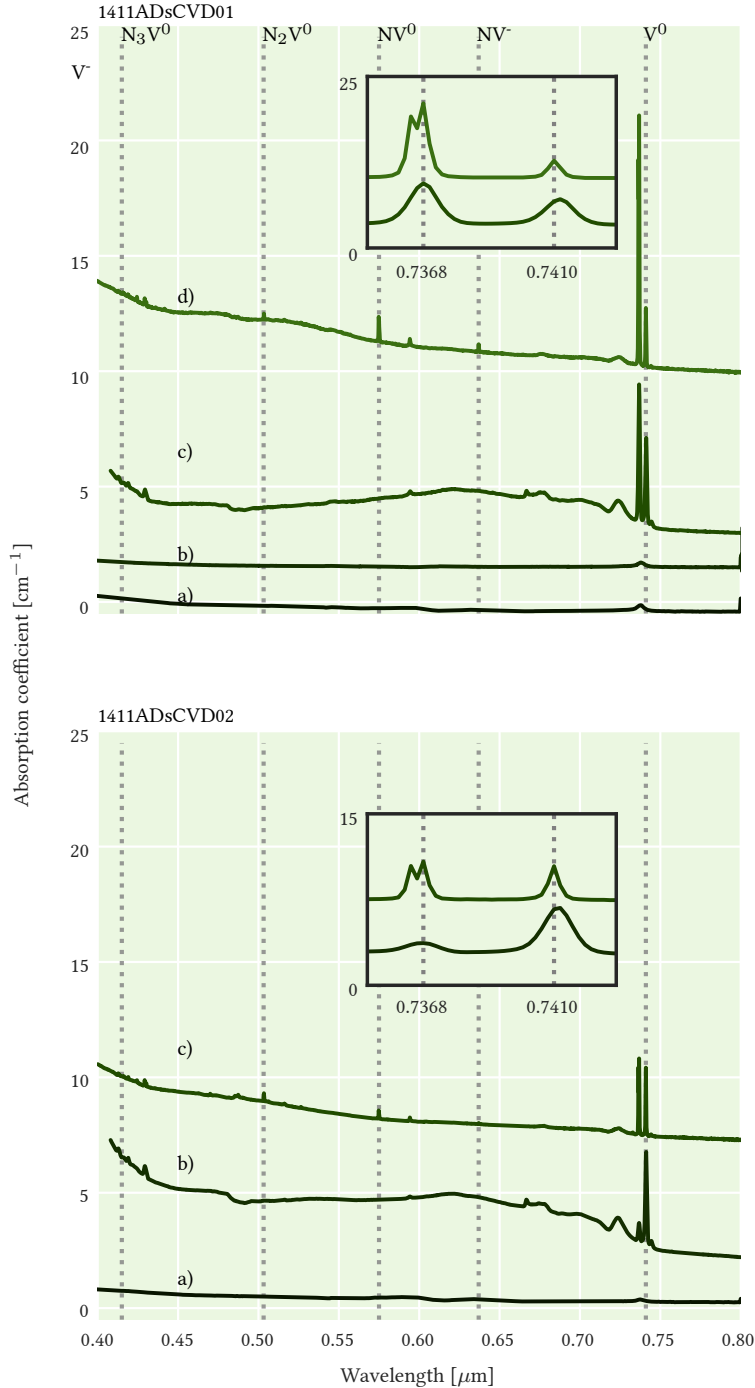


Figure 5.8: UV-VIS absorption spectra of samples 1411ADsCVD01 and 1411ADsCVD02 taken at liquid nitrogen temperature (77 K). Some spectra are cut off below $0.4 \mu\text{m}$ because the spectrometer was broken at the time of the measurements and full spectra couldn't be taken. Spectra are vertically shifted for visibility by a varying amount to account for the height of the ZPLs.

1411ADsCVD01:

- a) As received
- b) After HPHT treatment at 2200°C and 11 GPa for 20 minutes.
- c) After irradiation with $8 \cdot 10^{16} \text{ e/cm}^2$.
- d) After annealing at 800°C and atmospheric pressure for 3 hours.

1411ADsCVD02:

- a) As received
- b) After irradiation with $8 \cdot 10^{16} \text{ e/cm}^2$.
- c) After annealing at 800°C and atmospheric pressure for 3 hours.

tures are expected to be broadened and it is likely the features observed here are associated with the negative silicon-vacancy centre.

Low concentrations of NV^0 , ~ 0.1 and 0.03 ppm in sample 1411ADsCVD01 and 1411ADsCVD02, which reflect the low initial nitrogen concentration, were measured after irradiation and annealing.

Figure 5.9 shows the IR absorption spectra of sample 1409E6sCVD04 after the various steps of the synthesis process.

Before the final HPHT treatment step of the synthesis of this sample, the spectrum is almost identical to sample 1409E6sCVD03, with the exception that the broad feature at 1065 cm^{-1} and shoulder at 1240 cm^{-1} do not appear after irradiation and annealing. It is unknown why this is the case. The overall reduction in the peaks associated with nitrogen is consistent with assumption that nitrogen and NV aggregated, forming N_2V , which is more obvious in fig. 5.10.

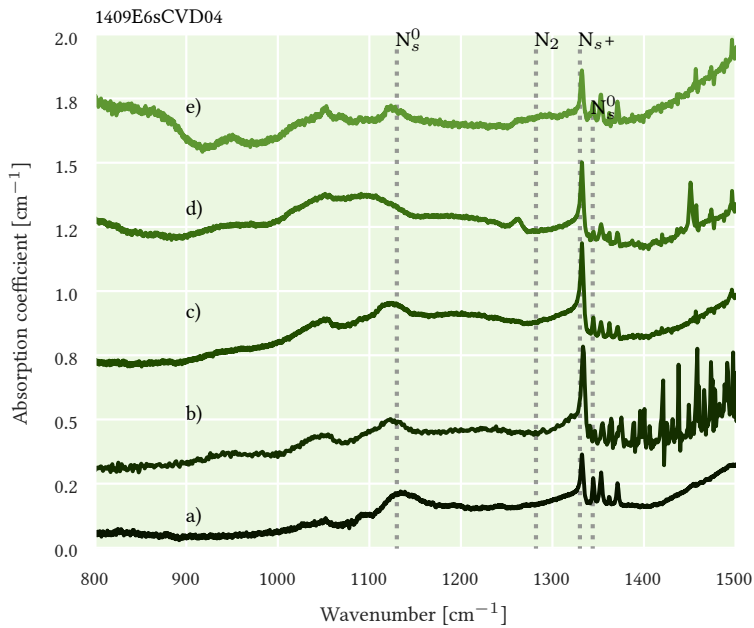


Figure 5.9: FTIR spectra of sample 1409E6sCVD04. Spectra are vertically shifted by 0.2 cm^{-1} for visibility.

- a) As received
- b) After irradiation with $1.6 \cdot 10^{17}\text{ e/cm}^2$.
- c) After additional irradiation with $8 \cdot 10^{16}\text{ e/cm}^2$.
- d) After annealing at 800°C and atmospheric pressure for 3 hours.
- e) After HPHT treatment at 1500°C and 7.5 GPa pressure for 48 hours.

Figure 5.10 shows the UV-VIS absorption spectra of sample 1409E6sCVD04 taken at liquid nitrogen temperature (77 K) after the various steps of the synthesis process. In plot b), after the first irradiation, it can be seen that vacancies are present predominantly as V^- , while V^0 appears after the second irradiation in plot c) (where the number of V^- could not be measured unfortunately). This was previously observed in sample 1409E6sCVD03, and indicates that the single nitrogen in the sample donate electrons to

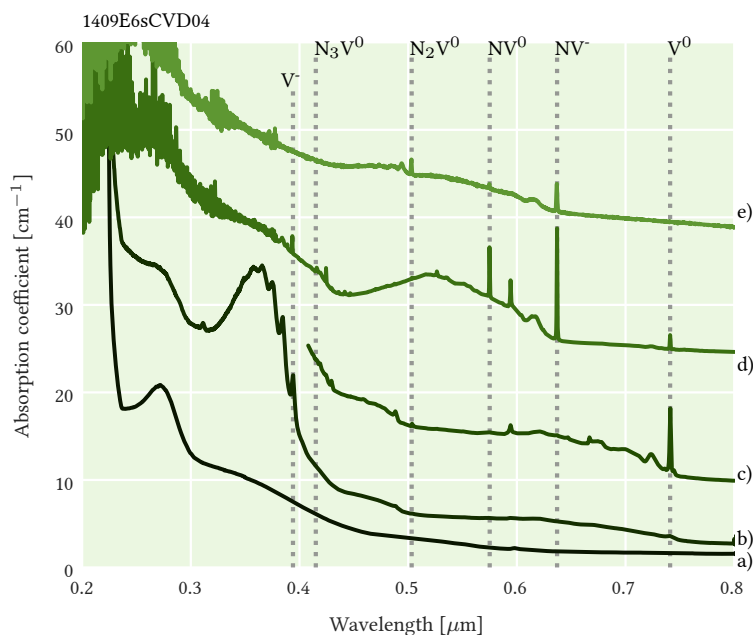


Figure 5.10: UV-VIS absorption spectra of sample 1409E6sCVD04 taken at liquid nitrogen temperature (77 K).

Spectra are vertically shifted for visibility by varying amounts, to account for the height of the spectral features appearing.

- a) As received
- b) After irradiation with $1.6 \cdot 10^{17}$ e/cm^2 .
- c) After additional irradiation with $8 \cdot 10^{16}$ e/cm^2 .
- d) After annealing at $800^\circ C$ and atmospheric pressure for 3 hours.
- e) After HPHT treatment at $1500^\circ C$ and 7.5 GPa pressure for 48 hours.

the vacancies.

The synthesis and evolution of spectroscopic features is, as expected, comparable to that of sample 1409E6sCVD03, discussed previously. Plot e) shows the sample after HPHT treatment at $1500^\circ C$ for 48 hours. As expected, the features for NV are reduced and those associated with N_2V^0 appear.

Figure 5.11 shows pictures of the samples before treatment and after the last step of treatment, and, if relevant, under UV light. The synthesis of NV in samples 1409E6sCVD02 and 1409E6sCVD03 is visible by the red coloration and the red luminescence under UV light. In samples 1411ADsCVD01 and 1411ADsCVD02 no changes in coloration were visible by the naked eye and no luminescence was seen under UV light. Sample 1409E6sCVD04 is shown before and after HPHT treatment. A slight decoloration of the sample, from dark red to light red, is consistent with the reduction of NV and the creation of N_2V^0 , which gives a yellowish color to the sample.

Table 5.1 and table 5.3 show an overview of the treatment details for the respective samples and the concentrations measured. Figure 5.12 shows a graphical representation of the defect concentrations for each treatment step where data was available.

In samples 1411ADsCVD01 and 1411ADsCVD02 a reduction of vacan-

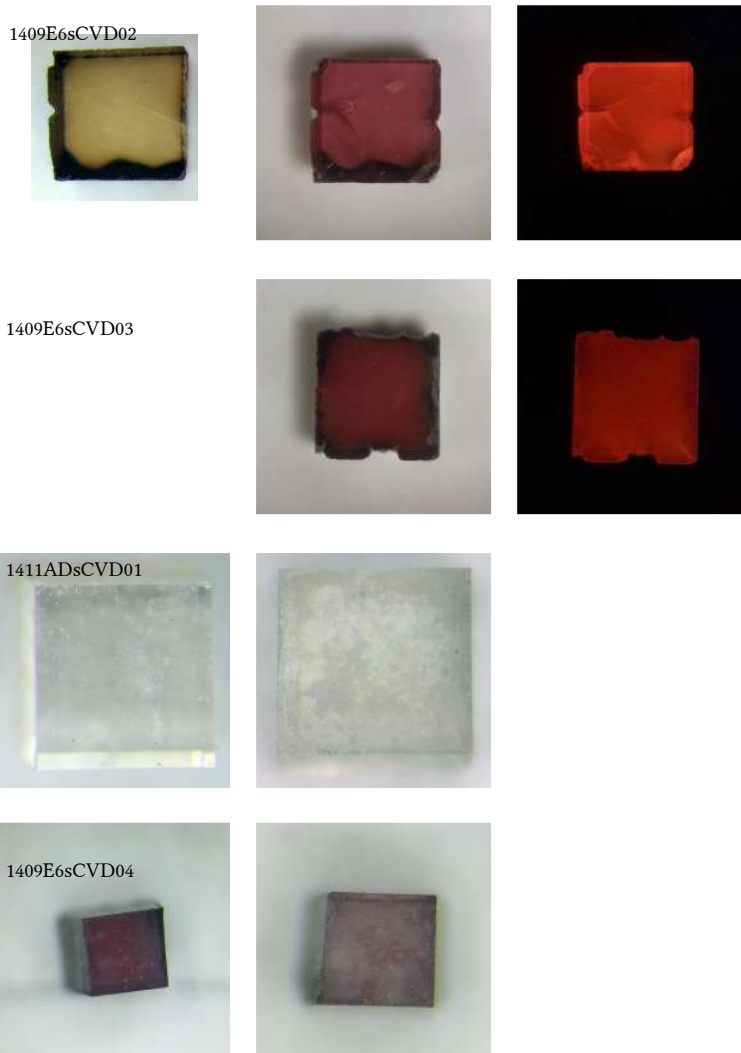


Figure 5.11: CVD diamond samples received as-grown and then treated

Left: Before treatment
Middle: After treatment
Right: After treatment under UV light

1409E6sCVD02 and 03 belong to a batch of brownish CVD samples with ~ 4 ppm of N_s in them according to EPR measurements performed on sample 1409E6sCVD05. 1409E6sCVD02 and 03 were both treated with the same irradiation and annealing treatment. Sample 1409E6sCVD02 has been HPHT treated before irradiation and annealing. Both samples show NV luminescence under UV light. Sample 1409E6sCVD02 has lost some of the brownish coloration after HPHT treatment.

Samples 1411ADsCVD01 and 02 are two samples with 0.3 and 0.11 ppm of N_s respectively according to EPR measurements. Sample 1411ADsCVD01 is shown before and after HPHT treatment.

Sample 1409E6sCVD04 has been irradiated and annealed and subsequently HPHT treated with a lower temperature at a prolonged time to aggregate NV into N_2V^0 . A slight paling of the red coloration can be seen after HPHT treatment.

cies is apparent, but only some of them go into the generation of NV, which is expected due to the low overall nitrogen concentrations in those samples. The rest might aggregate with other defects, which were not monitored in detail, or annealed out, as discussed in section 3.3.

For all the other samples an overall reduction of nitrogen and vacancies can be observed over the course of the synthesis and the appearance of NV. The numbers don't match, most likely due to the fact that the V^- concentration could not be monitored due to a broken spectrometer, and therefore the overall vacancy generation is unknown. For sample 1409E6sCVD04 the reduction of NV and the appearance of N_2V^0 is shown in the final treatment step.

CVD samples				
Treatment	Temperature [°C]	Pressure [GPa]	Time [min]	Dose [e/cm ²]
1409E6sCVD02				
HPHT	2200	11	20	
IRR				1.60E+17
ANN	800	AP	180	
IRR				1.60E+17
ANN	800	AP	300	
1409E6sCVD03				
IRR				8.00E+16
IRR				8.00E+16
ANN	800	AP	180	
IRR				1.60E+17
ANN	800	AP	300	
1409E6sCVD04				
IRR				1.60E+17
IRR				8.00E+16
ANN	800	AP	180	
HPHT	1500	7.5	2880	
1411ADsCVD01				
HPHT	2200	11	20	
IRR				8.00E+16
ANN	800	AP	180	
1411ADsCVD02				
IRR				8.00E+16
ANN	800	AP	180	

Table 5.1: Treatment details for CVD samples received as-grown. IRR = Irradiation
ANN = Annealing
HPHT = High Pressure High Temperature
AP = atmospheric pressure

All irradiation mentioned in this table has been performed with 4.5 MeV electrons at Synergy-Health

UV-VIS					
Sample	Treatment	N_2V^0 [ppm]	NV^- [ppm]	NV^0 [ppm]	V^0 [ppm]
1409E6sCVD02	INIT				
	HPHT				
	IRR	0.07 ± 0.01	<0.01	N/A	0.7 ± 0.2
	ANN	0.06 ± 0.01	0.42 ± 0.05	0.49 ± 0.03	0.15 ± 0.04
	IRR				
1409E6sCVD03	ANN	0.07 ± 0.01	0.61 ± 0.07	0.58 ± 0.04	0.09 ± 0.02
	INIT				
	IRR	0.05 ± 0.01	<0.01	N/A	0.8 ± 0.2
	ANN	N/A	0.58 ± 0.06	0.41 ± 0.02	0.11 ± 0.03
	IRR				
1409E6sCVD04	ANN	N/A	0.74 ± 0.08	0.65 ± 0.04	<0.01
	INIT				
	IRR	N/A	N/A	N/A	N/A
	IRR	0.12 ± 0.02	0.02 ± 0.01	N/A	1.2 ± 0.3
	ANN	N/A	0.78 ± 0.08	0.60 ± 0.04	0.12 ± 0.03
1411ADsCVD01	HPHT	0.50 ± 0.08	0.35 ± 0.04	0.10 ± 0.01	N/A
	INIT				
	HPHT				
	IRR	N/A	N/A	N/A	0.5 ± 0.2
	ANN	N/A	<0.01	0.10 ± 0.01	0.12 ± 0.03
1411ADsCVD02	INIT				
	IRR	N/A	N/A	N/A	0.6 ± 0.2
	ANN	N/A	N/A	0.03 ± 0.01	0.14 ± 0.03
IR					
Sample		N_2 [ppm]	N_4V [ppm]	N_S^0 [ppm]	N_s^+ [ppm]
1409E6sCVD02		N/A	N/A	N/A	<1
1409E6sCVD03		N/A	N/A	N/A	<1
1409E6sCVD04		<1	N/A	<1	<1

Top: Defect concentrations from UV-VIS measurements of as grown CVD samples as received (INIT) after HPHT treatment (HPHT), irradiation (IRR) and annealing (ANN). **Bottom:** Defect concentrations from IR measurements of as grown CVD samples after last treatment step. N/A - No signal for this defect could be detected

Table 5.3: Defect concentrations from absorption spectra of as grown CVD samples.

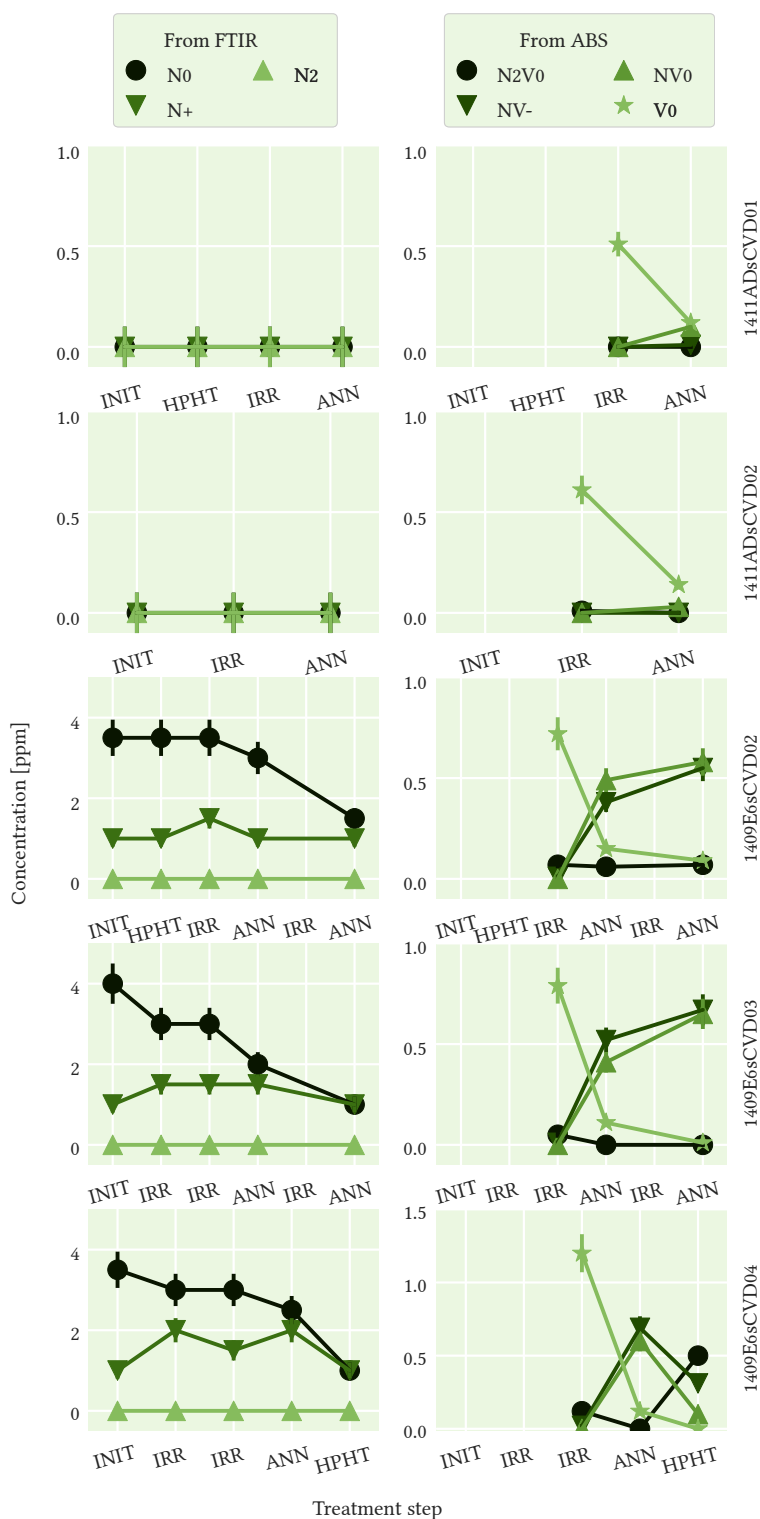


Figure 5.12: colour centre concentrations in CVD samples. Concentrations obtained from absorption spectra are indicated by circles. The lines in between are there to enhance the visibility. Missing circles indicate that no data was available after that treatment step.

About 1 ppm of NV was generated, equally split in NV⁰ and NV⁻ in sample 1409E6sCVD02 and 1409E6sCVD03.

About 0.1 ppm of NV was generated in sample 1411ADsCVD01, all present as NV⁰.

About 0.03 ppm of NV was generated in sample 1411ADsCVD02, all present as NV⁰.

In sample 1409E6sCVD04 ~0.7 and 0.6 ppm of NV⁻ and NV⁰ respectively transformed into ~0.5 ppm of N₂V⁰ and ~0.3 and 0.1 ppm of NV⁻ and NV⁰ after 48 hours of HPHT treatment at 1500°C.

Figure 5.13 shows the FTIR spectra of samples E6NV, E6H3A, E6H3B, E6H3C and E6H3D as received and after synthesis. The FTIR spectrum of sample E6NV shows the same features as that of sample 1411ADsCVD01 after HPHT treatment, irradiation and annealing (fig. 5.7). Those are two broad features at 1020 cm^{-1} and 1065 cm^{-1} and a narrower feature at 1265 cm^{-1} . Those features are absent in all E6H3 samples. A sharp peak between 1358 to 1380 cm^{-1} can be associated with platelets in the sample, but not much information is available for peaks in that spectral region [5]. In all of our samples there is peak at 1362 cm^{-1} , accompanied by a double peak at $1375 / 1378\text{ cm}^{-1}$ in all E6H3 samples before and after treatment, they are proposed to be linked to N_2VH^0 ²⁷ [10]. Another peak at 1405 cm^{-1} , most prominent in sample E6H3D, is present in all E6H3 samples before and after treatment and can be linked to a very temperature stable hydrogen-related feature [5]. Only in sample E6H3D a peak at 1437 cm^{-1} appears after treatment, which is not characterised in literature. A peak at 1451 cm^{-1} , present in all samples after irradiation and annealing, could possibly be associated with the H1a center found at 1450 cm^{-1} , a defect connected to interstitial nitrogen [5].

Features associated with single nitrogen are more prominent in the E6H3 samples than in E6NV. After irradiation and annealing the intensity of the peak associated with N_s^+ increased in all samples, which is in agreement with the appearance of NV^- (fig. 5.14).

Figure 5.14 shows the UV-VIS absorption spectra taken at liquid nitrogen temperature (77 K), of samples E6NV, E6H3A, E6H3B, E6H3C and E6H3D as received and after synthesis for the samples that were treated by us. The dominant feature in all irradiated and annealed samples is the appearance of NV. As discussed previously, split equally in sample E6NV and distributed towards NV^- in the E6H3 samples. The peak at 594 nm is linked to the so called 595 nm center, which is observed in any nitrogen containing diamond sample after irradiation and annealing and is believed to relate to a nitrogen vacancy centre [5].

Figure 5.15 shows pictures of the NV containing samples illuminated with a tabletop lamp and under UV light. All samples show a reddish colour and luminescence. Sample E6NV has a dark reddish colour, while the E6H3 samples look more violet. Sample E6H3D is a light violet to rose colour, with an orange looking luminescence.

Table 5.5 shows an overview of the concentrations measured in the samples. Figure 5.16 shows a graphical representation of the defect concentrations before and after treatment for the samples we irradiated and annealed.

As expected, all samples show a decrease of N_s^0 and a increase of NV,

²⁷ A nitrogen pair with a vacancy and a hydrogen

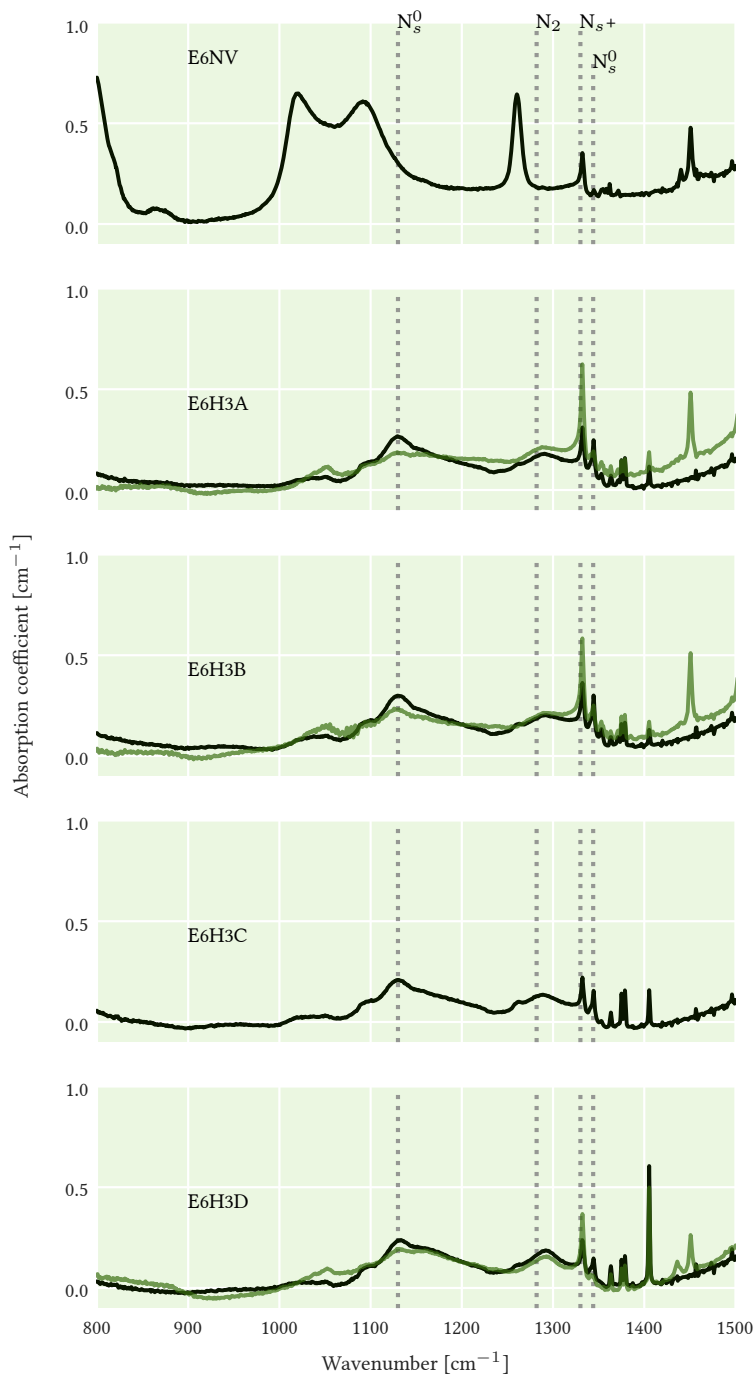


Figure 5.13: FTIR spectra of loaded CVD samples as received (dark lines) and after (light lines) treatment.

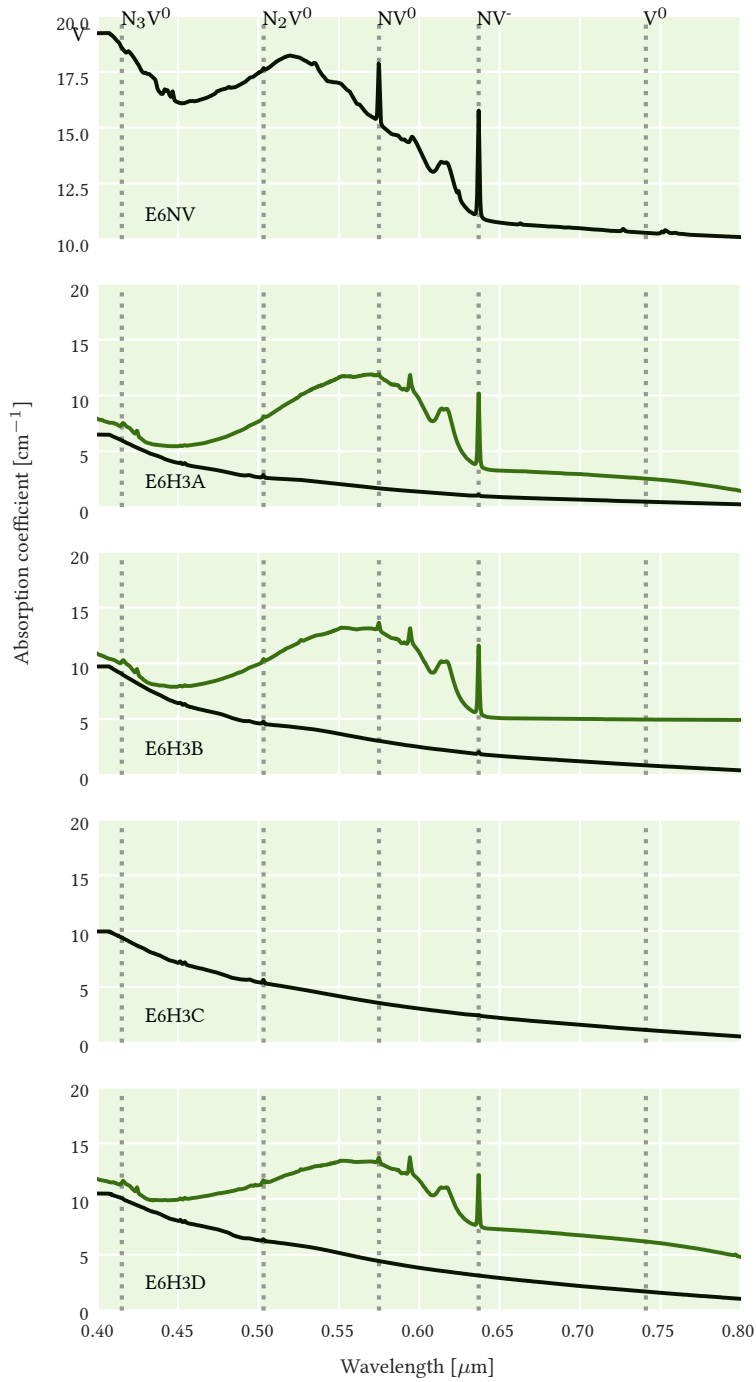


Figure 5.14: UV-VIS absorption spectra at liquid nitrogen temperature of loaned CVD samples as received (dark lines) and after (light lines) treatment.

E6NV

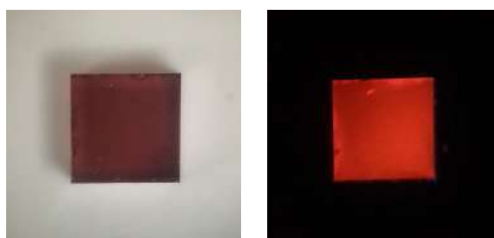
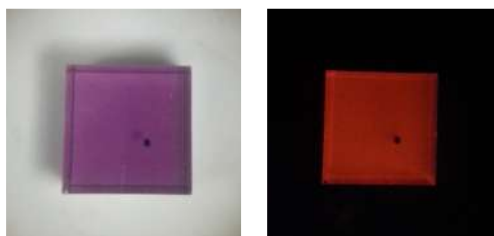


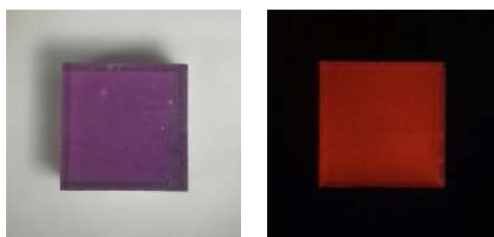
Figure 5.15: Pre-treated CVD diamond samples

Left: Before treatment (none available here)
Middle: After treatment
Right: After treatment under UV light

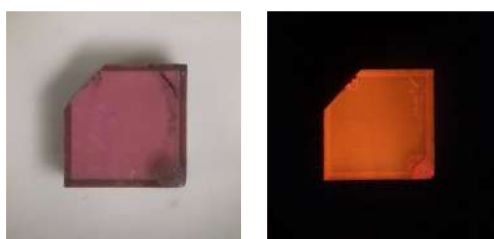
E6H3A



E6H3B



E6H3D



mostly in the form of NV^- , and an according increase of N_s^+ . The excess N_s^+ can be explained by the presence of other negatively charged centres in the samples, which we didn't measure in this work. For example N_2V^- or negatively charged nitrogen-hydrogen-vacancy complexes [10].

UV-VIS									
Sample	Treatment	N_2V [ppm]		NV^- [ppm]		NV^0 [ppm]		V^0 [ppm]	
E6NV	INITIAL	0.04	± 0.01	0.62	± 0.07	0.73	± 0.04	N/A	
E6H3A	INITIAL	0.08	± 0.01	<0.01		N/A		N/A	
	IRR								
	ANN	0.06	± 0.01	0.85	± 0.09	0.13	± 0.01	N/A	
E6H3B	INITIAL	0.07	± 0.02	<0.01		N/A		N/A	
	IRR								
	ANN	0.08	± 0.01	0.78	± 0.08	0.21	± 0.01	N/A	
E6H3C	INITIAL	0.11	± 0.02	<0.01		N/A		N/A	
E6H3D	INITIAL	0.05	± 0.01	N/A		N/A		N/A	
	IRR								
	ANN	0.11	± 0.02	0.56	± 0.06	0.19	± 0.01	N/A	
IR									
Sample	N_2 [ppm]		N_4V [ppm]		N_S^0 [ppm]		N_s^+ [ppm]		
E6NV	N/A		N/A		<1		<1		
E6H3A	<1		N/A		4	± 1	2	± 1	
E6H3B	<1		N/A		5	± 1	2	± 1	
E6H3C	<1		N/A		5	± 1	<1		
E6H3D	2	± 1	N/A		3	± 1	2	± 1	

Top: Defect concentrations from UV-VIS measurements of loaned CVD samples as received (INIT) after HPHT treatment (HPHT), irradiation (IRR) and annealing (ANN). **Bottom:** Defect concentrations from IR measurements of loaned CVD samples after last treatment step. N/A - No signal for this defect could be detected

Table 5.5: Defect concentrations from absorption spectra of loaned CVD samples.

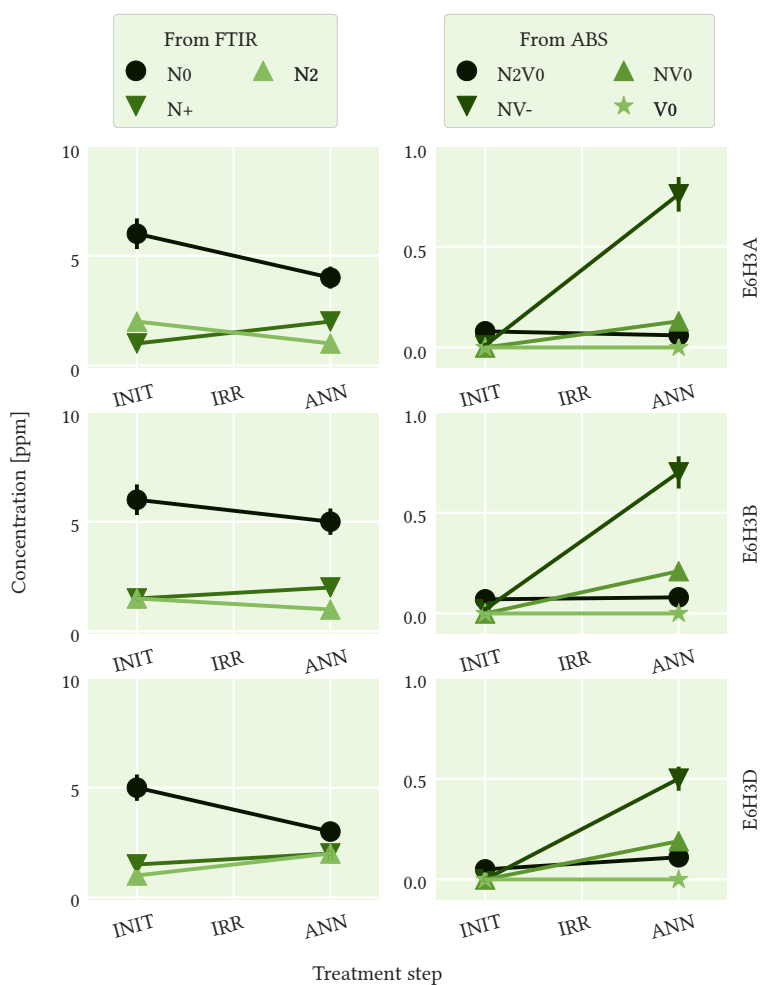


Figure 5.16: colour centre concentrations in E6 samples. Concentrations obtained from absorption spectra are indicated by circles. The lines in between are there to enhance the visibility. Missing circles indicate that no data was available after that treatment step.

In samples E6H3A and E6H3B ~ 0.9 ppm of NV was generated, predominantly in the form of NV⁻.

In sample E6H3D ~ 0.7 ppm of NV was generated, predominantly in the form of NV⁻. This sample had the highest N₂V⁰ concentration of all loaned samples at about ~ 0.1 ppm.

Figure 5.17 shows a comparison of the room temperature UV-VIS absorption spectra for all of the CVD samples introduced so far with NV concentrations in a range needed for laser assessment (~ 0.6 ppm of NV^- as discussed previously).

It can be seen that for samples E6H3A and E6H3B the shape of the phonon sideband is shifted with a peak at around 550 nm instead of 510 nm, as in the other samples. This is probably due to the NV population in those samples present mostly as NV^- . For sample E6H3D this is not as strongly the case (74% of total NV present as NV^- in comparison to 87% and 79% in E6H3A and E6H3B), but it is unclear why the shape is similar to samples with an equal distribution of NV^0 and NV^- . There might be another influence on the shape of the spectrum, which is not obvious from our data. In UV-VIS spectra taken at 77 K, the spectra of samples E6H3A, E6H3B and E6H3C look identical in shape (fig. 5.14).

From the samples received as grown, sample 1409E6sCVD02 shows the lowest background absorption of all samples. As discussed previously, this is due to the HPHT treatment reducing background absorption. From the pretreated samples, sample E6H3D has the lowest background absorption at the peak emission wavelength of NV^- .

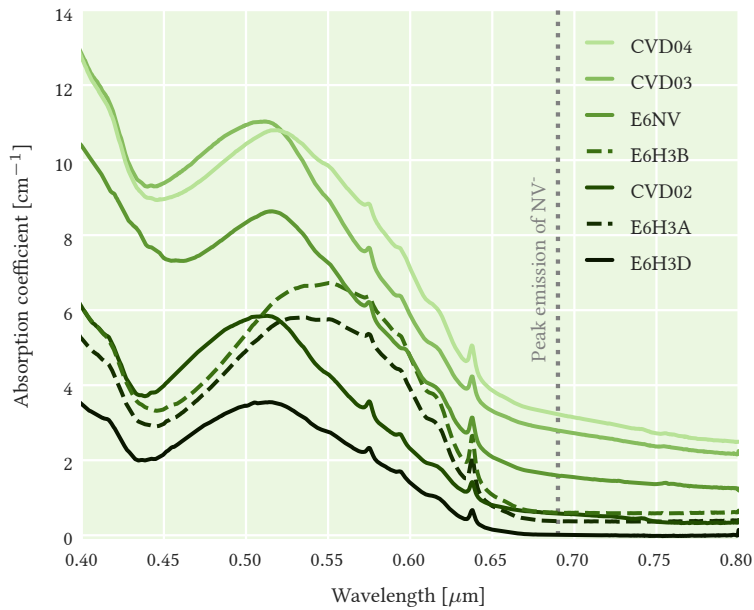


Figure 5.17: UV-VIS absorption spectra at room temperature of all CVD samples introduced so far after the last step of irradiation and annealing or as received in case of sample E6NV. The legend is sorted by the absorption coefficient at the peak emission wavelength of NV^- (690 nm, table 6.5) in descending order. Sample 1409E6sCVD04 is shown pre HPHT treatment.

In fig. 5.18, the overall NV concentration for the samples is plotted (left), as well as the ratio of the absorption coefficient at maximum emission for

NV⁻ (690 nm) to the absorption coefficient at maximum absorption for NV⁻ (565 nm), normalized to the highest value.

Samples 1409E6sCVD03 and E6NV have the highest absolute NV concentrations. Sample E6NV has a lower ratio of the absorption coefficients, mostly due to the lower absorption at 690 nm, as seen in fig. 5.17. For this reason sample E6NV has been chosen to be assessed for its laser related properties in chapter 7, Assessment of laser related properties.

Another sample, E6H3D, stands out for its low ratio of absorption coefficients, in comparison to other samples. Even though it had the lowest overall NV concentration, about half of the highest concentration, the NV concentration is still higher than the estimated minimum necessary for 50% pump absorption (0.6 ppm, see fig. 6.17, section 6.5). It was chosen to be assessed for its laser related properties due to the low absorption at the laser emission wavelength in comparison with a high absorption coefficient at the maximum absorption wavelength.

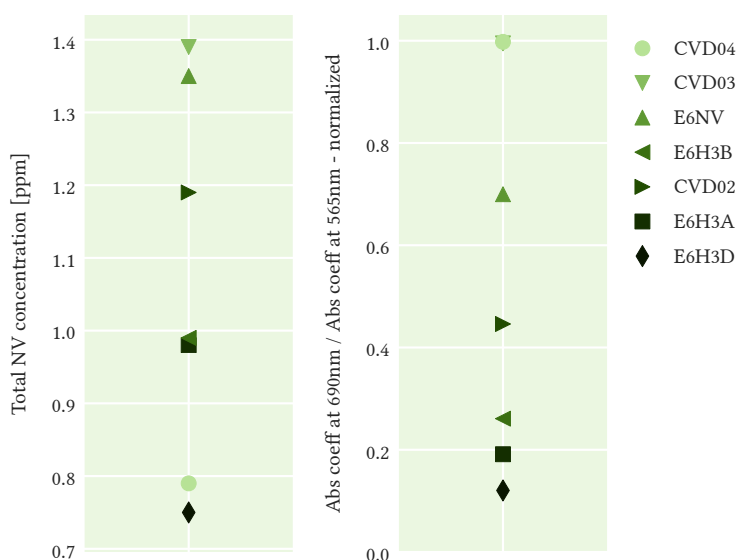


Figure 5.18:
Left: Total NV concentration of the samples.
Right: Ratio of absorption coefficient at 690 nm (maximum emission of NV⁻) to absorption coefficient at 565 nm (maximum absorption of NV⁻), normalized to the highest value.

Natural samples

Figure 5.19 shows the UV-VIS absorption spectrum taken at 77 K of one IaA natural diamond sample. All samples looked similar, as seen in fig. 5.20. It can be seen that while a large concentration of N_2V^0 was produced (1.8 ± 0.3 to 2.2 ± 0.4 ppm), the abundance of N_2 in the sample is responsible for the quenching of any luminescence. No traces of NV are visible in this sample. The small peak at ~ 594 nm is associated with irradiation damage [5].

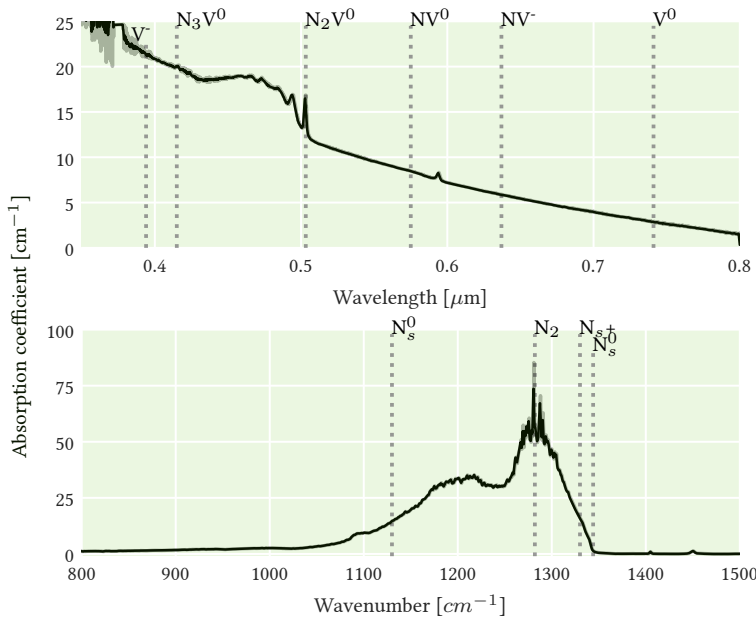


Figure 5.19: UV-VIS and FTIR spectrum of sample OR353-2 after the last step of synthesis.



Figure 5.20: Natural IaA diamond (OR358) sample after polishing

Figure 5.21 shows the FTIR spectra of natural IaB and IaAB samples before and after treatment.

In samples BRAZ62 and BRAZ70 most notably a reduction in the peak at around ~ 1360 cm^{-1} is observed. This peak is associated with B' ²⁸. The re-

²⁸ Platelets associated with a sharp line with a position varying between 1358 to 1380 cm^{-1}

duction of this peak is associated with the platlets breaking up into smaller clusters, possibly N_2 , N_4V and N_3V^0 ²⁹ centres [5]. No significant reduction of N_4V can be observed in sample BRAZ69. In BRAZ62 the peak for N_2 reduced by about 10%, while in sample BRAZ77 the peak for N_2 reduced by about 35% and the one for N_4V by about 10%. The peak at 1405 cm^{-1} , most clearly visible in sample BRAZ69, is associated with the presence of hydrogen [5].

²⁹ A vacancy and three substitutional nitrogen atoms with a C_{3v} symmetry (N_3)

Figure 5.22 shows the UV-VIS absorption spectra of polished natural IaB and IaAB samples taken at liquid nitrogen temperature (77 K).

Diamonds were only polished after treatment, as no polisher could be found in time before treatment was scheduled. Unfortunately this made it impossible to obtain UV-VIS spectra of the samples before treatment. In the absence of luminescence before treatment it is believed that N_2V^0 and N_3V^0 were generated in the samples after treatment. As expected, after HPHT treatment N_2V^0 and N_3V^0 were generated in the IaAB samples, and N_3V^0 in the IaB samples. This can be seen by the characteristic ZPLs in the low temperature absorption spectra in fig. 5.22. After additional irradiation and annealing, both BRAZ08 and BRAZ50 show a bright green luminescence (fig. 5.24), which can be associated with N_4V_2 [5, 27]. Neither of those samples contain N_2V^0 . In sample BRAZ50 the appearance of a peak associated with NV^- can be observed, which can be associated with the annealing and irradiation treatment. As seen before in the IaA sample, the peak at $\sim 594\text{ nm}$, associated with irradiation damage [5], is visible in both sample BRAZ08 and BRAZ50. In sample BRAZ62 about $2.2 \pm 0.4\text{ ppm}$ of N_2V^0 was generated, while in sample BRAZ77 $1.5 \pm 0.3\text{ ppm}$ was generated. It is not known why there is a difference of about 0.7 ppm of N_2V^0 in those samples. To determine the generation efficiency of N_2V , N_2V^- concentrations need to be monitored, which was not possible in this work. It is unclear if the reduction of the peak at $\sim 1360\text{ cm}^{-1}$, associated with B', is somehow related to the synthesis of N_2V^0 .

From these results it is not possible to propose a recipe for efficient N_2V^0 synthesis in IaAB diamond. But a possible correlation to the N_2 , N_4V and / or B' concentration can be proposed.

Figure 5.23 shows the IaB and IaAB samples before and after HPHT treatment and after treatment under UV light. Figure 5.24 shows the samples after polishing and in case of sample BRAZ08 and BRAZ50, after additional irradiation and annealing.

Polishing highlights one of the difficulties when working with natural samples. Samples can have inclusions and an uneven distribution of defects, depending on their growth. This can be seen most clearly in sample BRAZ50. Yellow-green luminescence in samples BRAZ50, BRAZ62 and BRAZ77 is caused by the presence of N_2V^0 , while blue luminescence is

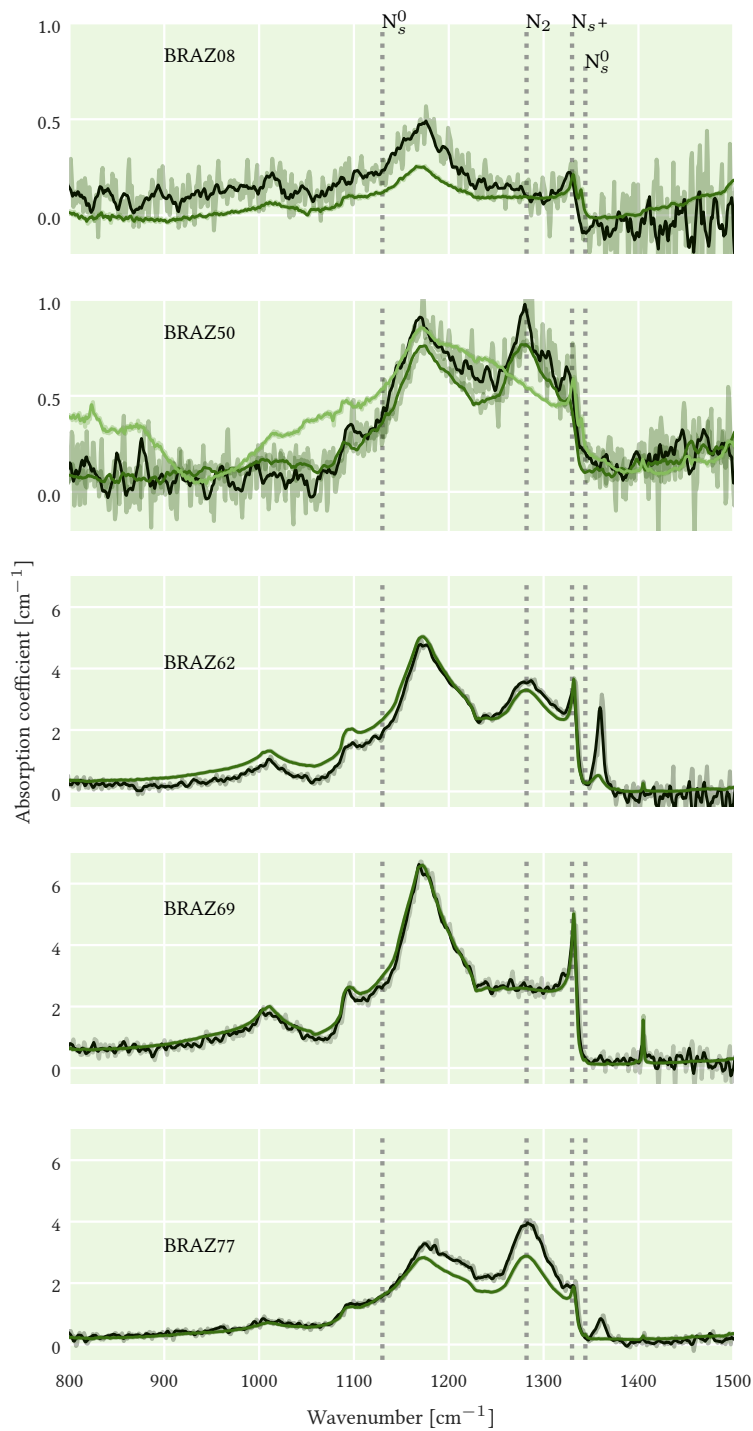


Figure 5.21: FTIR spectra of natural samples. Noisy data is smoothed using moving average, the original data is plotted in a lighter shade below.

Dark lines: Samples before treatment

Light lines: Samples after HPHT treatment

Additional light line in plot for BRAZ50 : Sample after irradiation and annealing

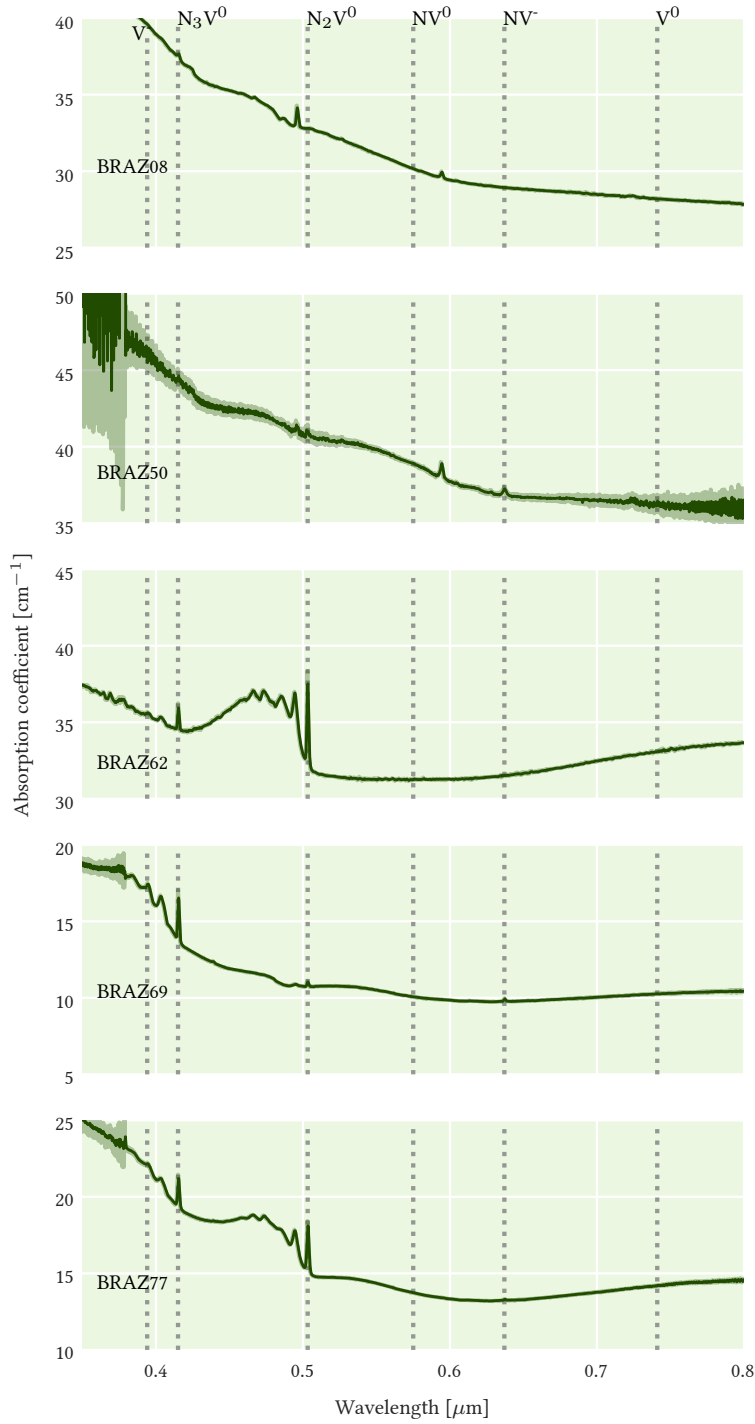


Figure 5.22: Absorption spectra of polished natural samples taken at liquid nitrogen temperature (77 K). Noisy data is smoothed using moving average, the original data is plotted in a lighter shade below.

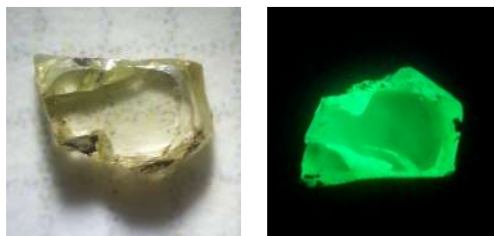
All spectra were taken after the last treatment step.



Figure 5.23: Natural diamond samples before and after HPHT treatment

Left: Before treatment
 Middle: After treatment
 Right: After treatment under UV light

BRAZ08



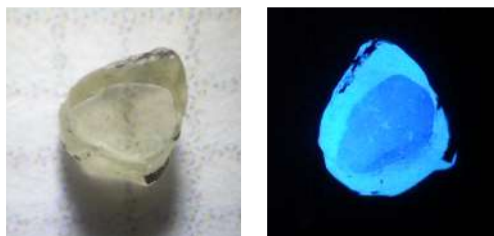
BRAZ50



BRAZ62



BRAZ69



BRAZ77

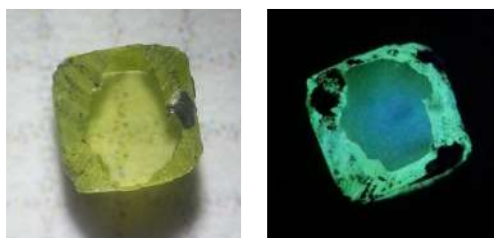


Figure 5.24: Natural diamond samples after polishing. Samples BRAZ08 and BRAZ50 have been irradiated and annealed. The other samples are in the same state as in fig. 5.23.

Left: Before treatment (none available here)

Middle: After treatment

Right: After treatment under UV light

Natural IaAB & IaB samples					
Treatment	Temperature [°C]	Pressure [GPa]	Time [min]	Dose [e/cm ²]	
BRAZ08					
HPHT	2100	11	3		
IRR				1.60E+17	
ANN	800	AP	300		
BRAZ50					
HPHT	2100	11	3		
IRR				1.60E+17	
ANN	800	AP	300		
BRAZ62					
HPHT	2100	11	3		
BRAZ69					
HPHT	2100	11	3		
BRAZ77					
HPHT	2100	11	3		

Table 5.6: Treatment details for natural samples.

IRR = Irradiation

ANN = Annealing

HPHT = High Pressure High Temperature

AP = atmospheric pressure

All irradiation mentioned in this table has been performed with 4.5 MeV electrons at Synergy-Health

IaB samples: BRAZ08, BRAZ69. All other samples are IaAB.

BRAZ08 and BRAZ50 have been irradiated and annealed additionally to HPHT treatment in order to convert any leftover N_s and N₂ with vacancies and enhance the number of NV or N₂V⁰.

UV-VIS								
Sample	N ₂ V ⁰ [ppm]			NV ⁻ [ppm]			NV ⁰ [ppm]	V ⁰ [ppm]
BRAZ50	N/A			0.09	±	0.04	N/A	N/A
BRAZ62	2.2	±	0.4	N/A			N/A	N/A
BRAZ69	0.13	±	0.02	0.05	±	0.02	N/A	N/A
BRAZ77	1.5	±	0.3	0.02	±	0.01	N/A	N/A

IR								
Sample	N ₂ [ppm]			N ₄ V [ppm]			N _s ⁰ [ppm]	N _s ⁺ [ppm]
BRAZ08	N/A			6	±	1	N/A	N/A
BRAZ50	2	±	1	21	±	2	N/A	N/A
BRAZ62	25	±	2	120	±	20	N/A	<1
BRAZ69	N/A			180	±	20	N/A	~1
BRAZ77	35	±	2	55	±	6	N/A	<1

Top: Defect concentrations from UV-VIS measurements of IaB & IaAB natural samples after treatment. A few ppm of N₂V⁰ could be produced in the IaAB samples with moderate nitrogen concentrations. **Bottom:** Defect concentrations from IR measurements of IaB & IaAB natural samples. N/A - No signal for this defect could be detected

Table 5.8: Defect concentrations from absorption spectra of IaB & IaAB natural samples.

caused by N_3V^0 . No luminescence was observed pre-treatment. The bright green luminescence of sample BRAZ08 and BRAZ50, after irradiation and annealing, despite little to no detectable concentration of N_2V^0 (figs. 5.22 and 5.25), is associated with N_4V_2 [5, 27].

Figure 5.25 shows the change in defect concentrations after each treatment step. In sample BRAZ08 a slight decrease in N_s^+ concentration and an increase in N_s^0 concentration could result from charge transfer, for example into vacancies generated during irradiation. No detectable concentrations of N_2V^0 or NV were found in the sample.

In sample BRAZ50 a reduction of the peak associated with N_2 after irradiation and annealing could indicate the generation of N_2V . N_2V^- could not be tracked with our measurements, but the slight increase in N_s^+ , an order of magnitude larger than the increase of NV^- , would allow for the possibility of some charge transferred to other defects in the sample.

In sample BRAZ69 traces of N_2V^0 and NV^- were generated (~ 0.1 ppm). In sample BRAZ62 >2 ppm and in sample BRAZ77 ~ 1.5 ppm of N_2V^0 were generated. It is unclear why the reduction of N_2 (about 10 ± 4 ppm for sample BRAZ62 and 15 ± 6 ppm for BRAZ77) does not match the generation of N_2V^0 . Judging from fig. 5.21, the concentration of N_4V seems not to be affected. No N_s^0 appeared in the samples and the concentration of N_s^+ didn't change, so it is unlikely that the N_2 centres dissociated into single nitrogen.

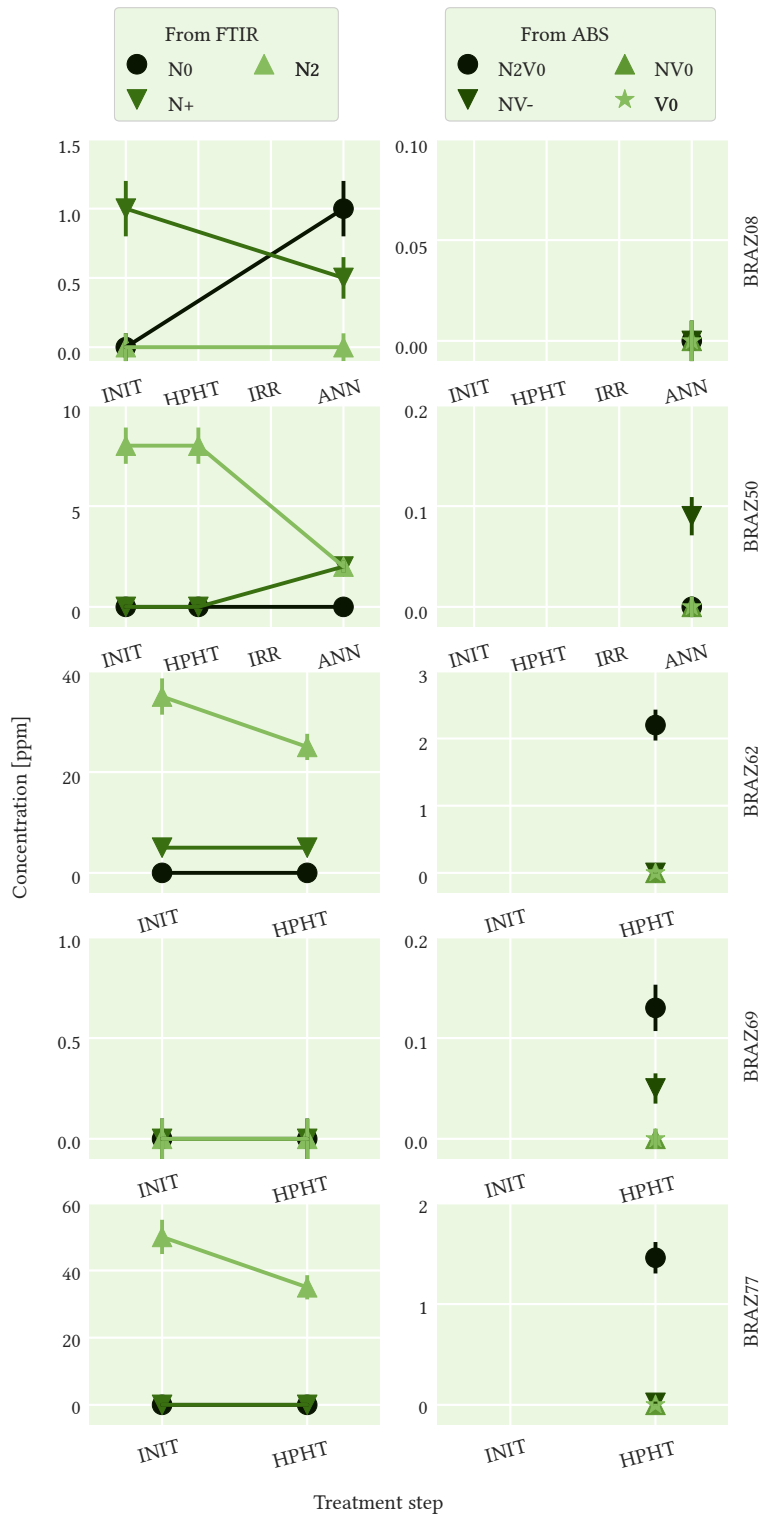


Figure 5.25: colour centre concentrations in natural diamond samples. Concentrations obtained from absorption spectra are indicated by markers. The lines in between are there to enhance the visibility. Missing markers indicate that no data was available after that treatment step.

5.5 Summary

THE SYNTHESIS of diamond samples with roughly 0.6 ppm of NV and 0.9 ppm of N_2V^0 was attempted in this work. Concentrations were estimated using literature parameters and assumptions discussed in detail in section 6.5, A potential diamond colour centre laser. Synthesis routes were discussed previously in chapter 3, Synthesis of colour centres in diamond.

For the synthesis of NV in CVD diamond, samples were irradiated with 4.5 MeV electrons and then annealed at 800°C for up to 5 hours. HPHT treatment of brownish synthetic CVD diamond significantly reduced background absorption at the target wavelength, in our case from 1.62 to 0.08 cm^{-1} at 690 nm (max NV^- emission wavelength). This step is costly in time and treatment expenses, and has a risk to damage the sample. As-grown material with low background absorption is always preferable, if available.

For the synthesis of N_2V^0 in CVD diamond, NV containing samples were HPHT treated at temperatures around 1500°C and 7.5 GPa for up to 48 hours. In one sample a reduction of 1 ppm of NV and the generation of 0.5 ppm of N_2V^0 was observed under these conditions. It is to be determined at what temperature the conversion efficiency is highest and if treatment times can be reduced by increasing the temperature by a few hundred degrees. Additionally, further experiments are needed to determine how much of the NV can be converted into N_2V^0 .

N_2V^0 was also generated by short HPHT anneals of brownish IaAB natural diamond samples at 2100°C and 11 GPa for 3 minutes, yielding luminescent samples with up to ~ 2 ppm of N_2V^0 . A systematic study is needed to determine the ideal time and temperature for maximum N_2V^0 yield in dependence on the starting material, in particular the concentrations of N_2 , N_4V and B' .

A maximum of 0.65 ppm of NV^0 , 0.85 ppm of NV^- and 2.2 ppm of N_2V^0 could be generated in different samples.

Samples E6NV and E6H3D, as well as BRAZ62 and BRAZ77, were considered for assessment of their laser related parameters in chapter 7. Sample E6H3D had a particularly low background absorption at the peak emission of NV^- (0.1 cm^{-1} at 690 nm & 2.34 cm^{-1} at 565 nm), and sample E6NV had a high concentration of NV (~ 1.3 ppm) with relatively low absorption at peak emission and high absorption at peak absorption for NV^- (1.59 cm^{-1} at 690 nm & 6.4 cm^{-1} at 565 nm). Samples BRAZ62 and BRAZ77 were the only luminescent samples with a high N_2V^0 concentration available.

The assessment of laser related properties is discussed in the next chapter 6, Progress towards a laser based on colour centres in diamond.

References

- [1] J. Solé, L. Bausá, and D. Jaque. *An Introduction to the Optical Spectroscopy of Inorganic Solids*. 2005. DOI: 10.1002/0470016043.
- [2] G. Huber, C. Kränkel, and K. Petermann. "Solid-state lasers : status and future". EN. In: *Josa B* 27.11 (Oct. 2010), pp. 93–105. ISSN: 0740-3224. DOI: 10.1364/JOSAB.27.000B93.
- [3] I. Aharonovich, A. D. Greentree, and S. Praver. "Diamond photonics". In: *Nature Photonics* 5.7 (June 2011), pp. 397–405. ISSN: 1749-4885. DOI: 10.1038/nphoton.2011.54. URL: <http://dx.doi.org/10.1038/nphoton.2011.54>.
- [4] R. P. Mildren and J. R. Rabeau. *Optical Engineering of Diamond*. Ed. by R. P. Mildren and J. R. Rabeau. Weinheim, Germany: Wiley-VCH, Apr. 2013. ISBN: 352741102X. DOI: 10.1002/9783527648603.
- [5] A. M. Zaitsev. *Optical Properties of Diamond : A Data Handbook*. Springer, 2001, p. 502. ISBN: 354066582X. DOI: 10.1007/978-3-662-04548-0.
- [6] M. A. Prelas et al. *Wide Band Gap Electronic Materials*. Vol. 1. Springer Science & Business Media, 1995. ISBN: 9789401040785. DOI: 10.1007/978-94-011-0173-8.
- [7] I. A. Dobrinets, V. G. Vins, and A. M. Zaitsev. *HPHT-Treated Diamonds*. Vol. 181. Springer, 2013. ISBN: 978-3-642-37489-0. DOI: 10.1007/978-3-642-37490-6.
- [8] S. Subedi et al. "Laser spectroscopy of highly doped NV-centers in diamond". In: *Solid State Lasers XXVII: Technology and Devices* 10511 (Feb. 2018). Ed. by W. A. Clarkson and R. K. Shori, p. 84. DOI: 10.1117/12.2290705.
- [9] C.-K. Lin et al. "Excitation properties of the H3 defect center in diamond: A theoretical study". In: *Chemical Physics Letters* 475.1-3 (June 2009), pp. 68–72. ISSN: 0009-2614. DOI: 10.1016/J.CPLETT.2009.05.011.
- [10] C. B. Hartland. *A study of point defects in CVD diamond using electron paramagnetic resonance and optical spectroscopy*. Aug. 2014. URL: <http://wrap.warwick.ac.uk/id/eprint/67156>.
- [11] M. D. Crossfield et al. "The role of defect interactions in reducing the decay time of H3 luminescence in diamond". In: *Journal of Physics C: Solid State Physics* 7.10 (May 1974), pp. 1909–1917. ISSN: 0022-3719. DOI: 10.1088/0022-3719/7/10/018.
- [12] I. A. Dobrinets, V. G. Vins, and A. M. Zaitsev. *Diamonds Used for HPHT Treatment*. Berlin, Heidelberg: Springer Berlin Heidelberg, 2013, pp. 5–25. ISBN: 978-3-642-37490-6. DOI: 10.1007/978-3-642-37490-6_2.
- [13] T. Yamamoto et al. "Extending spin coherence times of diamond qubits by high-temperature annealing". In: *Physical Review B - Condensed Matter and Materials Physics* 88.7 (2013), p. 75206. ISSN: 10980121. DOI: 10.1103/PhysRevB.88.075206.
- [14] Y. Chu et al. "Coherent optical transitions in implanted nitrogen vacancy centers Coherent optical transitions in implanted nitrogen vacancy centers". In: *Nano letters* 14.4 (2014), pp. 1982–1986. DOI: 10.1021/nl404836p.
- [15] J. Bernholc et al. "Mechanism of self-diffusion in diamond". In: *Phys. Rev. Lett.* 61.23 (Dec. 1988), pp. 2689–2692. DOI: 10.1103/PhysRevLett.61.2689.
- [16] A. Mainwood. "Nitrogen and nitrogen-vacancy complexes and their formation in diamond". In: *Physical Review B* 49.12 (Mar. 1994), pp. 7934–7940. ISSN: 01631829. DOI: 10.1103/PhysRevB.49.7934.
- [17] M. R. Brozel, T. Evans, and R. F. Stephenson. "Partial dissociation of nitrogen aggregates in diamond by high temperature-high pressure treatments". In: *Proceedings of the Royal Society of London A: Mathematical, Physical and Engineering Sciences* 361.1704 (1978), pp. 109–127. ISSN: 0080-4630. DOI: 10.1098/rspa.1978.0094.
- [18] T. Evans and Z. Qi. "The Kinetics of the Aggregation of Nitrogen Atoms in Diamond". In: *Proceedings of the Royal Society A: Mathematical, Physical and Engineering Sciences* 381.1780 (May 1982), pp. 159–178. ISSN: 1364-5021. DOI: 10.1098/rspa.1982.0063.
- [19] M. D. Crossfield et al. "The role of defect interactions in reducing the decay time of H3 luminescence in diamond". In: *Journal of Physics C: Solid State Physics* 7.10 (1974), pp. 1909–1917. ISSN: 0022-3719. DOI: 10.1088/0022-3719/7/10/018.
- [20] A. T. Collins, H. Kanda, and H. Kitawaki. "Colour changes produced in natural brown diamonds by high-pressure, high-temperature treatment". In: *Diamond and Related Materials* 9.2 (Mar. 2000), pp. 113–122. ISSN: 09259635. DOI: 10.1016/S0925-9635(00)00249-1.
- [21] A. T. Collins et al. "High-temperature annealing of optical centers in type-I diamond". In: *Journal of Applied Physics* 97.8 (Apr. 2005), p. 083517. ISSN: 00218979. DOI: 10.1063/1.1866501.
- [22] F. De Weerd and A. T. Collins. "HPHT annealing of natural diamond". In: *New Diam. Front. Carbon Technol* 17.2 (2007), pp. 91–103.
- [23] K. T. Takeru Nakashima, Shuichi Satoh. *Diamond laser crystal and method manufacturing the same*. Aug. 1990. URL: <https://www.google.com/patents/US4950625>.
- [24] PerkinElmer. *Technical Specifications for the LAMBDA 1050 UV/Vis/NIR and LAMBDA 950 UV/Vis/NIR Spectrophotometers*. Tech. rep. URL: <http://camcor.uoregon.edu/site/wp-content/uploads/2012/11/Lambda-1050-spec.pdf>.
- [25] M. W. Dale. "Colour centres on demand in diamond". PhD thesis. University of Warwick, 2015. URL: <http://wrap.warwick.ac.uk/id/eprint/80044>.
- [26] L. J. Rogers et al. "Electronic structure of the negatively charged silicon-vacancy center in diamond". In: *Physical Review B* 89.23 (2014), p. 235101. DOI: 10.1103/PhysRevB.89.235101.
- [27] R. Shor. "Fluorescence Produced by Optical Defects in Diamond: Measurement, Characterization, and Challenges". In: *Gems & Gemology* 49 (1) (2013), pp. 2–15. DOI: 10.5741/GEMS.49.1.2..

6

Progress towards a laser based on colour centres in diamond

Contents

6.1	Interaction of light and matter	130
	General Principles	130
	A short history of lasers	136
6.2	Key parameters for solid state lasers	139
	Host medium and Optically active centres	139
	Luminescence lifetime	141
	Luminescence quantum yield	142
	Emission and absorption cross sections	144
	Gain coefficient	145
6.3	Luminescence spectroscopy	146
	Integrating sphere measurements	146
	Correction of luminescence spectra for contributions of other centres	146
	Time-resolved luminescence spectroscopy	147
6.4	Diamond in laser engineering	149
	Diamond in comparison to other optical materials	149
	Doping diamond	150
6.5	A potential diamond colour centre laser	152
	Typical colour centre lasers in alkali halides	152
	The NV centre in diamond	155
	The N_2V^0 centre in diamond	160
	Predicted operation of a NV and N_2V^0 based laser	162
6.6	Summary	168
	References	169

6.1 Interaction of light and matter

ON THE PATH to test the suitability of a material as a laser gain medium, there are key laser related parameters to investigate. To give context to these parameters an introduction to laser physics is given in this section.

The general principles of light and matter interaction are introduced, followed by an introduction to laser physics, the components needed to build a laser and a brief historical overview of lasers.

Based on this the following sections will cover Key parameters for solid state lasers (section 6.2), Time-resolved luminescence spectroscopy (section 6.3) as a spectroscopic technique in addition to those presented previously in chapter 4, Defect quantification and spectroscopic methods, Diamond in laser engineering (section 6.4) with examples of areas where diamond is already utilized, and A potential diamond colour centre laser (section 6.5), a prediction of how a diamond laser based on NV¹ and N₂V⁰² might look like.

A laser based on colour centres³ in diamond could not be demonstrated in this work. The most promising samples produced during synthesis, according to their background absorption, luminescence spectra and colour centre concentration, presented in chapter 5, Results of the colour centre synthesis, were assessed for their laser related properties in chapter 7, Assessment of laser related properties.

General Principles

In this part we'll cover the general principles of laser physics based on [2, 3, 4, 5, 6].

Interactions of light and matter include absorption or emission processes. In the Rutherford–Bohr model, atoms are surrounded by electrons in discrete orbital shells. These electrons can move between different energy levels, absorbing or emitting energy. The simplest such system has two energy levels, E_1 and E_2 .

Three processes involving the interaction of matter with electromagnetic waves can take place:

- **Absorption:** An electron in the ground state (E_1) absorbs a photon of energy $E_p = E_2 - E_1 = h\nu$ and is excited to a higher energy level (E_2). h is Planck's constant and ν the frequency of the photon.
- **Spontaneous emission:** An electron in an upper energy level (E_2) emits a photon of energy $E_p = E_2 - E_1 = h\nu$ and decays into a lower energy

¹ A substitutional nitrogen adjacent to a vacancy with a C_{3v} symmetry

² The neutrally charged state of N₂V (H3)

³ A type of structural defect, which produces absorption and emission bands that are different to those of the pure crystal [1]

level (E_1). The emitted photon has a random direction and phase.

- **Stimulated emission:** An incoming photon with energy $E_p = h\nu$ causes the decay of an electron in an upper energy level by emission of a photon. The second photon has the same energy, direction and phase as the incident photon.

These processes, illustrated for a simple two level system in fig. 6.1, can be described as a change of the population in the respective levels.

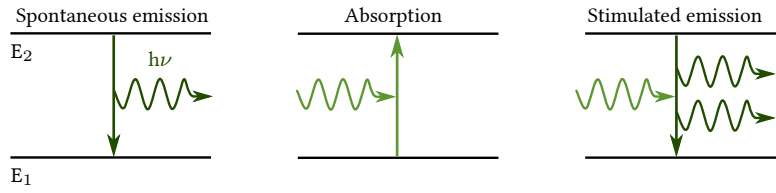


Figure 6.1: Types of light and matter interactions. Adapted from [7].

N_1 and N_2 are referred to as the **populations** of the energy levels E_1 and E_2 , respectively. The total concentration of optically active centres $N = N_1 + N_2$ is constant. The change of N_2 due to absorption can be described by:

$$\left(\frac{dN_2}{dt}\right)_{abs} = W_{12}N_1 \quad (6.1)$$

The rate of the absorption is defined by:

$$W_{12} = \sigma_{12} \cdot F \quad (6.2)$$

with the photon flux $F = I/(h\nu)$, the wave intensity I , and the **absorption cross section** σ_{12} . Cross sections have the dimensions of an area and are a representation of the probability of an interaction process occurring at a given wavelength.

The decay by spontaneous emission is characterized by the radiative **lifetime** of the excited state τ_r . In this simplification we assume that no non-radiative processes occur that could contribute to the depopulation.

$$\left(\frac{dN_2}{dt}\right)_{sp\ em} = -\frac{N_2}{\tau_r} \quad (6.3)$$

Stimulated emission, like absorption, can be described as a process triggered by the interaction with a photon:

$$\left(\frac{dN_2}{dt}\right)_{st\ em} = -W_{21}N_2 \quad (6.4)$$

with the transition probability and emission cross section for the transition from level 2 to level 1 in this case.

The overall time evolution of the population N_2 can be then written as:

$$\left(\frac{dN_2}{dt}\right)_{total} = W_{12}N_1 - W_{21}N_2 - \frac{N_2}{\tau_r} \quad (6.5)$$

with $(dN_2/dt) = -(dN_1/dt)$ for every process.

An electromagnetic wave with the frequency $\nu = (E_2 - E_1)/h$, which travels along the z axis of a material with energy levels E_1 and E_2 can trigger absorption and stimulated emission. The change in photon flux between z and $z+dz$, $dF(z)$, along a length dz is given by difference of the number of photons emitted and absorbed:

$$dF(z) = \sigma \cdot (N_2 - N_1) F(z) dz \quad (6.6)$$

with $\sigma = \sigma_{12} = \sigma_{21}$ for non-degenerate energy levels. If l is the length of the medium, as indicated in fig. 6.3, then the photon flux at the beginning of the medium $F(0)$ can be related to the one at the end of the medium $F(l)$ through:

$$F(l) = F(0) \cdot \exp(g \cdot l) \quad (6.7)$$

with the **gain coefficient**

$$g = (N_2 - N_1) \sigma \quad (6.8)$$

Light amplification by stimulated emission ($g > 0$) occurs if the population of the upper level is larger than the one in the lower level $N_2 > N_1$, which is referred to as **population inversion**.

For $N_2 < N_1$ the medium acts as an absorber.

At thermal equilibrium the distribution of the populations is determined by Boltzmann statistics:

$$\frac{N_2}{N_1} = \exp\left(-\frac{E_2 - E_1}{k_B T}\right) \quad (6.9)$$

with the Boltzmann constant k_B and the temperature T . Equation (6.9) shows that for $k_B T \ll E_2 - E_1$ the population N_2 is small in comparison to N_1 . This is true for transitions in the VIS⁴ and NIR⁵ at room temperature.

⁴ Visible (380-780 nm)

⁵ Near-InfraRed (0.78-3 μm)

The process to lift population from the ground state to the excited state is called **pumping**. It is needed to create population inversion. The change

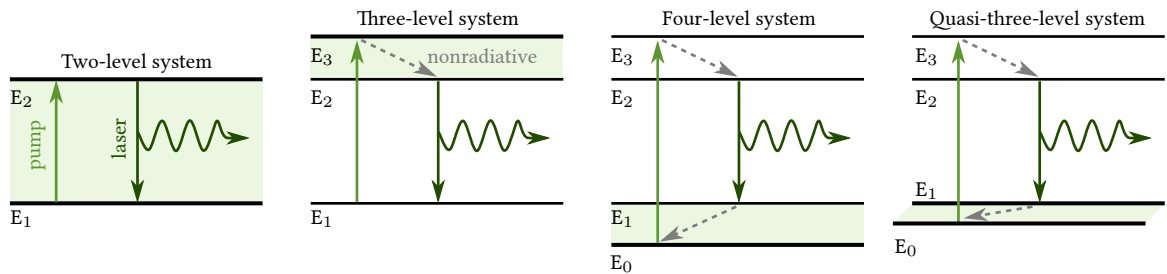
in the population of the excited state due to pumping is described by:

$$\left(\frac{dN_2}{dt}\right)_p = W_p N_g \quad (6.10)$$

with the pumping rate W_p and the population of the ground level of the system N_g .

In a two level system, if N_1 and N_2 become equal, absorption and stimulated emission compensate each other. This is referred to as **saturation**, the medium becomes transparent, and no population inversion can be achieved.

Multiple energy levels, as illustrated in fig. 6.2, are needed to separate the pump absorption and laser emission.



Three energy levels are the minimum to achieve population inversion in an optically pumped system. The third level prevents the depopulation of the upper laser level by the pump. The population is excited from the ground level E_1 to an energy level E_3 . From there it decays into the upper laser level E_2 by non-radiative processes. The laser transition is the transition between level E_2 and level E_1 . If the decay from level E_3 to E_2 is fast, there will be no population in level E_3 for stimulated emission of the pump to occur. Additionally, the pump doesn't influence the depopulation of the energy level E_2 . Three-level systems have a high laser threshold. The re-absorption of population in level E_1 into level E_2 by reabsorption of laser light will be a significant process. For this reason, to achieve net gain in such a system, strong pumping is needed in order to effectively get >50% of the initial population of E_1 up into E_2 . In principle, a three-level system could also have the radiative transition between E_3 and E_2 and the non-radiative between E_2 and E_1 . In this case the pumping requirements are not as strong. In practice, most laser lasers are four-level systems.

An example of a three-level system is the first laser that was realized using ruby.

Four energy levels facilitate the laser process, overcoming the problems of

Figure 6.2: Energy level diagrams of different laser systems. Adapted from [7]. In the two-level system on the left both absorption and emission occur between the energy levels E_1 and E_2 . For each addition of an energy level, the highlighted area marks the additional separation between the pump absorption and laser emission.

laser light reabsorption and the strong pump requirement in a three-level system.

The pump excites the population from level E_0 into E_3 , from where it decays into the upper laser level E_2 . From level E_2 it decays into the lower laser level E_1 . As before, the laser transition is the transition between level E_2 and level E_1 . The lower laser level is above the ground state and any population in it quickly decays into the ground state level ($N_2 \approx 0$), from where it can be excited by the pump again. This is also the reason why population inversion is so much easier to achieve in a four-level system.

Examples for four-level systems are some neodymium doped gain media, e.g. all the transitions in Nd:YAG, which is most commonly used at 1064 nm, except for the 946 nm transition, which is quasi-four-level.

If the lower laser level and the ground level are so close that the laser level is populated in thermal equilibrium at the operating temperature, that system is called quasi-four-level system. This is the case, for example, if the quantum defect of a gain medium is small. The quantum defect describes the energy difference between the pump and laser photon $q = h\nu_{pump} - h\nu_{laser}$. In such a system there will be some reabsorption of the laser light. This leads to an increase in the threshold power, but the slope efficiency isn't affected. Cooling the gain medium can counteract that by depopulating the lower laser level.

Examples of quasi-four-level systems are ytterbium-doped gain media or semiconductors.

To build a laser, a device that generates and amplifies a highly coherent, highly directional light beam, three components are needed:

- A medium that **amplifies** light by **stimulated emission**
- A pump source to generate **population inversion**
- A resonator to trap the light in to achieve **laser oscillation**

The principle setup is illustrated in fig. 6.3.

The **lasing medium** may be a solid, gas or liquid. It contains atoms or molecules that act as optically active centres. Different types of lasers are listed in table 6.1.

The **pump** adds energy to the system to generate population inversion. Pumps can be optical, for example different kinds of lamps or even other lasers, electrical or chemical.

The **optical resonator**, or optical cavity, surrounds the laser medium. In its simplest form it consists of two mirrors what are perfectly aligned to allow for the generated photons to be reflected back and forth through the

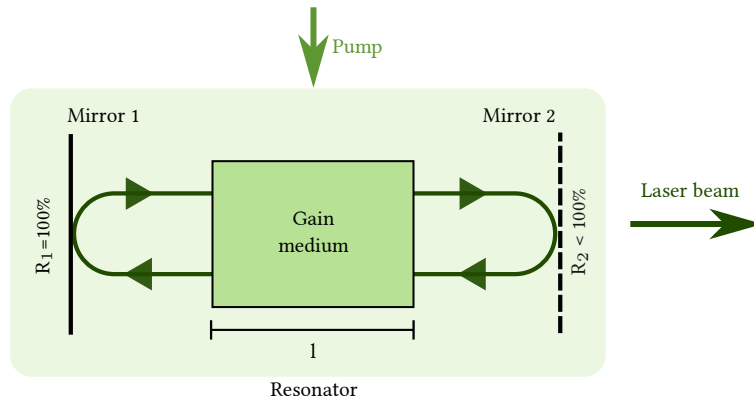


Figure 6.3: Illustration of a laser oscillator. Adapted from [6]

Laser type	Examples
Solid state	Doped crystals; colour centres
Semiconductor	Quantum well; Cascade lasers; VECSELS
Gas	Ions; Metal-vapor; Neutral non-metal
Dye	Organic dye; Solid-state dye
Other types	Raman; FEL

Table 6.1: An overview of different laser types.

laser medium, stimulating further emission with each round trip. One of those mirrors is partially transparent to allow the light beam to exit. This mirror is referred to as OC⁶.

⁶ Output Coupler

The population required to ensure the round trip gain equals the round trip loss γ is called critical inversion N_c :

$$N_c = \frac{\gamma}{2\sigma l} \tag{6.11}$$

Once the critical inversion is reached, stimulated emission, triggered initially by a few spontaneously emitted photons, can build up and in turn generate more photons by stimulated emission. This is referred to as **laser oscillation**.

The **threshold pump power** for a four-level laser, P_{th} , is the critical pump rate R_{cp} , the pump rate at which critical inversion is reached, multiplied with the pumped volume and the pump photon energy $h\nu_p$ over the pump efficiency η_p :

$$P_{th} = \frac{\gamma}{\sigma\tau} \cdot \frac{h\nu_p}{\eta_p} \cdot A \tag{6.12}$$

with the pump area A and the losses γ .

The **output power** P_{out} of a laser is then given by the difference between pump power P_p and threshold power P_{th} , multiplied with the **slope efficiency** η_s :

$$P_{out} = \eta_s(P_p - P_{th}) \quad (6.13)$$

The slope efficiency, $\eta_s = dP_{out}/dP_p$, is defined as the product of the *pump efficiency*, *output coupling efficiency*, *quantum defect*⁷, *quantum efficiency*⁸ and *transverse efficiency*⁹. It can range from less than 1% in low-efficiency lasers (like a HeNe) to 20-50% or higher in high-efficiency lasers [6].

⁷ the ratio of laser to pump photon energy

⁸ Also referred to as quantum yield (QY)

⁹ The ratio between transverse mode and pumping area

The **product of emission cross section and lifetime** $\sigma\tau$ is purely dependent on material properties and can be regarded as a figure of merit for a given laser [6].

A short history of lasers

The first laser was a solid state laser based on ruby, demonstrated in 1960 [8]. Despite advancements in other laser types, in particular semiconductor lasers, solid state lasers still play an important role in science, industry, and daily life. The quest for a *perfect solid state gain material* is still ongoing [9].

Laser is an acronym for *Light Amplification by Stimulated Emission of Radiation* [10]. It refers to the principle of operation, but it is used as a term for the device itself. The theoretical groundwork goes back to the idea of the existence of physical quanta of light, called photons. The mechanism for the absorption, spontaneous emission, and stimulated emission of photons was proposed by Einstein in 1917 [11].

Ideas for a device that would exploit this concept in order to amplify radiation were proposed in early 1950 and more famously in 1951 by Charles Townes. In 1953 such a device based on the amplification of microwaves using ammonia was realized. It was referred to as maser, where the m refers to microwaves. The first solid state maser followed in 1956. A ruby based maser was demonstrated a year later in 1957. This ultimately led to the idea by Maiman to harness ruby to build a laser, even though the outlook for ruby as a laser gain material was disputed at the time [8, 12].

Ruby is the historically used term for red samples of the mineral corundum, a crystalline form of aluminium oxide ($\alpha\text{-Al}_2\text{O}_3$). In this historical context other colourations of corundum were referred to as sapphire. There is no general agreement on where to draw the line in this characterization and it can lead to some confusion, especially when the material

Ti:sapphire¹⁰, a pink sapphire, will be discussed. It is interesting to point out that α -Al₂O₃ is to date considered to be the second best solid state host material regarding its thermo-mechanical properties. The best material right after diamond [9].

¹⁰ titanium-sapphire - Ti³⁺:Al₂O₃

From 1960 onwards many demonstrations of lasers followed. The ruby laser by Maiman, the first gas laser based on helium-neon and the first diode laser were all demonstrated in 1960. In 1964 the Nobel Prize in Physics was awarded to Townes, Basov and Prokhorov for *fundamental work in the field of quantum electronics, which has led to the construction of oscillators and amplifiers based on the maser-laser principle* [13].

Laser light has a set of very special properties that can be memorized using the three C's [14].

- One Colour: Laser light is monochromatic, it has a very narrow emission wavelength.
- Coherence: all the photons emitted are in the same quantum state, they are in phase and have the same polarization
- Highly Collimated: laser light is minimally divergent (with some differences due to cavity design)

The wavelength of the laser beam, its tunability and pulse length are dependent on the laser material. Additionally, possible designs of a laser vary with different laser types. New materials and laser designs are constantly being investigated in order to build better, more versatile lasers at custom wavelengths.

Lasers can be categorized in different types based on the lasing medium used and the cavity design.

In a gas laser an electric current is discharged through a gas to produce light. A laser based on HeNe¹¹ was the first laser to emit a cw¹² beam. Today different gases are used for different application. They are comparatively cheap, robust and flexible. Heat can be removed efficiently from the cavity. Additionally, optical distortions are low in the gas and most gas lasers can emit a high-quality beam. Gas lasers like those based on CO₂ produced high output powers. They are mostly used for engraving, cutting and welding. HeNe lasers can be operated on a range of discrete lines, but produce much lower output powers.

¹¹ Helium-Neon

¹² continuous wave

Gas lasers are used where certain wavelengths are needed that are difficult to obtain in solid-state lasers and because high optical powers can be achieved cost-efficiently [15].

Dye lasers have a liquid solution usually containing organic molecules as gain medium. They are broadly tunable and the generation of ultrashort pulses is possible. The power conversion efficiency is typically between 10 and 30%. Their biggest disadvantage is their complicated or dangerous handling. Many dyes are poisonous or carcinogenic and the solvents are often flammable. The dyes have long recovery times and degenerate after a while. This makes it necessary to have a steady flow of the dye going through the pump and for the dye to be replaced after some time.

Laser diodes, lasers based on semiconductors, are strictly speaking a category of solid state lasers, but are usually categorized separately. Compared to other laser types these are usually very compact, making them an ideal choice in small electronic devices. They are very power efficient (of the order of $\sim 50\%$ and above), but beam quality is inferior to other laser types. Large beam divergence, asymmetry of the radius and astigmatism, when the horizontal and vertical beam focus lies at different points in the beam path, require lenses for correction.

Solid state lasers are of particular interest for this work, as a laser based on colour centres in diamond falls into this class. They produce probably the widest range of outputs, often with the highest performance. They are based on a solid state laser medium, typically a glass, ceramic or crystal host doped with optically active ions or one including colour centres. Solid state lasers can have different geometries, most commonly rod, slab, disk or as waveguide structures such as fibres. To ease cooling a large ratio between the cooled surface and the pumped volume is beneficial. The closer the heat-sink used for cooling is to the pumped volume, the better.

Important solid state lasers based on rare earth ions are ytterbium-, neodymium-doped and erbium-doped materials. Common host materials for those include yttrium aluminium garnet (YAG), yttrium vanadate (YVO_4) among others. The ions are not strongly coupled to the host lattice vibrations, resulting in narrow absorption and emission features. The upper state lifetime of this kind of solid state lasers can be long, in the order or micro- to milliseconds, which can be utilized for pulsed operation. Average output powers of a few kW for bulk lasers and fibres are available commercially.

Solid state lasers based on transition metals include Ti:sapphire lasers and lasers based on chromium (e.g. Cr^{4+} :YAG, Cr^{3+} :LiSAF). The absorption and laser emission features in such materials are typically very broad, resulting from the strong coupling of the ions with lattice vibrations. Titanium sapphire is known for its tunability over a wide wavelength range and the generation of ultrashort pulses.

6.2 *Key parameters for solid state lasers*

THE KEY LASER PARAMETERS and their implication for the laser operation are outlined here. Linking spectroscopic properties of a sample to the laser parameters allows, in principle, to correlate those with crystal growth and synthesis parameters. In this way spectroscopic analysis is a powerful tool both to find new laser materials as well as improve existing ones.

Through iteration of colour centre synthesis in diamond, improved sample parameters can be approached and this data could be used to identify the improvements required to get closer to samples suitable for laser operation. At the time this thesis was written no working recipe is known to fabricate a lasing colour centre containing diamond sample.

The one literature report of a diamond colour centre laser provides very limited detail on the sample, and only general instructions for the fabrication of N_2V^0 in diamond [16]. Other attempts at making a colour centre containing diamond laser crystal are mentioned in more detail in section 6.5, A potential diamond colour centre laser.

Host medium and Optically active centres

It is important that the host material for a solid state laser has a range of excellent optical and thermo-mechanical properties [2, 3, 4, 5, 6]. It has to have a **high optical quality**, minimizing parasitic absorption and scattering caused by the presence of parasitic centres. Additionally, the un-doped material should have **high optical transparency** in the pump absorption and laser emission region. The variability of the **refractive index** should be small, to prevent the irregular propagation of the beam in the medium. **Chemical inertness** and **mechanical stability** is beneficial to ease the manufacturing process and prevent damage due to stress, deformation and fracture during laser operation. A **high thermal conductivity** is beneficial in any case to minimize effects caused by thermal deformation of the host material. This is especially important in high power lasers. It should be possible to grow the material uniformly and it should allow for homogeneous **doping** with laser-active centres.

Additionally, besides serving as a container, the choice of host material strongly **influences the radiative characteristics** of the optically active centres: In particular the cross sections for the pump and laser transitions, the bandwidth and the upper state lifetime. **Non radiative transitions** are influenced by the **maximum phonon energy** of the material. This can be detrimental to laser performance, by lowering the upper laser level population, or beneficial, by depopulating the lower laser level.

Optimizing all those attributes at the same time is not possible. For this reason a broad range of different materials with different advantages are investigated for their utility as host materials, depending on the specific requirements of the application they are intended for.

Optically active centres provide energy levels within the energy gap of the host material, so that optical transitions between those energy levels are possible [1]. In most cases, in the context of solid state lasers, this refers to dopant ions in a crystal. In a wider context this also includes lattice defects, which we have introduced as colour centres. The interaction of optically active centres with their environment has been covered in section 2.2, Fundamentals of crystallographic defects. Here, we will briefly describe the most important parameters to produce light amplification.

The laser operation of an optically active centre is characterized by a set of key parameters [4, 6]. Whether a good pump source is available and the efficiency of the pump absorption are determined by the **absorption wavelength and cross section**. The **emission wavelength region, the cross section and gain spectrum** determine at which wavelengths the laser can be operated and its tuning range. A broad gain spectrum is also necessary for the generation of ultrashort pulses. The **luminescence lifetime**, which is identical to the lifetime of the upper laser level, is one of the factors that determine the laser threshold that has to be overcome, as it determines the magnitude of losses through spontaneous emission. It is typically in the order of nanoseconds up to micro- or even milliseconds in rare earth doped media. Longer lifetimes are more suitable for Q-switched¹³ operation, due to the possibility to store large amounts of energy in the medium. A large **product of emission cross section and luminescence lifetime** ($\sigma \cdot \tau$) facilitates laser operation by lowering the critical pump rate to reach population inversion (see eq. (6.11) and eq. (6.12)). A high **quantum efficiency** indicates few losses by quenching and other parasitic absorption processes in the system. A small **quantum defect**, the difference in energy between the pump and laser photons, means less energy is transferred into heat by non radiative transitions. The **doping concentration** is correlated with the absorption and gain coefficients (eq. (6.24) and eq. (6.27)).

Many of those parameters influence each other. A small quantum defect usually means a three- or quasi three level behaviour, as in a four level system the spacing of the energy levels naturally imply that the quantum defect cannot be very small. A large gain bandwidth and cross-sections typically imply short lifetime (see eq. (6.25)). High doping densities may lead to quenching of the upper state lifetime and be detrimental to laser performance.

¹³ technique for pulse generation by modulation of the intracavity losses, and thus the Q(uality) factor of the laser resonator [15]

As with the host material, depending on the application in mind, a suitable choice of optically active centres needs to be made. In addition, the centres and the host material also need to be suitable for each other. This means that the centres need to fit into the lattice structure of the host without causing too much distortion of the lattice.

Luminescence lifetime

Time-resolved measurements of the luminescence intensity are used to determine the luminescence lifetime τ_{lum} of a system. A laser pulse is used to pump the population up into the excited state. Then the decay back down to the ground state is observed. Appropriate decay curves are fitted to the luminescence intensity, taken with a suitable spectrometer and excitation source as described further in section 6.3, Time-resolved luminescence spectroscopy.

The luminescence lifetime refers to the average decay time of a population N in an excited state, due to a combination of de-excitation effects like spontaneous emission (radiative lifetime τ_r) and nonradiative decay in the system (nonradiative lifetime τ_{nr}).

The time evolution of the excited state population of a system is described by:

$$\frac{dN(t)}{dt} = -N(t)/\tau_{lum} \quad (6.14)$$

with the total decay rate of the system $1/\tau_{lum}$ and the number of centres in the excited state N . In the simplest view of de-excitation channels, the total decay rate is the sum of the radiative ($1/\tau_r$) and nonradiative ($1/\tau_{nr}$) decay rates.

$$1/\tau_{lum} = 1/\tau_r + 1/\tau_{nr} \quad (6.15)$$

The solution of the differential eq. (6.14) leads to:

$$N(t) = N_0 \cdot e^{-t/\tau_{lum}} \quad (6.16)$$

with N_0 , the density of excited centres at $t = 0$, just when the excitation pulse has been absorbed. The emitted light intensity I_{em} is proportional to the rate of de-excitation.

It can be written as:

$$I_{em}(t) = A \cdot e^{-t/\tau_{lum}} \quad (6.17)$$

with the amplitude of the intensity A at $t = 0$.

A multi-exponential decay indicates the presence of different optically active centres with different luminescence lifetimes, or de-excitation pro-

cesses that affect the metastable level population with different decay rates. The former will be discussed later in this thesis (section 7.2, Assessment of NV containing samples) for the case when both NV^0 ¹⁴ and NV^- ¹⁵ contribute to the luminescence in a diamond sample. It is the sum of the contributing single-exponential decays τ_i with the respective amplitudes A_i [17]:

$$I_{em}(t) = \sum_{i=1}^n A_i \cdot \exp(-t/\tau_i) \quad (6.18)$$

For a double exponential decay, measurements can be fitted with a double-exponential decay function of the shape:

$$I_{em}(t) = A_f \cdot \exp(-t/\tau_f) + A_s \cdot \exp(-t/\tau_s) \quad (6.19)$$

where τ_f and τ_s indicate the fast and slow components of the luminescence and A_f and A_s the respective amplitudes.

To gain further information about the de-excitation processes in the system, it is useful to break apart the luminescence lifetime into its radiative and nonradiative components (eq. (6.15)). The luminescence lifetime as a function of colour centre concentration can be used to determine the point where concentration quenching sets in. As described in section 2.2, Fundamentals of crystallographic defects, non-radiative decay like quenching of the luminescence can have different causes. Mainly multi-phonon transitions to lower energy levels, energy transfer between optically active centres and to other defects in the crystal. If there is significant reabsorption in the system, the decay becomes non exponential [1].

The radiative lifetime can be measured directly if spontaneous emission is the only de-excitation process. This is the case for measurements taken at very low temperatures, where the non-radiative de-excitation channels are suppressed. Such measurements were not available in the scope of this work, but might be worth pursuing in future work as a direct determination of the radiative lifetime.

Values for the radiative lifetime within this work have been either taken from literature or determined by the measured luminescence lifetime and luminescence QY¹⁶ values obtained as explained below.

Luminescence quantum yield

The luminescence QY (Φ) is a measure for the efficiency of the luminescence. It is defined as the ratio of the number of photons emitted to the number absorbed. In other words, it represents the probability of an excited state to be depopulated by radiative decay rather than non radiative decay and therefore equates to a ratio of the radiative decay rate to the

¹⁴ The neutral form of NV

¹⁵ The negative form of NV

¹⁶ Quantum Yield

sum of radiative and non radiative decay rates (eq. (6.20)). Where there is significant self-absorption by the emitting centre, a correction needs to be undertaken in order to accurately extract the quantum yield, which will be described later in this subsection.

The value for the QY can be used to determine the radiative lifetime τ_r if the luminescence lifetime τ_{lum} has been measured [4]:

$$\begin{aligned}\Phi &= \frac{\# \text{ photons emitted}}{\# \text{ photons absorbed}} \\ &= \frac{1/\tau_r}{1/\tau_r + 1/\tau_{nr}} = \frac{\tau_{lum}}{\tau_r}\end{aligned}\quad (6.20)$$

Determination of the absolute QY through luminescence measurements can be difficult, as the luminescence is emitted in all directions, and hence collection is challenging. One way to collect the emitted light efficiently is by measurements with an integrating sphere, described in section 6.3, Luminescence spectroscopy.

Using a comparison method, described in detail in [18], luminescence integrating sphere QY measurements taken this way can be corrected for self-absorption of the emitting centre to calculate the absolute luminescence quantum yield QY of a sample [19].

This is done by comparing the transmittance of light T at the excitation wavelength and the integrate area under the luminescence spectrum A to those of a sample with known QY (eq. (6.21)).

The luminescence QY Φ_x of the sample is given by [18]:

$$\Phi_x = \Phi_s \cdot \frac{A_x}{A_s} \cdot \frac{1 - T_s}{1 - T_x} \cdot \left(\frac{n_x}{n_s}\right)^2 \quad (6.21)$$

Φ_s is the QY of a standard material. In this work a Ti:sapphire sample has been used with a reported QY of 0.7 ± 0.1 [20, 21, 22].

A_x and A_s are the integrated areas under the luminescence spectrum of the sample under study and the standard respectively. T_x and T_s are the transmittance values of the sample under the study and the standard respectively. n_x and n_s are the refractive indices of the sample and the standard.

The QY Φ_x has to be corrected for reabsorption effects caused by multiple reflections of the luminescence inside the integrating sphere.

To determine the probability of a emitted photon being reabsorbed, a , the emission spectra of two samples are necessary. The spectrum of the sample under study ($I_x(\lambda)$) and the spectrum from a sample with signif-

icantly lower concentration of the emitting centres ($I_{low}(\lambda)$). The long-wavelength tail of the luminescence spectrum is unaffected by reabsorption effects and therefore is independent of the concentration of the emitting centres. The emission spectrum of the sample with low concentration $I_{low}(\lambda)$ is then scaled so its long wavelength tail matches the one of the high concentration sample. This scaled spectrum ($I_{low,scaled}(\lambda)$) is then used to calculate a [18, 19]:

$$a = 1 - \frac{\int_0^\infty I_x(\lambda) d\lambda}{\int_0^\infty I_{low,scaled}(\lambda) d\lambda} \quad (6.22)$$

The absolute luminescence QY can be calculated from the uncorrected QY Φ_x (eq. (6.21)) and the parameter a (eq. (6.22)) with the equation [18, 19] :

$$\Phi = \frac{\Phi_x}{1 - a + a \cdot \Phi_x} \quad (6.23)$$

Emission and absorption cross sections

Cross sections quantify the likelihood of an optically induced transition. They have been defined previously in eq. (6.2). They are used to quantify the efficiency of the pump absorption, the reabsorption from the lower laser level and laser emission.

The ground state absorption cross section σ_{abs} is related to the concentration of active centres N and the absorption coefficient α via the Beer-Lambert law [6]:

$$\begin{aligned} I(\lambda) &= I_0(\lambda) \cdot \exp(-\alpha l) \\ &= I_0(\lambda) \cdot \exp(-N\sigma_{abs}l) \end{aligned} \quad (6.24)$$

with the length of the crystal l , the intensity of a light beam before $I_0(\lambda)$ and after $I(\lambda)$ being transmitted through the crystal.

The emission cross section $\sigma_{em}(\lambda)$ of the upper laser level can be calculated using the Füchtbauer-Ladenburg equation. This method requires knowledge of the radiative lifetime and a measured luminescence spectrum [23]. The emission cross section is related to the luminescence intensity $I(\lambda)$ normalized with respect to the instrument response function [6]:

$$\sigma_{em}(\lambda) = \frac{\lambda^5}{\tau_r \left(\int \lambda I d\lambda \right) 8\pi n^2 c} \cdot I(\lambda) \quad (6.25)$$

with the radiative lifetime τ_r , the wavelength λ , the refractive index n and the speed of light c .

With the simplification that the emission band of colour centres has Gaussian shape at the peak emission λ_0 , the equation can be expressed as described in [24]:

$$\sigma_{em}(\lambda_0) = \sqrt{\frac{\ln 2}{\pi}} \cdot \frac{\lambda^2}{4\pi n^2} \cdot \frac{\eta}{\tau_f} \cdot \frac{1}{\Delta\nu} \quad (6.26)$$

where $\Delta\nu$ is the width (FWHM) of the emission spectrum, η the QY and τ_f the fluorescence lifetime. Equation (6.26) is useful in illustrating the general dependencies, but was only used to determine the emission cross section value based on the sample thickness, reflectivity, and the parameters of Table 1 in [16].

The luminescence intensity $I(\lambda)$ has been corrected for the contribution of other centres as described in section 4.2, Dispersive spectroscopy.

Gain coefficient

The gain coefficient g , as previously introduced in eq. (6.8). The sign of the coefficient at a given wavelength determines the ability of a medium to absorb or amplify an optical signal.

All possible gain spectra can be calculated by a fractional distribution of the population between the upper laser level and the ground level, expressed through the inversion coefficient β , which is defined as the ratio between the populations in the upper laser level and in the ground level.

The gain coefficient can be calculated from the emission and absorption cross sections of a sample using the equation [6]:

$$g = N \cdot \beta \cdot \sigma_{em} - \alpha_{abs} \quad (6.27)$$

with the total concentration of colour centres in the sample N , and α_{abs} the absorption coefficient caused by centres different from the colour centre under study, which is unrelated to the inversion coefficient β . The absorption region of the colour centres under study is considered to be separated enough from the emission region in order to neglect their effect. β is defined as the ratio between the populations in the upper and lower laser levels. No ESA¹⁷ is assumed in this case.

¹⁷ Excited State Absorption

6.3 Luminescence spectroscopy

Integrating sphere measurements

Luminescence spectra were taken using a Ocean Optics S2000 spectrometer. It is equipped with a 2048-element linear CCD-array detector. Light is coupled into the spectrometer via an optical fibre and dispersed by a fixed grating. The detector is responsive from 200-1100 μm . The schematic setup was introduced previously in fig. 4.2.

An Thorlabs IS200 integrating sphere was used to collect the luminescence from the samples. An integrating sphere is illustrated in fig. 6.4. The interior of the sphere is covered with a diffuse white reflective coating, so that the luminescence, emitted randomly in all directions, can be scattered uniformly over the area of the sphere. In this way the total light emitted can be measured.

The spectrometer was connected to the detector port of the integrating sphere setup using a multi-mode fibre. The samples were suspended inside the integrating sphere using a piece of white thread glued to the surface of the sample on one side and to the end cap of the integrating sphere on the other. The samples were pumped through one of the input ports of the integrating sphere using cw lasers at 447 and 532 nm with 15 mW incident power.

Light sources used for luminescence measurements are listed in table 6.2.

Wavelength [nm]	Type	Manufacturer	Model
447	diode	Laserglow	LRD-0447
532	solid state	Elforlight	FCHPG-5000

Correction of luminescence spectra for contributions of other centres

To calculate the emission cross section of a colour centre, a pure luminescence spectrum is required. Other centres should not contribute to the spectrum. This is particularly difficult if the spectra overlap, as they do for N_2V^0 , NV^0 and NV^- . For many of our samples a combination of these defects were present at the same time.

The spectra of NV^0 and NV^- can be separated with a method described in [26]. A sample is pumped at 447 nm, where the luminescence spectrum is dominated by the contribution of NV^0 . For 532 nm pumping the spectrum shows contributions of both NV^0 and NV^- . Both spectra are then normalised to the ZPL¹⁸ of NV^0 and the NV^0 spectrum is subtracted from

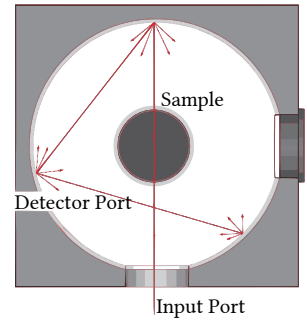


Figure 6.4: Thorlabs integrating sphere [25].

Table 6.2: Laser types used in experimental setups

¹⁸ Zero Phonon Line

the combined spectrum, leaving a pure NV^- spectrum.

If one colour centre was generated at a different treatment step, spectra taken at different times during the synthesis can be subtracted from one another. This is the case for some of the samples that were delivered to us with an initial N_2V^0 content, but with an insignificant amount of NV . The initial spectrum pumped at 447 nm is a pure N_2V^0 emission spectrum. After irradiation and annealing both N_2V^0 and NV^0 emission is observable when illuminating at 447 nm. To correct the NV^0 spectrum for the contribution of N_2V^0 both spectra were normalised to the N_2V^0 ZPL and the initial spectrum was subtracted from the final.

Time-resolved luminescence spectroscopy

Time resolved luminescence measurements allow the luminescence lifetime of a colour centre to be determined. Optically active defects, their interaction with each other and the resulting implications for the luminescence lifetime have been covered in section 2.2 (Fundamentals of crystallographic defects).

Luminescence lifetime can be measured directly [6]. Experimental techniques depend on the magnitude of the lifetime. For lifetimes in the order of micro- to nanoseconds, the excited state can be populated with a short laser pulse. The decay of the luminescence is then measured with a fast oscilloscope.

For small intensities TCSPC¹⁹ spectroscopy is suitable. A laser pulse is emitted at $t = 0$ and the first luminescence photon to be detected stops the timer and adds to the photon count at that time, as is illustrated on the right hand side of fig. 6.5. The sample is repeatedly excited by the pulsed light source and a histogram of counts versus time is recorded. For many measurements a probability distribution of decay times is generated. An illustration of a TCSPC spectroscopy setup and working principle is shown in fig. 6.5.

¹⁹ Time-Correlated Single Photon Counting

Measurements were taken at room temperature using an Edinburgh Instruments Mini-Tau TCSPC spectrometer. It has a blue or red sensitive single photon counting PMT²⁰ as a detector and is able to measure lifetimes ranging from 25 ps to 50 μ s. One of two pump sources were used for all measurements. A 448 nm pulsed diode laser with an average of 0.12 mW and pulse duration of 128 ps (20 MHz repetition rate) for the excitation of N_2V^0 and NV^0 . And a 562 nm pulsed LED²¹ with an average power of 0.09 μ W and a pulse duration of 1.5 ns (10 MHz repetition rate) for the excitation of NV^- . The setup has a filter wheel with 5 bandpass filters of approx. 10 nm width. They are centred at 450 nm, 500 nm, 550 nm,

²⁰ PhotoMultiplier Tube

²¹ Light-Emitting Diode

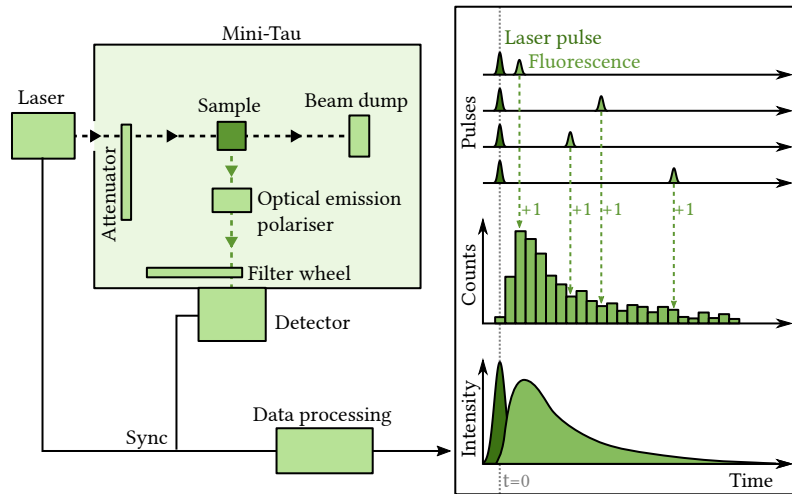


Figure 6.5: Edinburgh Instruments Mini-Tau spectrometer schematic [27] (left) and working principle [28] (right).

600 nm, and 650 nm.

To measure NV^- lifetimes bandpass filters at 640 nm, 670 nm and 700 nm with 10 nm width were used. These bands correspond to the ZPL, the maximum of the phonon sideband and the long-wavelength tail of the NV^- , respectively. Measurements using a long-pass filter > 640 nm were taken to compare the measurements taken here with literature data of the luminescence decay of NV^- in natural Ib diamond [29]. All filters blocked $>99.99\%$ of the light outside the bandpass region.

6.4 Diamond in laser engineering

THERE IS A WIDE RANGE of applications within laser engineering and optics that diamond is already used for. In this section the material properties of diamond will be compared to other optical materials. The challenge to dope diamond with laser active ions will be outlined.

Diamond in comparison to other optical materials

Diamond can be compared in many aspects to the material sapphire. Sapphire has been briefly introduced in section 6.1 in the context of ruby lasers and as the host of the laser gain medium Ti:sapphire. Synthetic sapphire is a strong, hard and chemical inert material. The optical transmission window is very large (see fig. 2.7). It is the third hardest mineral on the Mohs scale, it's resistant to tension (tensile strength) and has a high elasticity (Young's modulus). It has a very good thermal conductivity for an optical material and the expansion and change of refractive index with temperature (Thermal and Thermo-optical coefficients) are comparable to other laser hosts.

A comparison of some relevant material parameters of optical materials to those of diamond can be found in table 6.3.

Material	Thermal cond. [W/mK]	Young's modulus [GPa]	Thermal expansion [10 ⁻⁶ /K]	Thermo-optical coefficient [10 ⁻⁶ /K]	Tensile strength [MPa]
Diamond	2000	1100	1.0	9.6	2860
Sapphire	33	335	5	13	400
YAG	10.5	282	8	8.9	280
YVO ₄	6.6	133	11.4	8.5	53

Table 6.3: Comparison of material properties for CVD diamond and other optical materials [30, 31].

Diamond surpasses sapphire and other lasers materials in terms of thermo-optical properties. Together with the wide transparency (from 220 nm to over 50 μm, with an absorption band between ~2.5 and 6 μm. See fig. 2.7) it is a desirable material for thermal management in laser engineering.

Optical windows, lenses and output couplers in high power CO₂ and solid state lasers are sometimes made out of diamond. It is used for spectroscopic applications, semiconductor processing, medical applications, defence and aerospace applications [31].

Low birefringence single crystal diamond can be used as intra-cavity heatspreader [32]. Bonded directly to conventional laser materials it can alleviate deformation and help to extract heat efficiently very close to the

point of its generation [33]. Output power improvements of two orders of magnitude have been reported in semiconductor disk lasers when a diamond heatspreader was used in comparison to no heatspreader [30].

Another way to utilize diamond as a laser material without the need to dope it with laser ions, is through **Raman laser** light amplification. It is achieved due to stimulated Raman-scattering instead of stimulated emission of electronic transitions.

Raman scattering is the inelastic scattering of photons by atoms which are excited to higher vibrational energies. The re-emitted photon has a lower energy corresponding to the phonon frequency of the medium. With this technique in principle any laser wavelength can be generated, as long as it lies in the transparency region of the host material. The wavelength of the output light is determined by the pump wavelength and the phonon frequency.

A large Raman gain coefficient was measured in diamond [34]. This, together with the excellent thermo-mechanical properties of diamond and the improvements in growth quality, lead to the demonstration of cw [35, 36] and pulsed [37, 38, 39] lasers emission. Diamond Raman lasers cover emission wavelengths from the UV to the mid-IR [40, 41]. The feasibility of a monolithic diamond Raman laser with a conversion efficiency of 84%, using a micro-lens structure, and 59% in a plane-plane design, has been demonstrated [42].

Even though Raman lasers are a feasible way to utilize diamond as a laser material, they require bright pump sources (Intensities above tens of MW/cm^2) to reach threshold. In conventional inversion lasers pump energy can be accumulated and stored through shifting the population [43]. Utilizing diamond as a inversion laser through colour centres is a complementary approach to that of Raman amplification.

Doping diamond

The main reason diamond is still not harnessed as a laser host is its tight lattice structure. As discussed in section 2.2, Fundamentals of crystallographic defects, impurities in diamond can occupy substitutional and interstitial positions in the crystal lattice.

Only atoms with atomic radii similar to carbon can occupy substitutional sites. Figure 6.6 shows the calculated nearest-neighbour bond-lengths versus covalent radii for different atoms in comparison to carbon [44]. Nitrogen and boron are small enough to cause the least distortion to the diamond lattice [45].

In fig. 6.7 a diamond unit cell is compared to the sizes of nitrogen and boron and typical laser ions like ytterbium and neodymium. Laser ions are particularly big in comparison to the inter-atomic distances in diamond.

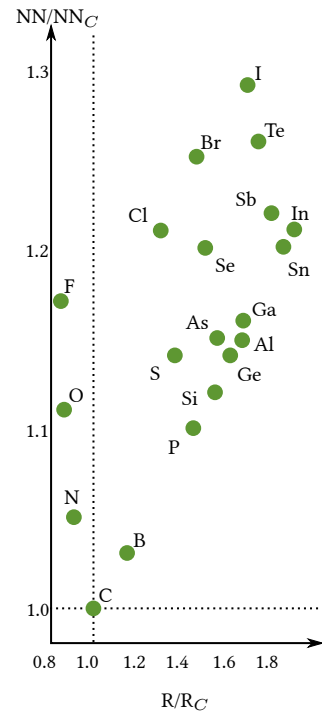
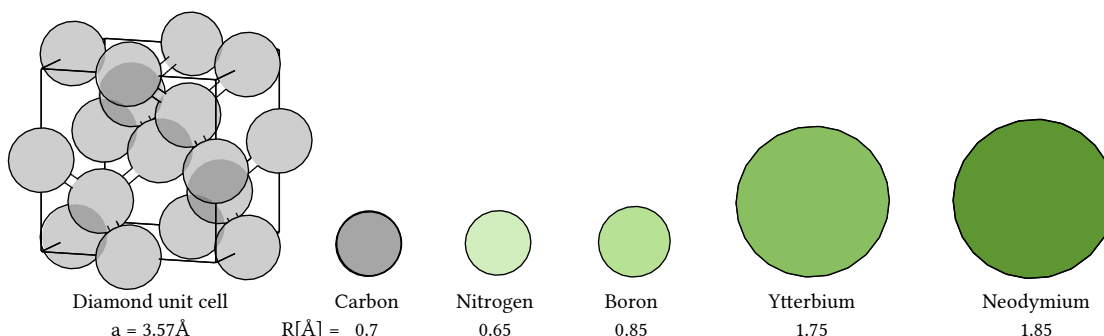


Figure 6.6: Calculated nearest-neighbor bond-lengths (NN) versus covalent radii (R) adapted from [44]. The closer the value to that of carbon, the easier it is to incorporate the element into the diamond lattice.



This makes the inclusion of such atoms into the lattice difficult, but not impossible. Diamond can be doped by ion implantation, ion assisted doping during growth or diffusion doping methods [45].

Incorporating dopants during diamond growth is a challenge. The bonding energy of the dopants is small in comparison to the bonding energy between carbon atoms. That makes them more likely to re-evaporate during the growth process [45]. Incorporating a critical concentration of laser ions into the lattice is challenging [30, 47]. Some methods to produce a diamond laser by doping have been discussed in literature [48], but no working sample has been reported.

While in the future doping diamond with laser ions might be possible, in the meantime another route of utilizing optically active centres, which are common in natural diamond, shows some promise. A comparison of the emission range of NV^- and N_2V^0 in diamond to common RE and TM ions is shown in table 6.4.

Their emission bandwidths are comparable to those of TM ions, suggesting the possibility of tunability and generation of ultrashort pulses. NV^- and N_2V^0 in diamond as a basis for a colour centre based diamond laser will be outlined in more detail in the next section.

Figure 6.7: Comparison of atomic radii of laser ions to space in the diamond lattice [46].

Laser ion	Wavelength [μm]	
Nd^{3+}	0.9, 1.06, 1.3	NIR RE
Yb^{3+}	1.0 - 1.1	
Tm^{3+}	2	
Ho^{3+}	2	
Er^{3+}	1.6, 3	
Pr^{3+}	0.52, 0.60	VIS RE
	0.64, 0.72	
Er^{3+}	0.55	
Ce^{3+}	0.3	UV RE
Ti^{3+}	0.68 - 1.1	TM
Cr^{3+}	0.7 - 1.1	
Cr^{4+}	1.2 - 1.6	
Cr^{2+}	2.0 - 3.0	
NV^-	0.57 - 0.8	CC
N_2V^0	0.48 - 0.63	

Table 6.4: Laser wavelengths of RE and TM ions [9] in comparison to the emission range of N_2V^0 and NV^- in diamond [45, 49].

6.5 A potential diamond colour centre laser

THE PROOF OF CONCEPT to use colour centres for a laser has been demonstrated in 1974 in colour centre containing alkali halides [50].

A laser based on colour centres in diamond has a attractive range of potential features, such as high power operation, high efficiency and operation at room temperature [45]. In the past a few attempts were made to study colour centres in diamond for the purpose of building a laser. Most famously these include the report of room temperature laser action at 530 nm using N_2V^0 centres in diamond with an efficiency of 13.5% [16]. Up to this date this is the only substantive report of laser action produced by colour centres in diamond in the literature.

Typical colour centre lasers in alkali halides

Stimulated emission from colour centres was first reported in 1965 in flash-light pumped potassium chloride containing lithium [51]. Ten years later a tunable colour centre laser operated in cw was demonstrated [50]. While colour centre laser have been around for a while, proving the general concept, those in alkali halides often have to be stored and operated at low temperatures. The thermal stability of colour centres in diamond is an advantage over colour centres in alkali halides.

A typical colour centre laser is based on colour centres in alkali halides²², since they can be most easily created there [45].

Colour centre lasers are four-level (fig. 6.8) and so there is little self-absorption, contributing to their efficiency ($\sim 50\%$) [45, 52]. They have a low saturation intensity, making them easy to pump, with a threshold of only a few tens of mW. Ultrafast pulsed and cw operation is possible [45]. The first commercial colour centre laser had to be operated at cryogenic temperatures in a suitable chamber, increasing the complexity of the setup and operation. An illustrating example of a colour centre laser that can be operated at room temperature is $LiF:F_2^-$ ²³. $NaCl:F_2^+ \cdot OH^-$ ²⁴ has been chosen as an example for a laser operated at cryogenic temperatures .

Classical colour centre lasers combine the tunability of dye lasers with the advantage of using a static laser medium. Operation of the laser is facilitated by removing hazardous dyes and making the complex jet stream setup needed to guarantee a continuous flow of the dye obsolete.

In table 2.3 can be seen that colour centre lasers combine large gain cross sections and emission bandwidths [53].

Disadvantages of classical colour centre lasers include light bleaching and discolouration under optical pumping and a low thermal stability. Many of them have to be stored and operated at low temperatures. There is non-

²² Alkali halides are a family of inorganic compounds consisting of an alkali metal as lithium, sodium, potassium, rubidium or caesium, and a halogen such as fluorine, chlorine, bromine or iodine

²³ Lithium fluoride with an F_2^- colour centre

²⁴ Sodium chloride with an F_2^+ colour centre in combination with hydroxide

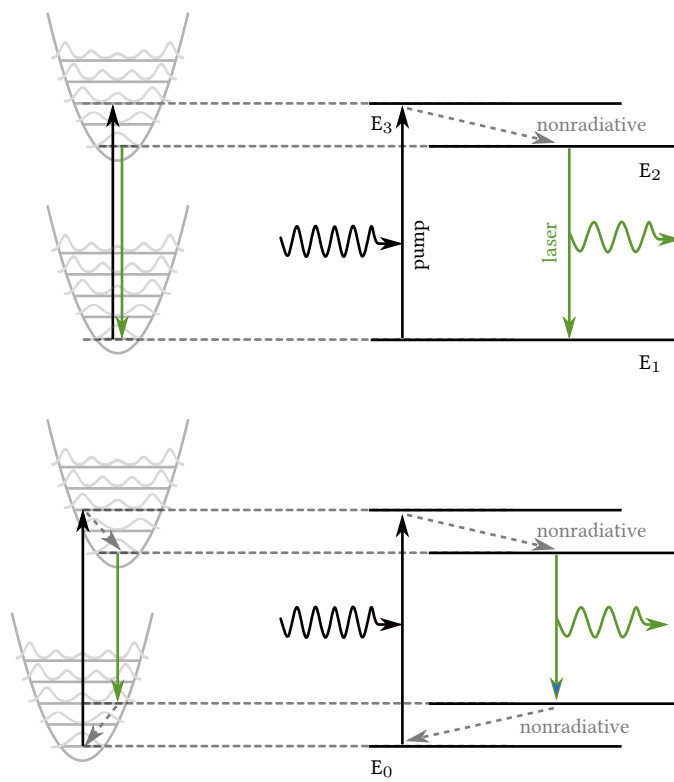


Figure 6.8: Configuration coordinate diagram with weak (top) and strong (bottom) lattice coupling. **Left:** Ground and first excited electronic states, the vibronic levels and wavefunctions. **Right:** Simplified four-level diagram, reduced to the most commonly excited vibronic levels of the normal and relaxed configuration. Adapted from [45].

linear loss because of excited state absorption. Different colour centres in the same crystal can cause parasitic losses and nonradiative transitions can compete with radiative transitions. The visible spectral region from blue to green can not be covered by classical colour centre lasers [45]

In contrast, colour centres in diamond have a high thermal stability and, depending on the colour centre type, a broad emission in the visible spectrum [54].

The NV centre in diamond

The NV colour centre is of particular interest to study laser emission. NV is the most well studied nitrogen related defect in diamond due to a wide array of possible and existing applications and its relatively easy synthesis [30].

NV is made up of a substitutional nitrogen atom with an adjacent vacancy (N-V) in a trigonal (C_{3V}) symmetry [54, 55]. This is shown in fig. 6.9

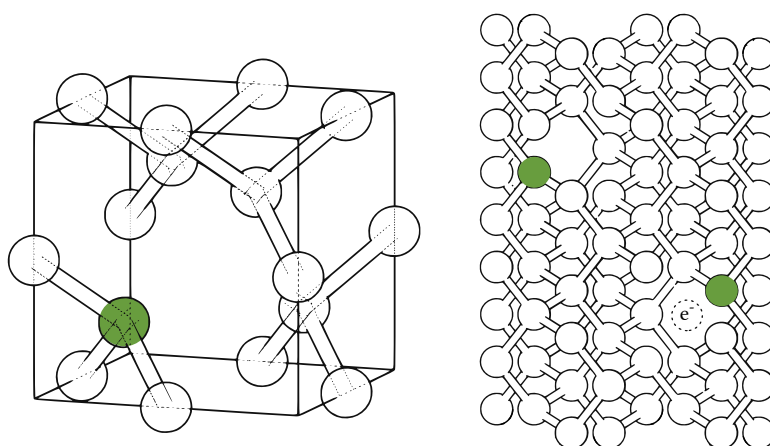


Figure 6.9: Representation of NV in the diamond lattice. NV is made up of one substitutional nitrogen atom adjacent to one vacancy (N-V) with (C_{3V}) symmetry [54, 55].

In literature, in particular in older work, sometimes NV is discussed without explicitly mentioning a charged state. In many of those cases the negatively charged state of NV, NV^- , is discussed. This becomes apparent when the ZPL is mentioned, which is 638 nm (1.945 eV) for NV^- and 575 nm (2.156 eV) for NV^0 [54]. An additional ZPL at 1046 nm (1.185 eV) has been observed during illumination with light < 637 nm (> 1.945 eV) has been associated with NV^- [56].

A representation of the electronic structure of NV can be seen in fig. 6.10.

The ground 3A and the excited 3E states in NV^- are triplets and show a zero-field splitting as illustrated in fig. 6.11.

Zero-field magnetic resonance occurs in NV^- between the $m_s = 0$ and $m_s = \pm 1$ spin sub-levels of the ground state 3A_2 at ~ 2.88 GHz [60] and between the spin sub-levels of the excited state 3E at ~ 1.42 GHz [61]. This makes NV^- detectable by EPR²⁵ [60] and ODMR²⁶ [62]. NV^0 does not show any detectable magnetic resonances associated with the ground and excited states [55].

²⁵ Electron Paramagnetic Resonance

²⁶ Optically Detected Magnetic Resonance

Two relaxation processes have been established for NV^- .

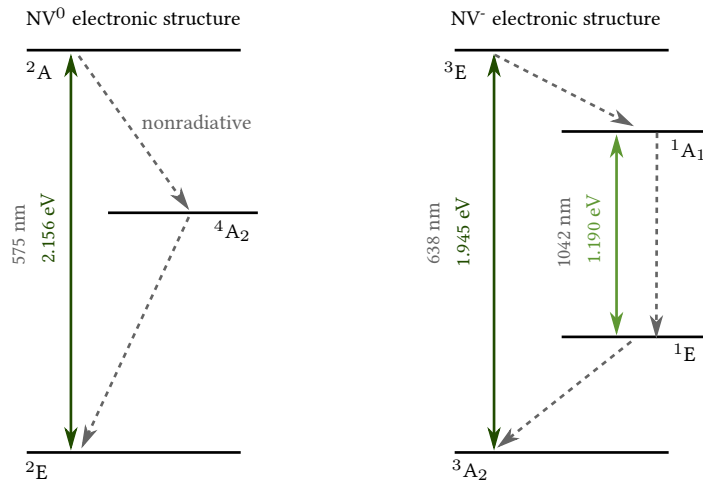


Figure 6.10: NV⁻ [57] and NV⁰ [58] energy structures. The optical ZPL transitions have been experimentally observed [56, 59]. The relative positions of the energy levels are currently unknown. Transitions indicated as in [55].

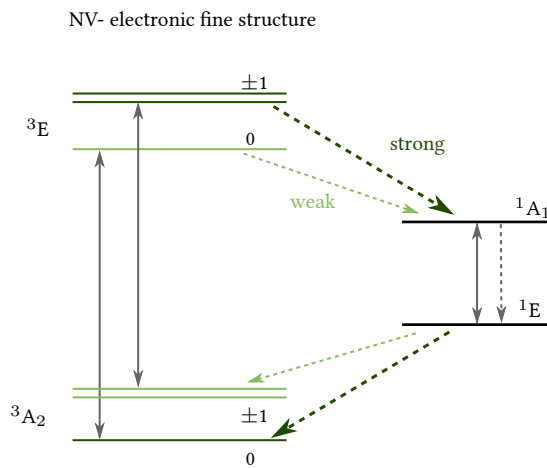


Figure 6.11: RT electronic fine structure of NV⁻ [55, 57]. The optical transitions are indicated by solid arrows. Nonradiative transitions are indicated by dashed arrows, divided into strong and weak interactions. Splitting between energy levels not to scale.

The first is the transition from the metastable state 1A to the ground state with a lifetime of $\tau = 265 \text{ ms}$ and spin-lattice relaxations between the 3A ground states with a lifetime of $\tau = 1.17 \text{ ms}$ [63], illustrated on the right hand side of fig. 6.11.

Even though this lifetime is significantly longer than the ns lifetime reported for the transition between the levels 3E and 3A , pictured on the left hand side of fig. 6.11, it will not affect the laser operation due to the mechanisms explained below. Initially, the spin sub-levels $m_s = 0$ and $m_s = \pm 1$ of 3A are thermally populated. A pump with suitable emission wavelength in the green drives the population towards the excited state 3E . As described before, the optical transition is spin-conserving ($\Delta m_s = 0$). The radiative relaxation is again spin-conserving. However, a part of the system relaxes non-radiatively and is not spin-conserving from the $m_s = \pm 1$ energy levels of 2E into the intermediate state 1A , from where it decays further into the $m_s = 0$ level of 3A . After a few cycles of excitation and decay, the population will be moved to the $m_s = 0$ sub-levels of 3A and 3E [55].

So far the transition between the energy levels have been discussed, without taking lattice vibrations into account. Lattice vibrations are responsible for the appearance of phonon sidebands in the spectra. This has been discussed previously in section 2.2, Optically active centres in a crystal and electron phonon coupling.

The ratio between the emission intensity in the ZPL to that in the phonon sidebands is expressed by the so called Debye–Waller, or Huang-Rhys factor. Both are related to one another via $H = -\ln(D)$, and $D = I_{ZPL}/I_{tot}$, where D is the Debye–Waller factor and H the Huang-Rhys factor. For NV^- Huang-Rhys factor is $H=3.7$, that means about 97% of the emission goes into the phonon sideband [64]. The temperature dependence of the factor is weak, it increases about 30% in a temperature range between 2 to 350 K [65]. In NV^0 the situation is similar with the Huang-Rhys factor $H = 3.3$ [54].

The emission part of the optical transitions is shown in fig. 6.12.

The demonstration of single photon generation from single NV^- centres [66] and the readout of the electronic spin [67] made the centre interesting for quantum information processing as a solid state spin qubit [55, 68, 69]. Other fields of applications include nano-technologies, sensing of magnetic and electric fields, temperature, pressure and biosensing [55, 70].

NV^0 has not received the same attention with regards to quantum applications and research interest has been focused on obtaining more information about it to increase understanding of NV^- and the charge transfer in the NV system [55]. Charge transfer between NV^0 and NV^- is believed to

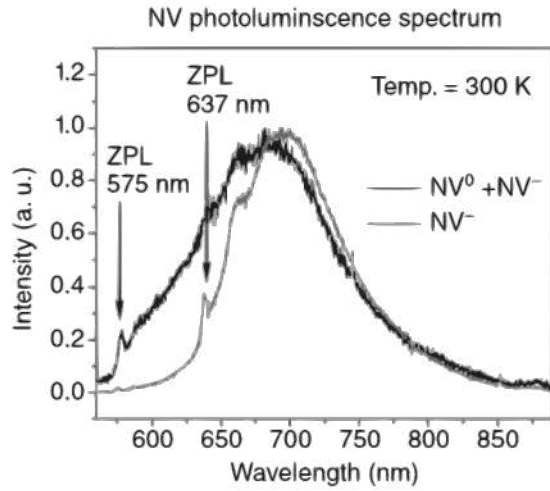


Figure 6.12: Emission spectrum of NV containing diamond. From [30].

occur between the optically excited levels via electron and hole transitions in the diamond valence and conduction bands [71].

Optical illumination, as is the case with optical pumping of a laser gain material, can drive charge transfer between NV^- and NV^0 [72, 73]. Charge transfer between NV^- and NV^0 is illustrated in fig. 6.13. Both ground and excited states of NV^- and NV^0 are shown in the bandgap. From the left the first two panels show the ionization process and the second two the recombination.

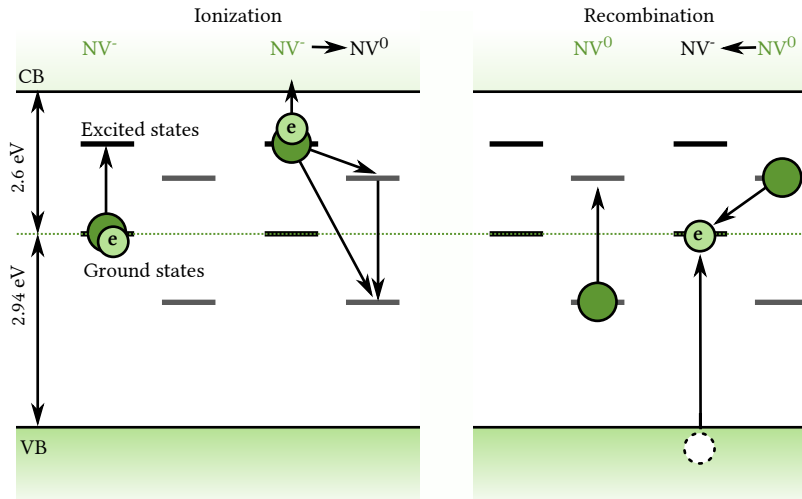


Figure 6.13: Charge transfer between NV^- and NV^0 based on an illustration in [72]. The dark green circle represents the state of the NV centre, from left to right:

Ionization
left) Excitation of NV^- by a photon.
right) Excitation of the electron into the conduction band and creation of NV^0 .

Recombination
left) Excitation of NV^0 by a photon.
right) Recombination of NV^0 and an electron from the conduction band and formation of NV^- .

For the ionization process NV^- is transferred into an excited state by photon absorption. Another photon then excites the the electron into the con-

duction band, generating NV^0 . For the recombination NV^0 is transferred into the excited state by photon absorption. Then an electron from the valence band is captured by NV^0 , generating NV^- again [72].

Using single-shot charge-state measurements it was shown that when excited at the absorption maximum of NV^- at about 580 nm, the NV^- concentration decreased to about 10% due to charge transfer into NV^0 [72]. For illumination at 450-610 nm the steady state concentration of NV^- is always below 75-80% of the total NV population. An excitation wavelength between 510-540 nm was found to be optimal for maximal fluorescence of NV^- , combined with low saturation power. Samples used in this study were ultrapure IIa CVD²⁷ diamonds [72, 74].

To date, to the best knowledge of the author, no work like that has been performed in diamond samples with a few ppm of NV^- and NV^0 .

Reports of luminescence lifetime in NV vary in literature, according to the type of diamond studied, the method of measurement and the defect composition in the sample [75]. Single exponential luminescence decay, when pumped with sources above 532 nm, has been attributed to NV^- , as NV^0 is not excited in this wavelength regime. The luminescence lifetime of NV^- varies according to the NV environment and is usually reported around 10 ns in bulk diamond [30] Collins et al. reported a luminescence decay time of 13 ± 0.5 ns for NV^- [29]. This value was measured in Ib natural diamond. A pump wavelength of 580 ± 20 nm and an emission spectral range of > 640 nm were chosen. Over a temperature range from 77 to 700 K there was no significant change for the value.

A luminescence decay time of 19 ± 2 ns for NV^0 was reported in synthetic CVD grown bulk diamond with an initial nitrogen concentration of less than 1 ppm, when excited at 467 nm. For this excitation source predominantly NV^0 are believed to be excited [75].

In some reports double exponential decay has been measured. Hanzawa et al. reported double exponential luminescence decay in synthetic diamond containing NV centers [76]. The sample under study was a Ib diamond pumped at 587 nm. A fast and slow component 2 and 8 ns were attributed to NV without the attribution to a particular charged state. Manson et. al showed that the double exponential decay could be attributed to different spin-projection states under certain circumstances [77]. The fast component of the lifetime is associated with the state $m_s = 0$ and the slow component with $m_s = 1$. The fast component should only be observable for low repetition rate pumping (< 10 Hz), or when a MW²⁸ field is added that would cause mixing of the population of the states.

Lifetime measurements with a MW field were done in [78]. A slow decay time of 7.8 ns and a fast decay time of 12 ns were measured.

²⁷ Chemical Vapour Deposition

²⁸ MicroWave

The N_2V^0 centre in diamond

The N_2V^0 colour centre is one of the most common centres that occur in natural diamond [54]. The structure is made up of two nitrogen atoms adjacent to one vacancy (N-V-N) with a rhombic-I (C_{2v}) symmetry [24, 79], illustrated in fig. 6.14

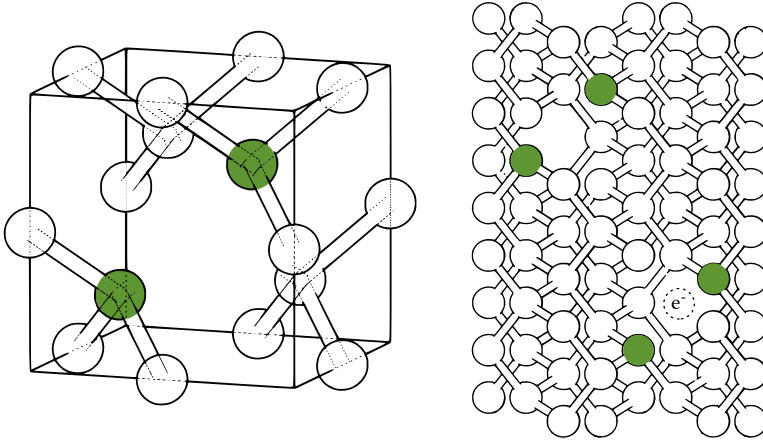


Figure 6.14: Representation of N_2V^0 in the diamond lattice. N_2V^0 is made up of two nitrogen atoms adjacent to one vacancy (N-V-N) with a rhombic-I (C_{2v}) symmetry [24, 79]. An additional electron is associated with the N_2V^- defect.

Electronic transitions occur between a non-degenerate ground state and a degenerate excited state as shown in fig. 6.15.

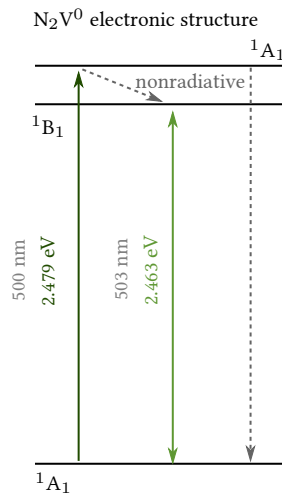


Figure 6.15: Energy levels of N_2V^0 adapted from [16, 54, 80]. A 1A_1 ground state exists, with vibronic energy levels above the excited state. Optical absorption occurs between the 1A_1 ground state and the 1B_1 and 1A_1 excited states. Nonradiative decay occurs between the 1A_1 excited state and both 1B_1 and 1A_1 ground state. The optical transition between the 1B_1 excited state and the 1A_1 ground state is associated with the N_2V^0 ZPL.

The optical transition occurs between the 1A_1 ground state and the 1B_1 excited state. There is another optically inactive 1A_1 state 16 meV above the 1B_1 state [16, 54, 81].

The ZPL of N_2V^0 is at 503.2 nm (2.463 eV) [54]. The presence of N_2V^0 results in a yellow colour of the sample, while the combination of N_2V^- ²⁹ and N_2V^0 absorption results in a yellow-green or green colour [82]. The radiative decay time $\tau_f = 17 ns$ is stable in a range from 77-700 K [54].

²⁹ The negatively charged state of N_2V (H_2)

The negative charged state is N_2V^- , with a ZPL at 986 nm (1.257 eV) [54]. The excited state of N_2V^- is believed to lie within the conduction band. This leads to a negligibly small efficiency of the radiative decay [83], reducing our interest in that centre for laser purposes. N_2V^- is bleached and the N_2V^0 center is enhanced when exposed to light with a wavelength shorter than 600 nm [84].

Similar as for NV, the Huang-Rhys factor in N_2V^0 is $H=4.2$, over 98% of the emission goes into the phonon sideband [85]. Typical optical transitions are shown in fig. 6.16.

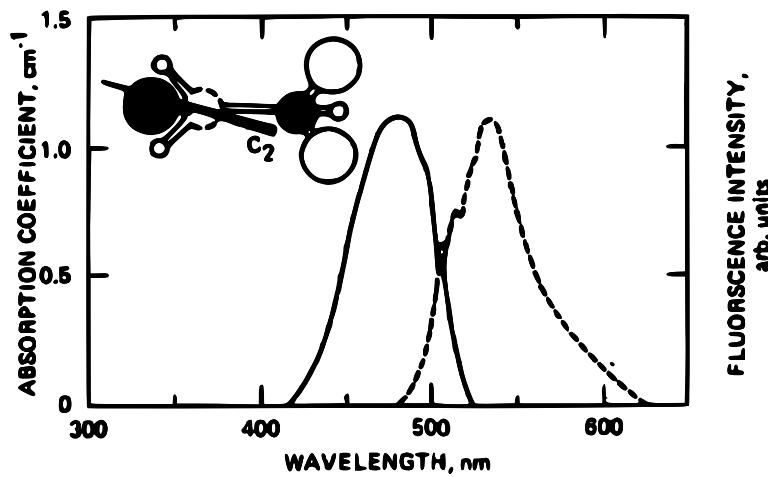


Figure 6.16: Absorption (solid line) and emission (dash line) spectra of N_2V^0 , as presented in [16].

Predicted operation of a NV and N₂V⁰ based laser

In table 6.5 a comparison of the literature values of the most important laser related properties of NV and N₂V⁰ is given.

	Literature values		
	NV ⁰	NV ⁻	N ₂ V ⁰
ZPL	575 [54]	638 [54]	503.2 [54]
Absorption range (nm)	~450 - 580 [54]	450 - 640 [83]	420 - 520 [45]
Peak absorption (nm)	520 [54]	565 [24]	490 [24]
Emission range (nm)	550-800 [54]	570 - 800 [86]	480 - 630 [45]
Peak emission (nm)	650 [54]	690 [24]	525 [24]
Abs cross-section (10 ⁻¹⁶ cm ²)			
(at max abs)	-	0.28 [87]	-
(at 532 nm)	-	0.31 [88] 0.95 [89]	-
(at 473 nm)	-	-	0.21 [90]
Em cross-section (10 ⁻¹⁶ cm ²)			
(at max em)	-	0.43 [87] 3.2 [24]	1.6 [24]
Luminescence lifetime (ns)	21 [91]	12-13 [29]	16 [54]
Quantum Efficiency	-	0.7 [92] 0.8 [93] 0.99 [45]	0.95 [16]
Radiative lifetime (ns)	17 [75]-19 [94]	12 for $m_s = 0$ & 7.8 for $m_s = \pm 1$ [87]	17 [54]
Gain coefficient (cm ⁻¹)			
(at 531 nm)	-	-	0.201 [16]

In fig. 6.17 the pump absorption depending on the NV⁻ and N₂V⁰ concentration calculated with eq. (6.24) is shown. According to this estimation a concentration of 0.6 ppm³⁰ of NV⁻ and 0.9 ppm of N₂V⁰ are needed to achieve 50% pump absorption, which provides a ballpark concentration to aim for when planning colour centre synthesis.

In table 6.6 estimated values for the critical inversion (eq. (6.11)), the concentration needed for 50% pump absorption (eq. (6.24)) and the threshold pump power (eq. (6.12)) of NV⁻ and N₂V⁰ containing diamond are given, assuming a 2 mm sample, cavity losses $\gamma = 0.1$, pump efficiency $\eta = 1$ and a pump beam radius of $r = 50 \mu m$. Calculated values are based on the literature values presented in table 6.5. The colour centre concentrations in this ball park have been achieved during synthesis, as discussed in chapter 5, Results of the colour centre synthesis.

N₂V⁰ looks suitable for GaN diode pumping in the blue and NV⁻ for pumping in the green either with frequency doubled Nd lasers or with green InGaN diodes, which are not as powerful yet, but developing rapidly.

Table 6.5: Important literature values and predictions for NV and N₂V⁰. Gain coefficient for N₂V⁰ estimated for a concentration of $N = 10^{16} \text{ cm}^{-3} = 0.9 \text{ ppm}$.
³⁰ parts per million
(1.77 · 10¹⁷ cm⁻³ for diamond)

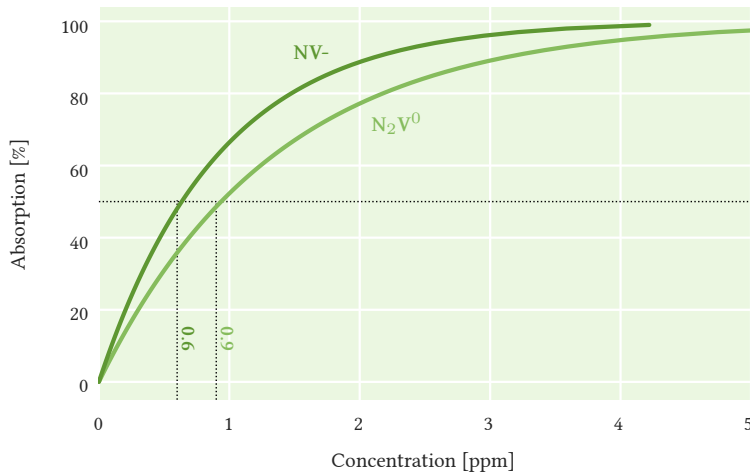


Figure 6.17: The pump absorption by NV^- and N_2V^0 , based on literature values for the absorption cross sections ($0.31 \cdot 10^{-16} \text{ cm}^2$ at 532 nm for NV^- and $0.21 \cdot 10^{-16} \text{ cm}^2$ at 472 nm for N_2V^0), calculated with eq. (6.24).

Cavity losses $\gamma = 0.1$, pump efficiency $\eta = 1$, pump beam radius $r = 50 \mu\text{m}$ and sample length $l = 2 \text{ mm}$.

Additionally, beam combining of several lower power sources is imaginable to reach higher output powers at the desired wavelength [15].

	Predicted values	
	NV^-	N_2V^0
Pump wavelength	532 nm	473 nm
Critical inversion N_c	9 ppb	18 ppb
Concentration for 50% pump absorption $N_{50\%}$	0.6 ppm	0.9 ppm
Threshold pump power P_{th}	0.70 W	1.2 W

Table 6.6: Predicted values for the critical inversion (eq. (6.11)), the concentration needed for 50% pump absorption (eq. (6.24)) and the threshold pump power (eq. (6.12)) of NV^- and N_2V^0 containing diamond. Chosen values for the calculations were:

Cavity losses $\gamma = 0.1$, pump efficiency $\eta = 1$, pump beam radius $r = 50 \mu\text{m}$ and sample length $l = 2 \text{ mm}$.

While no laser action has been demonstrated in NV^- up to date, NV^- colour centres have a theoretical gain coefficient that is almost twice as high as that of N_2V^0 , which makes them an excellent candidate to base a colour centre laser on [81]. This is, assuming other factors, such as charge transfer, don't inhibit laser oscillation.

Although laser amplification has not been reported, there have been observations of stimulated emission. Stimulated emission in the form of STED³¹ in NV^- has been detected indirectly by measurements of the reduction in the NV^- emission spectrum [26, 95]. STED based microscopy has been successfully implemented with NV^- . This technique takes advantage of the reduction of emission by strong optical illumination [96]. Although Jeske et al attribute the effect to stimulated emission, it is perhaps still too early to completely rule out other effects. For example, whether the reduction of

³¹ Stimulated Emission Depletion

emission is caused by stimulated emission or other effects. Jeske et al point out that ESA processes could potentially lead to a weaker stimulated emission, by driving the NV^- population into NV^0 [26]. The ionisation process is believed to be a two-photon process which scales with laser power [71, 72, 73].

Although laser action has not been reported from NV^- , the spectroscopic properties look reasonably promising, and there is at least some indirect evidence that has been tentatively attributed to stimulated emission, suggesting that further study is merited.

In contrast to the lack of a demonstration of laser action with NV centres, observation of RT³² laser action of N_2V^0 in type I diamond was reported most famously in 1985 at a laser emission wavelength of 530 nm with an efficiency of 13.5% [16].

³² Room Temperature (293 K)

The sample chosen had a peak absorption of 1.05 cm^{-1} at 480 nm. It was cut into a 1.85 mm thick sample with near parallel polished surfaces and a wedge angle of 0.36 degrees and put into a setup as shown in fig. 6.18. It was pumped at 490 nm with intensities above 30 MW/cm^2 . Laser output was measured at 530 nm with an efficiency of 13.5% (for 1.27 mJ of absorbed input energy, the output energy was $171 \mu\text{J}$) from 18% Fresnel reflections at the surfaces and a beam divergence of 70 mrad. The minimum pumping intensity was estimated to be 8 MW/cm^2 , with an inversion density of $N_{th} = 2.4 \text{ ppm}$ [16, 45].

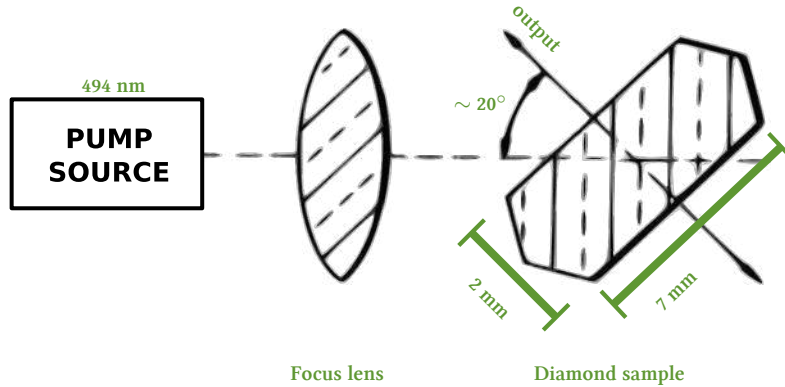
With such a huge round-trip loss from Fresnel reflections, a round trip gain of 15 dB was achieved. The estimation was made by Rand et al. that if losses were reduced to 4% per pass, using an external cavity, threshold inversion would be $N_{th} = 0.055 \text{ ppm}$. For a system pumped at 488 nm, with a pump spot size of $20 \mu\text{m}$ in diameter, threshold power for cw output was estimated to be $P_{th} = 0.14 \text{ W}$ [16].

In a patent Rand et. al describe a similar setup [97]. A green diamond was picked because of its bright luminescence from a selection of type I natural diamonds. The sample was cut to be 2 mm thick and 7 mm in diameter, with parallel polished surfaces. It was pumped using a 10 Hz pulsed dye laser at 494 nm. At an excitation beam intensity of 65 MW/cm^2 N_2V^0 centres were reported to lase, emitting at 540 nm, producing a coherent beam normal to the polished surfaces. The laser output was from 18% Fresnel reflections of the diamond surfaces, there was no external cavity and no mirror coatings. A representation of the setup is shown in fig. 6.18.

It was suggested that the addition of external mirrors and tuning elements would allow for laser output to be tunable in a 100 nm range. No bleaching of N_2V^0 was observed at excitation levels up to 70 MW/cm^2 [97].

Another demonstration of laser action was reported in 1988 as following:

Figure 6.18: Laser setup taken from and adjusted as described in [97].



A $3 \times 2 \times 2 \text{ mm}^3$ sample was side-pumped by a dye laser with 490 nm emission and a pulsewidth of 500 ns. The sample was placed in an external cavity with a 100% end mirror and a 97% OC with curvatures of 40 cm, separated by 35 cm. The laser was operated at room temperature. Laser emission in the yellow wavelength region was observed with a threshold of 3 MW/cm^2

In 1990 the research laboratories at Sumitomo Electric [98] describe their setup as following: N_2V^0 centres for laser purposes have been synthesized in a Ib synthetic diamond. Vacancies have been created by irradiation with 2 MeV electrons with a total dosage of 10^{18} cm^{-2} . Afterwards the sample was annealed at 1700°C and 5 GPa for 50 hours. Boron doping enhanced the concentration of N_2V^0 that was synthesized, while synthesis of N_2V^- and NV was suppressed. The diamond selected was a sample with a peak absorption of 3.5 cm^{-1} and a luminescence decay time of 9 ns. It was cut into a 1.6 mm thick plate with almost parallel polished surfaces with a wedge with an angle of 4° . The sample was placed in a two mirror cavity, both mirrors with a curvature of 40 cm, with 97% and 100% reflectivity. It was pumped with a flash-lamp dye laser with emission wavelength at 480 nm, pulse duration of 500 ns and a pulse energy of 10 mJ. Laser emission at 530 nm was reported with an output energy in the order of μJ , an efficiency of 0.1%, and threshold of $\sim 40 \text{ kW/cm}^2$ [98].

cw tunable laser action was reported at the University of Strathclyde in 1988 by [45, 81] as following: Two synthetic diamond samples containing N_2V^0 centres were cooled to 77 K and placed at Brewster's angle into a 3-mirror cavity. The pump laser used was an argon-ion laser with cw emission at 488 nm. The reported efficiency was very low with $6.6 \cdot 10^{-4}\%$, due to parasitic absorption by other defects present in the samples.

In the appendix to the thesis of G. Taylor [99] the findings were described as following: A laser setup was used as presented in fig. 6.19. The setup has a 5% output coupler and the minimum beam waist is approximately $100\ \mu\text{m}$. Laser operation at 300 K in natural diamond containing N_2V^0 was reported with an efficiency of $\sim 20\%$ and a threshold of 110 mW (fig. 6.19 bottom left). The crystal was pumped using the second harmonic of a Nd:YAG laser operating at 960 nm with 100 ps pulses. Laser operation at 77 K in synthetic diamond containing N_2V^0 , pumped with an cw Ar^+ laser emitting at 488 nm, was reported (fig. 6.19 bottom right).

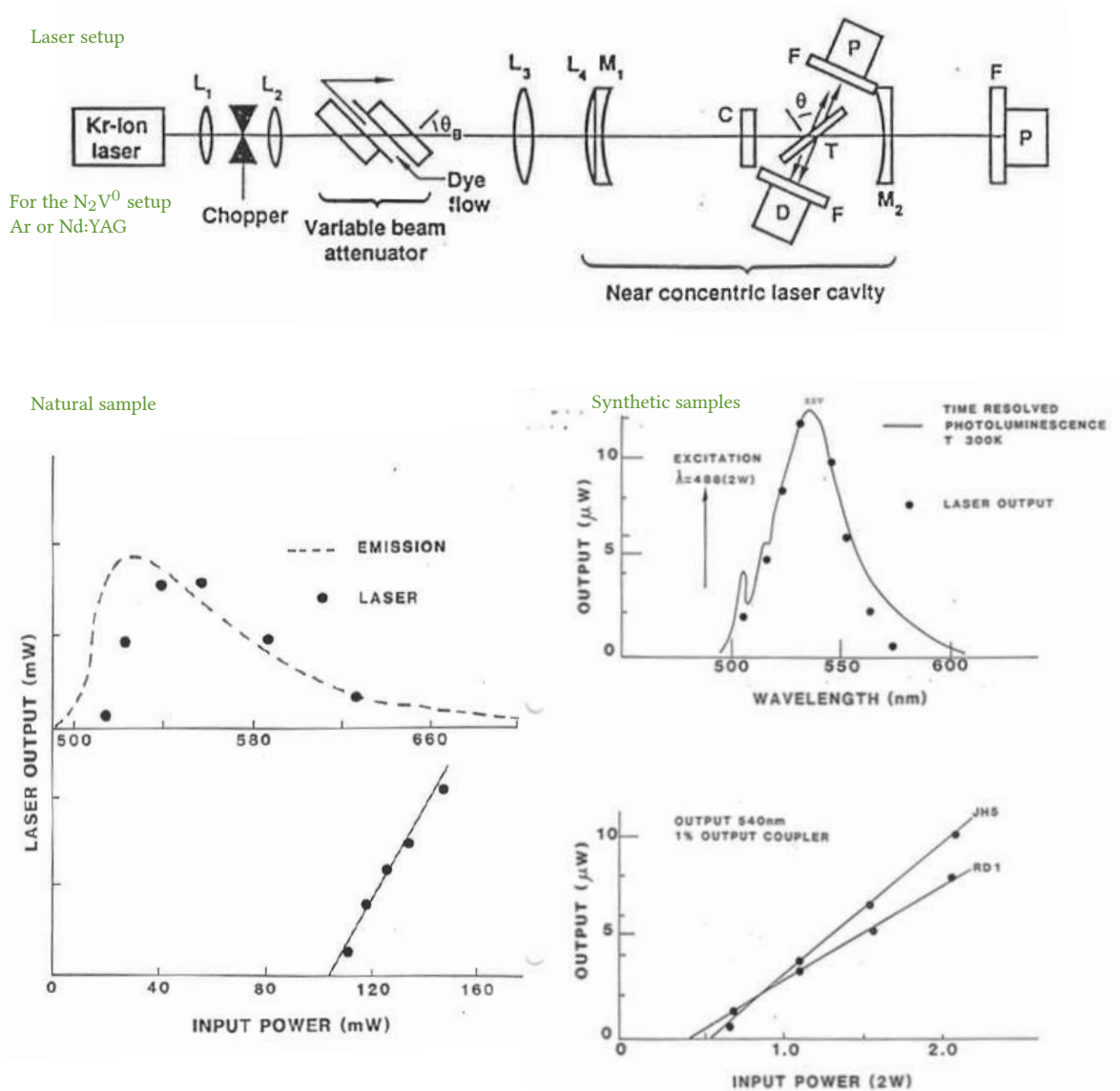


Figure 6.19: The laser setup (top) and experimental results for natural (bottom left) and synthetic (bottom right) N_2V^0 containing diamond [99].

Potential laser operation of NV and N_2V^0 colour centres in diamond may be compared to that of Ti:sapphire. Although the spectra of NV and N_2V^0 are narrower than that of Ti:sapphire, they are broader than some of the other materials widely used in fs / tuneable lasers, e.g. Yb-doped materials, and have emission in the otherwise poorly served visible spectral region.

Ti:sapphire is a material with a broad emission spectrum and relatively short lifetime ($3.2\mu s$), but large emission cross section ($4.1 \cdot 10^{-19} cm^2$) [15] and a sigma-tau product of $(\sigma \cdot \tau)_{TiS} = 1.3 \cdot 10^{-24} cm^2 s$. Literature values for NV⁻ and N_2V^0 suggest $(\sigma \cdot \tau)_{NV^-} \approx (0.5-4) \cdot 10^{-24}$ and $(\sigma \cdot \tau)_{N_2V^0} \approx 2.7 \cdot 10^{-24} cm^2 s$ respectively (see table 6.5). This is another indication that a laser based on NV and N_2V^0 , provided the literature values are reliable, is indeed plausible.

Figure 6.20 shows a comparison of the absorption and emission regions of Ti:sapphire to that of NV and N_2V^0 containing diamond.

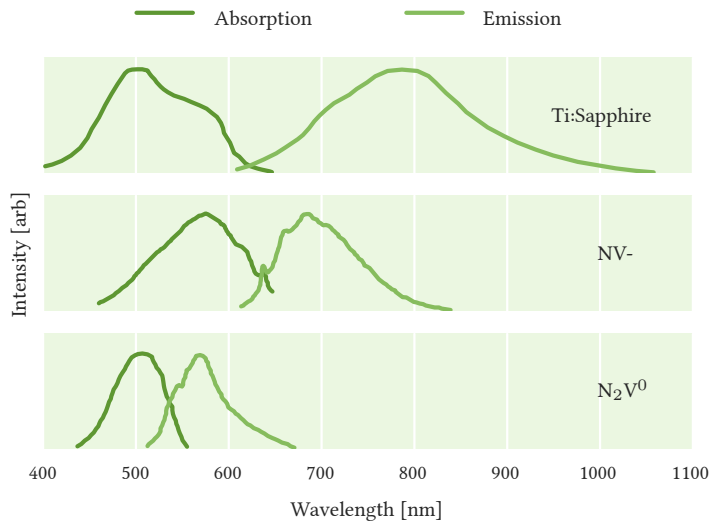


Figure 6.20: A comparison of the absorption and emission spectra of Ti:sapphire, NV⁻ and N_2V^0 [16, 54, 100].

6.6 Summary

DIAMOND IS A PROMISING MATERIAL for laser engineering, with its high thermal conductivity, high optical quality and mechanical stability and chemical inertness. In this work colour centres in diamond are inspected as a source of laser gain, as it is difficult to dope diamond with laser ions due to its compact crystal lattice. Proof of concept of colour centre lasers was shown in 1974 in colour centre containing alkali halides [50].

Classical colour centres often have the disadvantage of low thermal stability and bleaching when optically pumped. NV and N_2V^0 in diamond are both thermally stable and the broad emission spectrum in the visible make them interesting candidates for potential widely tunable and ultra-fast lasers.

The key laser parameters to characterise an optically active centre are the absorption and emission wavelengths and cross-sections, the luminescence lifetime and quantum efficiency. In this chapter the techniques to measure and calculate those parameters, in addition to the spectroscopic techniques introduced in chapter 4, are discussed.

Literature values for the figure of merit (sigma-tau product) for a laser based on NV⁻ and N_2V^0 are comparable to that of Ti:sapphire, a widely used and commercially available laser material. Preliminary calculations of some of the laser related properties, based on literature values, suggest a minimum concentration of ~ 1 ppm of the respective centres for 50% pump absorption (see section 6.5). This concentration was aimed for during the synthesis described previously in chapter 5.

The diamond samples used in the reported demonstrations of NV and N_2V^0 based lasers have not been characterised extensively and no *synthesis recipes* have been established to reproduce such samples. It was the aim of this work to reproduce these demonstrations, providing a more detailed characterisation of the samples.

The next chapter contains the assessment of key laser parameters of the most promising samples, in terms of optical quality and colour centre concentration.

References

- [1] J. Solé, L. Bausá, and D. Jaque. *An Introduction to the Optical Spectroscopy of Inorganic Solids*. 2005. DOI: 10.1002/0470016043.
- [2] C. Cohen-Tannoudji, B. Diu, and F. Laloe. *Quantum Mechanics*. Wiley, 1991. ISBN: 9780471164333.
- [3] A. E. Siegman. *Lasers*. University Science Books, 1986, p. 1283. ISBN: 0935702113.
- [4] O. Svelto. *Principles of lasers*. Boston, MA: Springer, 2010, pp. 1–620. ISBN: 9781441913012. DOI: 10.1007/978-1-4419-1302-9.
- [5] W. Koehner. *Solid-State Laser Engineering*. Springer Series in Optical Sciences. Springer, 2006. ISBN: 978-0-387-29338-7. DOI: 10.1007/0-387-29338-8.
- [6] F. Träger. *Springer handbook of lasers and optics*. Springer, 2012, pp. 87–156. ISBN: 9783642194085. DOI: 10.1007/978-3-642-19409-2.
- [7] G. Huber. *Solid-state lasers, Vorlesung WS 2008/2009, Universität Hamburg*.
- [8] T. H. Maiman. “Stimulated Optical Radiation in Ruby”. In: *Nature* 187.4736 (Aug. 1960), pp. 493–494. ISSN: 0028-0836. DOI: 10.1038/187493a0.
- [9] G. Huber, C. Kränkel, and K. Petermann. “Solid-state lasers : status and future”. EN. In: *Josa B* 27.11 (Oct. 2010), pp. 93–105. ISSN: 0740-3224. DOI: 10.1364/JOSAB.27.000B93.
- [10] R. G. Gould. “The LASER, Light Amplification by Stimulated Emission of Radiation”. In: *The Ann Arbor Conference on Optical Pumping*. Vol. 15. 1959, p. 128.
- [11] A. Einstein. “Zur Quantentheorie der Strahlung”. In: *Mitteilungen der Physikalischen Gesellschaft Zürich* 18.17 (1916), pp. 47–62.
- [12] S. Chu and C. Townes. “Biographical Memoirs V.83”. In: *Biographical Memoirs* (2003). URL: <https://www.nap.edu/read/10830/chapter/13>.
- [13] *The Nobel Prize in Physics 1964*. URL: http://www.nobelprize.org/nobel_prizes/physics/laureates/1964/ (visited on 04/20/2017).
- [14] G. Thomas and R. Isaacs. “Basic principles of lasers”. In: *Anaesthesia and Intensive Care Medicine* 12.12 (2011), pp. 574–577. ISSN: 14720299. DOI: 10.1016/j.mpaic.2011.09.013.
- [15] *RP Photonics Consulting GmbH - technical consulting on laser technology, nonlinear optics, fiber optics; simulation and design software; encyclopedia and buyer's guide*. URL: <https://www.rp-photonics.com/>.
- [16] S. C. Rand and L. G. Deshazer. “Visible color-center laser in diamond.” In: *Optics letters* 10.10 (Oct. 1985), pp. 481–483. ISSN: 0146-9592. DOI: 10.1364/OL.10.000481.
- [17] L. J. Curtis, H. G. Berry, and J. Bromander. “Analysis of Multi-exponential Decay Curves”. In: *Physica Scripta* 2.4-5 (Oct. 1970), pp. 216–220. ISSN: 0031-8949. DOI: 10.1088/0031-8949/2/4-5/015. URL: <http://stacks.iop.org/1402-4896/2/i=4-5/a=015?key=crossref.3edcd6e72534ecea9f7c9945d6f8b3a9>.
- [18] G. A. Crosby and J. N. Demas. “Measurement of photoluminescence quantum yields.” In: *J. Phys. Chem.* 75.8 (1971), pp. 991–1024. ISSN: 0022-3654. DOI: 10.1021/j100678a001.
- [19] T. S. Ahn et al. “Self-absorption correction for solid-state photoluminescence quantum yields obtained from integrating sphere measurements”. In: *Review of Scientific Instruments* 78.8 (Aug. 2007), p. 086105. ISSN: 00346748. DOI: 10.1063/1.2768926.
- [20] P. F. Moulton. “Spectroscopic and laser characteristics of Ti:Al₂O₃”. EN. In: *J. Opt. Soc. Am. B* 3.1 (Jan. 1986), pp. 125–133. ISSN: 0740-3224. DOI: 10.1364/JOSAB.3.000125.
- [21] P. Albers, E. Stark, and G. Huber. “Continuous-wave laser operation and quantum efficiency of titanium-doped sapphire”. EN. In: *Journal of the Optical Society of America B* 3.1 (Jan. 1986), pp. 134–139. ISSN: 0740-3224. DOI: 10.1364/JOSAB.3.000134.
- [22] Y. Li, I. Duncan, and T. Morrow. “Absolute fluorescence quantum efficiency of titanium-doped sapphire at ambient temperature”. In: *Journal of Luminescence* 52.5-6 (June 1992), pp. 275–276. ISSN: 00222313. DOI: 10.1016/0022-2313(92)90030-D.
- [23] B. F. Aull and H. P. Jenssen. “Vibronic interactions in Nd-YAG resulting in nonreciprocity of absorption and stimulated-emission cross-sections”. In: *IEEE Journal of Quantum Electronics* 18.5 (1982), pp. 925–930. ISSN: 0018-9197. DOI: 10.1109/JQE.1982.1071611.
- [24] V. G. Vins and E. V. Pstryakov. “Color centers in diamond crystals: Their potential use in tunable and femtosecond lasers”. In: *Diamond and Related Materials* 15.4-8 (Apr. 2006), pp. 569–571. ISSN: 09259635. DOI: 10.1016/j.diamond.2005.11.038.
- [25] *Thorlabs*. URL: <https://www.thorlabs.com/> (visited on 06/09/2017).
- [26] J. Jeske et al. “Stimulated emission from NV centres in diamond”. In: *Nature Communications* 8 (Jan. 2017), pp. 1–10. ISSN: 2041-1723. DOI: 10.1038/ncomms14000.
- [27] *The Mini-tau Product Features*. URL: https://www.edinst.com/wp-content/uploads/2015/07/Mini-Tau_Datasheet.pdf (visited on 08/08/2017).
- [28] W. Becker. “Fluorescence lifetime imaging by multi-dimensional time correlated single photon counting”. In: *Medical Photonics* 27 (May 2015), pp. 41–61. ISSN: 2213-8846. DOI: 10.1016/J.MEDPHO.2015.02.001.
- [29] A. T. Collins, M. F. Thomaz, and M. I. B. Jorge. “Luminescence decay time of the 1.945 eV centre in type Ib diamond”. In: *Journal of Physics C: Solid State Physics* 16.11 (1983), pp. 2177–2181. ISSN: 0022-3719. DOI: 10.1088/0022-3719/16/11/020.
- [30] R. P. Mildren and J. R. Rabeau. *Optical Engineering of Diamond*. Ed. by R. P. Mildren and J. R. Rabeau. Weinheim, Germany: Wiley-VCH, Apr. 2013. ISBN: 352741102X. DOI: 10.1002/9783527648603.
- [31] *Enable extreme performance photonics*. URL: https://e6cvd.com/media/catalog/category/Element_Six_Optical.pdf.

- [32] F. van Loon et al. "Intracavity diamond heatspreaders in lasers: the effects of birefringence". In: *Optics Express* 14.20 (2006), p. 9250. ISSN: 1094-4087. DOI: 10.1364/OE.14.009250.
- [33] R. Fork et al. "Integrated diamond sapphire laser". In: *Optics express* 11.20 (2003), pp. 2532–2548. DOI: 10.1364/OE.11.002532.
- [34] V. G. Savitski, S. Reilly, and A. J. Kemp. "Steady-state raman gain in diamond as a function of pump wavelength". In: *IEEE Journal of Quantum Electronics* 49.2 (2013), pp. 218–223. ISSN: 00189197. DOI: 10.1109/JQE.2012.2237505.
- [35] V. G. Savitski et al. "Characterization of single-crystal synthetic diamond for multi-watt continuous-wave raman lasers". In: *IEEE Journal of Quantum Electronics* 48.3 (Mar. 2012), pp. 328–337. ISSN: 00189197. DOI: 10.1109/JQE.2011.2179917.
- [36] O. Kitzler, A. McKay, and R. P. Mildren. "Continuous-wave wavelength conversion for high-power applications using an external cavity diamond Raman laser". In: *Optics Letters* 37.14 (2012), p. 2790. ISSN: 0146-9592. DOI: 10.1364/OL.37.002790.
- [37] A. McKay et al. "An efficient 14.5 W diamond Raman laser at high pulse repetition rate with first (1240 nm) and second (1485 nm) Stokes output". In: *Laser Physics Letters* 10.10 (2013), p. 105801. ISSN: 1612-2011. DOI: 10.1088/1612-2011/10/10/105801.
- [38] E. Granados, D. J. Spence, and R. P. Mildren. "Deep ultraviolet diamond Raman laser". In: *Optics express* 19.11 (2011), pp. 10857–10863. ISSN: 1094-4087. DOI: 10.1364/OE.19.010857.
- [39] J.-P. M. Feve et al. "High average power diamond Raman laser". In: *Opt. Exp.* 19 (2).2 (2011), p. 913. DOI: 10.1364/OE.19.000913.
- [40] A. Sabella, J. A. Piper, and R. P. Mildren. "Diamond Raman laser with continuously tunable output from 3.38 to 3.80 μm ". In: *Optics letters* 39.13 (2014), pp. 4037–4040. DOI: 10.1364/OL.39.004037.
- [41] D. C. Parrotta et al. "Tunable continuous-wave diamond Raman laser". In: *Optics express* 19.24 (2011), pp. 24165–24170. ISSN: 1094-4087. DOI: 10.1364/OE.19.024165.
- [42] S. Reilly et al. "Monolithic diamond Raman laser". In: *Optics Letters* 40.6 (Mar. 2015), p. 930. ISSN: 0146-9592. DOI: 10.1364/OL.40.000930.
- [43] R. J. Williams et al. "High Power Diamond Raman Lasers". In: *IEEE Journal of Selected Topics in Quantum Electronics* 24.5 (Sept. 2018), pp. 1–14. ISSN: 1077-260X. DOI: 10.1109/JSTQE.2018.2827658.
- [44] J. P. Goss et al. "Vacancy-impurity complexes and limitations for implantation doping of diamond". In: *Physical Review B - Condensed Matter and Materials Physics* 72.3 (July 2005), p. 35214. ISSN: 10980121. DOI: 10.1103/PhysRevB.72.035214.
- [45] M. A. Prelas et al. *Wide Band Gap Electronic Materials*. Vol. 1. Springer Science & Business Media, 1995. ISBN: 9789401040785. DOI: 10.1007/978-94-011-0173-8.
- [46] J. C. Slater. "Atomic Radii in Crystals". In: *The Journal of Chemical Physics* 41.10 (Nov. 1964), pp. 3199–3204. ISSN: 0021-9606. DOI: 10.1063/1.1725697.
- [47] A. Zunger. "Practical doping principles". In: *Applied Physics Letters* 83.1 (2003), pp. 57–59. ISSN: 00036951. DOI: 10.1063/1.1584074.
- [48] K. D. Jamison and H. K. Schmidt. *Doped diamond laser*. 1996. URL: <http://www.google.si/patents/US5504767>.
- [49] J. Storteboom et al. "Lifetime investigation of single nitrogen vacancy centres in nanodiamonds". EN. In: *Optics Express* 23.9 (May 2015), p. 11327. ISSN: 1094-4087. DOI: 10.1364/OE.23.011327. URL: <https://www.osapublishing.org/abstract.cfm?URI=oe-23-9-11327>.
- [50] L. F. Mollenauer and D. H. Olson. "A broadly tunable cw laser using color centers". In: *Applied Physics Letters* 24.8 (Apr. 1974), pp. 386–388. ISSN: 00036951. DOI: 10.1063/1.1655228.
- [51] B. Fritz and E. Menke. "Laser effect in KCl with FA(Li) centers". In: *Solid State Communications* 3.3 (Mar. 1965), pp. 61–63. ISSN: 00381098. DOI: 10.1016/0038-1098(65)90109-2.
- [52] W. T. Silfvast. *Laser Fundamentals*. Vol. 65. 9. Cambridge University Press, 1997, p. 932. ISBN: 0521833450. DOI: 10.1017/CB09780511616426.
- [53] L. F. Mollenauer and J. C. White. *Tunable Lasers*. Springer-Verlag Berlin Heidelberg, 1987, pp. 225–277. ISBN: 978-3-662-10637-2. DOI: 10.1007/978-3-662-10635-8.
- [54] A. M. Zaitsev. *Optical Properties of Diamond: A Data Handbook*. Springer, 2001, p. 502. ISBN: 354066582X. DOI: 10.1007/978-3-662-04548-0.
- [55] M. W. Doherty et al. "The nitrogen-vacancy colour centre in diamond". In: *Physics Reports* 528.1 (July 2013), pp. 1–45. ISSN: 03701573. DOI: 10.1016/j.physrep.2013.02.001.
- [56] L. J. Rogers et al. "Infrared emission of the NV centre in diamond: Zeeman and uniaxial stress studies". In: *New Journal of Physics* 10.10 (2008), p. 103024. ISSN: 13672630. DOI: 10.1088/1367-2630/10/10/103024.
- [57] M. W. Doherty et al. "The negatively charged nitrogen-vacancy centre in diamond: The electronic solution". In: *New Journal of Physics* 13.2 (2011), p. 25019. ISSN: 13672630. DOI: 10.1088/1367-2630/13/2/025019.
- [58] S. Felton et al. "Electron paramagnetic resonance studies of the neutral nitrogen vacancy in diamond". In: *Physical Review B* 77.8 (2008), p. 81201. ISSN: 1098-0121. DOI: 10.1103/PhysRevB.77.081201.
- [59] G. Davies. "Dynamic Jahn-Teller distortions at trigonal optical centres in diamond". In: *Journal of Physics C: Solid State Physics* 12.13 (1979), pp. 2551–2566. ISSN: 0022-3719. DOI: 10.1088/0022-3719/12/13/019.
- [60] J. Loubser and J. van Wyk. "Electron spin resonance in the study of diamond". In: *Reports on Progress in Physics* 41.December 1977 (1978), p. 1201. DOI: 10.1088/0034-4885/41/8/002.

- [61] P. Neumann et al. "Excited-state spectroscopy of single NV defect in diamond using optically detected magnetic resonance". In: *ArXiv: quant-ph* 11.1 (2009), pp. 1–11. ISSN: 13672630. DOI: 10.1088/1367-2630/11/1/013017.
- [62] E. V. Oort, N. B. Manson, and M. Glasbeek. "Optically detected spin coherence of the diamond N-V centre in its triplet ground state". In: *Journal of Physics C: Solid State Physics* 21.23 (1988), pp. 4385–4391. ISSN: 0022-3719. DOI: 10.1088/0022-3719/21/23/020.
- [63] D. Redman et al. "Two-beam coupling by nitrogen-vacancy centers in diamond." In: *Optics letters* 17.3 (1992), p. 175. ISSN: 0146-9592. DOI: 10.1364/OL.17.000175.
- [64] N. B. Manson, J. P. Harrison, and M. J. Sellars. "Nitrogen-vacancy center in diamond: Model of the electronic structure and associated dynamics". In: *Physical Review B* 74.10 (Sept. 2006), p. 104303. ISSN: 1098-0121. DOI: 10.1103/PhysRevB.74.104303.
- [65] V. M. Acosta et al. "Diamonds with a high density of nitrogen-vacancy centers for magnetometry applications". In: *Phys. Rev. B* 80.11 (Sept. 2009), p. 115202. DOI: 10.1103/PhysRevB.80.115202.
- [66] A. Drabenstedt et al. "Low-temperature microscopy and spectroscopy on single defect centers in diamond". In: *Phys. Rev. B* 60.16 (1999), pp. 11503–11508. ISSN: 0163-1829. DOI: 10.1103/PhysRevB.60.11503.
- [67] F. Jelezko et al. "Observation of coherent oscillation of a single nuclear spin and realization of a two-qubit conditional quantum gate". In: *Physical Review Letters* 93.13 (2004), p. 130501. ISSN: 00319007. DOI: 10.1103/PhysRevLett.93.130501.
- [68] I. Aharonovich et al. "Producing optimized ensembles of nitrogen-vacancy color centers for quantum information applications". In: *Journal of Applied Physics* 106.12 (2009), p. 124904. ISSN: 00218979. DOI: 10.1063/1.3271579.
- [69] P. Neumann et al. "Quantum register based on coupled electron spins in a room-temperature solid". In: *Nature Physics* 6.4 (2010), pp. 249–253. ISSN: 1745-2473. DOI: 10.1038/Nphys1536.
- [70] J. Jeske, J. H. Cole, and A. D. Greentree. "Laser threshold magnetometry". en. In: *New Journal of Physics* 18.1 (Jan. 2016), p. 013015. ISSN: 13672630. DOI: 10.1088/1367-2630/18/1/013015. arXiv: 1410.6239. URL: <http://iopscience.iop.org/article/10.1088/1367-2630/18/1/013015%20http://stacks.iop.org/1367-2630/18/i=1/a=013015?key=crossref.1001f1e0b109b31341fa12764aecb4b5>.
- [71] G. Waldherr et al. "Dark states of single nitrogen-vacancy centers in diamond unraveled by single-shot NMR". In: *Phys. Rev. Lett.* 106.15 (2011), p. 157601. DOI: 10.1103/PhysRevLett.106.157601.
- [72] N. Aslam et al. "Photo-induced ionization dynamics of the nitrogen vacancy defect in diamond investigated by single-shot charge state detection". In: *New Journal of Physics* 15.1 (Jan. 2013), p. 13064. ISSN: 13672630. DOI: 10.1088/1367-2630/15/1/013064.
- [73] P. Siyushev et al. "Optically controlled switching of the charge state of a single nitrogen-vacancy center in diamond at cryogenic temperatures". In: *Physical Review Letters* 110.16 (2013). ISSN: 00319007. DOI: 10.1103/PhysRevLett.110.167402.
- [74] X.-D. Chen et al. "Optical manipulation of the charge state of nitrogen-vacancy center in diamond". In: *Applied Physics Letters* 103.1 (2013), p. 13112. DOI: 10.1063/1.4813120.
- [75] G. Liaugaudas et al. "Luminescence lifetimes of neutral nitrogen-vacancy centres in synthetic diamond containing nitrogen". en. In: *Journal of Physics: Condensed Matter* 24.43 (Oct. 2012), p. 435503. ISSN: 0953-8984. DOI: 10.1088/0953-8984/24/43/435503.
- [76] H. Hanzawa, Y. Nisida, and T. Kato. "Measurement of decay time for the NV centre in Ib diamond with a picosecond laser pulse". In: *Diamond and Related Materials* 6.11 (1997), pp. 1595–1598. ISSN: 09259635. DOI: 10.1016/S0925-9635(97)00037-X.
- [77] N. B. Manson and R. L. McMurtrie. "Issues concerning the nitrogen-vacancy center in diamond". In: *Journal of Luminescence* 127.1 (2007), pp. 98–103. ISSN: 00222313. DOI: 10.1016/j.jlumin.2007.02.013.
- [78] A. Batalov et al. "Temporal coherence of photons emitted by single nitrogen-vacancy defect centers in diamond using optical rabi-oscillations". In: *Physical Review Letters* 100.7 (Mar. 2008), p. 077401. ISSN: 00319007. DOI: 10.1103/PhysRevLett.100.077401.
- [79] A. Mainwood. "Nitrogen and nitrogen-vacancy complexes and their formation in diamond". In: *Physical Review B* 49.12 (Mar. 1994), pp. 7934–7940. ISSN: 01631829. DOI: 10.1103/PhysRevB.49.7934.
- [80] P. Udvarhelyi et al. "Ab initio theory of N₂V defect as quantum memory in diamond". In: *arXiv.org* (2017). arXiv: 1704.07289.
- [81] G. Davies. *Properties and growth of diamond*. INSPEC, the Institution of Electrical Engineers, 1994, p. 437. ISBN: 0852968752.
- [82] A. T. Collins, H. Kanda, and H. Kitawaki. "Colour changes produced in natural brown diamonds by high-pressure, high-temperature treatment". In: *Diamond and Related Materials* 9.2 (Mar. 2000), pp. 113–122. ISSN: 09259635. DOI: 10.1016/S0925-9635(00)00249-1.
- [83] I. A. Dobrinets, V. G. Vins, and A. M. Zaitsev. *HPHT-Treated Diamonds*. Vol. 181. Springer, 2013. ISBN: 978-3-642-37489-0. DOI: 10.1007/978-3-642-37490-6.
- [84] Y. Mita et al. "Photochromism of H2 and H3 centres in synthetic type Ib diamonds". In: *Journal of Physics: Condensed Matter* 2.43 (Oct. 1999), pp. 8567–8574. ISSN: 0953-8984. DOI: 10.1088/0953-8984/2/43/002.
- [85] M. Kobayashi and Y. Nisida. "High Pressure Effects on Photoluminescence Spectra of Color Centers in Diamond". In: *Japanese Journal of Applied Physics* 32.S1 (Jan. 1993), p. 279. ISSN: 0021-4922. DOI: 10.7567/JJAPS.32S1.279.
- [86] J. Stortebom et al. "Lifetime investigation of single nitrogen vacancy centres in nanodiamonds". In: *Optics Express* 23.9 (2015), p. 11327. ISSN: 1094-4087. DOI: 10.1364/OE.23.011327.

- [87] S. Subedi et al. "Laser spectroscopy of highly doped NV-centers in diamond". In: *Solid State Lasers XXVII: Technology and Devices* 10511 (Feb. 2018). Ed. by W. A. Clarkson and R. K. Shori, p. 84. DOI: 10.1117/12.2290705.
- [88] T.-I. Wee et al. "Two-photon Excited Fluorescence of Nitrogen-Vacancy Centers in Proton-Irradiated Type". In: *The Journal of Physical Chemistry A* 111.38 (2007), pp. 9379–9386. ISSN: 1089-5639. DOI: 10.1021/jp073938o.
- [89] R. Chapman and T. Plakhotnik. "Quantitative luminescence microscopy on Nitrogen-Vacancy Centres in diamond: Saturation effects under pulsed excitation". In: *Chemical Physics Letters* 507.1-3 (2011), pp. 190–194. ISSN: 00092614. DOI: 10.1016/j.cpllett.2011.03.057.
- [90] C.-K. Lin et al. "Excitation properties of the H3 defect center in diamond: A theoretical study". In: *Chemical Physics Letters* 475.1-3 (June 2009), pp. 68–72. ISSN: 0009-2614. DOI: 10.1016/J.CPLETT.2009.05.011.
- [91] K. Beha et al. "Optimum photoluminescence excitation and recharging cycle of single nitrogen-vacancy centers in ultrapure diamond". In: *Physical Review Letters* 109.9 (Aug. 2012), p. 097404. ISSN: 00319007. DOI: 10.1103/PhysRevLett.109.097404.
- [92] F. Jelezko and J. Wrachtrup. "Single defect centres in diamond: A review". In: *Physica Status Solidi (A) Applications and Materials Science* 203.13 (Oct. 2006), pp. 3207–3225. ISSN: 18626300. DOI: 10.1002/pssa.200671403.
- [93] I. P. Radko et al. "Determining the internal quantum efficiency of shallow-implanted nitrogen-vacancy defects in bulk diamond". In: *Optics Express* 24.24 (Nov. 2016), p. 27715. ISSN: 1094-4087. DOI: 10.1364/OE.24.027715.
- [94] D. Gatto Monticone et al. "Systematic study of defect-related quenching of NV luminescence in diamond with time-correlated single-photon counting spectroscopy". In: *Physical Review B - Condensed Matter and Materials Physics* 88.15 (2013), p. 155201. ISSN: 10980121. DOI: 10.1103/PhysRevB.88.155201.
- [95] D. Wildanger, J. R. Maze, and S. W. Hell. "Diffraction Unlimited All-Optical Recording of Electron Spin Resonances". In: *Physical Review Letters* 107.1 (July 2011), p. 017601. ISSN: 0031-9007. DOI: 10.1103/PhysRevLett.107.017601.
- [96] E. Rittweger et al. "STED microscopy reveals crystal colour centres with nanometric resolution". In: *Nature Photonics* 3.3 (2009), pp. 144–147. ISSN: 1749-4885. DOI: 10.1038/nphoton.2009.2.
- [97] S. C. Rand and L. G. Deshazer. "Solid state laser employing diamond having color centers as a laser active material". In: (1985). URL: <https://www.google.com/patents/WO1986003347A1?c1=en>.
- [98] T. Nakashima and S. Yazu. "Optical properties and laser action of H3 center in synthetic diamond". In: *Proc. SPIE*. Vol. 1325. International Society for Optics and Photonics. 1990, pp. 10–16. DOI: 10.1117/12.22438.
- [99] G. T. Taylor. "An evaluation of the GR1, H3, H4 und NV1 diamond colour centres for use as a tunable laser source". PhD thesis. University of Strathclyde, Glasgow, 1989.
- [100] K. Wall and A. Sanchez. "Titanium Sapphire lasers". In: *The Lincoln laboratory journal* 3.3 (1990), pp. 447–462. URL: <https://pdfs.semanticscholar.org/0be0/0117536e932394af5e1d6d5c8acab06364d5.pdf>.

7

Assessment of colour centres for laser related properties

Contents

7.1	Sample selection	174
7.2	Assessment of NV containing samples	176
	Luminescence lifetime	177
	Luminescence quantum yield	180
	Emission cross section	182
	Gain spectrum	184
7.3	Assessment of N_2V^0 containing samples	188
	Luminescence lifetime	189
	Luminescence quantum yield	191
	Emission cross section	193
	Gain spectrum	194
7.4	Re-evaluation of laser potential	198
7.5	Summary	203
	References	204

7.1 Sample selection

EFFICIENT PUMP ABSORPTION in a laser material is a condition for efficient laser operation. Pump absorption dependent on sample size and colour centre ¹ density has been discussed in section 6.5 (Predicted operation of a NV and N₂V⁰ based laser). Neglecting other sources of losses, lower limits for the required colour centre concentrations for 50% pump absorption have been found to be 0.6 ppm² for NV⁻ ³ and 0.9 ppm for N₂V⁰ ⁴ in a 2 mm thick sample, assuming optical pumping at 532 nm and 473 nm. (two wavelengths for which literature values for the absorption cross sections were available table 6.6)

In practice, an Elforlight solid state laser emitting at 532 nm and a Laser-glow laser diode emitting at 447 nm were available for pumping (table 6.2).

Available samples, their synthesis and a comparison of colour centre concentrations as well as background absorption was given in chapter 5, Results of the colour centre synthesis. Samples were chosen based on their relatively high target centre concentration (up to ~ 0.6 ppm of NV⁰ ⁵, 0.8 ppm of NV⁻ and 2 ppm of N₂V⁰) combined with a comparably low absorption coefficient at the emission wavelength of the respective centre (between ~ 2 and 0.5 cm^{-1} at max emission of NV⁰, ~ 1.5 and 0.1 cm^{-1} for NV⁻ and 8 and 2.5 cm^{-1} for N₂V⁰). Those parameters are directly related to the magnitude of the gain coefficient, as shown in eq. (6.27) in section 6.2, Key parameters for solid state lasers.

Two synthetic CVD⁶ diamond samples, labelled E6NV and E6H3D have been selected for detailed study. Sample E6NV was selected for its large overall NV⁻ ⁷ concentration and a comparably low background absorption. Sample E6H3D was selected because it had the lowest background absorption at the peak emission of NV⁻ (See fig. 5.17 and fig. 5.18). Two natural diamond samples, BRAZ62 and BRAZ77, were chosen because of their luminescence and the highest amounts of N₂V⁰ present in any sample (~ 2 ppm).

Initial assessment of laser potential is based on measurements of the absorption and emission spectra, the luminescence lifetime, QY⁸, and the calculation of the emission cross section and gain spectra.

The defect concentrations have been calculated using FTIR⁹ spectra taken at room temperature and UV-VIS¹⁰ absorption spectra taken at 77 K. Low temperature absorption spectra were taken with the aim to obtain the area under the ZPL¹¹, after removing the background as shown in section 5.4, to determine defect concentrations. They were not corrected for the magnitude of background absorption and hence the absolute values of the absorption coefficients at any point cannot be compared among

¹ A type of structural defect, which produces absorption and emission bands that are different to those of the pure crystal [1]

² parts per million ($1.77 \cdot 10^{17} \text{ cm}^{-3}$ for diamond)

³ The negative form of NV

⁴ The neutrally charged state of N₂V (H3)

⁵ The neutral form of NV

⁶ Chemical Vapour Deposition

⁷ A substitutional nitrogen adjacent to a vacancy with a C_{3v} symmetry

⁸ Quantum Yield

⁹ Fourier Transform Infra Red

¹⁰ UltraViolet-Visible

¹¹ Zero Phonon Line

the samples measured at different occasions. UV-VIS and IR¹² spectra were taken as described in section 4.2, Dispersive spectroscopy, and section 4.3, Fourier transform spectroscopy, and concentrations were calculated as described in section 4.1, Defect quantification in diamond. Luminescence lifetime measurements have been carried out as described in section 6.3, Time-resolved luminescence spectroscopy, and section 6.2, Key parameters for solid state lasers. Where it was necessary, the spectra were corrected for spectral sensitivity of the detecting system as described in section 4.2, Dispersive spectroscopy.

¹² InfraRed (0.78-1000 μm)

The luminescence QY was calculated using eq. (6.20) and eq. (6.23) in section 6.2, Key parameters for solid state lasers. To determine the correction factor for self-absorption, a (eq. (6.22)), the spectrum of a sample with a low defect concentration was measured. This spectrum is matched to the long wavelength tail of the respective sample. For the assessment of NV⁻, the low concentration reference sample chosen was 1411ADsCVD01 ($N_{NV^0} = 0.03 \text{ ppm}$, $N_{NV^-} < 0.01 \text{ ppm}$). For the assessment of N₂V⁰ the low concentration reference sample chosen was E6H3C ($N_{N_2V^0} = 0.11 \text{ ppm}$, $N_{NV^-} < 0.02 \text{ ppm}$). Those were the best low concentration samples available to us.

The stimulated emission cross section was calculated using the Füchtbauer-Ladenburg equation (eq. (6.25)) as described in section 6.2, Key parameters for solid state lasers.

The gain spectrum for the respective defect, taking into account different values for the inversion coefficient β , was calculated using the calculated emission cross section, the defect concentration and the absorption spectrum taken at room temperature, with eq. (6.27), discussed in section 6.2, Key parameters for solid state lasers.

7.2 Assessment of NV containing samples

LASER RELATED PARAMETERS for NV centres based on measurement of samples E6NV and E6H3D are presented in this section.

Absorption spectra at liquid nitrogen temperature for samples E6NV and E6H3D were presented before in fig. 5.14. In fig. 7.1 the spectra after the last step of synthesis are compared to one another with an inset plot comparing the N_2V^0 ZPLs. As discussed previously, peaks for NV^- , NV^0 and some traces of N_2V^0 are present in both samples. The N_2V^0 concentration was ~ 0.1 and 0.04 ppm in sample E6H3D and E6NV, respectively. Sample E6NV had 0.62 ± 0.07 ppm of NV^- and 0.73 ± 0.04 ppm of NV^0 , present approximately equally split between both charged states. Sample E6H3D had 0.56 ± 0.06 ppm of NV^- and 0.19 ± 0.01 ppm of NV^0 , mostly present in the negatively charged state.

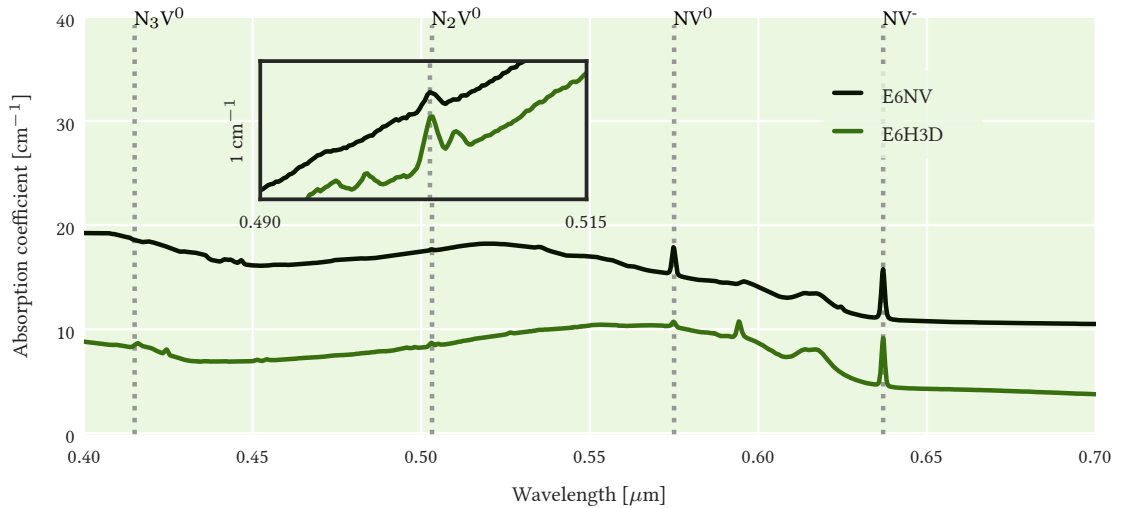


Table 7.1: Defect concentrations in samples estimated by the integrated ZPLs in absorption measurements taken at 77K.

CC	Concentrations [ppm]	
	E6NV	E6H3D
NV^0	0.73 ± 0.04	0.19 ± 0.01
NV^-	0.62 ± 0.07	0.56 ± 0.06
N_2V^0	0.04 ± 0.01	0.11 ± 0.02

Concentrations of single and aggregated nitrogen were calculated based on the FTIR spectra shown in fig. 7.2. Single nitrogen was about 5 and ~ 2 ppm for sample E6H3D and E6NV respectively (table 5.5).

The concentration of NV^- in both samples corresponds to the estimated concentration needed for 50% pump absorption, 0.6 ppm, as discussed in section 6.5, A potential diamond colour centre laser. As discussed in section 5.4, Spectroscopic analysis, sample E6H3D had the lowest background absorption at the maximum emission wavelength of NV^- (0.1 cm^{-1} at 690 nm). The absorption for E6NV was higher (1.56 cm^{-1} at 690 nm), but it was chosen for its large overall NV concentration (~ 1.3 ppm) and relatively high

Figure 7.1: Absorption spectra of samples E6NV and E6H3D, taken at 77 K. Spectra not corrected for background absorption and are offset for visibility.

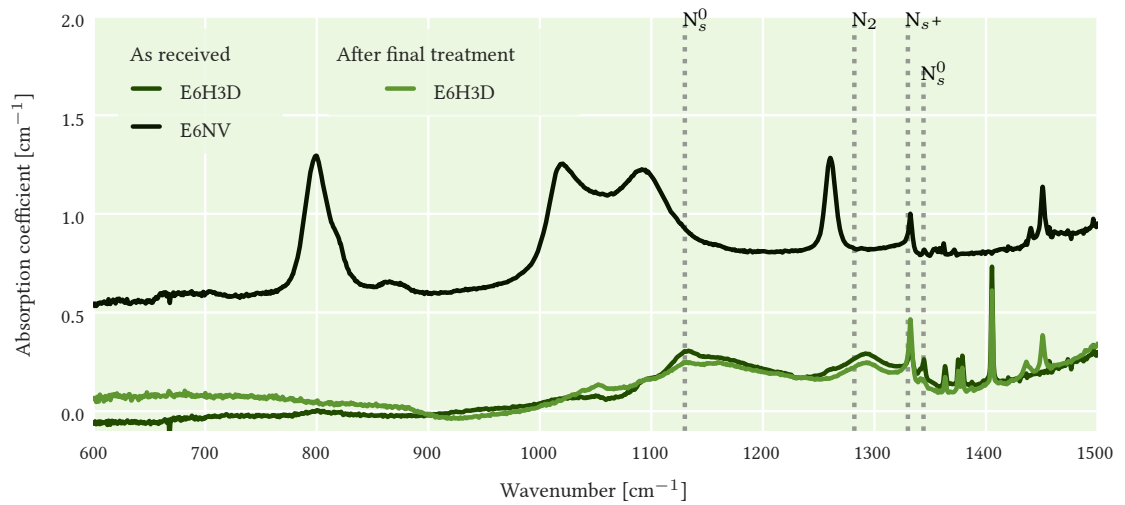


Figure 7.2: FTIR spectra for sample E6NV and E6H3D.

absorption at the maximum absorption wavelength to low absorption at the maximum emission wavelength of NV^- in comparison to other samples (1.59 cm^{-1} at 690 nm & 6.4 cm^{-1} at 565 nm , see fig. 5.18 and fig. 5.17).

Luminescence lifetime

Luminescence lifetime was measured with two pulsed light sources at 448 nm and 562 nm as described in section 6.3, Time-resolved luminescence spectroscopy. Luminescence measurements of bulk diamond at 10 K have shown that below 450 nm predominantly NV^0 is excited, and above 575 nm NV^- . In between the NV centre converts between the charged states [2]. For the setup here, we expect to see a contribution of only NV^0 at 448 nm , while both centres are excited at 562 nm and the emission spectrum is a superposition of the spectra of NV^0 and NV^- . Lifetime measurements are probed at different luminescence wavelengths, 640 , 670 and 700 nm and additionally $>640 \text{ nm}$, to distinguish between the contributions of NV^0 and NV^- when the emission spectra overlap. In previous studies [3, 4] the contribution of NV^0 was attributed for 65% of the light collected in the spectral region between 600 - 650 nm and for 37.5% between 700 - 800 nm . The contribution of NV^- was attributed for 35% and 62.5% , respectively.

The typical luminescence decay for the samples in the spectral region $>640 \text{ nm}$ is shown in fig. 7.3.

The decay is mono-exponential for pumping with 448 nm . The luminescence lifetime is $20 - 22 \text{ ns}$ for both samples, independent of the emission wavelength bands selected. The decay is double exponential when pumped with 562 nm . For the double exponential decay, measurements were fitted

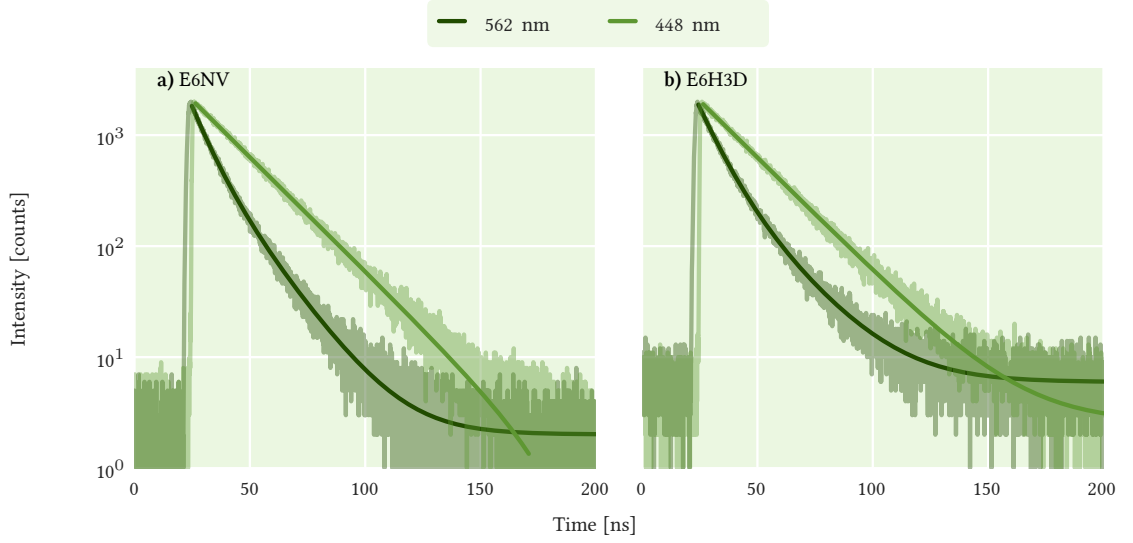


Figure 7.3: Luminescence decay of E6NV and E6H3D at emission wavelengths >640 nm, pumped at 448 and 562 nm.

with eq. (6.19) as described in section 6.2 (Key parameters for solid state lasers).

The results of the fitting are presented in table 7.2. The fast component of the lifetime, τ_f , was found to be between 7 and 9 ns, and the slow component, τ_s , was found to be between 17 and 21 ns, for sample E6NV and E6H3D. The only outlier is the measurement of the slow component in sample E6NV for wavelength band >640 nm, ~ 16 ns.

Sample		E6NV				E6H3D			
λ_{pump}	λ_{lum}	A_{sl}	τ_{sl}	A_f	τ_f	A_{sl}	τ_{sl}	A_f	τ_f
[nm]	[nm]		[ns]		[ns]		[ns]		[ns]
448	640		20				20		
	670		20				20		
	700		20				22		
	> 640		20				22		
562	640	921	17.5	1029	7.2	910	20.6	1108	8.9
	670	604	17.2	1321	7.7	633	19.3	1288	8.2
	700	457	17.5	1418	8	499	19.1	1424	8.2
	> 640	660	15.9	1254	7.1	501	19.4	1418	8.3

Table 7.2: Results of luminescence lifetime measurements

The difference in the luminescence decay times at the different pump wavelengths is attributed to the excitation of the different charged states of NV.

The difference in the samples could be related to the higher NV concentration in sample E6NV, possibly causing more quenching and therefore leading to shorter lifetimes. More studies are needed to confirm the concentration at which luminescence quenching appears in NV containing samples.

In table 7.2 an increase of the amplitude for the slow component (A_{sl}) can be observed when the selection of the emission wavelength bands is moved from 640 to 700 nm. The amplitude of the fast component (A_f) decreased for the same selection. This suggests that the contribution at 640 nm is predominantly determined by NV^0 and at 700 nm by NV^- . The respective maxima of the phonon sidebands in the emission spectrum are close to these values for the respective defects. For blue pumping no fast component is observed. The fast and slow components of the luminescence decay can therefore be associated with the decay of NV^- and NV^0 respectively.

Literature values for the radiative lifetime are listed in table 6.5. Luminescence lifetimes of NV^0 and NV^- in literature were measured by time-resolved luminescence spectroscopy in the spectral windows from 575 to 630 nm and 660 to 800 nm, respectively. Mono-exponential luminescence decay with a lifetime of 21 ns and 12 ns was found and attributed to NV^0 and NV^- [2].

The values measured here for excitation at 448 nm agree with literature values reported for NV^0 . We assume that at 448 nm mainly NV^0 is excited, while both NV^0 and NV^- are excited at 562 nm [2]. The shorter lifetimes measured at 562 nm excitation could be caused by non-radiative energy transfer mechanisms like photo-ionisation of NV^0 [3] or quenching due to other centres [5, 6].

Luminescence lifetimes measured for NV^- (~ 7.5 ns in sample E6NV and ~ 8.3 ns in E6H3D) are shorter than literature values ($\sim 12 - 13$ ns). Slightly lower luminescence lifetime values have been observed by [7], when comparing the lifetime of Ib natural diamonds with synthetic diamonds with about 10 times as much nitrogen in them. This is attributed to non-radiative decay mechanisms, for example from concentration quenching or energy transfer to other centres [7, 8].

Shorter luminescence lifetimes may indicate that the QY in a specific sample is lower, which is equivalent to a reduced laser potential for the sample. In the following subsection the estimation of the QY of both samples is discussed.

Luminescence quantum yield

The QY was introduced as a measure for the efficiency of the luminescence in section 6.2, represented by the ratio of luminescence lifetime over radiative lifetime (eq. (6.20)).

Two methods were used to calculate the QY in our samples, as described previously in section 6.2, Key parameters for solid state lasers. The QY value obtained by comparison of the luminescence spectra measured with the integrating sphere method is affected by parasitic absorption of the pump light in the respective sample. Comparison with the QY value obtained from the radiative and luminescence lifetime allows to judge the magnitude of parasitic absorption in the samples.

The luminescence lifetimes measured in the previous subsection indicate a quantum yield of $\sim 0.9-1$ for NV^0 and ~ 0.63 for NV^- in sample E6NV, and of ~ 1 for NV^0 and ~ 0.7 for NV^- in sample E6H3D, when compared to literature radiative lifetime values (17-19 ns for NV^0 [6, 8] and 12 ns for NV^- [9], see table 7.7).

Measured luminescence lifetimes associated with NV^0 (20-22 ns for excitation at 448 nm, see table 7.2) are similar or longer than the radiative lifetimes for bulk diamond given in literature. In a study of NV luminescence lifetime in nano-diamonds, average lifetimes of 22.59 ± 6.21 ns and 29.41 ± 6.98 ns for the negative and neutral charge state were found. The longer lifetimes in comparison to bulk diamond were attributed to suppression of the luminescence emission rate with decreasing diamond size. A variation in luminescence lifetime was attributed to a wide distribution of radiative and non-radiative decays among samples [4]. There are other possible causes for the suppression of the luminescence emission rate. For example, a connection between the suppression of NV^0 luminescence for excitation at 532 nm and moderate 1064 nm illumination was reported in [10]. While in our samples a suppression of the luminescence emission rate due to the sample size or at additional IR illumination is not plausible, there might be other, not yet fully understood, causes for it in our samples.

A QY value of 1 was reported for NV^- [11], but no information was given on the methods used to determine this value or the concentration of centres in the sample. There are no reported QY values for NV^0 up to date.

The QY values in those samples were also estimated by the comparison of the luminescence spectra measured with an integrating sphere, as discussed in section 6.2. The luminescence spectra of diamond samples E6NV and E6H3D and a Ti:sapphire¹³ crystal were measured using an integrating sphere setup with pumps at 532 and 447 nm are shown in fig. 7.4. The Ti:sapphire spectra are reduced to 1/3 of their intensity to improve the comparability with the other, less intense, spectra in fig. 7.4). The spec-

¹³ titanium-sapphire - $Ti^{3+} : Al_2O_3$

trum of 1411ADsCVD01 was matched to the long wavelength tail of E6NV to estimate the correction factor a as described in section 6.3.

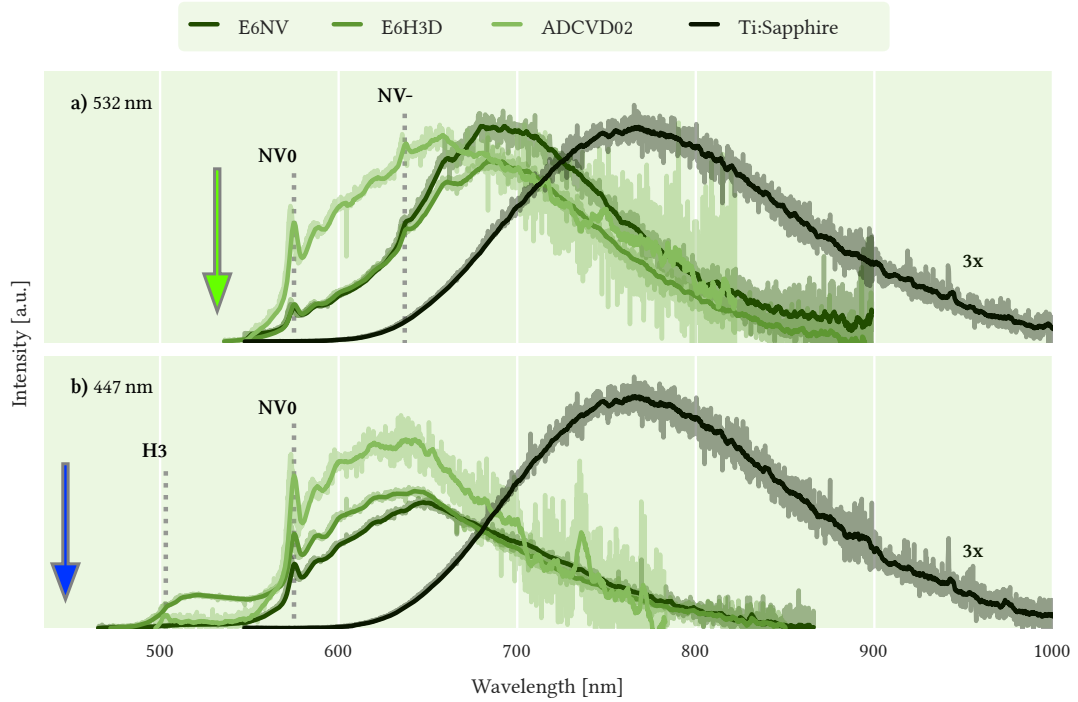


Figure 7.4: Luminescence spectra of E6NV and E6H3D and Ti:sapphire pumped at 532 nm and at 447 nm. The spectrum of Ti:sapphire has been reduced to 1/3 or its intensity for better comparability in this plot.

The results of the measurements are summarized in table 7.3.

Sample E6H3D has a relatively high concentration of N_2V^0 centres as can be seen by the characteristic shoulder at ~ 525 nm [12]. This will influence the accuracy in the calculation of parameter a . The integral over the spectrum of the sample in eq. (6.22) will be larger, causing the value for a to be smaller and ultimately leading to a lower estimation of the QY in eq. (6.23). Additionally, at a given pump wavelength several colour centres can cause absorption. This makes the determination of the exact transmittance value T_x for a specific colour centre difficult and will directly affect the accuracy of Φ_x (eq. (6.21)). Values presented in table 7.3 have been corrected for the reabsorption by the emitting center, but not for absorption by other centres.

Due to the challenges in the calculation of the QY the values given in table 7.3 should not be interpreted as QY values of a particular colour centre. They represent a QY value for the specific ensemble of centres present in the particular sample.

QY values for pumping at 447 nm (mostly exciting NV^0) are 0.17 and

Integrating sphere method						
Sample	Pump wavelength [nm]					
	447			532		
	Φ_x	a	Φ	Φ_x	a	Φ
E6NV	0.13 ± 0.06	0.25	0.17 ± 0.06	0.32 ± 0.1	0.3	0.4 ± 0.1
E6H3D	0.25 ± 0.1	0.17	0.28 ± 0.1	0.4 ± 0.1	0.24	0.48 ± 0.1

Luminescence lifetime / radiative lifetime			
Sample	Pump wavelength [nm]		
	448	562	
	τ_{sl}/τ_r (NV ⁰)	τ_{sl}/τ_r (NV ⁰)	τ_f/τ_r (NV ⁻)
E6NV	~ 1	0.9-1	0.63
E6H3D	~ 1	~ 1	0.7

0.28, and for pumping at 532 nm (mostly exciting NV⁻) are 0.4 and 0.48 for samples E6NV and E6H3D, respectively.

There is a difference between the results returned by the two QY measurement techniques, as can be seen in table 7.3. Measured luminescence lifetime divided by literature radiative lifetime gives a QY of 0.9-1 in both samples for NV⁰ and a range of 0.58-63 in sample E6NV and 0.65-0.7 in sample E6H3D for NV⁻. A QY of 0.17 at 447 nm and 0.4 at 532 nm for sample E6NV, and 0.28 at 447 nm and 0.48 at 532 nm for sample E6H3D, was measured using the integrating sphere method. This indicates a relatively strong absorption of the pump light by centres other than the target centre in the integrating sphere measurements, resulting in lower QY values than obtained by comparison to the QY obtained by measuring the luminescence lifetime. A low QY value and competing pump absorption from other defects are both factors that correlate negatively with the laser potential of a sample.

Emission cross section

In order to estimate the potential gain in our samples, the emission cross section needs to be determined. The luminescence spectra of E6NV and E6H3D were corrected for the contribution of other centres to obtain pure NV⁰ and NV⁻ spectra, as described in section 6.3, Luminescence spectroscopy. Figure 7.5 a) shows the correction of a mixed NV⁰ and NV⁻ spectrum when excited at 532 nm by subtraction of a pure NV⁰ spectrum excited at 447 nm, resulting in a pure NV⁻ spectrum, on the example of sample E6NV. Figure 7.5 b) shows the correction of a mixed N₂V⁰ and NV⁰ spectrum when

Table 7.3: **Top:** Results of quantum yield measurements by the integrating sphere method.

Bottom: Results for the quantum yield by measurements of luminescence lifetime. τ_r values taken from table 6.5 and τ_{sl} , τ_f values taken from table 7.2

excited at 447 nm by subtraction of a pure N_2V^0 spectrum excited at 447 nm, from the sample taken at a previous point in the synthesis when no NV was present in the sample, resulting in a pure NV^0 spectrum. The pure N_2V^0 spectrum was available from a previous state of the sample E6H3D, when no NV was yet generated in the sample. The noise in the NV^0 spectrum of E6H3D is due to the relatively low NV^0 concentration in the sample, resulting in an overall weaker signal.

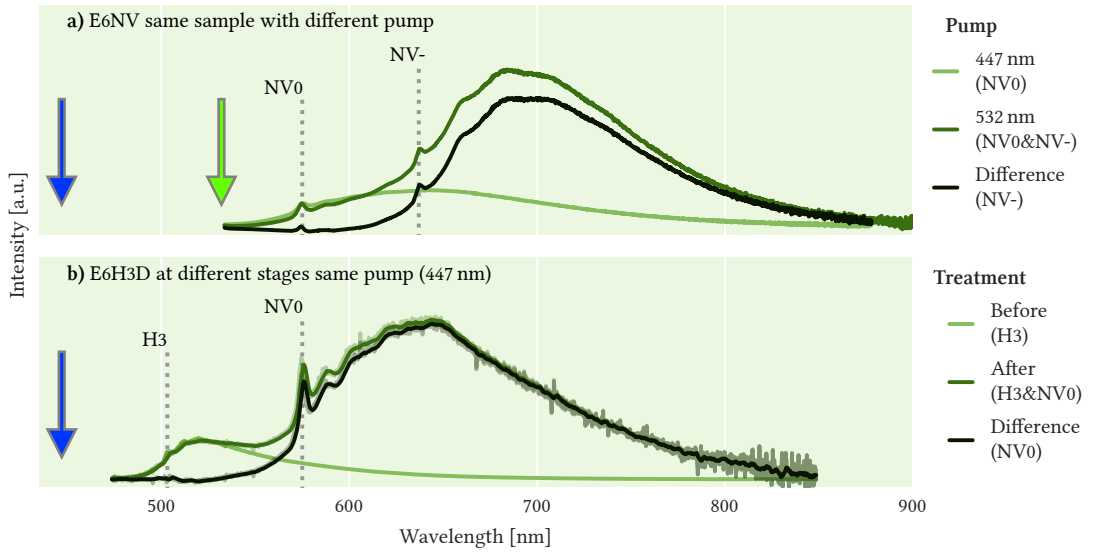
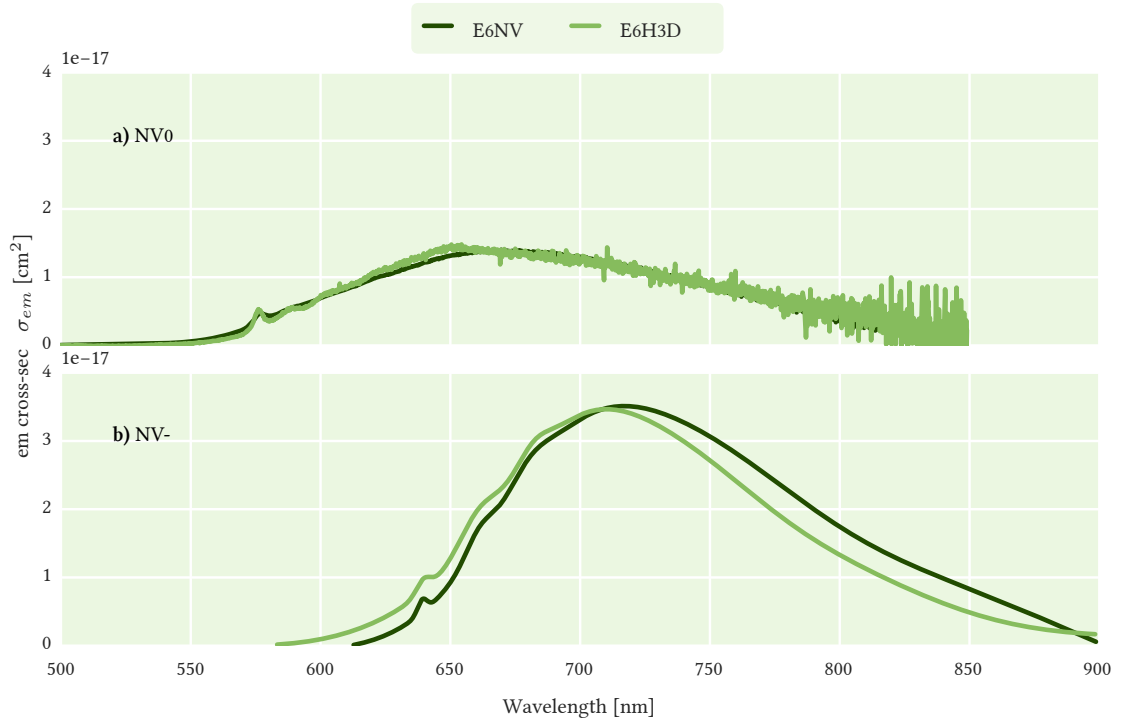


Figure 7.5: Correction of the luminescence spectra for the contribution of emission from NV^0 and N_2V^0 , pumped at 532 and 447 nm.

These corrected spectra were then used in eq. (6.25) to calculate the emission cross sections shown in fig. 7.6. The difference in the shape of the spectra is due to the relative contribution of the defects and the inaccuracy of the correction method. This can be seen, for example, in the emission cross section spectrum for NV^- of sample E6NV, in which the concentration of NV^0 is larger than in sample E6H3D, and the resulting spectrum is lower where the emission of NV^0 is strongest, and elevated towards longer wavelengths. Nonetheless, strong similarity in shape and magnitude of the spectra can be seen in fig. 7.6, despite the measurements coming from two very different samples.

For the calculations a radiative lifetime of 13 ± 0.5 ns [7] for NV^- and 20.7 ± 0.6 ns [2] for NV^0 was assumed. The peak of the emission cross section is estimated to be $\sigma_{em} = (3.6 \pm 0.1) \cdot 10^{-17}$ cm² at 710 nm for both samples for NV^- and in the range of $1.6 - 1.8 \cdot 10^{-17}$ cm² in the wavelength range of $\sim 660 - 670$ nm for NV^0 .

Literature values for the emission cross sections (table 6.5) are reported be-



tween 0.43 [9] and $3.2 \cdot 10^{-16} \text{cm}^2$ [12] for NV^- . The emission cross section value obtained here is in reasonable agreement with the value reported by [9].

Gain spectrum

The gain coefficient can be calculated with eq. (6.27) as described in section 6.2, Key parameters for solid state lasers. Two values of β are considered, representing different population inversion levels. The inversion level $\beta = 1$ represents an ideal situation when all population is in the upper laser level. A more realistic assumption to be achieved with the available pump intensity of $\sim 0.4 \text{ MW/cm}^2$ is an inversion level of $\beta = 0.3$ for both NV^0 and NV^- .

The absorption coefficient measured at room temperature, shown in fig. 7.7, is used for the calculation of the gain spectrum. In this calculation it is assumed that the major contribution to the absorption in the emission region of the respective centre is caused by centres different from the colour centre under study. This is especially valid for wavelengths further from the ZPL, but will lead to an underestimation of the gain closer to the ZPL and for lower values of β , by overestimation of the contribution of parasitic absorption.

Figure 7.6: The emission cross sections of NV^- and NV^0 (σ_{em}) for samples E6NV and E6H3D. The difference in the shape of the cross section spectra is attributed to the difference in colour centre concentrations and their contribution to the luminescence spectra.

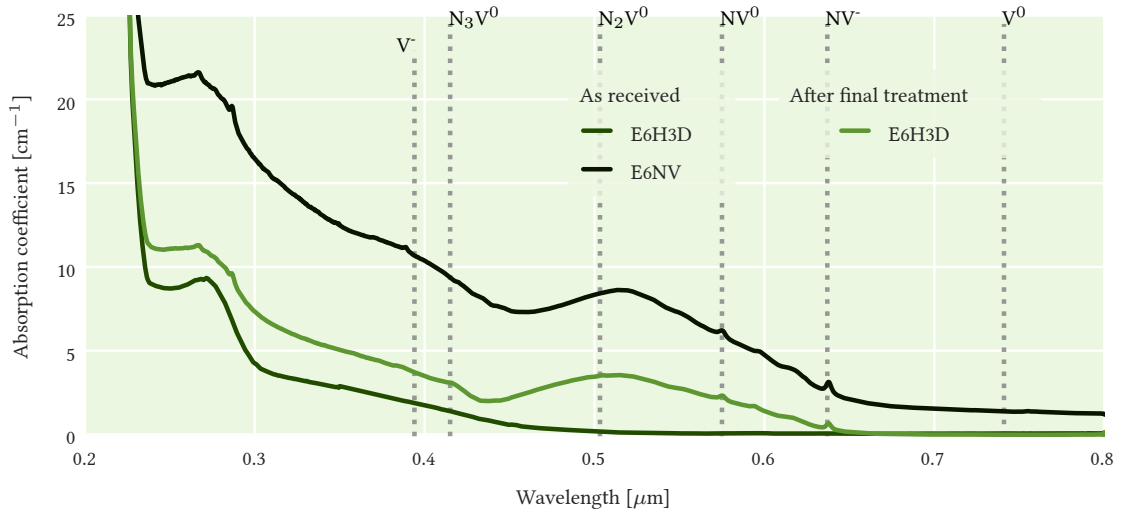


Figure 7.7: Room temperature unpolarised absorption spectra for sample E6NV and E6H3D.

The gain spectrum, calculated from eq. (6.27), for both inversion levels for NV^- and NV^0 , is shown in fig. 7.8. The upper plots show eq. (6.27) divided in the emission (for $\beta=1$) and absorption parts for the respective samples. The bottom plots show the calculated value for the gain for different inversion levels β . On the left side, measurements and values for NV^0 are shown and on the right for NV^- .

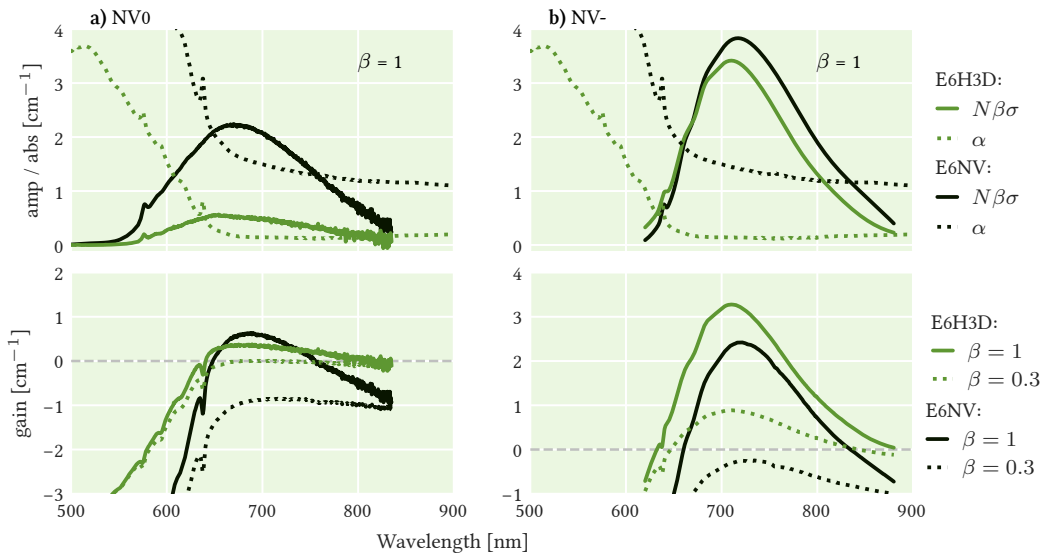
The ramp in the absorption towards lower wavelengths is caused by the absorption of NV^- and NV^0 . In the left top plot, it can be seen that the absorption of NV^- cuts into the emission of NV^0 . The emission of NV^- is further separated by the absorption of NV^0 , so this doesn't cause an issue (see top right plot). This decreases the potential gain bandwidth of NV^0 if NV^- is present in the sample or driven towards this state through temporary charge transfer. While charge transfer is an issue for the loss of population in an NV^- based laser, the problem of additional parasitic absorption doesn't arise here.

There is positive net gain ($\sim 1 \text{ cm}^{-1}$ max) for NV^- in sample E6H3D between 650 and 820 nm for $\beta = 0.3$, while no positive net gain is expected for sample E6NV for the same parameters. The biggest difference in the samples, contributing to the difference in gain, is the $\sim 1.5 \text{ cm}^{-1}$ larger absorption in sample E6NV, seen in the top plots in fig. 7.8. A short HPHT¹⁴ treatment of this sample, comparable to that of sample 1409E6sCVD02 as described in section 5.2, could yield a sample with a reduced parasitic background absorption of $\sim 1.5 \text{ cm}^{-1}$. But at the needed temperatures, treatment times would need to be as short as possible, not in excess of a few minutes, to prevent dissociation of the NV centres present in the sample.

¹⁴ High Pressure High Temperature

Additionally, further irradiation and annealing to regenerate NV centres after HPHT treatment can be considered.

This result makes sample E6H3D the most promising laser candidate of the two samples and advocates for the synthesis of diamond samples with an excess of 0.6 ppm of NV^- and a background absorption ideally lower than 0.1 cm^{-1} at peak emission of NV^- . It would be interesting to study samples with significantly higher NV^- concentrations, around 10 ppm, to determine at what concentrations quenching becomes a problem and where the concentration to luminescence ratio is ideal.



The maximum gain for NV^- in the ideal situation of $\beta = 1$ is about 3 cm^{-1} in sample E6H3D and about 2 cm^{-1} in sample E6NV at 710 nm. For NV^0 the gain coefficient stays below 1 cm^{-1} for all inversion levels and samples. For a more realistic inversion factor $\beta = 0.3$ there is a small net gain of 0.1 cm^{-1} estimated in sample E6H3D. The lower values in comparison to NV^- are mainly due to an overall smaller emission cross section of NV^0 , $1.5 \cdot 10^{-17} \text{ cm}^2$ as opposed to $3.5 \cdot 10^{-17} \text{ cm}^2$ (fig. 7.6).

The big difference in the amplification part for the two NV^0 spectra is due to the difference in concentration in the two samples, 0.73 and 0.19 ppm in samples E6NV and E6H3D. The concentration of NV^- is about the same in both samples.

Charge transfer has not been taken into account in this assessment, but plays a vital role to assess the suitability of NV or any other colour centre for laser purposes. In particular, charge stability and the loss of popula-

Figure 7.8: **Top:** The gain for NV^0 and NV^- in samples E6NV and E6H3D, separated in the absorption and amplification part of eq. (6.27), $g = N \cdot \beta \cdot \sigma_{em} - \alpha_{abs}$. Calculated for $\beta = 1$.

Bottom: Calculated gain spectra for NV^- and NV^0 in samples E6NV and E6H3D for different inversion factors $\beta = 1$ and $\beta = 0.3$.

tion due to charge transfer needs to be measured in a detailed study. The question whether charge transfer can be treated just as an additional loss, that can be addressed by a higher overall concentration of the target centre, needs to be addressed. If the dynamic drives too many colour centre into the undesirable charged state, while the rate of recovery is not large enough to ever get a large enough net concentration of the target charged state, then it will be impossible to operate a laser.

While positive net gain was calculated in sample E6H3D for NV^- , a laser based on this sample could not be built. ESA¹⁵ and charge transfer is suggested to reduce the laser potential for NV [9, 13]. Those effects act as additional losses in the system, possibly raising the threshold pump power and reducing the slope efficiency [14].

¹⁵ Excited State Absorption

Future experiments could include the measurement of the ESA cross section over the emission range for NV and the rate of charge transfer in order to determine if laser action is, in principle, achievable. In addition, samples with higher concentrations of NV should be investigated to determine if the additional amplification can overcome losses, before concentration quenching of luminescence and non-radiative charge transfer limit the benefit.

Based on the samples investigated in this work, a lower concentration of NV is not feasible for future experiments. Samples with at least comparable nitrogen concentrations to the samples presented here (3.5 ppm) or above should be considered for further synthesis, in order for the amplification part to overcome parasitic absorption and possibly overcome temporary losses of the concentration due to charge transfer.

An initial nitrogen concentration up to 20 ppm (yielding up to 2-10 ppm of NV), more, if concentration quenching doesn't limit the benefits of additional luminescence, is a better starting point, for samples with a background absorption ideally below 0.1 cm^{-1} (like sample E6H3D, which has the lowest background absorption at the emission wavelength).

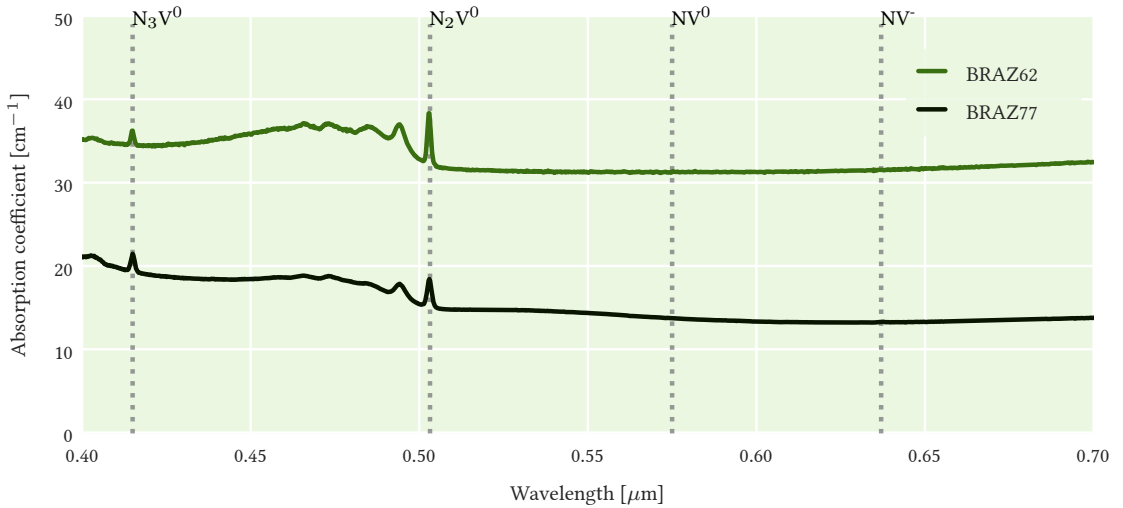
Laser related values for NV^0 and NV^- obtained in this work are less optimistic than literature values available at the start of this project. In particular for NV^0 , mostly due to reabsorption of the luminescence by NV^- .

In the following section 7.4, Re-evaluation of laser potential, the results of that will be discussed in more detail.

7.3 Assessment of N_2V^0 containing samples

THE MOST PROMISING N_2V^0 samples in this work were the natural samples BRAZ62 and BRAZ77. Those samples had the highest N_2V^0 concentrations (2.2 ppm and 1.5 ppm) and brightest apparent luminescence (by eye under UV¹⁶ light) of any N_2V^0 samples available.

Figure 7.9 shows the absorption coefficient measured at liquid nitrogen temperature without correction for the background. Low temperature absorption measurements were taken to calculate the colour centre concentrations, however, to assess the absorption coefficients of relevance to laser work, room temperature measurements were used (see fig. 7.14). In the region of interest it can be seen that N_2V^0 and N_3V^0 ¹⁷ is present while strong features for NV centres are absent. The N_2V^0 concentration is 1.5 ± 0.3 and 2.2 ± 0.4 ppm in samples BRAZ77 and BRAZ62, calculated from the area under the ZPL, respectively (see table 5.8).



Nitrogen concentrations were calculated based on the FTIR spectra shown in fig. 7.10. The spectra shown are shifted for visibility and do not represent the actual absorption coefficient.

These samples had a high overall nitrogen concentration in comparison to the CVD samples evaluated in the previous section. Nitrogen was present mostly in aggregated form. 35 ppm of N_2 ¹⁸ and 120 ppm of N_4V ¹⁹ were present before treatment, and 25 ppm of N_2 and 120 ppm of N_4V after treatment, in sample BRAZ62. 50 ppm of N_2 and 60 ppm of N_4V were present before treatment, and 35 ppm of N_2 and 55 ppm of N_4V after treatment, in sample BRAZ77. This is reflected in the similar characteristic peak

CC	Concentrations [ppm]	
	BRAZ62	BRAZ77
NV0	-	-
NV-	-	0.02 ± 0.01
N_2V	2.2 ± 0.4	1.5 ± 0.3

Table 7.4: Defect concentrations in samples estimated by the integrated ZPLs in absorption measurements taken at 77K.

¹⁶ UltraViolet (10-380 nm)

¹⁷ A vacancy and three substitutional nitrogen atoms with a C_{3v} symmetry (N3)

Figure 7.9: Absorption spectra of samples BRAZ62 and BRAZ77, taken at 77 K. Spectra not corrected for background absorption.

¹⁸ Two adjacent substitutional nitrogen atoms (A centre)

¹⁹ Four substitutional nitrogen surrounding a vacancy (B centre)

for N_2 centres at 1282 cm^{-1} in both spectra of both samples after treatment, as seen in fig. 7.10, and in the difference in the characteristic peak for N_4V centres at 1170 cm^{-1} . The reference spectra showing this in detail can be seen in fig. 4.1 in chapter 4, Defect quantification and spectroscopic methods. The noisy signal in the spectra before treatment is due to the use of the unpurged benchtop FTIR spectrometer. The peak at $\sim 1360\text{ cm}^{-1}$, associated with platelets (B' ²⁰), is significantly reduced after HPHT treatment.

The increase in N_s^+ ²¹ suggests that a negatively charged defect appeared, possibly N_2V^- ²², which was not measured in this work, as the low temperature absorption measurements were not taken in the wavelength region for N_2V^- .

²⁰ Platelets associated with a sharp line with a position varying between 1358 to 1380 cm^{-1}

²¹ Positively charged N_s

²² The negatively charged state of N_2V (H_2)

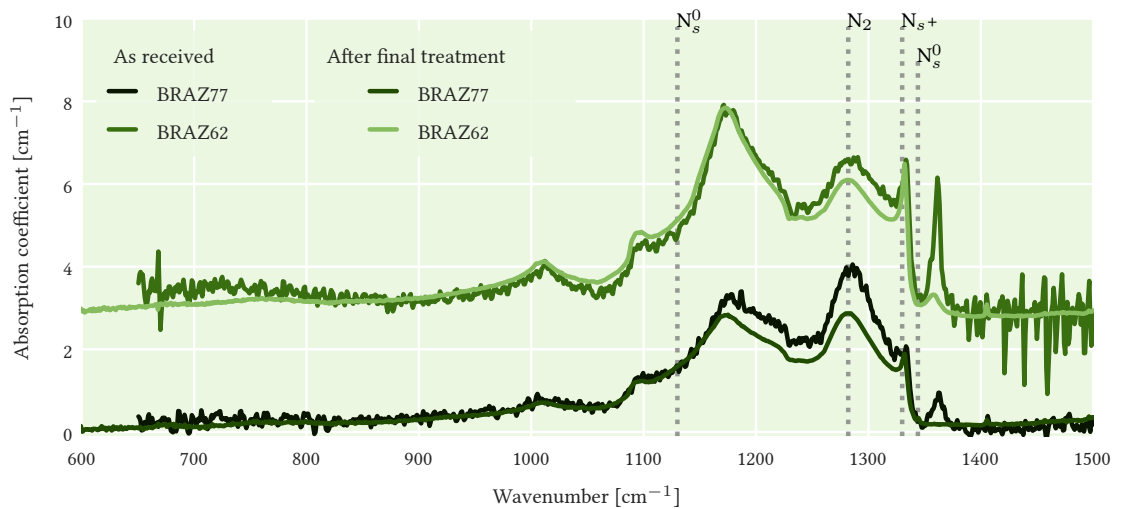


Figure 7.10: FTIR spectra for sample BRAZ62 and BRAZ77. Vertically shifted for visibility.

Luminescence lifetime

The luminescence decay for samples BRAZ62, BRAZ77 and the low concentration sample E6H3C (0.11 ± 0.02 ppm of N_2V^0) are shown in fig. 7.11.

The decay is mono-exponential for pumping with 448 nm for all samples. The luminescence lifetime ranges between 11.5 ± 1 ns sample E6H3C to 12.3 ± 1 and 12.5 ± 1 ns in samples BRAZ77 and BRAZ62. The results of the fitting are presented in table 7.5. Within error bounds the lifetime is assumed to be essentially the same in all samples. The N_2V^0 concentration differs by an order of magnitude between the BRAZ samples and E6H3C. Additionally, N_2 centres were present in concentrations up to 35 ppm and N_4V centres in concentrations up to 120 ppm. In sample E6H3C, N_2 centres were present in a concentration of about 1 ppm and no N_4V centres were detectable.

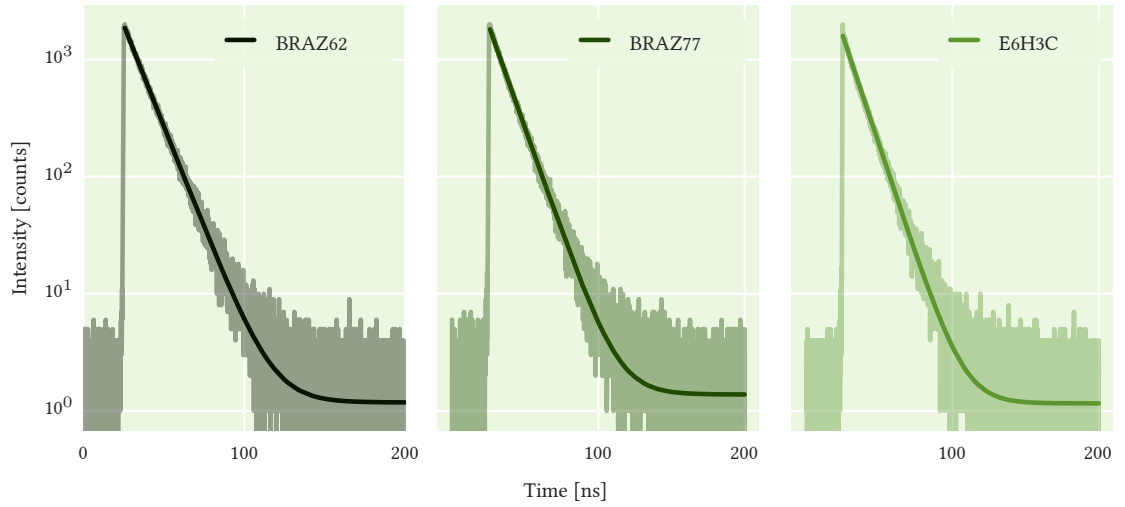


Figure 7.11: Luminescence decay of BRAZ62, BRAZ77 and E6H3C pumped at 448 nm.

Luminescence lifetime of N_2V^0 in literature was found to be 16 ns in highly homogeneous natural diamonds, and the radiative lifetime was found to be 17 ns in a temperature range between 77 and 700 K [11].

Literature values of luminescence lifetime were measured by cathodoluminescence emission of N_2V^0 in samples which were found to have naturally occurring N_2V^0 luminescence, but the N_2V^0 concentration was too small to be detected by conventional absorption spectroscopy [15].

Sample		BRAZ62	BRAZ77	E6H3C
λ_{pump} [nm]	λ_{lum} [nm]	τ [ns]		
448	520	13 ± 1	12 ± 1	12 ± 1

Table 7.5: Results of the luminescence lifetime measurements for samples BRAZ62, BRAZ77 and E6H3C

Our samples have a combined nitrogen concentration of 530 ppm (25 ppm N_2 and 120 ppm N_4V) in sample BRAZ62 and 290 ppm (35 ppm N_2 and 55 ppm N_4V) in sample BRAZ77. Significantly shorter lifetimes, as low as 7 ns, were found in samples with more than 0.05 atomic per cent (500 ppm) of nitrogen [15]. Concentration quenching of the luminescence by N_2 centres might be assumed to some degree in the BRAZ samples, as they have a higher overall nitrogen-aggregate concentration. It is unclear why we measured a similar lifetime in sample E6H3C, with only about 5 ppm of leftover single nitrogen and 1 ppm of N_2 centres.

The luminescence lifetime can go down to a few ns in diamonds with high N_2 concentration and internal stress [11]. Stress was not measured in our samples and the difference in internal stress for the samples is not

known.

Luminescence quantum yield

The luminescence lifetimes measured in the previous subsection indicate a quantum yield of ~ 0.76 in sample BRAZ62 and ~ 0.71 in sample BRAZ77, when compared to literature radiative lifetime values.

To estimate the QY by comparison of the luminescence spectra, the spectra of samples BRAZ62 and BRAZ77 and a Ti:sapphire crystal, pumped 447 nm were measured. The results are presented in fig. 7.12. Sample E6H3C was used to obtain the correction factor a for self absorption, as described previously in section 6.3, Correction of luminescence spectra for contributions of other centres. The peak intensity of the N_2V^0 luminescence of samples BRAZ62 and BRAZ77 is comparable to that of Ti:sapphire. The luminescence bandwidth is ~ 60 nm (FWHM) in both samples. Sample BRAZ77 has a lower luminescence intensity than sample BRAZ62, reflecting the higher N_2V^0 concentration and lower background absorption in the emission region (see fig. 7.15) in sample BRAZ62.

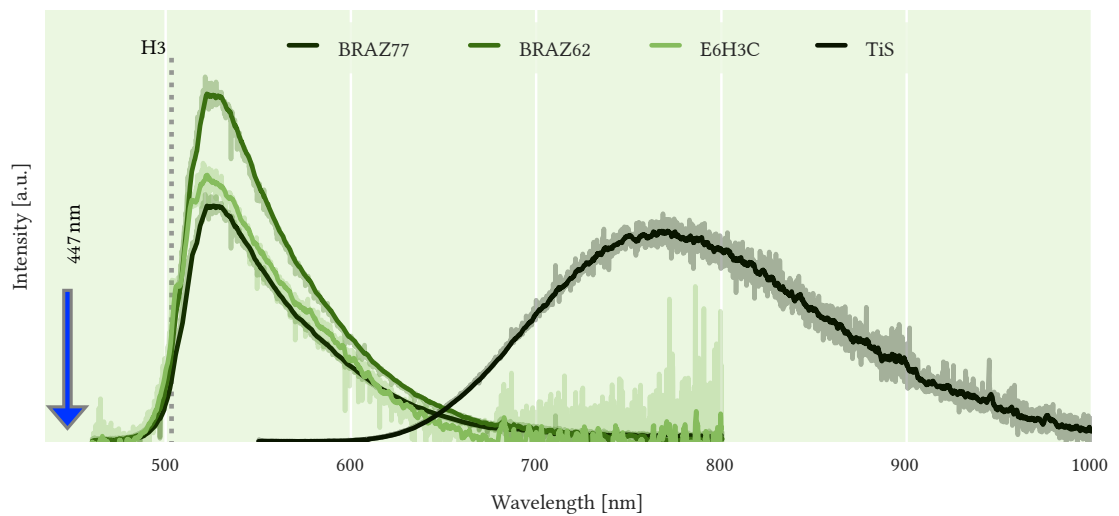


Figure 7.12: Luminescence spectra of BRAZ62 and BRAZ77 and Ti:sapphire pumped at 447 nm.

The results of the QY calculations are presented in table 7.6. The QY value for sample BRAZ62 approaches unity with an error of about 30% in our measurements, largely due either to random effects, which can be dealt with in future experiments by averaging of multiple measurements, and the reduction of systematic errors by improvement of the experimental setup, for example using a larger integrating sphere diameter (the one used here is 2") to improve accuracy of the measurements, by lowering the ratio of port to surface area of the sphere.

The value for BRAZ77 is 0.7 ± 0.2 . The value for a is small in both samples, suggesting that the effect of self absorption can be neglected. While the large error in the measurement makes it difficult to fully speculate on the nature of the data measured, it would make sense for the QY value of BRAZ77 to be lower, reflecting the parasitic reabsorption of luminescence in our measurement method, due to the higher absorption at the peak emission (525 nm) of this sample (8.7 cm^{-1}) in comparison to BRAZ62 (2.9 cm^{-1}).

Integrating sphere method			
Sample	Pump wavelength [nm]		
	Φ_x	a	Φ
BRAZ62	$\sim 1.0 \pm 0.3$	0.01	$\sim 1.0 \pm 0.3$
BRAZ77	0.7 ± 0.2	0.02	0.7 ± 0.2

Luminescence lifetime / radiative lifetime	
Sample	Pump wavelength [nm]
	τ_{lum}/τ_r (N_2V^0)
BRAZ62	0.76
BRAZ77	0.71
E6H3C	0.71

A QY value of 0.95 was reported in literature for N_2V^0 in samples as described in the previous subsection (with < 0.01 atomic per cent (100 ppm) of nitrogen, and no visible N_2V^0 feature in absorption measurements) [11, 15]. The QY values presented here, are, within error bounds, in reasonable agreement with literature values. Particularly taking into account, that the BRAZ samples here were affected by luminescence quenching of N_2 centres, as can be implied from the shorter measured luminescence lifetime.

The significantly lower NV QY, obtained by integrating sphere measurements, as compared to the one obtained by luminescence lifetime measurements, was attributed to a strong absorption of the luminescence by other centres than the target colour centre in the NV samples (section 7.2, table 7.3). The two QY measurements for N_2V^0 are in agreement with each other, within error bounds. N_2V^0 samples contained predominantly N_2V^0 , while the NV samples had an overlap of at least the two charged states of NV, and some had N_2V^0 in them additionally. The agreement in QY values

Table 7.6: **Top:** Results of quantum yield measurements by the integrating sphere method. **Bottom:** Results for the quantum yield by measurements of luminescence lifetime. τ_r values taken from table 6.5 and τ_{lum} values taken from table 7.5

is believed to reflect the colour centre purity of the N_2V^0 samples.

Emission cross section

The emission cross sections were calculated using the uncorrected luminescence spectra, as no other defects, in particular NV, were present in sufficient concentration to cause absorption or emission in the region of N_2V^0 luminescence. The calculated emission cross sections are shown in fig. 7.13.

There is better agreement in the shape of the emission cross section of the different N_2V^0 samples than of the NV sample spectra (fig. 7.6), since no correction for the overlap with other centres was needed.

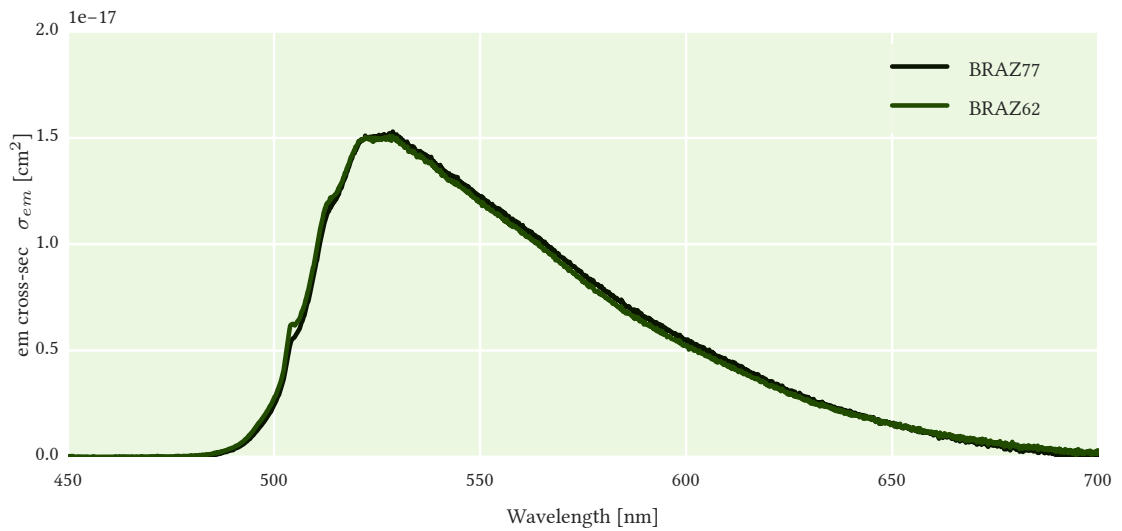


Figure 7.13: The emission cross sections of N_2V^0 (σ_{em}) for samples BRAZ62 and BRAZ77.

The emission cross section has a peak of $\sigma_{em} = 1.5 \cdot 10^{-17} \text{ cm}^2$ at 525 nm. A value ten times larger, $1.6 \cdot 10^{-16} \text{ cm}^2$, was reported for the emission cross section in N_2V^0 at maximum emission in literature [12], determined in HPHT treated natural type Ia diamond.

While no recent measurements of the emission cross section of N_2V^0 have been reported, the method to measure the emission cross section value in this work has already produced reliable values for NV, which are in better agreement with recent publications by [9] than the values previously published by [12].

In the first report of laser action based on N_2V^0 centres in diamond by Rand et al. [16], the inversion density at threshold was calculated to be

$\Delta N = 4.2 \cdot 10^{17} \text{ cm}^{-3}$ and the minimum pump intensity to achieve this was calculated with

$$I_t = \Delta N h \nu V / A \tau_p$$

to be 8 MW/cm^2 for the crystal thickness $V/A=0.185 \text{ cm}$. Furthermore, if losses were to be reduced to 4%, the authors claim that the threshold inversion would be $\Delta N = 9.8 \cdot 10^{15} \text{ cm}^{-3}$, which would allow for cw²³ excitation by a 488 nm Ar^+ laser with a $20 \mu\text{m}$ beam diameter, to reach threshold for a calculated incident power of 0.14 W.

²³ continuous wave

From the estimation of the threshold power by Rand et. al, using eq. (6.12), assuming pump efficiency of 100%, the emission cross section calculated should be $\sigma_{em} = 2.3 \cdot 10^{-17} \text{ cm}^2$. These values are close to the emission cross section calculated in this work, $\sigma_{em} = 1.5 \cdot 10^{-17} \text{ cm}^2$. Using this emission cross section value in the calculation above, the threshold power would be 0.21 W, in a setup as described by Rand et al. in [16].

Gain spectrum

Figure 7.14 shows the room temperature absorption coefficient for the samples, which was used in the calculation of the gain spectrum. The spectra are corrected and show the real absorption coefficients.

It can be seen that BRAZ77 has a higher background absorption than BRAZ62, despite having a lower N_4V concentration and a comparable N_2 concentration. The background absorption might be caused by the presence of other defects, which have not been studied in further detail in this work. Additionally, the large background absorption at the peak emission of N_2V^0 , 525 nm, (2.9 cm^{-1} for BRAZ62 and 8.6 cm^{-1} for BRAZ77) in comparison to the low background absorption of the CVD samples at the peak emission of NV⁻, 690 nm, (between 0.1 cm^{-1} for E6H3D and 3.2 cm^{-1} for CVD04, fig. 5.17) should be pointed out. This is another argument to synthesise N_2V^0 preferably in synthetic diamond, if the right technique to do so efficiently, can be established. The parasitic background absorption in natural diamond and the uneven quality of the samples are a major downside to using natural diamond as a laser material.

A direct comparison for the CVD samples at 525 nm is unfeasible, as the large amount of NV centres there cause a large absorption at this wavelength (between 2.8 cm^{-1} for E6H3D and 10 cm^{-1} for CVD04). Before treatment (and the generation of NV) those samples had absorption coefficients below 2.7 cm^{-1} .

The gain spectrum for both inversion levels $\beta = 1$ and $\beta = 0.3$ is shown in fig. 7.15.

Sample BRAZ62 shows a net gain of $\sim 2.5 \text{ cm}^{-1}$ in the unrealistic case

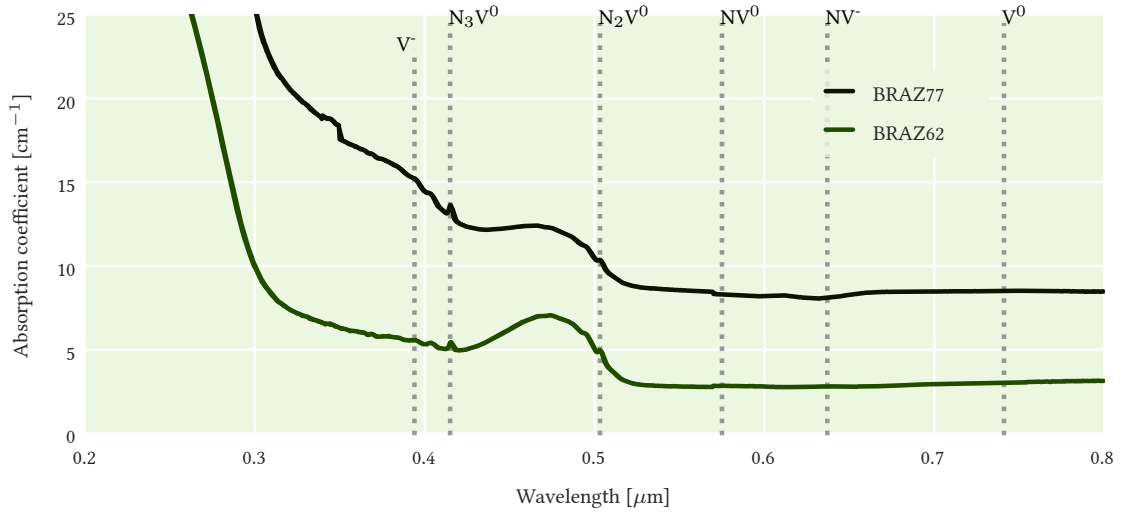


Figure 7.14: Room temperature unpolarised absorption spectra for samples BRAZ62 and BRAZ77.

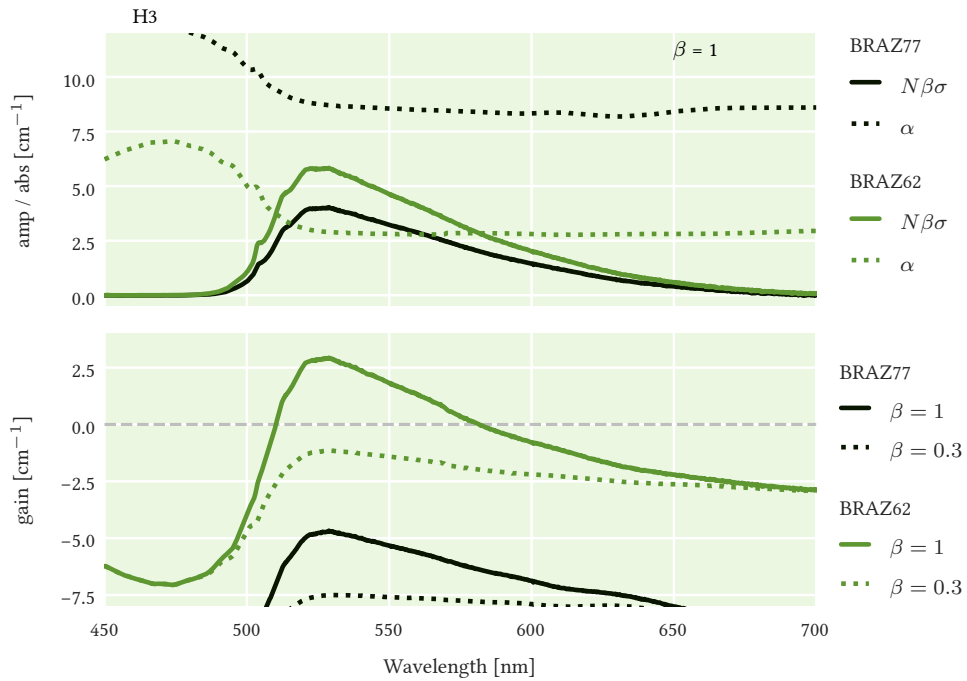


Figure 7.15: **Top:** The gain for N_2V^0 in samples samples BRAZ62 and BRAZ77, separated in the absorption and amplification part of eq. (6.27), $g = N \cdot \beta \cdot \sigma_{em} - \alpha_{abs}$. Calculated for $\beta = 1$. **Bottom:** Calculated gain spectrum for samples BRAZ62 and BRAZ77 for different inversion factors $\beta = 1$ and $\beta = 0.3$.

of full inversion. Positive net gain starts at $\beta > 0.5$. Additional HPHT treatment of such samples, ideally lowering background absorption and increasing the concentration of N_2V^0 , could lead to samples that show positive net absorption even for $\beta = 0.3$. If we assume the background absorption would not change, then an increase of 3 ppm, so a total of 5.2 ppm of N_2V^0 would be needed in sample BRAZ62 in order to get a net gain of 1 cm^{-1} for $\beta = 0.3$.

More work is merited to understand what is causing the background absorption in the natural diamonds and if it can be reduced further. Additional HPHT treatment of those samples could already yield a first indication if there is a possible reduction in absorption associated with it, as shown previously with the CVD grown samples. With these measurements, pre-treatment absorption spectra could not be taken due to the unpolished state of the diamonds and the schedule not permitting for polishing before HPHT treatment. In addition, further short HPHT treatment could increase the N_2V^0 concentration. Again, a more controlled starting material, like synthetic diamond, might be the better route to find a good ratio of high colour centre concentration to low background absorption.

The synthetic sample 1409E6sCVD04 (introduced in chapter 5, Results of the colour centre synthesis), had the largest concentration of N_2V^0 of any synthetic sample, 0.5 ppm. It was not included in the assessment of N_2V^0 samples, due to its large parasitic NV concentration, ~ 0.5 ppm, and the resulting background absorption at N_2V^0 peak emission of $\sim 3 \text{ cm}^{-1}$. The amplification part for $\beta = 1$ would be $N \cdot \beta \cdot \sigma = 1.32 \text{ cm}^{-1}$ (using the emission cross section determined previously). This makes it approximately as appealing as sample BRAZ62 in terms of background absorption.

In the next iteration of N_2V^0 synthesis using synthetic, NV containing samples, HPHT treatment at high temperatures can be considered to be included in the N_2V^0 synthesis protocol, to lower the overall background absorption. This has been discussed in section 5.2 for sample 1409E6sCVD02 in the NV synthesis. In fig. 5.2 it is clear that the overall background absorption of the sample has been lowered, and in fig. 5.17 it can be seen that even after NV synthesis, the background absorption remains lower than that of the comparison sample 1409E6sCVD03, which was not HPHT treated, but had an identical synthesis protocol besides. We assume that, provided full NV to N_2V^0 synthesis is possible, the background absorption of a sample can be efficiently lowered by prior high temperature HPHT treatment.

The maximum N_2V^0 concentration is limited up to $\sim 1/2 \cdot 3.8 = 1.9$ ppm (based on the initial single nitrogen concentration) in sample 1409E6sCVD04, in the most ideal situation that all N_s ²⁴ could be transformed to N_2V^0 . This

²⁴ Single substitutional nitrogen (C centre)

is likely not enough to overcome the losses in this sample.

The CVD samples in this work had a background absorption ranging from $3\text{--}10\text{ cm}^{-1}$ at the peak emission of N_2V^0 . In HPHT grown samples available to us (not introduced in this work in detail), with approximately 100 ppm of initial single nitrogen, the absorption ranged between $\sim 10\text{--}20\text{ cm}^{-1}$ in the same wavelength region (with up to 2 ppm of NV^- present in those samples). The N_2V^0 concentration needed in order for the amplification to match this background absorption would be ~ 6 ppm (for an absorption of 11 cm^{-1} and $\beta = 0.3$) and ~ 11 ppm (for an absorption of 20 cm^{-1} and $\beta = 0.3$).

It would be reasonable to include samples with higher initial N_s concentration for further synthesis of N_2V^0 samples in synthetic diamond. Samples with low background absorption and initial nitrogen concentration of at least $\sim 20\text{--}30$ ppm (allowing for the generation of $10\text{--}15$ ppm of NV and up to that amount of N_2V^0 , assuming full conversion of NV to N_2V^0 is possible) seem suitable for further experiments.

From a laser engineering point of view the reduction of background absorption is the favourable route to get a sample with net gain, but from a synthesis point of view, the strategy depends very much on the material available. In any case, both routes, and possibly a combination of both, should be investigated in further synthesis planning.

While CVD grown diamond is still not commercially available in concentrations between $10\text{--}50$ ppm, possibly allowing for the generation of $5\text{--}25$ ppm of NV , and possibly up to that amount of N_2V^0 , it seems that a suitable natural diamond might be a better starting point to get a sample with a good enough ratio of N_2V^0 concentration to background absorption at peak emission.

N_2V^0 synthesis in natural diamond requires HPHT anneals at high temperatures ($\sim 2100^\circ\text{C}$ at 11 GPa) for a few minutes, which are easier to maintain than long anneals ($>48\text{h}$) at moderate conditions ($\sim 1500^\circ\text{C}$ at 7.5 GPa), used for NV assisted N_2V^0 synthesis. Both routes are costly and have a moderate to high risk of damaging or destroying the sample. An ideal scenario would skip this step entirely and rely on N_2 centres being grown directly into low-absorption synthetic diamond. Unfortunately, such a technique is not yet known.

7.4 Re-evaluation of laser potential

THE PROSPECTS for a laser based on NV and N_2V^0 colour centres, in the most promising samples available to us, will be studied in this section. In section 6.5, A potential diamond colour centre laser, the potential of a colour centre diamond laser based on literature values was discussed and compared to colour centre based lasers in alkali halides and to another source with a broad emission, Ti:sapphire. In table 7.7 literature values for NV and N_2V^0 centres are compared to those measured in this work, and to values for Ti:sapphire and two types of colour centres in alkali halides.

Absorption cross sections in table 7.7 were estimated by taking the difference between the absorption coefficient at the given wavelength after the final treatment step and pre-treatment (when no target colour centre was present), divided by the concentration of the target colour centre in the sample, and averaged over all the samples introduced in the previous chapters.

in fig. 7.16 the absorption and emission cross-sections for NV and N_2V^0 are plotted. Their absorption part was adjusted to match the emission at the ZPL. Values for NV⁻ and N_2V^0 agree with the calculated ones shown in table 7.7. For NV⁰ the absorption cross section in table 7.7 seems to be overestimated. Most likely due to the overlap of NV⁰ and NV⁻ in that spectral range. The calculated value is plotted as a dotted line, while the one adjusted to the ZPL is plotted as a solid line.

In this work luminescence lifetime and emission cross section values for NV and N_2V ²⁵ were measured and calculated:

$$\tau_{lum} = 20 \text{ ns} \text{ and } \sigma_{em} = 0.17 \cdot 10^{-16} \text{ cm}^2 \text{ for NV}^0,$$

$$\tau_{lum} = 8 \text{ ns} \text{ and } \sigma_{em} = 0.36 \cdot 10^{-16} \text{ cm}^2 \text{ for NV}^-, \text{ and}$$

$$\tau_{lum} = 12 \text{ ns} \text{ and } \sigma_{em} = 0.15 \cdot 10^{-16} \text{ cm}^2 \text{ for } N_2V^0.$$

With these $\sigma \cdot \tau$ values of 3.4, 2.9 and $1.8 \cdot 10^{-16} \text{ cm}^2 \text{ ns}$ were calculated, for the respective centres.

²⁵ A vacancy and two substitutional nitrogen atoms in C_{2v} symmetry

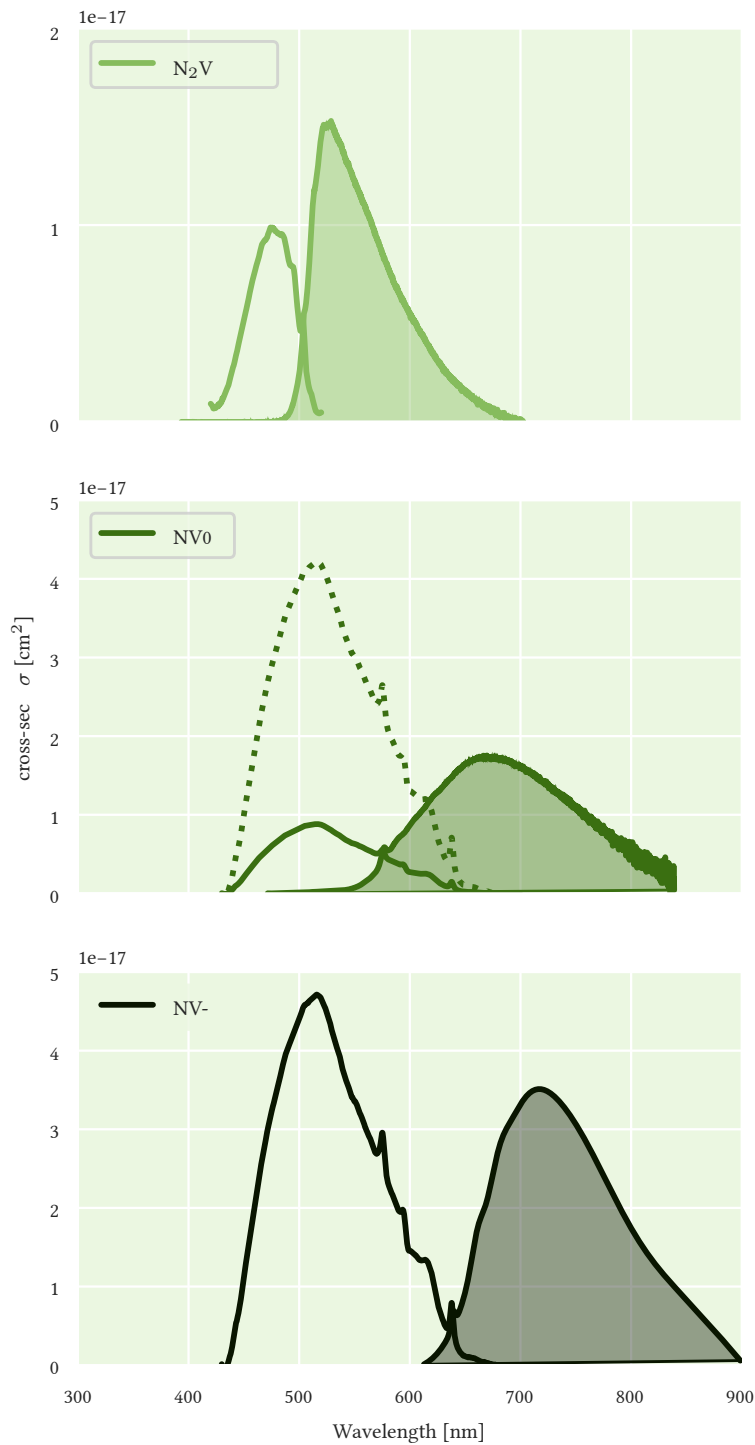


Figure 7.16: Illustration of emission and absorption cross section spectra for N_2V^0 , NV^0 and NV^- . The absorption cross section was calculated for all the samples introduced in this work, with the measured colour centre concentrations and absorption cross sections according to eq. (6.24).

For N_2V^0 and NV^- the ZPLs in absorption and emission overlap. For NV^0 the absorption cross section is likely overestimated due to the spectrum not being separated for NV^0 and NV^- . The calculated spectrum (dotted line) and the spectrum adjusted to the ZPL (solid line) are plotted.

	NV ⁰	NV ⁻	N ₂ V ⁰	Ti:Sapphire	Typical CC laser	
					NaCl:F ₂ ⁺ :OH	LiF:F ₂
ZPL	575 [11]	638 [11]	503.2 [11]	617.7 [17]	-	-
Absorption range (nm)	~450 - 580 [11]	450 - 640 [18]	420 - 520 [19]	420 - 600 [20]	800 - 1200 [21]	800 - 1100 [21]
Peak absorption (nm)	520 [11]	565 [12]	490 [12]	480 [20]	1050 [21]	1000 [21]
Emission range (nm)	550 - 800 [11]	570 - 800 [22]	480 - 630 [19]	650 - 1200 [20]	1300-1800 [21]	1000-1250 [21]
Peak emission (nm)	650 [11]	690 [12]	525 [12]	790 [20]	1450 [21]	1180 [21]
Abs cross-section (10 ⁻¹⁶ cm ²)						
(at max abs)	-	0.28 [9]	-	0.00092 [23]		
	0.43	0.48	0.01			
(at 532 nm)	-	0.31 [24] 0.95 [25]	-			
(at 473 nm)	-	-	0.21 [26]			
Em cross-section (10 ⁻¹⁶ cm ²)						
(at max em)	-	0.43 [9] 3.2 [12]	0.23 [16], 1.6 [12]	0.0041 [14]	≥ 1 [27]	≥ 1 [27]
	0.17	0.36	0.15			
Luminescence lifetime (ns)	21 [2]	12-13 [7]	16 [16]	3.2 · 10 ³ [14]	~100 [21]	~100 [21]
	20	8	12.1			
$\sigma \cdot \tau$ (10 ⁻¹⁶ cm ² ns)	-	5 [7, 9], 42 [7, 12]	3.6 [16], 26 [12]	13 [14]	~100 [21, 27]	~100 [21, 27]
	3.4	2.9	1.8			
Quantum Efficiency	-	0.7 [28] 0.8 [29] 0.99 [19]	0.95 [16]	0.8 [17]	~1 [30]	~1 [27]
	~ 1	0.6	0.7			
Radiative lifetime (ns)	17 [6], 19 [8]	12 for $m_s = 0$ 7.8 for $m_s = \pm 1$ [9]	17 [11]	3.85 · 10 ³ [17]		
Gain coefficient (cm ⁻¹)						
(at 531 nm)	-	-	0.201 [16]			
(at max) for $\beta = 1$	< 1	< 3.5	< 2.5			
(at max) for $\beta = 0.3$	< 0	< 1	< 0			
Concentration (cm ⁻³)	< 1.1 · 10 ¹⁷ (0.65 ppm)	< 1.5 · 10 ¹⁷ (0.85 ppm)	< 3.9 · 10 ¹⁷ (2.2 ppm)	4.56 · 10 ¹⁹ (for 0.1 at%) [14]	~ 10 ¹⁷ [31]	~ 10 ¹⁷ [31]
Operation temperature (K)	RT	RT	RT	RT	77 K [27]	RT [27]

Table 7.7: Typical colour centre laser parameter compared to Ti:sapphire and values for N₂V⁰ and NV.
Bold: Values obtained in this work.

To illustrate the difference in the prediction of a NV or N_2V^0 based laser, made previously in section 6.5, Predicted operation of a NV and N_2V^0 based laser, and after assessment of the samples in this work, a comparison of the threshold pump powers can be made. As mentioned before in section 6.2, the product of the emission cross section and the upper state lifetime can be regarded as a figure of merit for a given laser. It is inversely proportional to the threshold power (eq. (6.12)).

The laser threshold was estimated previously, using literature values (and the assumption of cavity losses $\gamma = 0.1$, pump efficiency $\eta = 1$, pump beam radius $r = 50 \mu m$ and sample length $l = 2 mm$). For comparison the value for cavity losses doesn't reflect the actual samples we have, but an ideal sample. For NV⁻, a laser threshold of 0.7 W (table 6.6) was estimated with $\sigma = 3.2 \cdot 10^{-16} cm^2$ [12]. This value is increased to 10.2 W with the $\sigma \cdot \tau$ value obtained in this work. A comparison of literature values and values obtained in this work can be found in table 7.7. The anticipated laser threshold of 1.2 W for N_2V^0 (table 6.6), estimated with $\sigma = 1.6 \cdot 10^{-16} cm^2$, is increased to 18.3 W with the $\sigma \cdot \tau$ value obtained in this work.

There are no literature values available for NV⁰. With a luminescence lifetime of 20 ns and the same parameters as used in the calculation above, the estimated threshold would be 8.6 W with the emission cross section obtained here.

The luminescence QY of the samples was also measured in two ways: by collecting the total luminescence using an integrating sphere and by comparing the luminescence lifetime to the radiative lifetime.

The former returned the QY of the sample overall, factoring in the effect of absorption by other centres; the latter returned an estimate of the yield of particular centres. The QY of NV⁻ and NV⁰ in these samples was relatively high and similar for the two samples: 60-70% for NV⁻ and approaching 100% for NV⁰. However, parasitic absorption in the samples meant the QYs from the samples overall were substantially lower: 20-30% for pumping at 447 nm, exciting mainly NV⁰, and 40-50% for pumping at 532 nm, exciting both NV⁰ and NV⁻.

The steep reduction of the QY for NV⁰ when looking at the overall sample indicates a high parasitic absorption, mostly likely by NV⁻, which absorbs in the NV⁰ emission region. This might be an intrinsic downside of trying to base a laser on NV⁰, as having large quantities of it requires a large quantity of single nitrogen in the sample, which, in turn, makes it more likely to have electron donors close by, producing NV⁻.

For NV⁻ it seems the intrinsic QY is lower than unity, possibly indicating concentration quenching or quenching from stress in the sample. Again, these measurements should be repeated using a wider range of NV concentrations, in order to determine the onset and magnitude of concentration quenching of NV luminescence.

Gain of up to 1 cm^{-1} for $\beta = 0.3$ was estimated for NV^- in sample E6H3D, and no positive net gain was found in any other sample for any colour centre for $\beta = 0.3$.

No laser action could be achieved in any of the samples, in particular not in the only promising sample E6H3D, indicating that the effects of photo-ionization and ESA need to be investigated before making further assumptions about the potential of such samples for a laser gain material.

It seems that the initial estimations of the $\sigma \cdot \tau$ values of NV^- and N_2V^0 , based on values reported by [12], were too optimistic. The smaller $\sigma \cdot \tau$, between a quarter and a sixth of the Ti:sapphire value, indicate that lasers based on these colour centres likely require high brightness or pulsed pumps and will have a high threshold, as already discussed previously.

While this makes them less attractive in terms of practicality, there is still value in continued research for an intrinsic laser in diamond. In particular, as integrated diamond electronics are advancing. With the wide range of colour centres in diamond, it might very well be that another colour centre turns out to be a better candidate for a diamond laser.

7.5 Summary

THE MOST PROMISING SAMPLES, regarding the concentration of NV and N_2V^0 , respectively, and residual background absorption, were evaluated for their laser related properties in this section. These include the background absorption at peak emission at room temperature, the luminescence lifetime and quantum yield, the emission cross section and potential laser gain.

Promising net gain of $g \approx 1 \text{ cm}^{-1}$ for $\beta = 0.3$ was determined for NV⁻ in one sample (E6H3D), but no laser action could be established. Additional work is needed to understand the effect of ESA and charge transfer in the depopulation of the excited state of NV, reducing the laser potential for this colour centre as suggested by [9].

No N_2V^0 sample with positive net gain for $\beta = 0.3$ could be produced. An inversion of $\beta > 0.5$ would be required for positive net gain in sample BRAZ62. Additional HPHT treatment of natural samples to find the maximum N_2V^0 could yield even more promising samples in terms of N_2V^0 concentration and background absorption.

For synthetic samples, diamonds with higher initial nitrogen concentrations (starting from $\sim 20\text{-}30$ ppm) for the synthesis of a suitable N_2V^0 laser sample are suggested. As with NV, measurements of ESA and charge transfer effects are advisable.

References

- [1] J. Solé, L. Bausá, and D. Jaque. *An Introduction to the Optical Spectroscopy of Inorganic Solids*. 2005. DOI: 10.1002/0470016043.
- [2] K. Beha et al. "Optimum photoluminescence excitation and recharging cycle of single nitrogen-vacancy centers in ultrapure diamond". In: *Physical Review Letters* 109.9 (Aug. 2012), p. 097404. ISSN: 00319007. DOI: 10.1103/PhysRevLett.109.097404.
- [3] N. Aslam et al. "Photo-induced ionization dynamics of the nitrogen vacancy defect in diamond investigated by single-shot charge state detection". In: *New Journal of Physics* 15.1 (Jan. 2013), p. 13064. ISSN: 13672630. DOI: 10.1088/1367-2630/15/1/013064.
- [4] J. Storteboom et al. "Lifetime investigation of single nitrogen vacancy centres in nanodiamonds". EN. In: *Optics Express* 23.9 (May 2015), p. 11327. ISSN: 1094-4087. DOI: 10.1364/OE.23.011327. URL: <https://www.osapublishing.org/abstract.cfm?URI=oe-23-9-11327>.
- [5] G. Liaugaudas et al. "Luminescence-lifetime mapping in diamond." In: *Journal of physics. Condensed matter: an Institute of Physics journal* 21.36 (Sept. 2009), p. 364210. ISSN: 0953-8984. DOI: 10.1088/0953-8984/21/36/364210. URL: <http://stacks.iop.org/0953-8984/21/i=36/a=364210?key=crossref.10614e3e690024bbe6f4728857534dda>.
- [6] G. Liaugaudas et al. "Luminescence lifetimes of neutral nitrogen-vacancy centres in synthetic diamond containing nitrogen". en. In: *Journal of Physics: Condensed Matter* 24.43 (Oct. 2012), p. 435503. ISSN: 0953-8984. DOI: 10.1088/0953-8984/24/43/435503.
- [7] A. T. Collins, M. F. Thomaz, and M. I. B. Jorge. "Luminescence decay time of the 1.945 eV centre in type Ib diamond". In: *Journal of Physics C: Solid State Physics* 16.11 (1983), pp. 2177-2181. ISSN: 0022-3719. DOI: 10.1088/0022-3719/16/11/020.
- [8] D. Gatto Monticone et al. "Systematic study of defect-related quenching of NV luminescence in diamond with time-correlated single-photon counting spectroscopy". In: *Physical Review B - Condensed Matter and Materials Physics* 88.15 (2013), p. 155201. ISSN: 10980121. DOI: 10.1103/PhysRevB.88.155201.
- [9] S. Subedi et al. "Laser spectroscopy of highly doped NV-centers in diamond". In: *Solid State Lasers XXVII: Technology and Devices* 10511 (Feb. 2018). Ed. by W. A. Clarkson and R. K. Shori, p. 84. DOI: 10.1117/12.2290705.
- [10] L. P. Neukirch et al. "Observation of nitrogen vacancy photoluminescence from an optically levitated nanodiamond". In: 12 (2013). DOI: 10.1364/OL.38.002976.
- [11] A. M. Zaitsev. *Optical Properties of Diamond: A Data Handbook*. Springer, 2001, p. 502. ISBN: 354066582X. DOI: 10.1007/978-3-662-04548-0.
- [12] V. G. Vins and E. V. Pestryakov. "Color centers in diamond crystals: Their potential use in tunable and femtosecond lasers". In: *Diamond and Related Materials* 15.4-8 (Apr. 2006), pp. 569-571. ISSN: 09259635. DOI: 10.1016/j.diamond.2005.11.038.
- [13] S. D. Subedi et al. "Saturation spectroscopy of NV centers in diamond". In: *Laser Congress 2018 (ASSL)*. Optical Society of America, 2018, AM6A.11. DOI: 10.1364/ASSL.2018.AM6A.11. URL: <http://www.osapublishing.org/abstract.cfm?URI=ASSL-2018-AM6A.11>.
- [14] *RP Photonics Consulting GmbH - technical consulting on laser technology, nonlinear optics, fiber optics; simulation and design software; encyclopedia and buyer's guide*. URL: <https://www.rp-photonics.com/>.
- [15] M. D. Crossfield et al. "The role of defect interactions in reducing the decay time of H3 luminescence in diamond". In: *Journal of Physics C: Solid State Physics* 7.10 (May 1974), pp. 1909-1917. ISSN: 0022-3719. DOI: 10.1088/0022-3719/7/10/018.
- [16] S. C. Rand and L. G. Deshazer. "Visible color-center laser in diamond." In: *Optics letters* 10.10 (Oct. 1985), pp. 481-483. ISSN: 0146-9592. DOI: 10.1364/OL.10.000481.
- [17] P. Albers, E. Stark, and G. Huber. "Continuous-wave laser operation and quantum efficiency of titanium-doped sapphire". EN. In: *Journal of the Optical Society of America B* 3.1 (Jan. 1986), pp. 134-139. ISSN: 0740-3224. DOI: 10.1364/JOSAB.3.000134.
- [18] I. A. Dobrinets, V. G. Vins, and A. M. Zaitsev. *HPHT-Treated Diamonds*. Vol. 181. Springer, 2013. ISBN: 978-3-642-37489-0. DOI: 10.1007/978-3-642-37490-6.
- [19] M. A. Prelas et al. *Wide Band Gap Electronic Materials*. Vol. 1. Springer Science & Business Media, 1995. ISBN: 9789401040785. DOI: 10.1007/978-94-011-0173-8.
- [20] K. Wall and A. Sanchez. "Titanium Sapphire lasers". In: *The Lincoln laboratory journal* 3.3 (1990), pp. 447-462. URL: <https://pdfs.semanticscholar.org/0be0/0117536e932394af5e1d6d5c8acab06364d5.pdf>.
- [21] J. Yao and Y. Wang. *Nonlinear Optics and Solid-State Lasers*. Vol. 164. Springer Science & Business Media, 2012. ISBN: 978-3-642-22788-2. DOI: 10.1007/978-3-642-22789-9.
- [22] J. Storteboom et al. "Lifetime investigation of single nitrogen vacancy centres in nanodiamonds". In: *Optics Express* 23.9 (2015), p. 11327. ISSN: 1094-4087. DOI: 10.1364/OE.23.011327.
- [23] R. L. Aggarwal et al. "Magnetic and optical measurements on Ti:Al₂O₃ crystals for laser applications: Concentration and absorption cross section of Ti³⁺ ions". In: *Applied Physics Letters* 48.20 (May 1986), pp. 1345-1347. ISSN: 0003-6951. DOI: 10.1063/1.96904.
- [24] T.-I. Wee et al. "Two-photon Excited Fluorescence of Nitrogen-Vacancy Centers in Proton-Irradiated Type". In: *The Journal of Physical Chemistry A* 111.38 (2007), pp. 9379-9386. ISSN: 1089-5639. DOI: 10.1021/jp073938o.
- [25] R. Chapman and T. Plakhotnik. "Quantitative luminescence microscopy on Nitrogen-Vacancy Centres in diamond: Saturation effects under pulsed excitation". In:

- Chemical Physics Letters* 507.1-3 (2011), pp. 190–194. ISSN: 00092614. DOI: 10.1016/j.cplett.2011.03.057.
- [26] C.-K. Lin et al. “Excitation properties of the H3 defect center in diamond: A theoretical study”. In: *Chemical Physics Letters* 475.1-3 (June 2009), pp. 68–72. ISSN: 0009-2614. DOI: 10.1016/J.CPLETT.2009.05.011.
- [27] L. F. Mollenauer and J. C. White. *Tunable Lasers*. Springer-Verlag Berlin Heidelberg, 1987, pp. 225–277. ISBN: 978-3-662-10637-2. DOI: 10.1007/978-3-662-10635-8.
- [28] F. Jelezko and J. Wrachtrup. “Single defect centres in diamond: A review”. In: *Physica Status Solidi (A) Applications and Materials Science* 203.13 (Oct. 2006), pp. 3207–3225. ISSN: 18626300. DOI: 10.1002/pssa.200671403.
- [29] I. P. Radko et al. “Determining the internal quantum efficiency of shallow-implanted nitrogen-vacancy defects in bulk diamond”. In: *Optics Express* 24.24 (Nov. 2016), p. 27715. ISSN: 1094-4087. DOI: 10.1364/OE.24.027715.
- [30] G. Lifante, J. Tocho, and F. Cusso. “Photoacoustic determination of the luminescent quantum efficiencies of F2+ and (F2+) H centres in NaCl: OH-crystals”. In: *Journal of Physics: Condensed Matter* 2.13 (1990), p. 3035. DOI: 10.1088/0953-8984/2/13/013.
- [31] J. F. Pinto, E. Georgiou, and C. R. Pollock. “Stable color-center laser in OH-doped NaCl operating in the 1.41- to 1.81- μm region”. In: *Opt. Lett.* 11.8 (1986), pp. 519–521. ISSN: 15394794. DOI: 10.1364/OL.11.000519.

8

Summary and future work

Contents

8.1 Synthesis	208
8.2 Assessment of laser related properties	211
8.3 Further work	212
References	215

IN THIS THESIS NV¹ and N₂V⁰² colour centres³ in diamond were synthesised with the aim to produce samples that allowed for the assessment of laser related parameters.

Synthesis techniques including HPHT⁴ treatment, irradiation with MeV electrons and annealing were used to generate NV and N₂V⁰ in synthetic and natural diamond samples. UV-VIS⁵ and FTIR⁶ absorption and photoluminescence measurements have been used to investigate the type and concentration of the respective defect, its laser related properties and background absorption at the emission wavelength range.

8.1 Synthesis

NV or N₂V⁰ were synthesised in single crystal diamond, while preserving optical quality of the samples, to assess their laser potential. This was done in order to initiate and guide a subsequent campaign of iterative improvement towards a laser grade sample.

Preliminary calculations for 50% pump absorption suggested required target concentrations of 0.6 ppm in NV⁻⁷ samples and 0.9 ppm in N₂V⁰ samples. Samples with ideal N_s⁸ levels could not be obtained. As grown starting material available to us was CVD⁹ diamond with single nitrogen concentrations ranging from 0.1 to 3.8 ppm. These samples were subjected to a mix of electron irradiation, annealing and HPHT treatment, to generate NV and N₂V⁰ colour centres. Pre treated and natural samples became available and were used to extend this picture. Pre treated CVD grown diamond loaned to us by Element Six Ltd. and natural diamond loaned to us by Professor Jeff Harris from Glasgow University.

NV synthesis, including irradiation with 4.5 MeV electrons and subsequent annealing at 800°C, in CVD grown samples with ~ 3.8 ppm of initial single nitrogen yielded a range of samples with a conversion up to 36% of the initial nitrogen concentration into NV. The charged states were almost equally split into NV⁰¹⁰ and NV⁻, due to a residue of N_s electron donors.

The highest concentration of NV was produced in samples 1409E6sCVD02, with 0.61 ± 0.07 ppm¹¹ of NV⁻ and 0.58 ± 0.04 ppm of NV⁰, and 1409E6sCVD03, with 0.74 ± 0.08 ppm of NV⁻ and 0.65 ± 0.04 ppm of NV⁰. In samples with initial nitrogen concentrations of 0.3 and 0.11 ppm the conversion was 33 and 27%, respectively, with NV present almost purely in the form of NV⁰, due to less nearby single nitrogen overall to act as electron donor.

A conversion of up to 50% of the initial nitrogen concentration into NV would be expected [2]. At least 2.8 ppm of vacancies were generated in total over the whole synthesis procedure in samples 1409E6sCVD02 and 1409E6sCVD03. Nevertheless, not more than 1.2 and 1.4 ppm of NV were generated in total in those samples. As the total nitrogen concentration

¹ A substitutional nitrogen adjacent to a vacancy with a C_{3v} symmetry

² The neutrally charged state of N₂V (H3)

³ A type of structural defect, which produces absorption and emission bands that are different to those of the pure crystal [1]

⁴ High Pressure High Temperature

⁵ UltraViolet-Visible

⁶ Fourier Transform Infra Red

⁷ The negative form of NV

⁸ Single substitutional nitrogen (C centre)

⁹ Chemical Vapour Deposition

¹⁰ The neutral form of NV

¹¹ parts per million (1.77 · 10¹⁷ cm⁻³ for diamond)

in those samples was established by EPR¹² measurements of one sample in the series (3.8 ppm in sample 1409E6sCVD05) it is not clear if the low conversion is simply due to less initial nitrogen being available in the other samples.

¹² Electron
Resonance Paramagnetic

In loaned, pre-treated E6H3 CVD samples with 5-7 ppm of initial single nitrogen, between 0.04 – 0.08 ppm of N_2V^0 was present initially. In one case (sample E6H3D) this concentration could be doubled from 0.05 to 0.11 ppm after irradiation and annealing. The N_2V^0 concentration was too low for those samples to be considered for N_2V^0 related laser assessment. Their relatively high single nitrogen concentration, in comparison to other samples available to us, together with low background absorption, made them ideal NV samples. Therefore they were irradiated and annealed as part of this work.

NV concentrations between 0.7 – 1 ppm were generated, with $\sim 70 - 80\%$ available as NV^- , due to a larger concentration of leftover single nitrogen available as electron donors in these samples. All of the loaned samples had comparable concentrations of NV^- (from 0.56 ± 0.06 to 0.85 ± 0.09 ppm), with lower NV^0 concentrations (from 0.13 ± 0.01 to 0.21 ± 0.01 ppm).

Sample E6NV, another loaned and pre-treated sample from a different batch than the previous samples, was obtained with 0.62 ± 0.07 ppm of NV^- and 0.73 ± 0.07 ppm of NV^0 .

Residual background absorption at the emission wavelength is a crucial parameter for a laser sample. Within this work the favourable effects of HPHT treatment on the background absorption in brownish CVD grown diamond, mentioned in literature [3], were replicated. Lowering the background absorption of sample 1409E6sCVD02 at the peak emission of NV^- from 1.62 to 0.08 cm^{-1} . After irradiation and annealing the absorption was still lower than in the reference sample, which was not HPHT treated before. After the full synthesis, the absorption at the peak emission of NV^- in sample 1409E6sCVD02 was 0.57 cm^{-1} and 2.79 cm^{-1} (1.34 cm^{-1} before treatment) in sample 1409E6sCVD03.

The total nitrogen concentration, at least at the concentration levels available to us, did not have a noticeable effect on the background absorption, as can be seen in fig. 5.17, where the background absorption of samples with nitrogen concentrations between ~ 1 to 7 ppm is plotted. The background absorption is not increasing with overall nitrogen concentration. In addition, as the example of sample 1409E6sCVD02 and 1409E6sCVD03 shows, the reduction of brown colouration in samples with identical nitrogen concentrations reduces the background absorption significantly. It would be of interest to future experiments to examine sam-

ples with nitrogen concentrations between 10-50 ppm, a range that wasn't available to us, and determine the influence of the nitrogen concentration on the background absorption or other effects, like quenching of luminescence.

N_2V^0 synthesis in synthetic diamond, with the initial nitrogen concentrations available to us, was considered infeasible through the route of nitrogen aggregation and subsequent irradiation and annealing, due to the low aggregation rate at such concentrations. A detailed discussion of these considerations can be found in section 3.3, Diffusion, aggregation and dissociation of defects. Instead, two alternative routes were exploited, N_2V^0 synthesis through NV assisted aggregation and synthesis in natural diamond.

The NV assisted synthesis was attempted with a long term (48 hours) HPHT run at 1500°C and 7.5 GPa in sample 1409E6sCVD04, where previously 0.78 ± 0.08 ppm of NV^- and 0.6 ± 0.04 ppm of NV^0 were synthesised.

0.5 ppm of N_2V^0 were generated after HPHT treatment. The conversion of at least $\sim 26\%$ of the initial single nitrogen concentration into N_2V^0 , through NV assisted aggregation, was the highest that could be achieved in any low nitrogen CVD sample available to us. In comparison, an aggregation of only 0.12% would be expected at at 1500°C and 7.5 GPa for 48 hours using the appropriate aggregation rate constant in the literature (table 3.3). The leftover NV concentration of about 0.5 ppm was relatively high. This is a disadvantage for lasing purposes, as NV^0 absorbs in the emission region of N_2V^0 and acts as a source of parasitic loss.

The goal of 0.9 ppm N_2V^0 could not be reached in the synthetic samples available to us. This motivated the alternative route of N_2V^0 synthesis in natural diamond, to obtain samples with sufficient N_2V^0 for the assessment as laser samples. Luminescent samples containing N_2V^0 could be produced with natural IaAB diamond samples. 2.2 ± 0.4 and 1.5 ± 0.3 ppm were the maximum concentrations of N_2V^0 achieved, produced by short HPHT treatment of samples BRAZ62 and BRAZ77, containing about 35 ± 2 and 50 ± 6 ppm of N_2 ¹³ initially. The samples were treated at 2100°C and 11 GPa for 3 minutes.

Further experiments are needed to establish the ideal synthesis parameters and the exact route of the N_2V^0 synthesis with this method. The maximum concentration possible should be determined with a succession of short HPHT anneals at one temperature, and careful monitoring of the concentrations in between each anneal. Ideally, this should be performed for a range of different temperatures, at least between 2100 and 2300°C, to determine the most suitable temperature for the process. It is suggested in literature that HPHT treatments up to 2300°C could yield a substantial additional concentration of N_2V^0 [4], but no quantitative comparisons were

¹³ Two adjacent substitutional nitrogen atoms (A centre)

available. Additional experiments of brown IaAB samples, as suggested in literature, at different temperatures between 2100-2300°C, with careful tracking of defect concentrations, would be helpful to quantify the N_2V^0 yield using this synthesis route.

IaA samples could be suitable for the synthesis of luminescent samples. Natural IaA samples with fully aggregated nitrogen are available, simplifying the aggregation to electron irradiation and annealing to form N_2V^0 . Additionally, the lack of leftover N_s guarantees no parasitic NV will be formed in those samples after irradiation and annealing. Even though 1.8-2.2 ppm of N_2V^0 were generated in the various IaA samples, and no leftover NV were present, all luminescence was quenched by the leftover N_2 concentration (~ 1000 ppm). Judging from luminescent IaAB samples with N_2 up to 50 ppm, a good N_2 concentration for luminescent IaA samples should be 50 ppm or below. No such samples were available to us.

8.2 Assessment of laser related properties

A selection of four samples were chosen for the assessment of laser related properties, based on their combination of high target colour centre concentration and low background absorption at the emission region, in comparison to other samples available. Laser related parameters for NV were measured in samples E6NV and E6H3D, and for N_2V^0 in samples BRAZ62 and BRAZ77.

Luminescence lifetimes of $\tau_{lum} = 20$ ns for NV^0 , $\tau_{lum} = 8$ ns for NV^- , and $\tau_{lum} = 12$ ns for N_2V^0 were measured by TCSPC¹⁴ spectroscopy.

Peak emission cross sections values calculated are $\sigma_{em} = 0.17 \cdot 10^{-16}$ cm² for NV^0 , $\sigma_{em} = 0.36 \cdot 10^{-16}$ cm² for NV^- , and $\sigma_{em} = 0.15 \cdot 10^{-16}$ cm² for N_2V^0 .

QY¹⁵ values were measured by two different approaches. One used the luminescence lifetime of the respective centre and the other the relation between pump absorption and emission spectrum of the sample as a whole. In this way the first value is a quantification of the QY of the respective centre and the potential a sample containing solely this centre, if no other non radiative quenching effects or parasitic absorption occurs. The second value is a representation of the potential a specific sample has.

The luminescence QY for the respective centres was estimated by comparison of the literature radiative lifetimes to the luminescence lifetimes measured here. It was ~ 1 for NV^0 , 0.6 for NV^- and 0.7 for N_2V^0 . Literature values range between 0.7-0.99 [5, 6, 7] for NV^- and 0.95 [8] for N_2V^0 .

QY values measured using an integrating sphere included self-absorption effects in the respective samples. Those values were lower in the NV sam-

¹⁴ Time-Correlated Single Photon Counting

¹⁵ Quantum Yield

ples, < 0.3 for pumping at 447 nm (exciting NV^0), and < 0.5 for pumping at 532 nm (exciting NV^-). In the N_2V^0 samples pumped at 447 nm, these QY values ranged between $\sim 0.7 \pm 0.2$ and $1 - 0.3$.

The luminescence of NV^0 is affected most strongly by reabsorption in the sample, which is likely caused by the overlap of emission region of NV^0 and absorption region of NV^- . This strong reduction of QY lowers the chances of NV^0 to be a viable candidate for a colour centre based laser. For NV^- and N_2V^0 the two values were closer to each other, suggesting less additional reabsorption in the samples available.

Gain spectra were estimated for the respective centres at two different inversion levels. Only in one sample and for one centre, NV^- , positive net gain was estimated at an inversion of $\beta = 0.3$. For N_2V^0 , an inversion of $\beta > 0.5$ would be required to achieve positive net gain in the most promising sample. The preliminary results, positive net gain in one sample, look promising for the first iteration towards a laser focussed synthesis protocol.

8.3 Further work

Further research is needed to determine the optimal balance between starting nitrogen concentration and yield of NV and N_2V^0 centres in synthetic diamond, while keeping the background absorption as low as possible. Constant advancements in the quality, versatility and customizability of synthetic diamond samples and the included impurities [9, 10] could lead to a greater selection of suitable samples for laser assessment in the future.

It was possible to generate luminescent natural diamond containing N_2V^0 , but positive net gain was only predicted for sample BRAZ62 with an inversion of $\beta > 0.5$. For the next iteration of the N_2V^0 synthesis the generation of samples with positive net gain at $\beta = 0.3$ is desirable, in order to achieve positive net gain.

From the results in this thesis it seems that similar IaAB samples with either lower background absorption or about double the N_2V^0 concentration are needed to obtain positive net gain. Natural samples with low background absorption at the N_2V^0 emission range and similar concentrations of N_2 and N_4V ¹⁶ centres could be a better starting material, if available. A concentration of 5 ppm of N_2V^0 for sample BRAZ62 and 12 ppm for sample BRAZ77 would be sufficient to reach a gain coefficient of 1 cm^{-1} at $\beta = 0.3$. Prolonged HPHT treatment or HPHT treatment at higher temperatures might yield additional N_2V^0 in similar samples, as discussed previously and indicated in literature. Quantitative results of N_2V^0 concentrations in natural diamond after HPHT treatment at temperatures above 2100°C and pressures above 11 GPa for a range of treatment times, are rare

¹⁶ Four substitutional nitrogen surrounding a vacancy (B centre)

in the literature. Further work is needed to determine the optimal treatment time to generate a specific concentration of N_2V^0 in a given sample.

Additionally, natural IIa diamond with less than 50 ppm of N_2 could be of interest as a starting material. Judging from the results using natural IaAB diamond, samples with such concentrations of N_2 and 1-2 ppm of N_2V^0 are luminescent. To determine the ideal amount of N_2 to prevent quenching, luminescence measurements with a range of samples are needed, ideally between 10-50 ppm.

The downsides of natural samples were the irregular sample size, impurities and inclusions in the samples, and a high background absorption in comparison to synthetic diamond.

N_2V^0 synthesis in synthetic diamond is therefore considered to be the more promising route for a reproducible and reliable laser sample. But unless synthetic diamond can be grown including nitrogen in the form of N_2 in the future, aggregation in low nitrogen concentration samples is a problem for the N_2V^0 synthesis. NV assisted N_2V^0 synthesis, although much more efficient than aggregation of single nitrogen at the same temperatures and pressures, was only successful in one of our samples, as the HPHT procedure is hard to stabilize over long periods of time. The leftover NV concentration in the sample was about the same as the concentration of generated N_2V^0 .

Longer HPHT runs at the same conditions, or runs at higher temperatures, between 1600-1800 °C, should be considered to study if the total amount of N_2V^0 and can be increased, while lowering residual NV. Such samples could combine the low background absorption of synthetic diamond with the high N_2V^0 yield during NV assisted synthesis, provided the ratio of N_2V^0 to NV can be maximized during the process.

For all colour centres under study, bleaching through charge transfer and possible ESA¹⁷ should be studied in greater detail. Transient-absorption spectroscopy can be used to measure changes in the absorption of the sample as a function of wavelength or time. Such work has been outlined in [11] for NV^- . First results in a CVD grown synthetic diamond with 200-300 ppm of single nitrogen and about 25.7 ppm of NV^- , indicate that stimulated emission of NV^- is suppressed by photoionization and ESA, reducing the usability of NV^- to base a diamond laser on. The optimization of colour centre concentration and excitation wavelength for NV^- and NV^0 are parameters considered for further research.

To the authors knowledge no such measurements were published for N_2V^0 up to this date. It would be of interest to know if the charge transfer in N_2V^0 is as detrimental to stimulated emission, as it is in NV^- , and if ESA can be measured.

¹⁷ Excited State Absorption

Several successful attempts at the control of the charged state of NV in diamond have been made [12, 13], raising the question whether electrical control of the charge transfer from NV^0 to NV^- in large enough numbers would work to counteract the detrimental effects of charge transfer induced by the pump in laser experiments. In [13] current-injecting graphitic microelectrodes were fabricated in bulk diamond, and an electrically-induced increase of the NV^- luminescence of up to 40% was detected from the NV centres in the $9\ \mu m$ gap between the electrodes.

With advances in the fabrication of diamond and an increase in knowledge about NV and other colour centres, there are a lot of potential applications to be examined. Even though N_2V^0 hasn't received the same attention in recent publications as NV, it is still a promising candidate for a laser sample if colour centre concentrations can be increased while lowering background absorption.

NV looks less promising for a laser candidate in comparison to previous estimations in literature [8, 14], but there might be a sweet spot between the concentration in the samples, the emission wavelength and other factors, like sample design, that has not been discovered yet. Additionally, many of the over five hundred known colour centres in diamond are yet to be synthesised and explored in synthetic diamond. Within those, a centre suitable for lasing might be hidden.

References

- [1] J. Solé, L. Bausá, and D. Jaque. *An Introduction to the Optical Spectroscopy of Inorganic Solids*. 2005. DOI: 10.1002/0470016043.
- [2] C. B. Hartland. *A study of point defects in CVD diamond using electron paramagnetic resonance and optical spectroscopy*. Aug. 2014. URL: <http://wrap.warwick.ac.uk/id/eprint/67156>.
- [3] I. A. Dobrinets, V. G. Vins, and A. M. Zaitsev. *Diamonds Used for HPHT Treatment*. Berlin, Heidelberg: Springer Berlin Heidelberg, 2013, pp. 5–25. ISBN: 978-3-642-37490-6. DOI: 10.1007/978-3-642-37490-6_2.
- [4] A. T. Collins et al. “High-temperature annealing of optical centers in type-I diamond”. In: *Journal of Applied Physics* 97.8 (Apr. 2005), p. 083517. ISSN: 00218979. DOI: 10.1063/1.1866501.
- [5] F. Jelezko and J. Wrachtrup. “Single defect centres in diamond: A review”. In: *Physica Status Solidi (A) Applications and Materials Science* 203.13 (Oct. 2006), pp. 3207–3225. ISSN: 18626300. DOI: 10.1002/pssa.200671403.
- [6] I. P. Radko et al. “Determining the internal quantum efficiency of shallow-implanted nitrogen-vacancy defects in bulk diamond”. In: *Optics Express* 24.24 (Nov. 2016), p. 27715. ISSN: 1094-4087. DOI: 10.1364/OE.24.027715.
- [7] M. A. Prelas et al. *Wide Band Gap Electronic Materials*. Vol. 1. Springer Science & Business Media, 1995. ISBN: 9789401040785. DOI: 10.1007/978-94-011-0173-8.
- [8] S. C. Rand and L. G. Deshazer. “Visible color-center laser in diamond.” In: *Optics letters* 10.10 (Oct. 1985), pp. 481–483. ISSN: 0146-9592. DOI: 10.1364/OL.10.000481.
- [9] *DIAMOND PUREOPTICS™: ACHIEVE EVER HIGHER POWER DENSITIES*. URL: https://e6-prd-cdn-01.azureedge.net/mediacontainer/medialibraries/element6/documents/brochures/element_six_diamond_pureoptics.pdf.
- [10] *CVD DIAMOND: THE ELEMENT SIX CVD DIAMOND HANDBOOK*. URL: https://e6-prd-cdn-01.azureedge.net/mediacontainer/medialibraries/element6/documents/brochures/element_six_cvd_diamond_handbook.pdf.
- [11] S. Subedi et al. “Laser spectroscopy of highly doped NV-centers in diamond”. In: *Solid State Lasers XXVII: Technology and Devices* 10511 (Feb. 2018). Ed. by W. A. Clarkson and R. K. Shori, p. 84. DOI: 10.1117/12.2290705.
- [12] C. Schreyvogel et al. “Active charge state control of single NV centres in diamond by in-plane Al-Schottky junctions”. In: *Scientific Reports* 5.1 (Dec. 2015), p. 12160. ISSN: 2045-2322. DOI: 10.1038/srep12160.
- [13] J. Forneris et al. “Electrical control of deep NV centers in diamond by means of sub-superficial graphitic micro-electrodes”. In: (July 2016). DOI: 10.1016/j.carbon.2016.11.031. arXiv: 1607.05553.
- [14] V. G. Vins and E. V. Pestryakov. “Color centers in diamond crystals: Their potential use in tunable and femtosecond lasers”. In: *Diamond and Related Materials* 15.4-8 (Apr. 2006), pp. 569–571. ISSN: 09259635. DOI: 10.1016/j.diamond.2005.11.038.